Computer simulations of Fréchet dendrimers in solution

Stephen Charles Simpson

A Thesis Presented for the Degree of
Doctor of Philosophy

Computational Chemistry
Department of Chemistry
University of Cape Town
South Africa

Dedicated to

Min, Pops, Grannamoradogbiscuits and Angelpuddingpie

Computer simulations of Fréchet dendrimers in solution

S. Charles Simpson

Abstract

The structure and dynamics of dendrimers in solution are studied through nanosecond atomistic Molecular Dynamics (MD) simulations of explicitly solvated Fréchet dendrimers, generations G1 to G5. The properties of these dendrimers are investigated in four solvent environments: vacuum and water (representatives of poor solvents), and tetrahydrofuran (THF) and chloroform (representatives of good solvents). To establish the effect of the quality of the solvent on the conformation of the dendrimer, additional nanosecond MD simulations of dendrimers are performed, from both initially folded and unfolded conformations. Free energy calculations of model dendritic units are employed to provide an energetic rational for the folding behaviour of these dendrimers.

These simulations require a solution force field that accurately represents Fréchet dendrimers solvated in chloroform, THF and water. Here we develop a new fully relaxed, all-atom chloroform force field. Models for THF and water were sourced from the available literature. In the dendrimer force field, the ether linkage (which governs the flexibility of the dendrimer) is relaxed to offer an improved match with quantum mechanically derived rotational energy profiles.

Employing this force field, MD simulations show that the dendrimers do not fold in chloroform and THF. Spatially averaged distribution functions (SDFs) show the core of the dendrimer is readily accessible by the reaction medium, even when the dendrimer is folded, and backfolding of the terminal groups can be accounted for largely by the hyperbranching inherent to dendrimers. Calculated diffusion coefficients, intrinsic viscosities and longitudinal relaxation rates afford a good match with available experimental data. A close correlation is observed between the flexibility of a dendrimer and its intrinsic viscosity. A new expression for calculating intrinsic viscosities is suggested, which is a function of the size, shape and flexibility of the polymer. The potentials of mean force (PMF) of folding indicate that a dendrimer folds at least two generations deep. Slight differences in these PMFs in chloroform and THF suggest that solvent shells encapsulating the dendrimer are more easily disrupted in THF than in chloroform.

Declaration

The work in this thesis is based on research carried out at the Computational Chemistry Research Group, the Department of Chemistry, University of Cape Town, South Africa. No part of this thesis has been submitted elsewhere for any other degree or qualification and is all my own work unless referenced to the contrary in the text.

Signed by candidate

Acknowledgements

Supervising a Ph.D. is no easy task. Therefore, my first point of thanks is to my supervisor, Professor Kevin J. Naidoo, whose mentoring stretched beyond the principles of computational chemistry and polymer science and into the art of conducting thorough, probing scientific investigations. Most of all, I appreciate our many engaging discussions from which I learnt a great deal and was certainly not limited to science. I would also like to thank my co-supervisor, Professor John R. Moss, who made valuable suggestions and was constantly interested in the developments made during this thesis, even though the topic was not synthetically orientated.

To the past and present members of the Computational Research Group at U.C.T. and the members of Biophysical Chemistry Research Seminars, many thanks for the hours of engaging and thought provoking discussions. In particular, I would like to make special mention of Drs Michelle Kuttel, Robert Best, Anton Lopis and Jeff Chen, for helpful suggestions, proof reading and patience in the laboratory.

I thank Dr Rick Venable of the National Institute of Health USA, Professor Manfred Zeidler of Rheinisch-Westfälische Technische Hochschule in Aachen Germany, Professor Jozef Kowalewski of Stockholm University and the members of the Computational Chemistry mailing List for fruitful discussions and encouragement.

A word of thanks to the National Research Foundation (Pretoria) for some financial assistance.

My heartfelt gratitude to the staff and management of Open Box Software for their support, encouragement and understanding over the past year.

And finally, but certainly not least of all, my loving family both here in South Africa and Mauritius, who have continuously supported and encouraged me. To you I can never express my gratitude. Especially my parents, who are an inspiration to us all and my late grandmother who will always be remembered with great affection. And last of all, to my wife Anabelle - this thesis was as much an effort and sacrifice on your part and is a testament to your patience, commitment and support. For each Ph.D. awarded, there should be an accompanying award for the partner. Merci beaucoup ma rose.

List of Abbreviations

AMBER Assisted Model Building and Energy Refinement

AFM Atomic Force Microscopy

amu atomic mass unit

atm atmospheres

CHARMM Chemistry at Harvard Macromolecular Mechanics

DAB diaminobutane poly(propylene imine) dendrimers

fs femtosecond

FEP Free Energy Perturbation

GROMOS Gronigen Molecular Simulation program

kcal kilocalories

MC Monte Carlo

MD Molecular Dynamics

ms millisecond

NVE constant number of particles, volume and energy ensemble

NVT constant number of particles, volume and temperature ensemble

NPT constant number of particles, pressure and temperature ensemble

NMR Nuclear Magnetic Resonance

nOe Nuclear Overhauser Effect

ns nanosecond

PAMAM polyamidoamine dendrimer

PBPE poly(benzyl phenyl ether) dendrimer

PDF Pair Distribution Function

PFGSE Pulse Field Gradient Spin Echo

PMF Potential of Mean Force

PPI poly(propyleneimine) dendrimer

POPAM poly(propyleneimine) dendrimer

ps picosecond

QM Quantum Mechanics

RDF Radial Distribution Function

$\mathbf{R_g}$ Radius of Gyration

SANS Small Angle Neutron Scattering

SAXS Small Angle X-ray Scattering

SDF Spatial Distribution Function

THF tetrahydrofuran

WHAM Weighted Histogram Analysis Method

Contents

List of Figures

List of Tables

Chapter 1

Introduction

1.1 Dendrimers - the molecular tumbleweeds

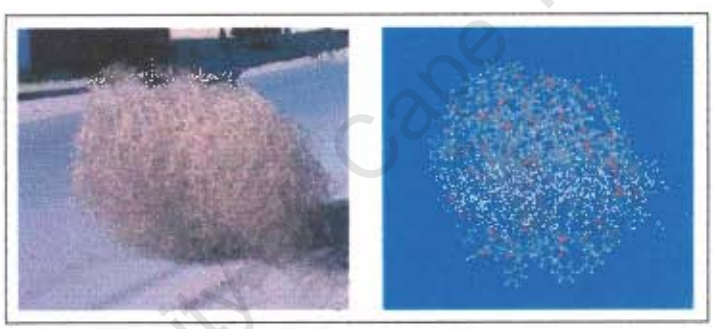

Figure 1.1: A tumbleweed compared with a fifth generation Fréchet dendrimer.

A dendrimer is a monodispersed, perfectly hyperbranched, fractal-like macromolecule that emanates from a central *focal point* (also known as an initiator or core group). The term dendrimer is derived from the Greek "dendra" (tree) and "meros" (part) and describes graphically the structure of dendrimers which resemble the architecture of a tree. [1] Dendrimers are also referred to as Cayley trees, arborols, cascade molecules and starburst polymers. However, we prefer the analogy of a molecular "tumbleweed" due to the dendrimer's ball-like structure (Figure 1.1). A dendrimer is made up of several *dendritic wedges*, or branches, that contain repeat units arranged in one or more concentric *topological layers*, or internal generations (Figure 1.2). These topological layers are denoted in lower case (i.e., g1 to g5). The *parent layer* of topological layer g_i is one layer in to the core from the current layer (i.e., layer g_{i-1}) and the *child layer* is one layer out from the current layer (i.e., layer g_{i+1}). Each successive layer is connected to the adjacent layers by

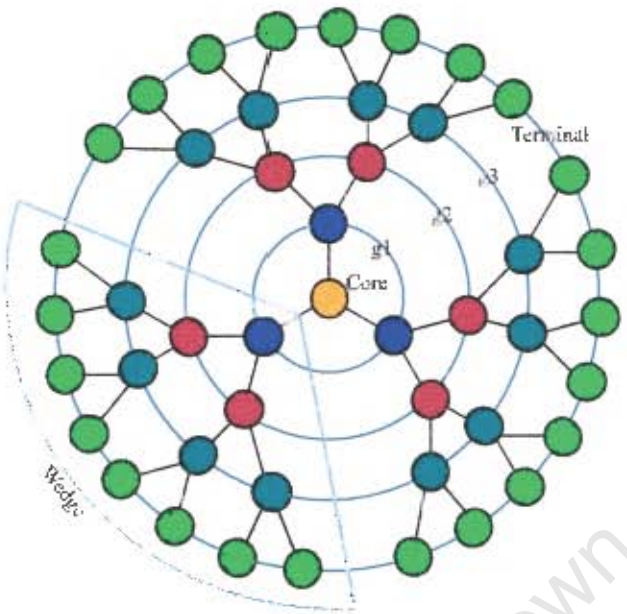

Figure 1.2: A schematic diagram of a third generation (G3) dendrimer, showing the core, topological layers (or internal generations) labelled g1, g2, g3 and terminal, and a wedge. We identify specific layers in lower case (g1 to g5), the whole dendrimer in upper case (G1 to G5) while wedges are prefixed with a "W" (WG1-WG5).

a *spacer*. The outermost layer contains a large number of *terminal groups*, which are also known as leaves or surface groups. A *dendritic wedge* is a single branch of a dendrimer and does not contain the core group.[1] The size of a dendrimer is denoted by its *generation*, or how many topological layers it comprises. In this thesis, the size of a dendrimer is specified in upper case (i.e., G1 to G5) while wedges are prefixed with a "W" (i.e., WG1 to WG5). However, there is some inconsistency in literature over the naming convention; in some cases the terminal layer is included when referring to the size of a dendrimer, while other instances the terminal layer is excluded. For example, a dendrimer containing only a single terminal layer attached to the core may be referred to as generation zero (G0) or generation one (G1), depending on the convention applied. We adopt the former convention, where the generation of the dendrimer refers to the number of internal layers. Here, the number of layers excludes the *terminal layer*, which is the outer most layer of the dendrimer. The *preterminal layer* is the parent layer of the terminal layer. An *internal layer* refers to any topological layer other than the terminal layer. Finally, *Backfolding*

[1] Wedges are often referred to in literature as dendrimers, which is a common source of confusion.

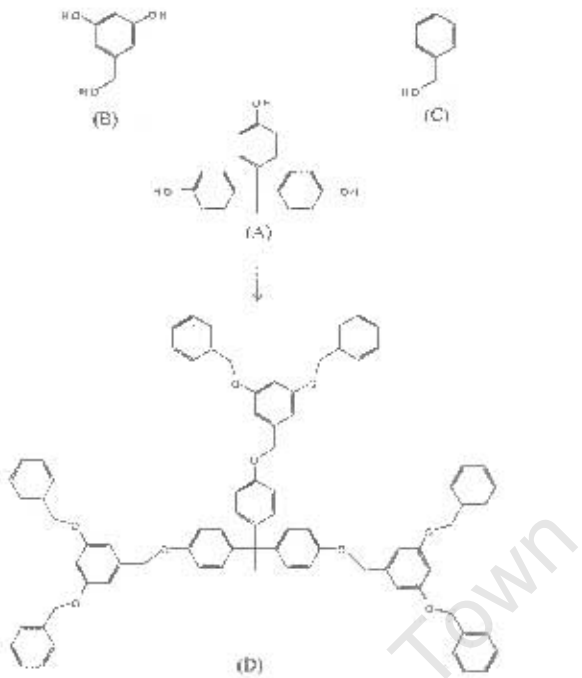

Figure 1.3: The three distinct chemical units making up a Fréchet dendrimer (D): (A) the core, (B) the repeat unit and (C) the terminal group [2]

refers to the terminal groups folding back in toward the focal point of the dendrimer, resulting in the terminal groups being dispersed throughout the dendrimer.

There are countless varieties of dendrimers available (see Section 1.2 for a review of dendrimer synthesis and design). The most popular dendrimers include variations of the polyamidoamine (PAMAM), [3] poly (aryl ether) (Fréchet or poly(benzyl phenyl ether)-PBPE), [4] polypropyleneimine [5] (PPI, POPAM or DAB) and carbosilane [6] dendrimers. In this thesis, we investigate a series of Fréchet dendrimers, generations one (G1) to five (G5). Fréchet dendrimers comprise three distinct chemical units: the core molecule, 1,1,1-tris(4-hydroxyphenyl)-ethane (Figure 1.3(A)); the main repeat-unit, 3,5-dihydroxybenzyl alcohol (Figure 1.3(B)); the terminal functionality, benzyl alcohol (Figure 1.3(C)). Figure 1.4 illustrates a WG4 Fréchet dendritic wedge and its linear isomer. [7]

Fréchet dendrimers were selected for this work for several reasons. Firstly, Fréchet dendrimers are readily synthesised, stable and are used in a wide variety of applications. [8] Secondly, due to the relatively large size of its repeat units, the collective steric effects of these groups will be appreciable for smaller dendrimers compared to dendrimer series with monomers consisting of single atom chains such as the PPI, carbosilane and PAMAM dendrimer families. Thus, the theoretical limiting generation [9] (beyond which idealised

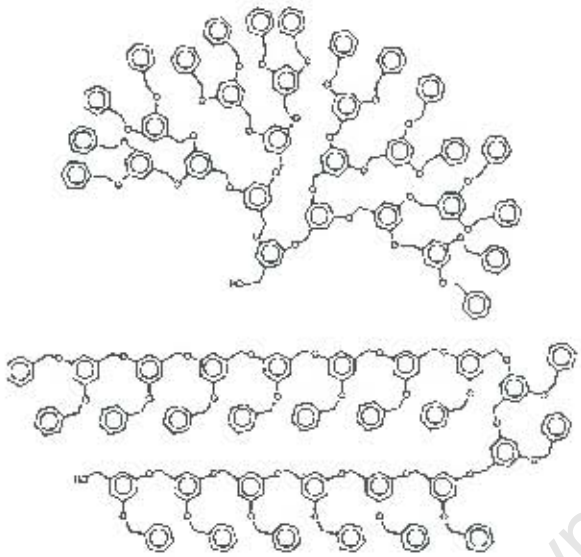

Figure 1.4: The fourth generation Fréchet dendritic wedge (WG4) and its linear isomer. [7]

perfect dendritic growth is no longer sterically possible) of Fréchet dendrimers is likely to be smaller than those of other popular dendritic systems. Hence, a smaller series of dendrimers (G1 to G5) are necessary to generate reliable trends for dendrimers. Thirdly, there are a number of experimental reports (Section 1.4 for details) and some vacuum computational simulations (Section 1.3) of Fréchet dendrimers in the literature. Finally, a force field has been developed in our laboratory specifically to describe Fréchet dendrimers, to investigate the use of these dendrimers as catalytic supports. [2, 10]

Computer simulations can offer unique insights into the structural and dynamical properties of dendrimers and provide a mechanism to study the atomistic details of these polymers in a manner analogous to a powerful microscope. While computer simulations of dendrimers have been conducted in vacuum, only a few studies have been reported for explicitly solvated systems. No studies have been reported in literature of a series of dendrimers simulated in the condense phase with an explicit solvent on a timescale of several nanoseconds.

To place dendrimers in context, in the following section we present a review of methodologies employed in dendrimer design and synthesis, and practical applications where dendrimers have been employed. In Sections 1.3 and 1.4, we review the theoretical and experimental studies of dendrimers presented in literature.

1.2 Dendrimer synthesis, design and application

Dendrimers have caught the attention of researchers since they were first discovered over 25 years ago. [11] The intense interest in dendrimers has been spawned not merely by academic curiosity but also by the industrial sector because of the extraordinary diverse areas where dendrimers have found application. These range from medicinal purposes, such as antiviral agents [12] and drug delivery systems, [1] to light harvesting devices [13] and recoverable catalytic supports [14]. The diverse uses for dendrimers is a result of the enormous variety of dendrimers currently available, yet all dendrimers are synthesised through one of two main synthetic strategies: divergent and convergent approaches.

In the divergent approach, the dendrimer is grown from the core outwards in an iterative synthetic procedure comprising activation and coupling steps, of which a simplified version is illustrated in the schematic diagram in Figure 1.5. This synthetic route was the first approach used to synthesize dendrimers and during the 1980's, virtually all the dendritic polymers were produced in this way. [15] For a number of industrial manufacturers of dendrimers, the divergent route is the preferred commercial synthetic pathway. [15] However, the difficulty of this approach is that it is imperative to ensure that each layer of the dendrimer is completely functionalized before adding further layers. As the number of functional groups increases exponentially with each layer, so too does the probability of incomplete functionalization or side reactions occurring increase exponentially. [16] Thus, at higher generations when the periphery becomes congested, the dendrimer can contain an appreciable number of structural flaws. Further, there is the added difficulty of removing imperfect dendrimers as they are very similar to the intended product. [16] PAMAM, carbosilane and PPI dendrimers are most commonly synthesized using this approach. [8]

In the convergent synthetic route, pioneered by Fréchet and co-workers, [4] the opposite approach is taken - the dendrimer is grown from what will eventually be the periphery, in towards the core (Figure 1.6). The terminal groups are coupled to each branch of a branch monomer to form a first generation wedge. These wedges may either be added to the core, or themselves added to the branch monomer to produce a second generation wedge. The process is repeated until the desired size wedges have been synthesised. Thereafter, the wedges are coordinated with the core group to produce a complete dendrimer. This process also involves activation and coupling steps for each layer of dendrimer. A simplified schematic diagram illustrating the convergent synthetic approach is shown in Figure 1.6. The advantage of the convergent synthetic route is that it is possible to separate a purer

product with less synthetic flaws as the differences between the perfect dendrimer and the reactants and any side products is substantial. Further, the synthetic versatility of this process makes it readily possible to introduce unique structural variations into the dendrimer, even to a single monomer unit. [16] Some of the possible structural variations from the typical dendrimer are illustrated in Figure 1.8. The disadvantage of this synthetic route compared with the divergent synthetic pathway is that as the size of the dendrimer increases, the difficulty of coordinating the wedge to the core increases exponentially due to steric inhibition. [16] The most common dendrimers synthesized using this approach are the Fréchet-type PBPE dendrimers and variations of these including poly(phenylene), poly(alkyl ester), poly(aryl alkene), and poly(alkyl ether) dendrimers. [16] The polyether dendrimers are currently the only dendrimers that are commercially available on the same scale as the dendrimers produced using the divergent methodology. [16]

There are other synthetic routes that do not fall exactly into either of the two classical approaches. An example for Fréchet-type dendrimers was developed by Hecht and Fréchet (Figure 1.8). [17] They devised a method to synthesize a six wedged poly aryl dendrimer with a fully substituted benzene core. They connect two wedges via an acetylenic moiety and then through a [2 + 2 + 2] cycloaddition process, three of these double sided wedges form a central benzene core. The advantage over alternative synthetic routes is that this approach results in an extremely clean reaction, with no partially reacted products due to the nature of the cycloaddition reaction. However, the disadvantage of this approach is that the steric crowding around the nascent core makes the reaction more difficult for larger generations.

Early attempts to functionalize dendrimers for specific uses or to enable a desirable characteristic or property were focused on the uniform derivitisation of the periphery of the dendrimer. With advances in the synthesis of dendrimers enabling rapid selective chemical transformations to tailor dendrimers to specific structural characteristics (such as those illustrated in Figure 1.8), all regions of the dendrimer have become potential targets for the synthetic chemist. In general there are three main targets: the surface, the interior and the core. A functionalised periphery is popular for recoverable catalytic supports, [14] light harvesting applications, [13] redox sensors [18] and mimics for biological molecules [19] among many others. When the core is the focus of attention, it can either be an active group, such as a metalloporhyrin catalyst [20] or biological mimic, [21] or comprise host capable features such as cyclophane cores. [21] The core can also be completely removed

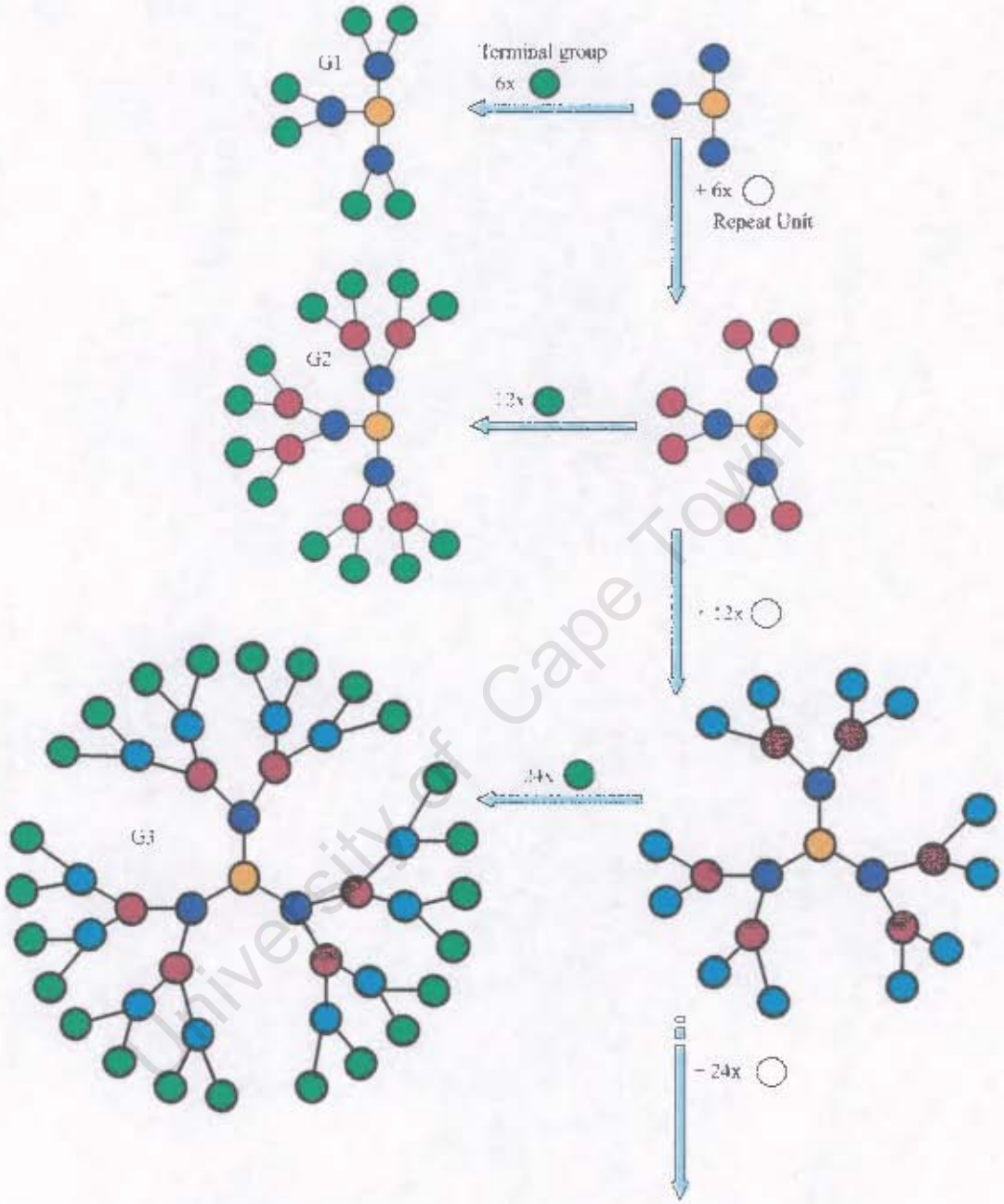

Figure 1.5: A schematic diagram of the *divergent method* to construct dendritic macromolecules in which the synthesis begins from a polyfunctional core and continues radially outwards by a successive stepwise process. The different colours represent various topological layers that result (yellow = core, red = g1, blue = g2, cyan = g3, green = terminal layer)

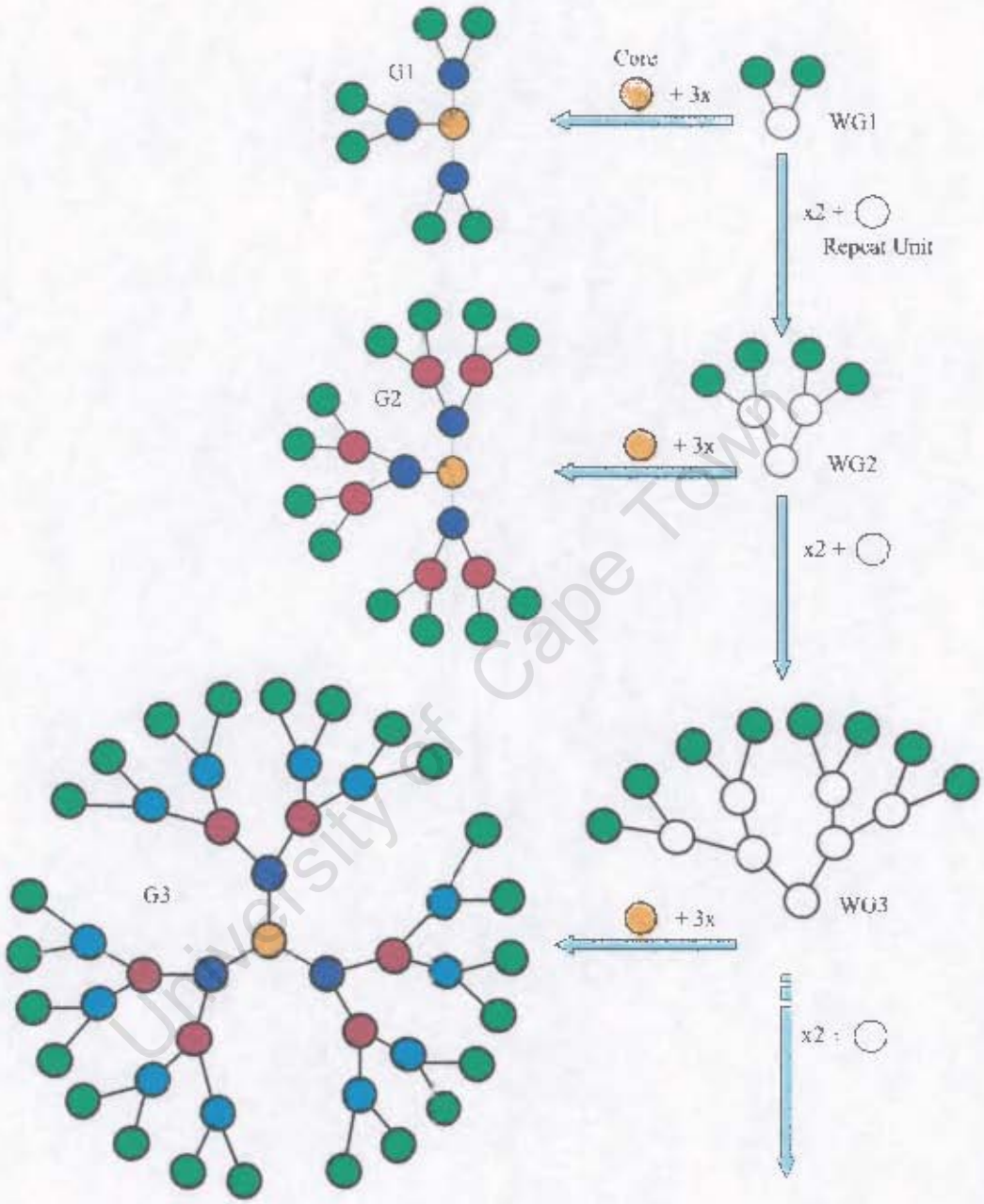

Figure 1.6: A schematic diagram of the *convergent method* to construct dendritic macromolecules in which the synthesis begins at what will be the periphery of the final macromolecule and proceeds inwards. The different colours represent various topological layers that result (yellow = core, red = g1, blue = g2, cyan = g3, green = terminal layer) [15]

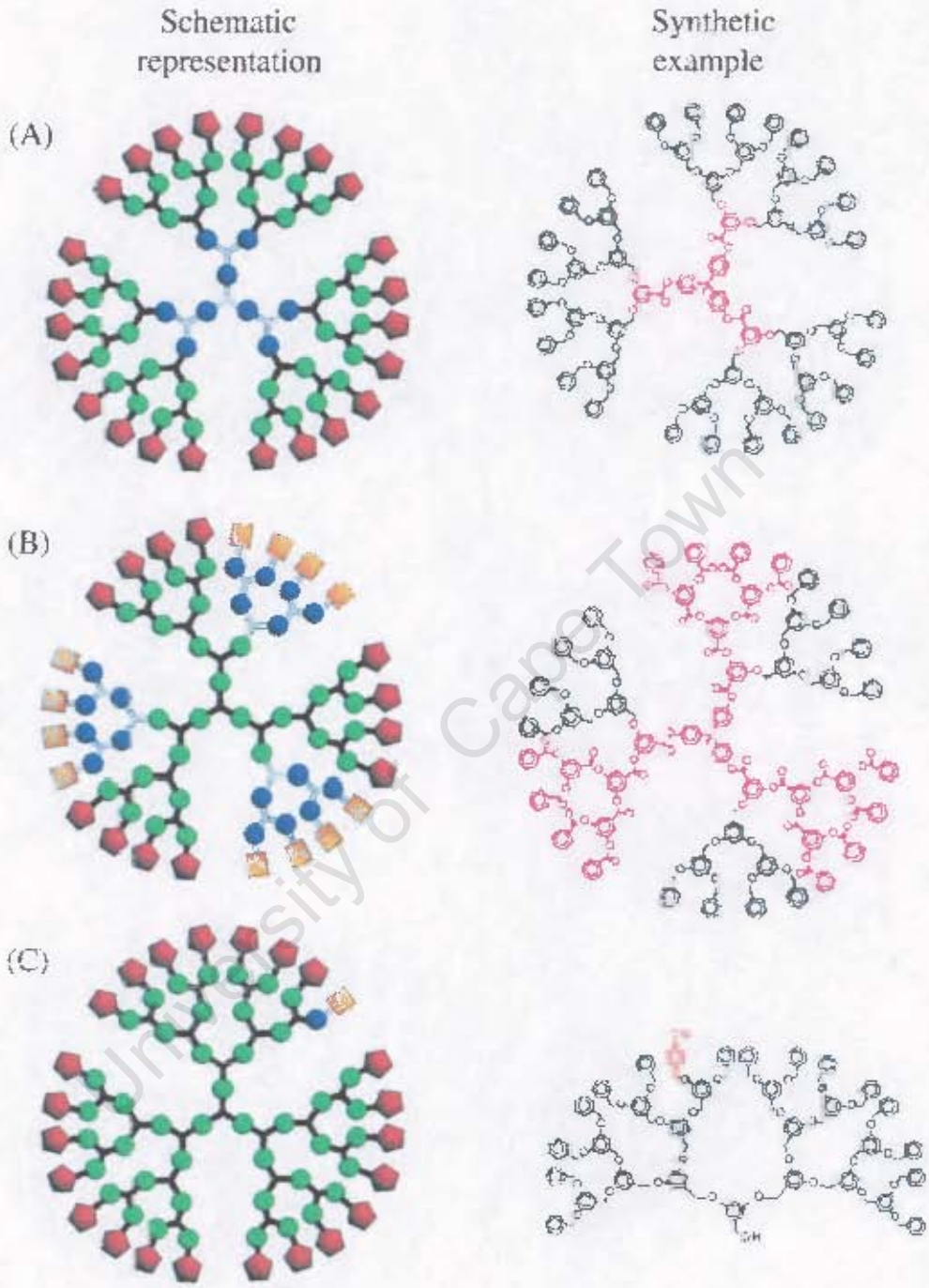

Figure 1.7: Schematic diagram of some of the possible synthetic modifications to dendrimers including (A)layered (B) segmented and (C) tailored dendrimers. Actual synthetic examples are also included [16]

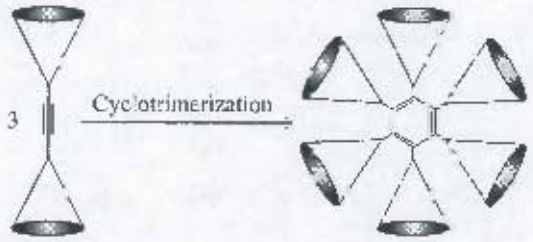

Figure 1.8: Cyclotrimerization of wedge-functionalized alkynes devised by Hecht et al. to produced Fréchet-like dendrimer with a fully functionalised benzene core. [17]

from the dendrimer, or "cored", to enhance its properties for drug delivery, recognition systems and catalysis. [22] Because there are cavities within the dendrimer, the internal generations can also be functionalised. [23] The advantage of functionalizing the interior of the dendrimer is that the exterior of the dendrimer may form a protective layer isolating the core or interior from the surrounding reaction medium, such as for oxygen sensitive catalysts in water soluble dendrimers where the exterior is hydrophilic and the interior is hydrophobic. [19] In medicinal applications, this hydrophilic exterior and hydrophobic interior can help delivery and adsorption of hydrophobic drugs. [19]

1.3 Theoretical studies

Since the synthesis of the first dendrimer was reported in literature, the fractal structure of dendrimers has fascinated theoretical chemists. The pioneering theoretical study was performed by de Gennes and Hervet. [9] They employed a modified version of the self-consistent field (SCF) method to investigate the limiting conditions beyond which perfect dendritic growth was no longer possible. Although de Gennes and Hervet showed that the limit to perfect fractal growth was a function of the spacer length between the trifunctional monomers of the dendrimer, the density profile indicating a global minimum at the centre of the dendrimer drew the most attention. This density profile became known as "hollow core" or "dense shell" and was a result of the assumption that each successive layer of monomers of the dendrimer occupied a concentric shell. The possible applications of dendrimers as delivery agents where smaller guest molecules are hosted within cavities of the dendrimer or as molecular scaffold on which functional groups such as homogenous catalysts were attached, sparked some excitement. However, atomic-level force field MD simulations performed by Naylor and co-workers indicated no evidence to support the

concentric shell assumption of De Gennes and Hervet. [24] Shortly thereafter, further doubt was thrown on this assumption by Lescanec and Muthukumar, employing a self-avoiding walk algorithm to kinetically grow bead model dendrimers. [25] The authors showed that the end groups traversed the entire molecule and were not confined to the surface as assumed by de Gennes and Hervet. This was the first evidence of "backfolding" observed in dendrimers and the decrease in density from the core to the periphery became known as the "dense core" model. However, as this study did not include any atomic detail, or solvent effects or dynamics of any sort, it was doubtful that the conformations of the bead dendrimers derived by Lescanec and Muthukumar were a realistic representation of the equilibrium conformation of dendrimers in solution. As a result of these early studies, the debate on dendrimer structure was born. The discussion has centred around the influence of the architecture and solvent quality on the size and shape of the dendrimer, the dynamics of dendrimers in solution and their physical properties.

In the years following these pioneering studies, there was an explosion in the number of theoretical and computational studies of dendrimers, with ever increasing complexity and detail. The theoretical studies can be loosely divided into two groups: those employing atomic-level molecular mechanics force fields (such as Naylor and co-workers' study) and those employing monomer-level, coarse grain or bead models (such as Lescanec and Muthukumar's study). The number of studies employing bead models to represent the dendrimer reported in literature are approximately three fold greater than the number of atomic-level studies of dendrimers. This is primarily due to the computational expense of atomic-level simulations. An advantage of coarse grain models is that the results are described in terms of dendrimers in general that have similar molecular architecture (for example the degree of branching) while the atomistic simulations are specific to only that type of dendrimer and the results are not transferable to other dendrimers. Further, when comparing with SANS data, course-grained models are adequate as SANS does not have atomistic resolution. [26] An additional advantage of implementing bead models, is that if it is assumed that the beads adequately represent the monomer constituents of the dendrimer, more complex problems may be investigated which would be computationally too expensive to study if atomic-level details were considered. For example, the first extensive atomic-level simulations following those of Naylor et al., were reported in 1998 by Smith and Gorman, [27] and Cavallo and Fraternali, [28] and Scherrenberg and co-workers. [29] During the same period, there were over five times as many reports

in literature of monomer-based dendrimer models. Topics included, the hydrodynamic properties of dendrimers by Mansfield and Klushin among others, [30–34] the conformation of dendrimers, including the calculation of structure factors [35] and analysis of the "dense core" and "dense shell" models by numerical methods [36, 37] and Monte Carlo simulations. [38–43] In addition, pioneering work was done to determine the effect of the quality and ionic strength of the solvent on the conformation of the dendrimer, performed by Murat and Grest [44] and Welch and Muthukumar respectively. [45] As a result of these studies, a picture of the structure of dendrimers began to emerge which favoured the "dense core" model, in particular that the end groups were located throughout the volume of the dendrimer. [21]

However, there was evidence suggesting that the first few internal generations of the dendrimer were extended and constrained to specific regions, particularly from the simulations that attempted to account for solvents effects. [38, 44] Employing a continuum solvent model, Murat and Grest concluded that the solvent quality had only a limited effect on the conformation of the dendrimer. [44] They reported that the density profile of dendrimers at all solvent conditions exhibit high-density near the core. An increase in solvent quality reduced the extent to which the layers of the dendrimer overlap. At the same time, Boris and Rubinstein employed a self-consistent mean field model (which they assumed to be within the good solvent limit) to verify the Flory theory predictions and to determine the density profile within a dendrimer. [37] They concluded that the density decreases monotonically from the core of the dendrimer to its periphery. Later, Welch and Muthukumar showed, by employing a Debye-Hückel potential to approximate the ionic strength of the solvent, that they were able to dramatically change the conformation of a dendrimer from "hollow shell" to "dense core", and the vice versa, depending on the concentration of the salt (Figure 1.9). [45] Atomic-level simulations around this time were consistent with the findings of Murat and Grest and with the bead model simulations, that the terminal groups exhibited a substantial degree of backfolding. [2, 27–29, 46] However, Smith et al. showed that the flexibility of the repeat unit could have a significant impact on the conformation of the dendrimer (degree to which the dendrimer is extended). Further, Mazo et al. and Scherrenberg et al. reported for different dendrimer systems, that the distribution of the density plateau within the dendrimer and the amount of backfolding was decreased with an increase in the solvent quality. [29, 46]

More recently, monomer-level simulations have continued to be at the forefront of

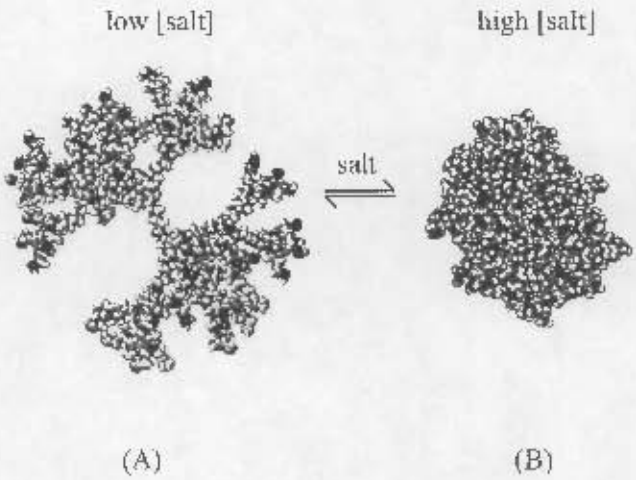

Figure 1.9: The effect of the salt concentration on the conformation of dendrimers as documented by Welch and Muthukumar. [45] (A) "Hollow core" or "dense shell" model and (B) "dense core" model

dendrimer simulations. Of particularly interest to this thesis is the effect of solvent quality on the dynamics and structure of the dendrimer, including radii of hydration and gyration, radial density profiles, location of the terminal groups, and the flexibility and diffusion of dendrimers. [47–56] These simulations offered further support for the dense-core model with the terminal groups distributed throughout the volume of the polymer. This is even the case in an implicit "good solvent" environment. Varying the quality did not have the dramatic change in conformation as was observed by Welch and co-workers (Figure 1.9). Instead, the maximum in the density profile is shifted toward the periphery in a similar manner to that reported by Murat and Grest. However, in all these cases, the solvent is treated implicitly, except for Karatasos et al. who explicitly represented the solvent as beads. [50]

Despite the promising results from monomer-level simulations and their close correlation with experimental results, [57] there is a need to ensure that these models do in fact realistically represent the atomic details of the dendrimer. Recent advances in computer technology, especially the development of commodity-off-the-shelf Beowulf clusters, make large scale atomic simulations viable options. As a result, the number of atomistic simulations have grown since 1998 and now atomistic simulations are routinely employed for all the major types of dendrimers including PAMAM [58–65], PPI, [29,66–68] carbosilane, [46,61,69,70] glycodendrimers [71,72] and Fréchet dendrimers. [27,73–77]

The first atomistic simulations of Fréchet dendrimers were reported by Smith and Gorman. [27, 73] They investigated the effect of the flexibility of the repeat unit, or the conformational flexibility of the dendrimer, on the overall size and shape of the dendrimer. Smith et al. showed that the more rigid the repeat units were, the more the distribution of the terminal groups was shifted to the periphery of the dendrimer. They also showed that the interior of the dendrimer exhibits solid-like behaviour, while the terminal layer exhibits more liquid-like behaviour. Moreover, the authors illustrated that the requisite number of hyperbranches would bring the terminal groups in to the core. [73] Shortly after Smith et al.'s original paper, [27] Hughes et al. reported an extensive investigation of MD simulations of a series of organic and organometallic-terminated Fréchet dendrimers (G1 to G5) in vacuum. [10] Their aim was to investigate whether dendrimers were suitable catalytic supports. Hughes et al. showed from the time evolution of the radius of gyration in vacuum, the dendrimers fold rapidly (in the order of tens of picoseconds) and remain contracted for the duration of the simulation. Using radial distribution profiles, the authors showed that all the dendrimers adopted a "dense core" conformation. In addition, they suggested backfolding was equally prevalent in the organic and organochromium dendrimers in the smaller generations (G1 to G3), while in the larger generations (G4 and G5) the terminal groups of the organochromium terminal groups do not penetrate to the core as readily as the organic terminal groups. The authors concluded that despite the compact nature of the dendrimers, the terminal groups were readily accessible to act as catalysts in a chemical reaction. Ortiz and co-workers essentially repeated the simulations conducted by Hughes (G1 to G4), using the PCCF force field. This force field allows for electron delocalization in aromatic rings. [77–79] They observed similar radial distribution profiles to Hughes et al., although the average radii of gyration calculated by Ortiz et al. were slightly larger than those reported by Hughes et al. Ortiz et al. also reported significant back folding, especially in the larger generations. From donor/acceptor distances and Förster energy-transfer rates calculated as a function of dendrimer generation, Ortiz and co-workers demonstrated, among other points, that the wrapping of peripheral groups to the core of the dendrimer was comparatively rare.

Initial atomistic simulations of dendrimers either did not include solvent effects at all (based on the findings of Murat and Grest), [2, 61, 63, 76] or included extra intramolecular non-bonded repulsive force field parameters. [27, 29, 69, 73] More recently, atomistic simulations have begun to include explicit solvent models. These vary in complexity from

Lennard-Jones particles to simulate a CCl_4 solvent, [70] through solvent molecules comprising pseudo-atoms, [68] to all atom explicit solvent models, including SPC and TIP3P water models. [62,72,75] The most detailed study of explicitly solvated dendrimers to date was recently reported by Maiti et al. [65] This investigation comprised two parts: a series of Monte Carlo simulations of PAMAM dendrimers G1 to G11 in vacuum, followed by a second series of Monte Carlo simulations of PAMAM dendrimer G4 to G6 in explicit water. In the former study, the authors modelled the complete range of PAMAM dendrimers up to the limiting generation G11 (close to 300 000 atoms). In the later study, Maiti et al. investigated not only the effect of an explicit good solvent (water) on the conformation of these dendrimers, but also the effect of pH. They showed that the presence of water leads to significant swelling in the dendrimer and that this swelling could also be affected by the pH of the solution. Further, they reported significant backfolding of the terminal groups into the interior of the dendrimer. However, Maiti and co-workers also noted the interior of the dendrimer was relatively open, with cavities available for hosting guest molecules as solvent penetrated into the body of the dendrimers at all pHs.

Despite the growing number of computational studies of dendrimers, there has yet to be a study of MD (or MC) computer simulations of a series of explicitly solvated dendrimers on the order of several nanoseconds. In addition, the folding of dendrimers has not been thoroughly investigated. In the following section, a brief review of the experimental studies of the of dendrimers further emphasises the need for nanosecond MD simulations of explicitly solvated dendrimers.

1.4 Experimental studies of dendrimers

Soon after the pioneering theoretical work by de Gennes et al., Lescanec et al. and Naylor et al., the debate over the structure of dendrimers began to attract the attention of experimental chemists. However, it quickly became apparent that there were also experimental difficulties to overcome. The secondary and tertiary structural characteristics of dendrimers proved difficult to resolve as the size and fractal nature of dendrimers limited the success of methods such as X-ray crystallography (dendrimers are difficult to crystallise), and NMR (dendrimers are usually made up of identical repeat units which makes identifying specific areas of the dendrimer problematic). Therefore, other methods have been employed such as small angle neutron and X-ray scattering, chromatographic

techniques and atomic force microscopy along with viscosimetric and other rheological studies. Here we treat the experimental papers in two sections, those pertaining to the overall structure of the dendrimer (dense core vs. dense shell) and those pertaining to the unique hydrodynamic properties of dendrimers (Ball Bearing effect).

Dense core versus dense shell

The difficulties associated with crystallising dendrimers have meant that only a few first generation dendrimers have had their crystal structures resolved [80–84] while some higher generation wedges have also been crystallized (see Figure 1.10 for an example of a dendrimer crystal structure). [80] These X-ray structures showed multiple interactions between the different end groups of the dendrimer, suggesting a dense core arrangement. [81] This is not surprising as a dendrimer is composed of 50% of terminal groups. In addition, in the crystal environment there are no solvent molecules with which the dendrimer can interact.

However, the structural, chemical and physical properties of dendrimers in solution are of most interest, considering the fact that the majority of the current and foreseeable applications of dendrimers are in solution. Advanced multidimensional NMR techniques, such as total correlation spectroscopy (TOCSY) and nuclear Overhauser enhancement spectroscopy (NOESY) NMR, have had great success in macromolecular systems such as proteins. However, these techniques have only been sparingly applied to dendrimers. [85–87] Despite promising results showing the clear conformational changes in response to solvent type and the identification of specific nOe interactions between the PPI dendrimer and its guest molecule, these techniques require high-end NMR facilities, such as a 750 MHz spectrometer. Thus the hardware requirements make these experiments currently exotic rather than commonplace.

Therefore, alternative methods have been employed to resolve the structure of dendrimers. These include small-angle neutron- and X-ray scattering (SANS and SAXS respectively) on dendrimers in solution. [8, 57] Bauer et al. were the first to employ these techniques on solvated dendrimers [88] which were expanded later by, amongst others, Prosa et al., [89] Scherrenberg et al. [29], Ramzi et al., [90, 91] Pötschke et al. [92–94] and Ballauf et al. [57, 95] The accumulated scattering data heavily favours the "dense-core" model. It was recently claimed that the debate over dendrimer structure has been resolved and the "dense-core" model is the correct model for dendrimers. [57] However, as this conclusion was drawn from a comparison of scattering data on dendrimers in good

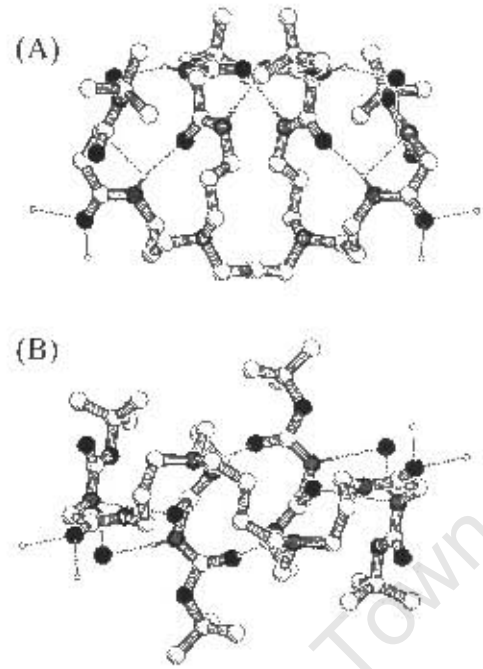

Figure 1.10: One of the few crystal structures available for dendrimers. This crystal structure is of a first generation *N*-t-BOC-glycine-functionalized dendrimer resolved by Bosman et al. [21] (A) Side and (B) top views as denoted by Bosman et al.

solvents with computer simulations of dendrimers in vacuum (i.e., a poor solvent) and in the light of the conflicting evidence presented here, we suggest that further investigation is still required.

However, not all measured data reflects the "dense core" model. Topp et al. showed in a SANS investigation of solvated PAMAM and PPI dendrimers, that the terminal groups were concentrated near the surface of the dendrimer. [96–98] Funayama et al. reported for PAMAM dendrimers in water that a layered model with water penetration gave the best fit with SANS data. [99] They reported a smaller segment density at the surface of the dendrimer although the segment chains were extended. Recently, Rosenfeldt and co-workers investigated the spatial dimensions of fully aromatic dendrimers which were incapable of backfolding because of the complete absence of flexible repeat units. [26] The authors concluded that the rigid dendrimer structure can best be described by the dense-shell model. However they also concluded that this was only possible for dendrimers that were made up of rigid repeat units and postulated that flexible dendrimers would exhibit dense-core structures.

In the NMR analysis of dendrimers, greater consistency between experimental mea-

surements has been achieved. NMR analysis of dendrimers began with a detailed study by Meltzer et al., of the proton and carbon relaxation parameters of PAMAM dendrimers, to investigate the mobility of the various layers of the dendrimer and their relationship to the size of the dendrimer. [100, 101] Meltzer et al. showed that there was a clear difference in the relaxation rates of the terminal groups in comparison with the relaxation rates of the internal layers; the spin-lattice relaxation times (T_1) of the terminal groups were longer than those of the internal generations. Further, the relaxation rates of the terminal groups were found to decrease with an increase in dendrimer size while the internal generations were independent of the size of the dendrimer. Similar trends are observed for a variety of types of dendrimers, in a variety of solvents. [17, 102–105] This includes investigations of the longitudinal relaxation rates for Fréchet and Fréchet-type dendrimers. [17, 102] Paramagnetic NMR atomic probes have also been employed to study the structure of dendrimers. [102, 106–110] Epperson et al. employed paramagnetic cobalt(II) complexes as external paramagnetic NMR probes to study the structure of PAMAM dendrimers. [110] They concluded that the dendrimers had a shell-like structure rather than a "dense-core" structure and that the dendrimers had sizeable cavities within the dendrimer capable of hosting guest molecules. Others have employed similar techniques, such as site-specific stable-isotope-labelling, rotational-echo double-resonance (REDOR) NMR measurements on Fréchet dendrimer wedges in the solid state. [108, 109] With the exception of the solid state measurements, all of these techniques pointed toward an extended conformation, i.e., the "dense-shell" model. Numerous pulsed field gradient spin echo (PFG SE) NMR measurements, including diffusion ordered 2D-NMR (DOSY) measurements, have been performed on a variety of dendrimers to further detail their hydrodynamic properties, in particular their diffusion coefficients and hydrodynamic radii. [105, 111–115] These included the study of diffusion of dendrimers under different pHs [112] and concentrations [114]. In these studies they showed that the dendrimer could adopt a closed or open conformation depending on environmental variables such as pH and concentration.

The "Ball Bearing" effect

Apart from the "dense core" versus "dense shell" debate, dendrimers exhibit curious hydrodynamic properties which have been documented for a variety of solvent-dendrimer systems. The so-called "Ball Bearing Effect" [116] of dendrimers is a characteristic trend

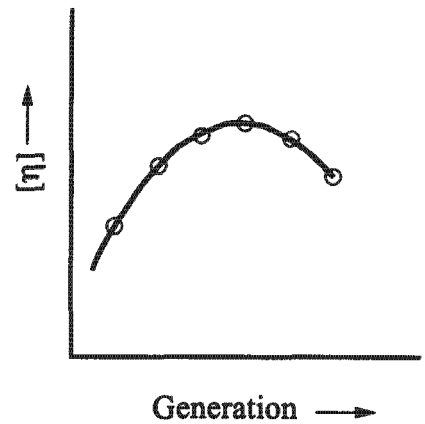

Figure 1.11: The classic "Ball Bearing Effect" - the dendrimer intrinsic viscosity increases up to a limiting generation where after it decreases

in the intrinsic viscosity, $[\eta]$.[2] Here, $[\eta]$ increases up to a limiting dendrimer size, where after $[\eta]$ decreases with an increase in the size of the dendrimer, as illustrated in Figure 1.11. Although the behaviour is clearly related to the size of the dendrimer, no conclusive explanation has been proposed that adequately accounts for the ball bearing phenomena. [116–118] However, this trend in viscosity, which is often referred to as a feature *unique* to dendrimers is in fact not unique to perfect dendrimers but also occurs in hyperbranched polymers, even for polymers with a very low degree of branching and randomly branched polymers. [32, 34, 119] Widmann and Davies showed that for high degrees of branching, a variety of hyperbranched polymers exhibited almost perfect dendrimer-type behaviour, while Aerts found similar results including polymers with low degrees of branching. Further, not all dendrimer-solvent combinations exhibit this trend. Scherrenberg and co-workers reported that viscosimetry measurements of PPI dendrimers did not produce a maximum in $[\eta]$ in water or in acetone. [29] Instead, the authors reported a plateau in $[\eta]$ for dendrimers G3 to G5.

Of most significance for this thesis are the studies of the hydrodynamic properties of Fréchet dendrimers. Mourey et al. published a detailed analysis of the intrinsic viscosity profiles of Fréchet dendrimers and dendritic wedges. [120] From viscosity detection in size exclusion chromatography, they noted a maximum in the intrinsic viscosity while the refractive index passed through a minimum at the same sized dendrimer. They concluded

[2] According to the IUPAC naming convention $[\eta]$ is formally referred to as the *reduced viscosity*. However, in literature $[\eta]$ is most commonly referred to as the *intrinsic viscosity*

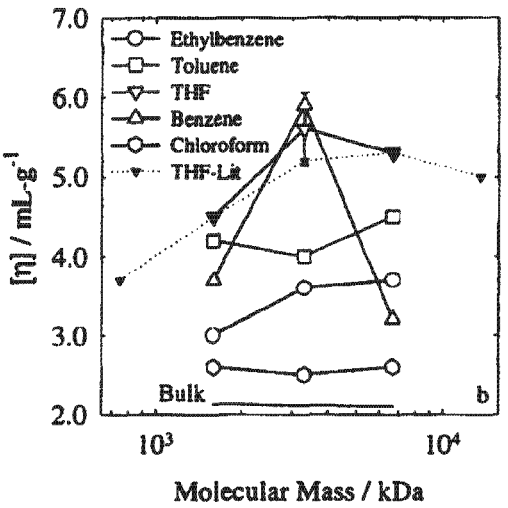

Figure 1.12: Intrinsic viscosity, $[\eta]$, for the Fréchet dendritic wedges WG3 to WG5 in various solvents at 30°C as a function of molecular mass as reported by Jeong et al. [118] The curve labelled THF-Lit represents data for Fréchet dendritic wedges WG2 to WG6 in THF reported by Mourey et al. [120]

that the dendrimers were extended to approximately two-thirds of the theoretical, fully extended length. Similar results were reported Jeong et al. [118, 121] From viscosimetric measurements of dendrimers, it has been suggested that this characteristic trend (or lack thereof) is an indicator of the degree of extension of the dendrimer, thereby affording a useful measure of the quality of the solvent for a dendrimer according to their solubility parameters. [118, 121, 122] However, Jeong et al. conducted measurements for dendritic wedges, generations WG3 to WG5 and excluded the wedges WG1 and WG2. [118] Although they observed a maximum in $[\eta]$ for wedges WG3 to WG5 in tetrahydrofuran (THF) and not in chloroform (Figure 1.12), this does not preclude an increase from generations WG1 to WG3 in chloroform, followed by a plateau from generations WG3 to WG5. This trend would be qualitatively similar to the trend observed for viscosimetric measurements of PPI dendrimers. [29, 123] Similarly, Matos et al. showed that for Fréchet-type dendrimers (the core of the dendrimer was a porphyrin ring), a maximum in $[\eta]$ in THF and dimethylformamide (DMF) was not always observed. [124] Most recently, Evmenenko and co-workers reported almost identical radii of gyration for Fréchet dendrimers in THF and toluene from SANS measurements, which is inconsistent with the trends in the radii of hydration derived from $[\eta]$ measurements. [118, 125] Therefore, this suggests that $[\eta]$

is more complicated than simply dependent on the folded state of the dendrimer. The conflicting experimental data highlights the need for computer simulations of explicitly solvated dendrimers as a means of resolving these issues.

However, returning briefly to the computational simulations, there are also inconsistencies in this literature. In all cases where $[\eta]$ have been calculated, the dendrimers were in their folded state with the majority of studies lacking any atomic detail altogether and several confined to sampling lattice conformations. An example is the study of Mansfield and Klushin. [30] Although their results compared favourably with measurements of PAMAM dendrimers, they implemented a bead model where the conformations were not equilibrium states but those calculated using the kinetic growth algorithm, detailed by Lescanec and Muthukumar. [25] However, Cai and Chen showed that a more rigorous version of Mansfield's calculations afford no maximum. [33] Later, Mansfield again investigated the transport properties of dendrimers, this time using a method analogous to electrical polarizability tensor. [126] Again the author found a maximum, however on this occasion at G6 ($[\eta] = 112.4$) compared with G4 ($[\eta] \simeq 4.5$) in the previous study. However, considering that the kinetic growth model and rigid lattice models simulations were analogous to a Θ solvent system (at best), it is somewhat surprising that the calculated results compared favourably with experimental results for dendrimers in *good* solvent systems.

1.5 Objectives

The debate over the structure of dendrimers has captured the interest of researchers world wide. The fact that the structure of dendrimers is still unclear a quarter of a century after the synthesis of the first dendrimer adds to the allure of the debate. Recently, there have been encouraging developments in computational simulations of dendrimers, especially in atomistic explicitly solvated systems. Yet due to the shear size of the simulations (number of atoms), these simulations have all been relatively short, in the order of several hundred picoseconds or less. It is unlikely that this is sufficient time for systems containing such large numbers of atoms to completely reach equilibrium. Therefore, the aim of this thesis is to investigate the equilibrium structure and dynamics of a series of dendrimers in a variety of explicit solvents.

Before commencing with such simulations, it is necessary to ensure that the force field employed is as accurate as possible. Therefore, as a precursor to the nanosecond solvated

simulations we develop a force field that not only accurately represents the solvent and the dendrimer separately, but as well as the interactions between the two.

Conducting the nanosecond simulations is a challenge in itself. However, the analysis of the simulation trajectory is where the real challenge lies. Traditional computational analytical methods such as time series analysis of the radius of gyration and moments of inertia, and radial average distribution functions have proved indispensable tools to describe the size, shape and distribution of a variety of properties of the dendrimer. In literature, there have been some attempts to visualise the simulated solvated dendrimer in three dimensions. While the results from these analytical methods proved interesting, the methods have not been readily adopted. A further aim of this thesis is to develop an analytical method which would allow easy visualisation of dendrimers in three dimensions using a spatially averaged distribution function commonly employed to study the structure of solvent about a solute carbohydrate molecule. This method is to be employed not only to gain a better understanding of the structure of the dendrimer in three dimensions but also to critically analyse the conclusions drawn from the two dimensional radially averaged methods. In particular, the qualitative descriptions "dense-core" and "dense-shell" are to be scrutinised.

The folding and unfolding of other polymers, particularly carbohydrates and proteins, is an area of active research. However, the folding of dendrimers has received relatively little attention. The final aim of this thesis is therefore to analyse the folding and unfolding dynamics of a dendrimer during nanosecond Molecular Dynamic simulations in explicitly poor and good solvents. A novel approach to exploring the free energy of folding of dendrimers is to calculate the first Potential of Mean Force (PMF), thereby quantifying the folding behaviour of a dendrimer in a variety of solvent environments. From the difference of the PMF of the dendrimer in vacuum and the explicit poor solvent, the aim is to quantitatively examine the effect of a poor solvent on the behaviour of a dendrimer in comparison with the behaviour of the dendrimer in vacuum.

1.6 Thesis overview

Chapter 2 contains a brief introduction of Molecular Mechanics and Molecular Dynamics simulations of dendrimers, with emphasis on force fields and simulation methods used in this thesis. The chapter closes with a description of the methods used to calculate the

Potential of Mean Force of model dendrimer systems, including the application of Adaptive Umbrella Sampling and the Weighted Histogram Analysis Method.

In Chapter 3, the analytical methods developed and employed in this thesis for condensed phase dendrimer simulations are outlined and discussed. The initial techniques detailed are those commonly employed during the analysis of dendrimer simulations, including radius of gyration, moments of inertia and radial distribution functions. Spatially averaged distributions functions follow, including the spatial distribution function developed during this work to describe the distribution of the groups of the layers of the dendrimer in three dimensions. This is followed by a description of Voronoi analysis for the geometrical description of solvent structure. The techniques used to analyse the dynamics of the system follow, starting with a brief overview of correlation functions followed by specific techniques employed in this thesis including diffusion coefficients, and rotational and longitudinal relaxation rates. This chapter closes with a brief description on the various methods available to calculate the intrinsic viscosity of dendrimers from simulations. Chapters 2 and 3, may be omitted by readers familiar with these techniques.

Chapter 4 sets the foundation of the simulation work in this thesis. In this chapter the development of a solution force field to accurately simulate dendrimers in the condense phase is described. Four solvent environments were employed in this thesis; vacuum, water, THF and chloroform. (The TIP3P water model, developed by Jorgensen et al. was the water model of choice and is described in Chapter 2.) The development of a new, relaxed all-atom chloroform model is detailed, along with a comparison of the structural characteristics of the THF solvent employing Girard and Müller-Plathe's modified Helfrich-Hentschke united atom THF model. [127] This includes radial and spatial distribution functions and Voronoi analysis as described in Chapter 3. Thereafter, analysis and modification of ether linkage dihedral angle of Hughes et al.'s force field for Fréchet dendrimers is discussed. Further validation of the solution force field is provided through an analysis of the combination of the dendrimer and solvent force fields, and of possible factors that could contribute to inaccuracies in the simulation.

Chapter 5 reports the nanosecond Molecular Dynamics simulations of Fréchet dendrimers, G1 to G5, in THF and chloroform. A comparison is drawn with the vacuum Molecular Dynamics simulations of Hughes et al. where appropriate. The application of the analytical methods detailed in Chapter 3 is presented with specific emphasis on any difference between the dendrimers in THF and chloroform. A discussion of the difficulties

associated with radial averaged analytical methods, particularly radial density distribution functions, is presented. This discussion includes an analysis of the use of the terms "dense core" and "dense shell" to qualitatively discuss the density distribution about the dendrimer. The size, shape and structure of the dendrimer is described by employing the spatially averaged distribution functions to detail the overall size and shape of the dendrimer along with the internal layers of the dendrimer. The final section involves an analysis of the dynamics of the dendrimer, including diffusion coefficients of the dendrimer, intrinsic viscosity profiles, the diffusion of the layers of the dendrimer and finally, longitudinal relaxation rates calculated from the simulations are presented in comparison with available experimental data.

Chapter 6 addresses the folding dynamics of dendrimers using qualitative analysis followed by quantitative PMF calculations. First the overall folding of Fréchet dendrimers in water are compared with the unfolding of these dendrimers in chloroform. This is followed by a report of the calculation of the potential of mean force of folding for model dendritic units, to probe the folding back of a terminal group one and two generations deep. Particular focus is placed on the difference between the water and vacuum systems, and the between the THF and chloroform systems.

Finally, Chapter 7 contains conclusions and suggests future avenues of investigation.

Chapter 2

Methods for Force Field Simulations

2.1 Introduction

The experimental determination of the secondary and tertiary structure of dendrimers (the relative orientation and position of linked monomers and the large-scale overall folding of the dendrimer respectively) has proved challenging. As a result of their starburst hyperbranched structure, dendrimers are extremely difficult to crystallise. To date, knowledge of their structure is speculative, with only a limited number of crystal structures available for a few first generation dendrimers. [80] The use of spectroscopic techniques has also only achieved limited success because only the average detail for each layer of the dendrimer can be determined. This is true even if molecular probes are employed, such as those used by Gorman et al. [102]

Therefore, computational methods can offer unique insights into this problem. Computer simulations provide the mechanism for a detailed study of these polymers analogous to a powerful microscope. However, before any computational study is undertaken, it is essential to understand the complexities of the molecular simulation. Further, one must ensure that any simplifications made are valid and identify any underlying assumptions. It is also important to be aware of the effects that these assumptions and simplifications may have on the simulation results.

In this thesis, force field computational methods are employed. In general these methods encompass Molecular Mechanics (MM) and Molecular Dynamics (MD) simulations.

Here the energy calculations are simplified by ignoring electronic motions and the energy of the system is a function of nuclear coordinates only, using a classical "ball-and-spring" model for atomic interactions. Despite their apparent simplicity, suitable force field models can provide answers that are as accurate as high low-level quantum mechanical (QM) calculations at a fraction of calculation time and are thus an efficient and appropriate choice for complex systems. [128] This is clearly advantageous as nanosecond QM MD simulations are at present beyond the capability of the most advanced supercomputers and empirical MD or Monte Carlo (MC) simulations are the only viable option for simulations of nanosecond (or greater) time scales. MD has the advantage over MC in that MD provides a time evolution of molecular interactions and conformational changes, while MC methods generate time-unrelated configurations based on random changes to the system. Therefore, MD is the sampling method employed in this thesis.

Molecular force field simulations are ever growing in popularity and there is a wide variety of software packages available for simulating solvated polymeric systems. Among some of the most popular academic packages are GROMOS, [129] AMBER, [130] DL_POLY, [131] NAMD, [132] and CHARMM. [133] CHARMM is the simulation package used in this thesis.

This chapter provides a brief overview of Molecular Mechanics and Dynamics simulation methods and their application to the study of dendrimers, focusing on techniques used in this thesis. The chapter closes with a discussion on the statistical mechanics associated with computer simulations of solvated polymeric systems, followed by a discussion of non-Boltzmann Molecular Dynamics for free energy calculations. For a broader treatment the reader is referred to the general texts on molecular modelling, such as those by Allen and Tildesley, [134] Leach [128] and Haile. [135]

2.2 Molecular Dynamics Simulations

The Born-Oppenheimer approximation assumes that the motion of the atomic nuclei is so much slower than the electrons that the electronic contribution to the energy can be integrated out as a function of nuclear coordinates. As a result, the kinetic energy of the system can be described in terms of simpler classical behaviour. In MD simulations, the motions of the atoms are described using Hamiltonian dynamics (Equation (2.1)) which has an advantage over Newtonian dynamics, since this formalism does not have an explicit

dependence on the applied forces.

$$H(r^N, p^N) = \frac{1}{2}\sum_i \frac{1}{m_i} p_i{}^2 + U(r^N) = E \tag{2.1}$$

The Hamiltonian is expressed as a function of the position (r^N) and momentum (p^N) of all N atoms in the molecular system. The first term refers to the kinetic energy of the system where m_i and p_i refer to the mass and momentum of the i^{th} atom respectively, while $U(r^N)$ refers to the potential energy as function of all N atomic positions. The classical equations of motion are integrated with respect to time, from which it is possible to obtain the time evolution of the molecular system. However, since the motions of all the particles in the system are interrelated, the resulting many-body problem does not have a true analytical solution. Therefore, integration using finite difference methods is required. There are several integration methods, for example Verlet, [136] Leap Frog, [137] Velocity Verlet, [138] Beeman [139] and Gear Predictor-Corrector. [140] In all the integration methods, the position and dynamic properties of the particles are represented using a truncated Taylor series expansion. Low order expansion algorithms, such as the Verlet [136] (and related algorithms) are generally used for long duration simulations. The more accurate but computationally more expensive higher-order expansion Predictor-Corrector methods are usually used for short duration simulations, typically in implementation of Nosé-Hoover thermostats. [141, 142]

In this thesis, the Leap-Frog integrator [137] (which is a variation of the Verlet algorithm) is used to integrate the equations of motion. In the Leap-Frog method, the velocities (μ) are calculated at $\frac{1}{2}\delta t$ as follows

$$r(t + \delta t) = r(t) + \delta t \mu(t + \frac{1}{2}\delta t) \tag{2.2}$$

$$\mu(t + \frac{1}{2}\delta t) = \mu(t - \frac{1}{2}\delta t) + \delta t a(t) \tag{2.3}$$

Hence the positions (r) are calculated at integral values of the time step δt, while the velocities "leap-frog" over at $\frac{1}{2}\delta t$ intervals. The Leap-frog method avoids floating point arithmetic errors which are inherent in the Verlet algorithm because it avoids the calculation of the $\delta t^2 a(t)$ term.

The choice of the integration time step size is also of importance. If the time step is too large (typically greater than 10fs for all-atom MD) instabilities in the calculation can occur.

A typical consequence is a gradual decrease in energy computed for the system. Ideally, the time step should be as small as possible. However, the smaller the time step, the longer the required simulation time. To allow for valid use of larger integration time steps, intramolecular bonds involving hydrogen atoms are constrained, since such interactions have high vibrational frequencies. Care must be taken to ensure that the convergence tolerance for the constraint algorithm is small enough to ensure that fluctuations in the simulation are larger than any constrained fluctuations. In the current work the SHAKE algorithm was used for constraining atoms. [143]

2.2.1 Molecular Mechanical Force Fields

There are numerous methods for describing the potential energy term ($U(r^N)$) of the Hamiltonian in Equation (2.1). Currently, the most sophisticated method is the quantum mechanical *ab initio* molecular dynamics method developed by Car and Parrinello. [144] However, this is computationally expensive and *ab initio* MD simulations have only been used to study small clusters of molecules, for periods of only a few picoseconds. [145] This is not sufficient for study of relaxation processes that take place on a time scale of several hundred picoseconds, or the microsecond relaxation times typical to NMR. An alternative method to include a quantum mechanical description into the model is a hybrid QM/MM approach where only a small section of the molecular system is described quantum mechanically (such as the active site in an enzyme) while the rest of the molecule is described with an empirical MM model.

Fortunately, in most cases a quantum mechanical description of the molecular system is not required. A relatively simple empirical MM model is adequate for systems where electronic effects are negligible, which is the case when there is no rearrangement of covalent bounds in the molecular system. In MM the electrons of a molecule are described as an average potential field which is a function of the nuclear coordinates: the bonds between atoms are described as simple harmonic springs, with spring constants parameterized from either vibrational spectroscopy or *ab initio* calculations.

There are several approaches for describing bonded interactions between atoms in MM force fields (FF), ranging from simple harmonic descriptors such as Hooke's law to the more complex Morse potential. Additional quadratic and cubic terms may be added to the harmonic descriptors to afford realistic behaviour. However, the greater the complexity of the potential functions, the greater the penalty in calculation time.

A variety of force fields have been used in computer simulations of dendrimers, including CHARMM, [133] AMBER, [130] MM3, [146] and CVFF [147]. In this thesis we employ a CHARMM-like force field (Equation (2.4)). [133] The development of the force field used to describe the dendrimers in this thesis is discussed in Chapter 4. The CHARMM force field takes the form:

$$\begin{aligned}\mathcal{V}(\mathbf{r}_i \ldots \mathbf{r}_N) = & \sum_{\text{bonds}} k_b(r - r_0)^2 + \sum_{\text{angles}} k_\theta(\theta - \theta_0)^2 \\ & + \sum_{\text{dihe}} k_\phi(1 + \cos(n\phi - \delta)), \text{where } n = 1, 2, 3, 4, 6 \\ & + \sum_{\text{impr dihe}} k_\omega(\omega - \omega_0)^2 \\ & + \sum_{\text{pairs}(i,j)} \left(\epsilon_{ij} \left[-\left(\frac{R_{min(ij)}}{r_{ij}} \right)^6 + \left(\frac{R_{min(ij)}}{r_{ij}} \right)^{12} \right] + \frac{q_i q_j}{\epsilon_l r_{ij}} \right)\end{aligned} \tag{2.4}$$

The first four terms describe local bonded interactions for bond and angle stretching and torsional rotation. Here k_b, k_θ, k_ϕ and k_ω are the bond, angle, torsional and improper torsional force constants respectively; r_0, θ_0, ϕ and ω are the equilibrium bond, angle, torsion angle and improper torsion angel equilibrium values respectively and n and δ are the multiplicity and phase angle respectively. These deformations are assumed to be at ordinary temperatures and in the absence of chemical reactions. The bond stretching and bond angle bending terms are described by Hooke's law. Torsional interactions are described using a simple cosine series expansion, while interactions involving improper torsion angles (used to fix atoms in a plane) are described in the form of a quadratic expression, analogous to the angle descriptor. In rigid force fields, the bond lengths and angles are held fixed at their equilibrium values. This simplification allows for longer simulation times as the calculations for changes in the bond lengths and angles are excluded from Equation 2.4.

It is important to note that in the CHARMM force field, there are no cross terms coupling the internal coordinates. As a consequence, bond stretching interactions, for example, do not explicitly affect the bond angle bending or torsional interactions and vice versa.

The remaining terms are the non-bonded or "through space" interactions. In CHARMM, the 6-12 Lennard-Jones potential is used to describe the van der Waals interactions. One of the advantages of the Lennard-Jones potential is its simplicity. It requires only two pa-

rameters, namely the well depth of the minimum interaction energy, ε_{ij}, and the collision diameter, σ_{ij} between atoms i and j where $E_{elec} = 0$. σ_{ij} is related to the position of the energy minimum, $R_{min(ij)}$ by $2^{1/6}\sigma$. Further, a substantial reduction in computational expense is obtained because the r^{-12} repulsive term can be calculated by squaring the attractive r^{-6} term and the r^{-6} term can be calculated directly from the distance without requiring a computationally expensive square root calculation. [128] Electrostatic interactions are modelled using Coulomb's Law. The terms ε_{ij}, $R_{min(ij)}$, r_{ij} and ϵ_l refer to the Lennard-Jones well depth, the minimum interaction radius for atoms i and j, the distance between atoms i and j and the dielectric constant respectively.

Atomic Detail of the Force Fields

Atomic detail in a large macromolecular system is often not essential if only a description of macroscopic behaviour is sought. This is the case for polymers which are almost entirely made up of identical repeat units, such as dendrimers. As atomic detail comes at great computational expense, models employed in early dendrimer computer simulations tended to avoid such details and apply various approximations. A popular approach is to describe the dendrimer in terms of a coarse-grain model, where individual particles do not represent atoms but instead represent a collection of atoms. [8] This collection is usually one or more monomer units of the dendrimer. [8] This method is frequently used in conjunction with a diamond lattice model, where the positions of the particles are restricted to a defined lattice or grid, resulting in all bond lengths and angles of the dendrimer being of equal value. [8] This too results in a substantial reduction in simulation costs. However, with the coarse-grained model, all atomic detail is lost and with such large approximations in place, care has to be taken with the interpretation of the results.

An alternative approach is to combine the hydrogen atoms with their neighbouring heavy atom. This is commonly referred to as an extended or united atom force field. For example, in chloroform models the hydrogen atom is often not explicitly represented: the hydrogen and carbon atoms are united and are represented a single CH group, centred at the carbon atom. The carbon force field parameters are adapted to incorporate the effect of the absorbed hydrogen. (In the all-atom approach, all atoms, including hydrogens, are explicitly accounted for.) An advantage of the united atom method is to significantly reduce the number of atoms, which in turn results in fewer non-bonded interactions and allows for a larger dynamics integration step size because the small hydrogen atoms require

smaller time steps. Disadvantages include difficulty with accurately representing hydrogen bonding, the loss of dipole and quadrupole moments which can effect the accuracy of interactions with neighbouring groups, loss of steric effects and shape associated with the hydrogen atoms and loss of hydrogen coordinates, which can be used in comparison with various analytical methods, including NMR and neutron diffraction studies.

Water Force Fields

There are a number of water models that are extensively used in computer simulations of aqueous polymer solutions. The most popular models include SPC (simple point charge) force field of Berendsen et al. (SPC, [148] SPC/E [149]) and the TIP (transferable intermolecular potential) FF of Jorgensen (TIP3P, [150] TIP4P [151] and TIP5P [152]).[1]

Jorgenson's TIP3P model was selected for this thesis because the dendrimer force field originated from a carbohydrate force field that was specifically parameterized for, and extensively tested with, TIP3P. Further, the TIP3P water model adequately reproduces most experimental measurements under the operating conditions of the simulations in this thesis. Furthermore, although the SPC models achieved good results in pure water simulations, this was achieved by over estimating the water-dimer interactions, thereby upsetting the balance between the solvent-solvent, solvent-solute and solute-solute interactions. [149] There are more sophisticated water models available, such as the TIP5P model of Jorgensen which has shown an exceptional fit with experimental data over an extensive temperature and pressure range. [152, 153] The TIP3P model is a 3-atom or 3-sited model that comprises only the hydrogen and oxygen atoms while in TIP4P and TIP5P extra "particles" or sites are included to shift the negative charge from being centred on the oxygen atom. Hence, the TIP3P model in comparison is a relatively simple model. However, the extra computational overheads of the four-site and five-site models were beyond our computational resources at this time.

2.2.2 Truncation of Long-Range Forces

The number of non-bonded interactions is of the order of the square of the number of atoms in the system. This is computationally expensive. However, it is not necessary to calculate the interactions between every pair of atoms in the system, as Van der Waals

[1] Older water FF such as BNS and ST2 were not considered for this thesis.

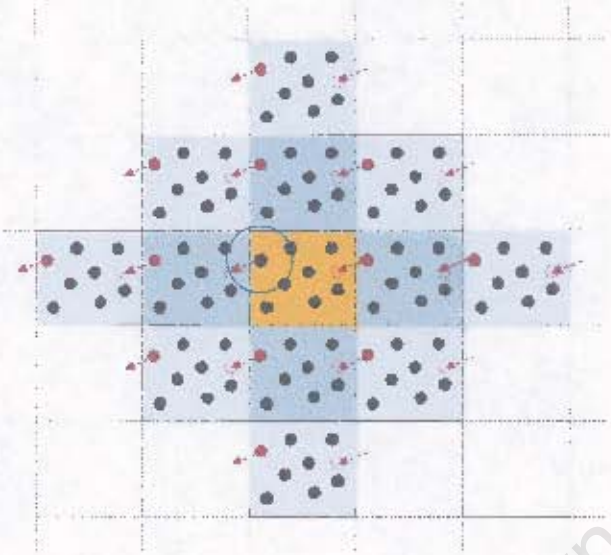

Figure 2.1. By periodically replicating a single cell, an infinite lattice is created. In the figure, the solid red particle exits the primary simulation cell to the left (arrow) and its image re-enters on the right. The circle indicates the closest image particles used to calculated the non-bonded interactions with the solid red particle by applying the minimum image convention and a cut-off less than half the length of the periodic cell.

method of choice, as it is the most "correct" way to accurately include all effects of the long-range forces into the simulations. [128] Alternative techniques include the reaction field [157] and the cell multipole [158–160] methods. In this thesis, all the molecular systems were of neutral charge, hence long-range methods such as these were not implemented due to their substantial computational expenses. However, in Chapter 4, we briefly investigated the effect of Ewald summations on the outcome of the simulation.

2.2.3 Periodic Boundary Conditions

In solvated dendrimer simulations one is mostly interested in the properties of the dendrimer in bulk solution. Interactions with the container walls must be removed because this will result in the system being dominated by surface artefacts. In essence, boundary conditions define what happens to an atom or molecule when it reaches the boundary of the simulation cell.

The method of periodic boundary conditions is a common way to define cell boundaries. The algorithm is relatively simple and we shall consider the case of a cubic simulation cell; if a particle crosses the boundary from the primary cell, its coordinates are modified so

that it reappears on the opposite side of the primary cell. Effectively it appears as though an identical image of the particle has moved into the box from the opposite neighbouring cell. The resulting effect is that of an infinite lattice of image cells identical to the primary cell, as shown in two dimensions in Figure 2.1. When using this method it is only necessary to store the details for the primary cell.

Non-bonded interactions are calculated using an analogous algorithm to that used in the periodic boundary conditions, namely the minimum image convention (Figure 2.1). In the minimum image convention, each atom interacts with only the closest image of every other atom in the system. [128] However, care must be taken to ensure that a particle does not interact with its image in a neighbouring cell. Special attention needs to be taken when dealing with long-range interactions, such as electrostatic interactions involving ions or dipolar molecules. Typically methods such as Ewald summations, [156] are used in such cases.

Geometrically there are a limited number of space-filling polyhedra which can form an infinitely repeating periodic system. In this thesis, the two most popular periodic systems, namely the cube and truncated octahedron, have been employed. Each has its own advantages; the cube is the simplest method to simulate and implement, while the truncated octahedron increases the distance between adjacent cells compared to a cubic system with the equivalent number of particles.

Although periodic boundary conditions remove surface and other boundary effects, they introduce periodicity into the system. Further, as real world isolated systems (NVE) are confined to vessels which in turn disrupt linear momentum, periodic boundary conditions artificially add the extra constraint of constant linear momentum, $\mathcal{P}$, which results in a loss of 3 degrees of freedom ($\mathcal{P}_x, \mathcal{P}_y, \mathcal{P}_z$). Furthermore, it is not possible to simulate fluctuations with wavelengths greater than the length of the cell, as these are suppressed.

Hence, great care still needs to be taken when employing a method which avoids boundary constraints. In general, the errors resulting from periodic boundary conditions are considered to be negligible compared to other systematic errors. [134, 135]

2.2.4 Ensemble Sampling

In addition to the selection of a suitable force field and method of integration, an additional factor to consider is the description of the simulation environment. There are a number of macroscopic thermodynamic states, or ensembles, suitable for MD simulations. In

this work the microcanonical (NVE), canonical (NVT) and isothermal-isobaric (NPT) ensembles were used.[2]

The canonical ensemble is appropriate for use during the heating and equilibration phases of the simulation. In this ensemble, the velocities of all the particles are altered in order to reach and maintain the desired temperature. One method is to scale the velocities by a factor of the ratio of the actual temperature of the system and the desired temperature of the system. [134] Alternatively, the velocities can be re-assigned according to a Maxwell-Boltzmann distribution. The advantage of the second approach is that it ensures an even distribution of kinetic energy in the system and prevents non-isothermal mixing from occurring, i.e., regions of hot and cold temperatures are prevented from forming. The frequency at which the velocities are reassigned is an important factor to consider. Artificial behaviour in the dynamics system will occur if this process is performed too frequently, while prohibitively long periods of equilibration are necessary for infrequent velocity assignments. [128]

When modelling solute-solvent systems, the solute may undergo a substantial change in conformation which results in a significant volume change. Such an effect may occur for the unfolding of a branch of a dendrimer and this may create an unrealistic increase in the local density around the unfolding arm. This would in turn artificially raise the energy barrier for this conformational change. To avoid such computational artefacts from occurring, an isothermal-isobaric (NPT) ensemble may be used. Andersen's extended pressure-coupling method is employed in this thesis. [161] Andersen assigned the system an additional degree of freedom - namely the volume. An analogy can be made to a piston and cylinder, where the potential energy applied by the piston is related to the pressure and volume of the cylinder or system. The kinetic energy of the system is related to the "mass" of the piston and the square of the rate of change of the volume. The "mass" of the piston in this case is the degree of coupling with an imaginary external pressure reservoir. The overall Hamiltonian includes the effects of this piston. The selection of the coupling constant is important. If the piston is assigned an infinite mass, the isothermal-isobaric ensemble is essentially a canonical ensemble. The volume of the system varies in order to maintain a balance between the internal pressure and the external pressure reservoir (the

[2]The thermodynamic constants, N, P, V, E and T are the number of particles, pressure, volume, energy and temperature respectively.

latter is set at the desired pressure value).

The method of temperature control used in sampling the isothermal-isobaric ensemble was developed by Nosé and later extended by Hoover. [141, 142] This method utilises essentially the same concept as the Andersen method, except now the notion of a "piston" is more abstract. It represents the "inertia" of the artificial thermal reservoir with which the system is in contact. The velocities are scaled in a similar manner to the way that the coordinates are scaled in a pressure calculation. Similar to the constant volume system, there are also kinetic and potential energy terms associated with this degree of freedom. Despite the fact that the final form of the energy operator is non-Hamiltonian, the overall energy is conserved and the ensemble samples the isobaric-isothermal phase space. This is an advantage compared to alternative methods, such as Berendsen's method, which does not represent any standard thermodynamic ensemble.

Once the system under investigation has been equilibrated, a microcanonical ensemble can be used to sample phase space and thus various transport and relaxation properties can be calculated (this is the procedure used in this thesis). The result is that a constant-energy surface of phase space is sampled ensuring that the coordinates and velocities are not artificially altered in any way, allowing direct correlations of the Newtonian dynamics of the system to be investigated. [134]

2.3 Statistical Mechanics of Dendrimer Simulations

Analysis of MD or MC simulation data allows one to determine macroscopic behaviour from microscopic behaviour, such as the diffusion and molecular relaxation properties of a dendrimer. However, in order to calculate macroscopic properties it is necessary to ensure that the phase space of the polymeric system has been sufficiently sampled in order to gain a true representation of the behaviour of the system. Central to this condition is the *ergodic hypothesis*. [134] This states that for a system undergoing a stationary random process containing N particles, the calculated time average, t, of a particular property A (which is a function of the momentum, **p** and coordinates, **r**) is related to the macroscopic

observable value, A_{obs}[3] as follows

$$A_{obs} = \int \int A(\mathbf{r}_N, \mathbf{p}_N) e^{-\beta V(\mathbf{r}_N, \mathbf{p}_N)} d\mathbf{r_N} d\mathbf{p_N} = \lim_{t \to \infty} \frac{1}{t} \int_0^{\infty} A(\mathbf{r}_N(t), \mathbf{p}_N(t)) dt \qquad (2.7)$$

For even a very small system of 100 atoms it is impossible to sample all available phase space in a single simulation. However, there is a significantly lower probability of sampling points in phase space that have relatively high energies. Hence a large proportion of the configurations of the molecular system are extremely unlikely, such as the situation where two atoms are superimposed. More formally stated, the probability of sampling a particular point on an isothermal surface of phase space, E(**r**,**p**), at a temperature T, is related to the Boltzmann distribution factor (k_B) through the partition coefficient,

$$q = e^{-\beta E(\mathbf{r},\mathbf{p})} \qquad (2.8)$$

where $\beta = 1/k_B T$. Since the contribution of energetically disfavoured areas of phase space to ensemble averages is extremely small, they can be neglected. Hence, it is not essential to sample every possible conformation of a dendrimer during a simulation.

It is important to evaluate statistically whether phase space has been sufficiently sampled. From the central limit theory, [135] as long as the sampling is random, a relatively small sample of phase space is sufficient to form a statistically representative set of configurations. There are several methods for conformational sampling, ranging from the Metropolis Monte Carlo method (the most stochastic sampling method) to molecular dynamics (the most deterministic sampling method). The deterministic nature of MD becomes essentially chaotic through molecular interactions because the correlation times of the velocities and coordinates are relatively very small. [135]

The main difficulty when sampling by both Monte Carlo and MD simulations is that if large energy barriers exist which split configuration space into disconnected regions, it is very improbable that a short simulation will be capable of crossing such barriers. Therefore, a short time average may not represent complete sampling. Moreover, it is possible that the simulation will appear to have converged (in terms of average properties), while instead it has only converged within some local minimum. It is important to be aware

[3]The use of the symbol 'A' as that for a generic parameter should not be confused with Helmholtz Free Energy.

of such problems - one simple method to check for this is to start several simulations from different configurations.

When comparing the sampling methods, the most significant advantage of MD over purely stochastic methods is that time dependent properties, such as diffusion coefficients or atomic relaxation times, can be calculated and compared to experimental data. In this thesis, we employed only varieties of MD integration methods - no stochastic methods were applied. However, to calculate free energies of the molecular system, the entire potential energy surface must be taken into account, including the improbable high energy regions. To sample such high energy regions, non-Boltzmann MD is required.

2.3.1 Non-Boltzman MD Free Energy Calculations

The calculation of properties that are functions of entropy including the chemical potential energy and Gibbs and Helmholtz free energy, is one of the most challenging areas in computational chemistry. Unlike pressure and internal energy, free energy cannot be defined in terms of a time average over the samples of phase-space and hence cannot be calculated directly. [135] This is because free energy requires the inclusion of high-energy regions of phase-space as well as the low energy regions. A standard MD simulation would inadequately sample high energy regions and the time average of the free energy would not give an accurate true free energy of the molecular system.

Entropically-based properties are functions of the canonical partition coefficient, Q. For a system where N, V and T are independent, the Helmholtz free energy is simply defined as:

$$A = -kTlnQ \tag{2.9}$$

where k is the Boltzmann constant and T is the temperature of the system.

One method for calculating the free energy differences of a system is via thermodynamic integration. The dependence of a thermodynamic property involving an independent variable (for example T or P) is determined from the integration of the appropriate Maxwell relation. [135] Another popular method is the free energy perturbation method. Both methods require several simulations along a reactant-product mutation pathway. This pathway need not be an actual physical pathway since free energy is a state function. The main disadvantage of such free energy difference calculations is that they only yield

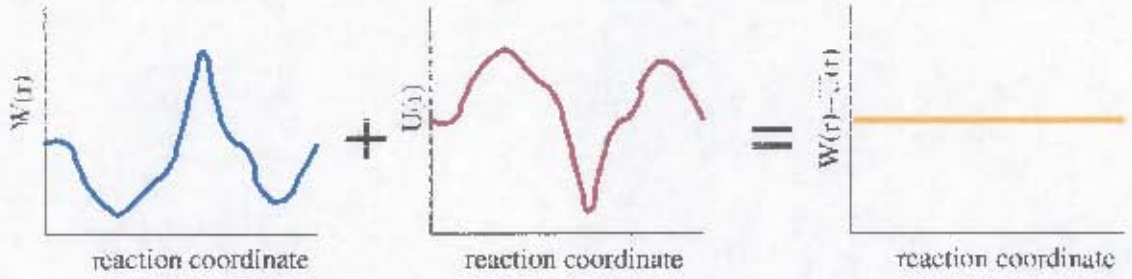

Figure 2.2: By adding the inverse of the real potential, $U(r)$, to the actual potential, $W(r)$, there resulting potential is completely flat and all points phase space have an equal probability of being sampled

an energy difference between the two states and do not describe the complete free energy pathway.

A more complete understanding of the free energy of the system requires the calculation of the potential of mean force (PMF) along the reaction coordinate(s). Unfortunately, PMF's are difficult to calculate. In principle, one could run an exceptionally long simulation, but this does not guarantee that all regions of phase space would be adequately sampled. Generally, energy barriers greater than $2kT$ would not be crossed and the full energy surface would be incompletely explored.

One approach for calculating PMFs is umbrella sampling, first developed by Patey, Vallean and Torrie. [162,163] Here, the sampling probability of a simulation is modified by applying a weighting factor to the energy of areas with high probability. The high energy regions that would be undersampled by standard Boltzmann dynamics become more highly sampled. The difficulty is that for efficient sampling one needs prior knowledge of the nature of the weighting function. This implies that in order to calculate the potential of mean force, one must actually know this potential!

Mezei [164] and Paine and Scheraga [165] developed an iterative procedure used to refine or the initial PMF function. Starting with a completely unbiased weighting function, a simulation is run. The probability function $P(r)$ is then calculated from a simple histogram as a function of r. The PMF, $W(r)$ is calculated from:

$$W(r) = -kTlnP(r) \tag{2.10}$$

where k is the Boltzmann constant and T is the absolute temperature. The inverse of this calculated PMF, the so-called umbrella potential ($U(r)$), is then used as the penalty

function for the next iteration of the simulation. This is done by modifying the unbiased Hamiltonian of the system (H_i) such that $H = H_i + U(r)$. For each successive iteration, histograms of the biased population distributions are combined using Weighted Histogram Analysis Method (WHAM). [166] WHAM is an iterative algorithm that determines an optimal estimate for the actual unbiased distribution function by combining overlapping distribution functions of several iterations of biased simulations. This is done by determining the optimal weighting factors for the weighted sum of the biased distributions. The convergence criterion is that the maximum difference between the weighting factors is less than a particular tolerance level, typically 0.001. Once the WHAM algorithm has converged, the potential is smoothed to avoid discontinuous or sudden changes in the umbrella potential and is extrapolated to previously unsampled regions. The extrapolation should direct the simulation into unsampled regions without introducing additional local minima into which the system could become trapped. [167] The method to extrapolate the umbrella potential to unsampled regions emulates the system of Bartels and Karplus but in a single dimension. [168] The unsampled regions are set to the maximum value of the umbrella potential. To ensure a smooth transition between explored and unexplored areas, the unsampled bins that are directly adjacent to a sampled bin are set to the average value of the neighbouring bins. The unsampled cells adjacent to the cells bordering the sampled region regions are set to the average of the surrounding cells plus half the difference between the average and the maximum values. In this way, sharp discontinuities in the umbrella potential were avoided. Any remaining discontinuities in the new umbrella potential are removed by smoothing the potential at least twice using the following smoothing function [168]

$$U'_{k,i} = \frac{1}{3}\left(-0.3U_{k-2,i} + 1.3U_{k-1,i} + U_k + 1.3U_{k+1,i} - 0.3U_{k+2,i}\right) \tag{2.11}$$

where $U'_{k,i}$ new smoothed umbrella potential of cell k of iteration i.

When the iterative procedure to calculate the umbrella potential is completed, the combination of the umbrella potential $U(r)$ and the true potential $W(r)$ is a flat potential, thereby allowing even sampling of the reaction coordinate. This process is illustrated in Figure 2.2. The system is deemed to be converged when the sampling is essentially uniform along the reaction coordinate. In this thesis we considered the system converged once the ratio of the population of most sampled region and the population of the least sampled region was less that 1.5. The exact converged umbrella potential would be $-W(r)$ with

the probability distribution of such a potential described by:

$$P(r) = e^{W(r)/kT} \tag{2.12}$$

In this thesis, W is the function of a scalar parameter (end-to-end distance) which indicates how difficult it is to stretch or compress a dendrimer in a particular solvent. However, the same iterative algorithm can be applied to any multidimensional parameter.

Chapter 3

Analytical Methods

3.1 Introduction

An important feature of computational chemistry is that properties computed from a simulation can be compared directly with measured values from physical experimental techniques, such as small-angle neutron and X-ray scattering (SANS and SAXS) or nuclear magnetic resonance (NMR) spectroscopy. Comparison of experimental measurements and computational calculations allows not only molecular mechanics models to be validated and improved, but also the interpretation of experimental data in terms of detailed atomic models obtained from simulations. For chemistry in general, the combination of experimental with computational techniques has resulted in an increased understanding of macromolecular structure and dynamics.

A number of physical techniques are routinely employed to investigate dendrimers including SAXS and SANS and a variety of NMR and rheology techniques. [8] However, NMR is most frequently used to provide detailed information on primary, secondary and even tertiary conformations of dendrimers. [17,85,105,106,108,109,111–113] The advantage of NMR over other experimental methods, such as X-ray crystallography, is that we can determine both structural detail and atomic motions. This is especially relevant in the case of dendrimers, where crystal structures have proved challenging to obtain and where solution properties are of most interest.

There are a variety of analytical methods use to analyse computer simulations of MD simulations. In MD simulations, the time evolution of the system simulated is recorded as a series of snapshots of the atomic configuration, usually in the form of a simple collection

of atomic coordinates. The simulation is typically written to disk and analysed separately at a later date. The frequency at which the frames of molecular position are recorded is a compromise between accuracy and computational resources. It is impractical for every frame of a simulation to be recorded, as the storage requirements would be prohibitively large, especially in the case of nanosecond simulations of large solvated polymeric systems. Further to ensure statistical accuracy each frame used in analysis must be independent from the next frame. Further, the computational time, power and memory required for the analysis of large data sets would make thorough analysis of these simulations impractical. The alternative is to record a subset of the trajectory frames of the simulation, sampling at a regular frequency. However, the smaller the frequency of sampling, the greater the risk of producing erroneous analysis due to disregarding the finer detail of the simulation. Simple analyses can be performed on a trajectory file first to check that the simulation is valid or that it has reached a desired point before commencing with expensive detailed analysis.

In the previous chapter we addressed the theoretical aspects of simulating solvated dendrimer systems in a computational environment. This chapter describes the computational analytical methods applied in this thesis. First we describe methods for calculating structural properties of a molecular system. These include the radius of gyration and moments of inertia to describe the size and shape of a dendrimer; radial and spatial distribution functions to analyze the distribution atoms about a central point; calculations of the solvent accessible surface to illustrate which regions of the dendrimer are most easily accessible by the solvent and finally, Voronoi analysis to give detailed description of the geometric arrangement of the pure solvent. This is followed by a description of the methods for calculating dynamical properties. These include correlation functions used to determine relaxation rates; mean squared displacement of each layer of a dendrimer to classify whether the motion is restricted (solid-like) or unrestricted (liquid-like); diffusion coefficient and intrinsic viscosity measurements of a dendrimer to describe its overall transport properties in the various solvents. Where possible, we make comparisons with physical NMR measurements of our calculated NMR properties, such as diffusion coefficients and longitudinal relaxation times.

3.2 Molecular Structure

3.2.1 Radius of Gyration

The radius of gyration, R_g, is the simplest measure of molecular size of macromolecules. A time series of the R_g is commonly used to analyse an MD trajectory to determine when a dendrimer has reached a stable conformation. The dendrimer is said to be equilibrated when there is no change in mean R_g over an extended period (typically several hundred picoseconds) except for small fluctuations about the mean. R_g is defined as the mean squared displacement of a set of N atoms each of mass m_i from the centre of mass, $\mathbf{r}_{com}$:

$$R_g = \sqrt{\frac{\sum_{i=1}^{N} m_i(\mathbf{r}_i - \mathbf{r}_{com})^2}{\sum_{i=1}^{N} m_i}} \tag{3.1}$$

Thus R_g is easily computed from a simulation time series. The values obtained from computational models can be compared with R_g measured from a number of techniques. [92, 96] For example, for small scattering angles in SANS measurements, the scattering intensity of an isolated particle can be expressed as a function of the radius of gyration, according to Guinier's approximation [169] :

$$\ln(I) = \ln(I_0) - \frac{(qR_g)^2}{3} \tag{3.2}$$

where I is the absolute intensity of coherent scattering, q is the scattering vector (which is a function of scattering angle) and I_0 is a function of the contrast of the scattering length of the solvent and the partial volume of the solute. Alternatively, R_g can be calculated from the diffusion coefficient measured from viscosimetric measurements or NMR pulsed field gradient (PFG) and diffusion ordered spectroscopy (DOSY) techniques. For Einstein spheres (spherical non-interacting solvent molecules) the hydrodynamic radius, R_h, is related to the limiting diffusion coefficient of the dendrimer, D_0, according to the Stokes-Einstein relation :

$$R_h = \frac{k_B T}{6\pi\eta D_0} \tag{3.3}$$

where k_B is Boltzmann's constant, T is the temperature and η is the viscosity of the solvent. For a spherical dendrimer of uniform density, R_g is related to R_h by a factor of $\sqrt{3/5}$. [90, 95, 96, 170]

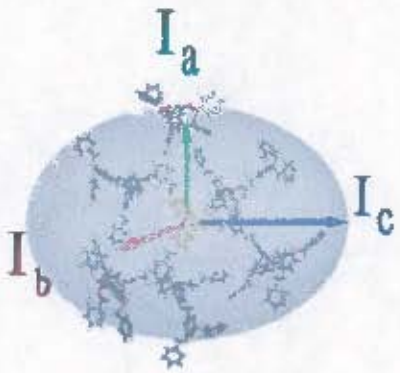

Figure 3.1: Distribution of a dendrimer's mass about its principal axes, where $I_a < I_b < I_c$.

The debate over the structure of dendrimers centres around the density distribution within the dendrimer, the location of the terminal groups and whether the dendrimer is folded (or contracted) or unfolded (extended). However no formal definition has been given to define when the dendrimer is "contracted" or "extended". We use the radius of gyration (R_g) as a quick method to quantitatively identify when the dendrimer is folded or unfolded. In this thesis we define the dendrimer to be completely folded or contracted when its conformation (or R_g) is similar to that of the average equilibrium conformation of the dendrimer in the vacuum Molecular Dynamics simulations. The dendrimer is said to be completely unfolded when the dendrimer has an R_g equal to the energy minimized conformation of the dendrimer in vacuum. The vacuum simulation is used as the basis of this definition as each conformation is only dependent on dendrimer force field and is independent of solvent effects.

3.2.2 Moments of Inertia

The principal moments of inertia for a dendrimer are closely related to R_g. These can be used to analyze the distribution of a macromolecule's mass along its principal axes with respect to its centre of mass (Figure 3.1). Calculation of moments of inertia is employed in a wide range of applications in macromolecular conformational analysis, [171] including dendrimers. [24, 27, 171]

The moments of inertia for a molecule can be calculated from a simulation in the following way. For each frame of the simulation, the moment of inertia tensor, $\bar{\mathrm{I}}$, is

calculated about the centre of mass $x_{com}, y_{com}, z_{com}$ of the polymer (Equation (3.4)). This tensor is subsequently transformed to align with its principal axes by diagonalizing $\overline{\mathbf{I}}$ with its eigenvectors, $\overline{\mathbf{X}}$, and the inverse thereof (Equation (3.5)). In the resulting diagonal matrix, $\overline{\mathbf{D}}$, the non-zero diagonal terms are the principal moments of inertia, where we define $I_A \leq I_B \leq I_C$.

$$\overline{\mathbf{I}} = \begin{pmatrix} \sum_k m_k(y_k^2 + z_k^2) - (y_{com}^2 + z_{com}^2)\sum_k m_k & -\sum_k m_k x_k y_k + x_{com}y_{com}\sum_k m_k & -\sum_k m_k x_k z_k + x_{com}z_{com}\sum_k m_k \\ -\sum_k m_k x_k y_k + x_{com}y_{com}\sum_k m_k & \sum_k m_k(z_k^2 + x_k^2) - (z_{com}^2 + x_{com}^2)\sum_k m_k & -\sum_k m_k x_k y_k + x_{com}y_{com}\sum_k m_k \\ -\sum_k m_k x_k z_k + x_{com}z_{com}\sum_k m_k & -\sum_k m_k y_k z_k - y_{com}z_{com}\sum_k m_k & \sum_k m_k(x_k^2 + y_k^2) - (x_{com}^2 + y_{com}^2)\sum_k m_k \end{pmatrix} \tag{3.4}$$

$$\overline{\mathbf{D}} = \overline{\mathbf{X}}^{-1}\,\overline{\mathbf{I}}\,\overline{\mathbf{X}} \tag{3.5}$$

The ratios of the principal moments, I_C/I_A and I_A/I_B, indicate the asphericity and acylindicity of a dendrimer. [8]

3.2.3 Radial Distributions

The R_g and the moments of inertia do not provide any structural information for a molecule other than its size and overall shape. Often one is interested in the position of side chains; in the case of dendrimers, the positions of the wedge. The radial disposition of monomeric groups within a dendrimer can be described by adapting the standard radial distribution function (RDF) definition. In general the radial distribution function, $g(r)$, is a standard method for analyzing the local structure of a solvent and is typically defined as:

$$g(r) = \frac{V}{N^2}\left\langle \sum_i \sum_{j \neq i} \delta(\mathbf{r} - \mathbf{r}_{ij}) \right\rangle \tag{3.6}$$

$g(r)$ relates the probability of finding a pair of atoms at distance r apart and is normalised by the probability of all the atoms being evenly distributed in the system at the

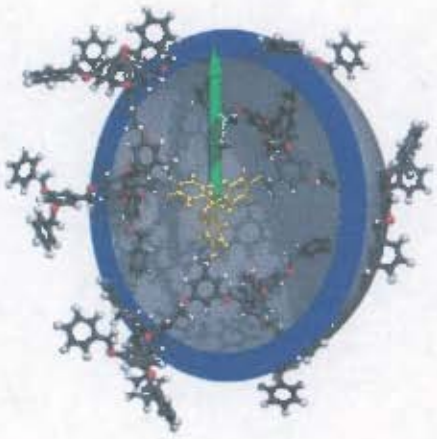

Figure 3.2: Schematic diagram of the radial distribution function $g(r)$ for a dendrimer at a particular r value. The particle density is evaluated within a thin spherical shell of radius r centred on the point of interest.

same density. Not only does $g(r)$ provide insight into the structure of a liquid (commonly referred to as pair distribution functions or PDFs) but it also can be used to calculate the ensemble average for any structural pair, for example the distribution of the aryl rings of the dendrimer. In addition, radial distributions constitute an integral part of potential of mean force calculations (Section 2.3.1). Hence, radially averaged density distributions, RDFs, are arguably the most common method used to describe the structure of dendrimers. RDFs are not only used to characterise the density distributions within dendrimers and to identify regions of low congestion suitable for hosting guest molecules, they are also used to identify the location of the terminal groups, their distribution within the polymer and subsequently the degree of backfolding. $g(r)$ can also be compared with experimentally-determined values. In SAXS and SANS measurements a variety of pair distribution functions, including the centre-of-mass probability distribution, $g^{(000)}_{n_i n_j}(r)$, and several orientational probability distributions can be calculated from a Fourier-inversion of the structure factor.

The radial density distribution function for a solute molecule differs slightly from that of the solvent in that the distribution of the monomers of the dendrimer are all with respect to the focal point or core of the dendrimer. If one assumes that the core is at the geometric centre of the polymer, then this too can be compared with scattering experiments in a

similar manner to that used for $g(r)$ of the solvent, except in this case the Fourier-inversion generates the shape function $T(r)$. [93]

If the distribution is not normalised by the volumes of each shell, then the radial distribution is of the population or the number of atoms within each shell. This is referred to as the number density function (NDF), $N(r)$. To avoid confusion and to highlight the difference in the radial distribution functions used in the analysis of dendrimer structure, we refer to the radial density distribution as $\rho(r)$. More specifically, the distribution of the total density of a dendrimer is referred to as $\rho_T(r)$ and an individual topological layer's density distribution as $\rho_l(r)$. Furthermore, $P(r)$ is the number density normalised by the total number of atoms in the population, i.e., a percentage of the total population. The integration of this curve represents the radial accumulation of atoms as we progress to the periphery of the dendrimer.

3.2.4 Spatial Distributions

A disadvantage of radial density distributions is that they do not provide a clear indication of exactly where each of the various chemical groups of the molecule is located. Further, we make the assumption that the core of the molecule is located at the geometric centre of the dendrimer and it will be shown that this is not always the case. In order to better understand the structure of dendrimers, a three dimensional probability distribution function designed for studying solvated polysaccharides [172] was modified specifically for dendrimers.

In this method, each frame of an MD trajectory is translated and rotated to align the core atoms about a common orientation. The density of selected atoms, in this case the carbon atoms of the phenyl rings, are summed in a 3D histogram (Figure 3.3). Using the following 3D Gaussian distribution :

$$g(\mathrm{r}) = \left(\frac{a}{\pi}\right)^{3/2} \exp\left(-ar^2\right) \tag{3.7}$$

the density of the atoms are distributed over neighbouring bins such that 90% of the binned density for an atom is within its van der Waals radius. This is determined by appropriate selection of the constant a for each atom. The resultant histogram is subsequently normalised with respect to the bulk density of the polymer. The advantage of this method over the methods mentioned thus far is that radially averaged errors are eliminated. An identical approach can be used to look at the structure of the solvent,

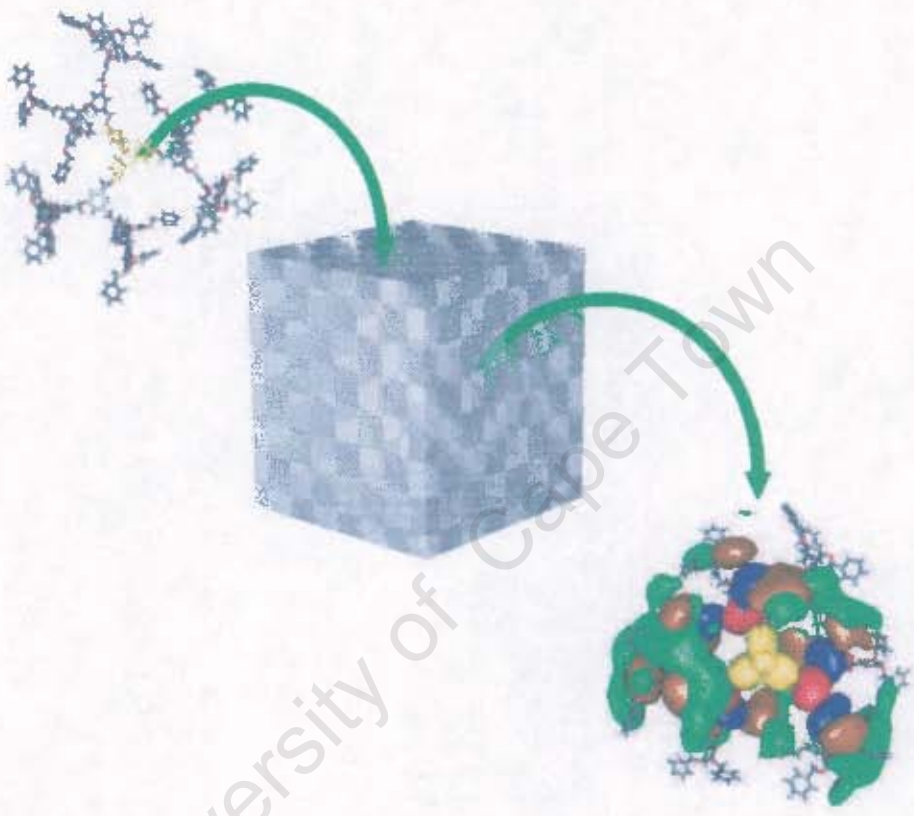

Figure 3.3: Schematic diagram of the procedure used to calculate the spatially averaged distribution of the layers corresponding to different generations of a dendrimer during MD simulations. The polymer is placed within a regular three-dimensional grid and the particle density calculated for each cell within the grid, allowing for a contoured representation of the mean density over the simulation. The contours are rendered using the opensource software gOpenMol [173, 174]

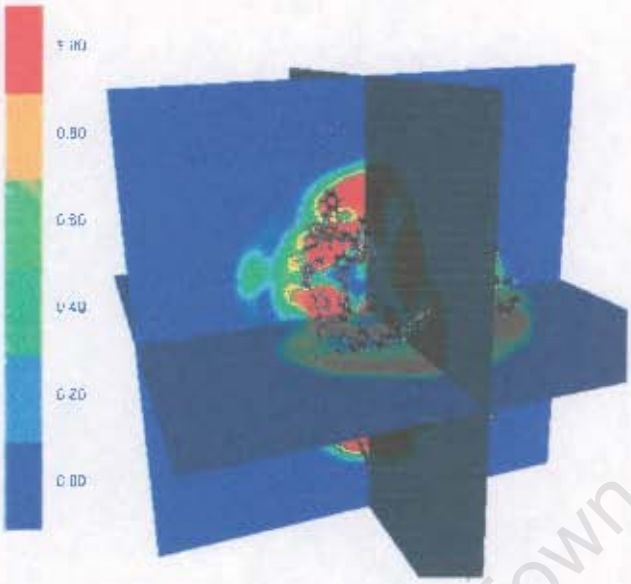

Figure 3.4: Cutplanes through the SDF of the terminal and core layers of a dendrimer. The key represents the probability distributions: from bulk probability or greater (red) to zero probability(blue).

except that in this case the density distribution of the solvent is normalised by its bulk density. [175]

While the overall structure of a dendrimer is immediately clear, representing a 3D method in 2D makes the perception of depth very difficult. For example, in Figure 3.3, in the SDF representation of the dendrimer, the vertical displacement of the terminal groups relative to the core is not clear. The result is that a group appearing directly above the core could be either a few angstroms from the core or twenty to thirty angstroms form the core. Furthermore, the internal features of the SDFs are hidden by the overall structure of the dendrimer. Therefore, SDFs are best viewed in relation with cutplane through the centre of the SDF (Figure 3.4) or to show the SDF of each layer on an individual basis (Figure 3.5).

The best option proved to be a combination of the complete set of SDFs for a dendrimer together with a series of cutplanes through the SDFs. To simplify this representation and because the location of the terminal groups is of primary interest, only the terminal layer and the core (for orientation purposes) are considered in the cutplanes. Any region where the probability is greater than that of bulk density is represented in red while lower probability levels are indicated in the key in Figure 3.4.

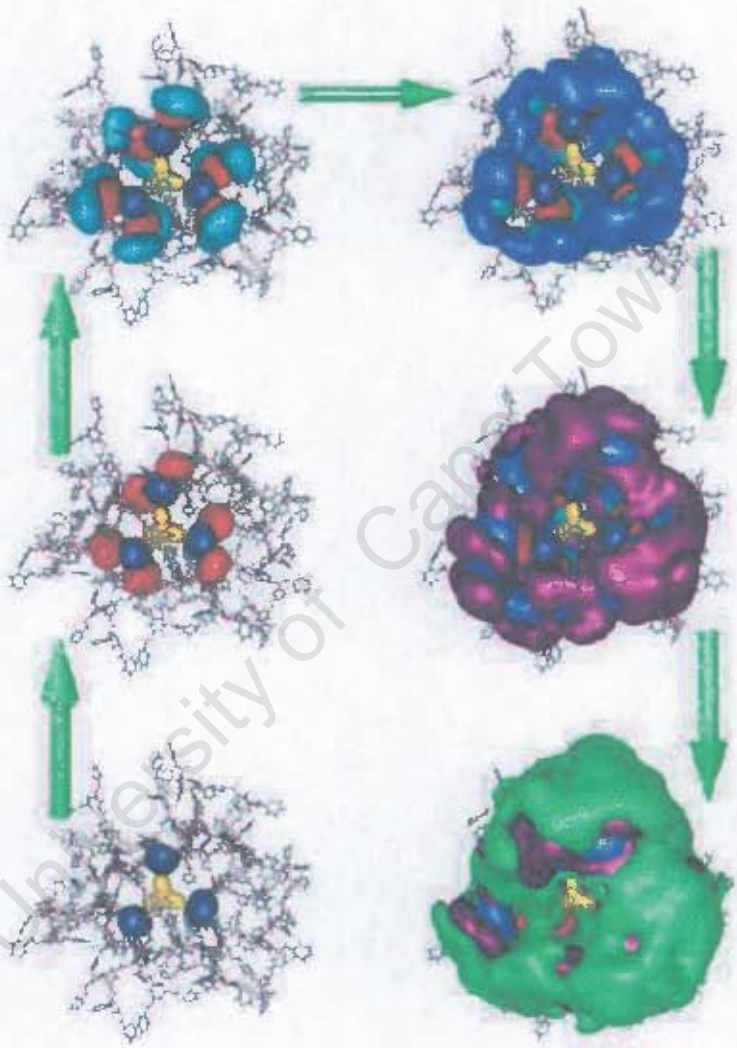

Figure 3.5: The stepwise inclusion of the SDFs of each layer of a G5 dendrimer revealing its internal structure.

3.3 Solvent Structure

Radial and spatial distributions are commonly used methods to describe the structure of a pure solvent. Voronoi Analysis can also be used to investigate the structure of a liquid. Voronoi analysis is the tessellation of the simulation coordinate space with Voronoi polyhedra (VP). A VP is defined as the region of space (described by a convex polyhedron) surrounding an atom that is closer to this atom than any other atom in the system. Therefore, it is a means of unequivocally defining the space occupied by each particle and describing its coordination with its nearest atomic environment. It is a purely geometrical approach and is not restricted to particles in a particles first coordination shell. A VP usually includes particles belonging to the second or third solvation shell. [176]

In this thesis, Voronoi Analysis is used to describe the structure of various solvents. The VP are formed from the centre of mass of each solvent molecule. From Voronoi analysis a variety of data can be obtained. V_i is the volume of the polyhedra of the i^{th} solvent molecule and indicates the space belonging to this molecule, while the reciprocal is a measure of the local density around the molecule in question. The number of faces of the VP indicates the number of neighbouring solvent molecules, while the area of each face indicates the distance to that neighbour. Therefore, the shape of the VP reflect the arrangement of the molecules about the each other. The shape of the VP is described in terms of its asphericity parameter, η, which quantifies how much the shape of the VP differs from a perfect sphere where $\eta = 1$. The number of faces is an indication of how structured the surrounding structure is: the larger the number of faces, the larger the larger the number of neighbouring particles and the larger the local density. The area of the i^{th} face A_i is defined as :

$$A_i = \frac{1}{2} \sum_{j=2}^{n_v^{(i)}-1} |(\bar{r}_j^{(i)} - \bar{r}_1^{(i)}) \times (\bar{r}_{j+1}^{(i)} - \bar{r}_1^{(i)})| \tag{3.8}$$

where n_v is the number of vertices pertaining to the i^{th} face, $\bar{r}_1^{(i)}$, $\bar{r}_j^{(i)}$ and $\bar{r}_{j+1}^{(i)}$ are the vectors of the first, j^{th} and $j+1$ vertex of the i^{th} vertex respectively. The total volume, V, surface area, S, and asphericity parameter, η, of a polyhedra are calculated from

$$V = \frac{1}{6}\sum_{i=1}^{N_f}\sum_{j=2}^{n_v^{(i)}-1} |(\bar{r}_1^{(i)} \times \bar{r}_j^{(i)}) \cdot \bar{r}_{j-1}^{(i)}| \tag{3.9}$$

$$S = \sum_{i=1}^{N_f} A_i \tag{3.10}$$

$$\eta = \frac{S^3}{36\pi V^2} \tag{3.11}$$

(3.12)

respectively. [176] The probability distribution function, $P(r)$, of each of these calculated values allows the solvent environment to be quantitatively characterised. Exponential tails of the distribution of a property of the VP, for example the volume of the VP, indicates a deviation from structural uniformity, while a Gaussian-like distribution indicates a uniform arrangement of points. [177]

3.4 Dynamical Properties

3.4.1 Correlation Functions and Transport Properties

MD generated configurations are connected in time, hence time-dependent properties such as diffusion coefficients, rotational times and similar transport properties can be extracted from a MD trajectory. A correlation function provides a numerical value that quantifies the strength of correlation of a property at different times in the simulation. The use of correlation functions links the trajectory of a MD simulation to fundamental statistical mechanics and hence to experimental measurements. Using correlation functions, analysis of statistical errors is also possible. In general, an autocorrelation function, $C(t)$, for a time-dependent equilibrium variable, $A(t)$, sampled at equal time intervals of τ, is given by:

$$C(t) = \lim_{T\to\infty}\int_0^T A(t+\tau)A(\tau)d\tau \tag{3.13}$$

This equation is more commonly written in the ensemble average form:

$$C(t) = \langle A(0)A(t)\rangle \tag{3.14}$$

Using the direct method, for a trajectory containing N points, $C(t)$ can be evaluated by the following summation:

$$C(t) = \left(\frac{1}{N - t/\delta t}\right) \sum_{i=1}^{N-t/\delta t} A_i A_{i+t/\delta t} \tag{3.15}$$

Here δt is the duration of a time step, $t/\delta t$ accounts for the end of the simulation where $A_{i+t/\delta t}$ is not defined and A_i is the value of A at time step i. [178] Uncorrelated properties average to zero, while correlated properties can either be positive or negative. The decay of the time series to zero indicates how quickly the properties become uncorrelated. This decay is usually assumed to be exponential with the general form $Ae^{-\frac{1/\tau}{t}}$ where τ is known as the correlation time. Frequencies of regular motion may be obtained from calculating the power spectrum of the correlation function by Fourier transformation. [175]

Mean Square Displacement Time Series and Diffusion Coefficients

One of the simplest correlation functions is the mean square displacement (MSD) time series:

$$\Delta r^2(t) = \frac{1}{N} \sum_{i=1}^{N} [\mathbf{r}_i(t) - \mathbf{r}_i(0)]^2 \tag{3.16}$$

We employ two MSD time series in this thesis. The first is the time series of the average MSD of each topological layer of the dendrimer, with respect to the core, i.e., the overall translational diffusion of the dendrimer is removed by reorientating each frame of the trajectory using the core of the dendrimer as the frame of reference. From this series, the dynamics of the internal generations of the dendrimer can be characterised as fluid-like or solid-like. [135] A group of atoms (such as a monomer of a dendrimer) is said to have solid-like behaviour when the MSD increases over a very short period, thereafter remaining constant at this value for the remainder of the time series. This is indicative of constrained dynamics where the group is confined to specific volume, for example the unit cell in a crystal. On the other hand, if the MSD continues to increase, the dynamics are said to be liquid-like and not constrained to a particular volume. This is illustrated in Figure 3.6.

The second MSD time series utilised in this thesis is the MSD of the centre of mass of the entire dendrimer. A dendrimer's diffusion coefficient may be determined from this time series by calculating the velocity autocorrelation function of the centre of mass of the dendrimer. From the Green-Kubo relation,

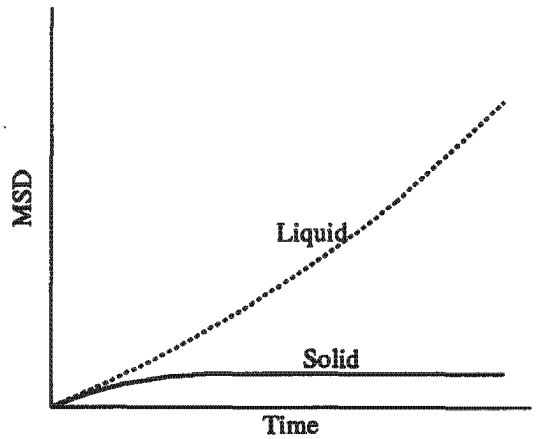

Figure 3.6: A schematic representation of solid-like (solid line) and liquid-like (dashed line) mean squared displacement (MSD) time series profiles.

$$D = \frac{1}{3}\int_0^\infty \langle \mathbf{v}(t).\mathbf{v}(0)\rangle \, dt \tag{3.17}$$

the equilibrium diffusion coefficients can be calculated, which in turn can be compared to experimentally derived values. For very long time series, the Green-Kubo relation is simplified to the Einstein relation,

$$D = \lim_{t\to\infty} \frac{\left\langle |\mathbf{r}(t) - \mathbf{r}(0)|^2 \right\rangle}{6t} \tag{3.18}$$

where D is related to the slope of the mean squared displacement autocorrelation function of the centre of mass of the diffusing molecule.

For a simulation containing N solvent molecules, the statistical accuracy of the self-diffusion coefficient is greatly improved by calculating the average, D, over all N molecules, ensuring that their positions have not been adjusted by any periodic boundary effects. [134]

In calculating a dynamical property, it is important to ensure that the sample time is sufficiently long for the Ergodic assumption to hold (Section 2.3). This is especially true in the case of the diffusion of a single molecule. The calculation should be performed over a very long simulation period (typically at least 0.5 ns) to remove any non-Brownian type motion. Illustrated in Figure 3.7 are two possible paths taken by a solute molecule. The diffusion coefficient for these two paths would differ substantially, suggesting that the molecule diffuses at different rates. To prevent this, one must either perform the measurement over a longer period or in the case of the diffusion of the solvent, calculate

Figure 3.7: The importance of a sufficiently long sample period for the diffusion calculation. (A) gives the impression of a very slow rate of diffusion while (B) gives the opposite impression. (C) Shows a more accurate representation of the diffusion if the simulation is taken over a sufficiently long period.

the average value for many molecules, preferably all the solvent molecules.

The diffusion of the solvent within the dendrimer is also of interest. Does the solvent move freely within the channels of the dendrimer as suggested from Connolly surfaces of dendrimers [24] or does the solvent remain trapped within the dendrimer? One approach is to calculate the diffusion coefficient of the solvent as a function of the distance from the core. However, if Fréchet dendrimers are not spherically symmetrical and the assumption is that the core is at the geometric centre of the dendrimer then this approach is potentially flawed. An alternative is to calculate the spatial distribution of the diffusion coefficients by using a modified version of the spatial distribution function discussed earlier (Section 3.2.4). In this case the histogram records the solvent diffusion coefficients about the solute instead of the solvent density. [175]

With the advent of pulsed NMR techniques over two decades ago, pulsed field gradient spin echo (PFG-SE) techniques have become the method of choice for the measurement of diffusion coefficients [113, 114]. The diffusion coefficient, D, is determined from the slope of amplitude of the Fourier transform of a series of acquired signals, A_G, in the gradient field with respect to the field gradient strength, G, as illustrated below: (3.19)

$$\ln A_G = f(\gamma, G, \delta, \Delta)D + \ln A_0 \tag{3.19}$$

Here A_0 is the echo amplitude without a magnetic field gradient and f is a function of γ, the gyromagnetic ratio of the nucleus, Δ, the gradient pulse interval and G.

An alternative method of measuring diffusion coefficients is using Diffusion-ordered NMR spectroscopy (DOSY). [179–181] DOSY NMR is similar to PFG-SE NMR techniques

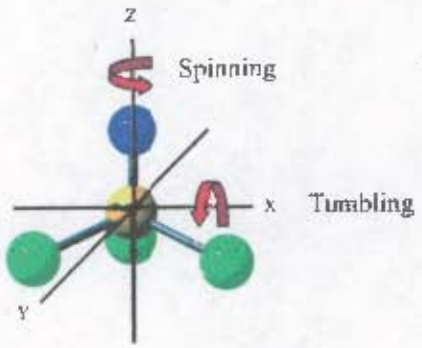

Figure 3.8: The anisotropic rotational relaxation modes of a molecule with a C_{3v} axis of symmetry (for example, chloroform)

in that the signal decays exponentially according the diffusion behaviour of individual molecules. However, the DOSY spectrum is a two dimension NMR spectrum where the one dimension represents the chemical shift and the other represents the diffusion coefficient. An advantage of this technique over PFG-SE NMR is that the sample can contain a mixture of molecules. The chemical shifts of similar molecules which normally overlap in one dimensional NMR become separated on the diffusion coefficient axis. This is also a means of determining if the sample has any impurities from incomplete reactions during the synthetic process.

3.4.2 Rotational Relaxation

Another method to quantify the accuracy of a solvent model is through a comparison of its calculated reorientational behaviour with available experimental and QM data. These rotational relaxation times (τ_{rot}) are calculated from integration of the time correlation function of an l-rank Legendre polynomial for the rotation of a solvent molecule about a reference vector.

$$C_l(t) = \langle P_l[\cos\theta(t)]\rangle \tag{3.20}$$

$$\tau_l = \int_0^\infty C_l(t)dt \tag{3.21}$$

For a symmetric top molecule (a molecule with a C_{3v} symmetric axis), such as chloroform, the rotational motion with respect to the top axis is anisotropic; the motion perpendicular to the top axis (tumbling) is hindered to a different extent from the motion

parallel (spinning) to its top axis (Figure 3.8). These relaxation modes can be measured using infra-red, Raman and NMR techniques.

The overall correlation time, $\tau_{c,l}$, for the l-rank spherical harmonic is a function of θ (which is the angle between a reference vector and the top axis) and the integral correlation times, $\tau_{(l,m)}$, of the normalized time autocorrelation function of the spherical harmonic $Y_{l,m}(\theta,\phi)$.

$$\tau_{c,1} = \cos^2\theta\tau_{1,0} + \sin^2\theta\tau_{1,1} \quad (3.22)$$

$$\tau_{c,2} = \frac{1}{4}(3\cos^2\theta - 1)^2\tau_{2,0} + 3\cos^2\theta\sin^2\theta\tau_{2,1} + \frac{3}{4}\sin^4\theta\tau_{2,2} \quad (3.23)$$

By setting the reference vector parallel or perpendicular to the top axis, the anisotropic effects from spinning and tumbling can be determined. For contribution from tumbling motion, Equation 3.22 and 3.23 simplify to $\tau_{1,0}$ and $\tau_{2,0}$ respectively. [182] The spinning contribution is characterized by $\tau_{l,m}$ where $m \neq 0$.

Internal and Overall Orientational Relaxation

Longitudinal or spin-lattice relaxation (T_1) and spin-spin or horizontal relaxation times (T_2) along with nuclear Overhauser enhancement (nOe) factors (η) for ^{13}C is dominated by the fluctuating dipolar interactions between the heteronucleus and the directly attached proton. The dipolar coupling itself is directly dependent on the motion of the internuclear r_{XH} vector. Therefore, the relaxation rate can be described by an angular autocorrelation function of the r_{XH} vector which is expressed in terms of a power series for the fluctuating $X-H$ dipole moment:

$$C(t) =< P_2\mu_{XH}(0).\mu_{XH}(t) > \quad (3.24)$$

One solution for this power series is with a second-order Legendre polynomial $P_2 = 1/2(3x-1)^2$. Here, $x = \cos\gamma$ and γ is the angle between the dipole moment unit vectors. Hence, $C(t)$ is dependent on γ only.

The spectral density, from which the relaxation parameters will be determined, is calculated from the Fourier transform of Equation 3.24.

$$J(\omega) = 2\int_0^\infty C(t)\cos\omega t dt \quad (3.25)$$

The T_1 relaxation rates are given by the following well established relations:

$$T_1^{-1} = \frac{1}{4}D\left(J(\omega_H - \omega_X) + 3J(\omega_X) + 6J(\omega_X + \omega_H)\right) \tag{3.26}$$

Here, ω_H and ω_C are the Lamour frequencies and D is the dipolar coupling constant which is a function of the distance between the nuclei X and H, r_{XH} and their respective magnetogyric ratios,γ_H and γ_C. Equivalent equations exist for T_2 and nOe calculations.

A practical difficulty arises for calculating NMR relaxation parameters from a simulation where the correlation function $C(t)$ in Equation 3.25 does not decay to zero in the time over which it can be reliably calculated. To overcome this difficulty, the correlation function is factored into contributions of slow molecular tumbling ($C_O(t)$) and rapid internal motions $C_I(t)$:

$$C(t) = C_O(t)C_I(t) \tag{3.27}$$

$C_I(t)$ is represented by Equation (3.24). $C_0(t)$ is represented by an exponential decay of $e^{\frac{1}{\tau_M}}$ where τ_M is the rotational correlation time of the dendrimer evaluated from a vector rigidly fixed to the core of the dendrimer.

T_1 relaxations can be measured using inversion recovery pulse sequence (Figure 3.9). The equilibrium nuclear magnetization is inverted with a 180° pulse followed by short delay time of τ. During this period the nuclei undergo partial spin-lattice relaxation. This is followed by a 90° pulse which rotates the remaining vector onto the y axis where it is measured. This process is repeated for a number of τ and the intensity of the peaks $I(\tau)$ against their delay τ is a simple exponential

$$I(\tau) = I(0)\left[1 - 2e^{-\tau/T_1}\right] \tag{3.28}$$

3.4.3 Intrinsic Viscosity

The intrinsic viscosity,[1] $[\eta]$, of dendrimers is probably the most common property reported in literature due to the curious "ball bearing" effect as described in Chapter 1 of this thesis. Briefly, the intrinsic viscosity of a polymer is the capability of this polymer to increase

[1]According to the IUPAC naming convention $[\eta]$ is formally referred to as the *reduced viscosity*. However, in literature $[\eta]$ is most commonly referred to as the *intrinsic viscosity*

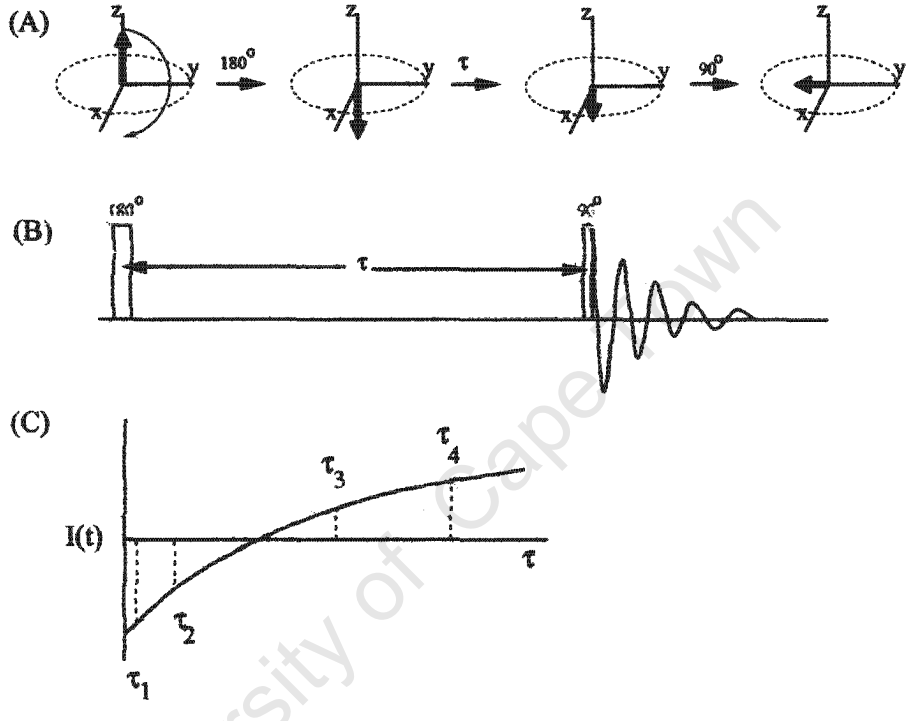

Figure 3.9: The inversion recovery pulse sequence. The nucleus magnetization vector, M, (blue arrow) is inverted by a 180° pulse followed by a an interval τ where the nucleus undergoes partial spin-lattice relaxation. This is followed by a 90° pulse which rotates M into the XY plane. The free induction decay is then acquired and Fourier transformed to determine the peak intensities for the various τ. (A) The vector representation of M during the pulse sequence. (B) The pulse sequence. (C) Observed peak intensity as a function of the delay (τ).

the viscosity of the solution. The intrinsic viscosity is the value in the zero limit of the polymer concentration :

$$[\eta] = \lim_{\rho \to 0} \left[\frac{1}{\rho} \frac{\eta - \eta_0}{\eta_0} \right] \tag{3.29}$$

where ρ is the concentration of the dendrimer and η_0 and η are the viscosity of the pure solvent and the viscosity of the solution respectively.

In the literature, several methods have been employed to calculate the viscosity based on a single average conformation of a polymer. [25,30,32,34,126,183,184] More precisely, most of these methods are used to calculate the size of the dendrimer based on measured $[\eta]$. However, the simplest means to calculate $[\eta]$ is to assume that the dendrimer is a rigid, non-interacting, non-draining spherical polymer which can be represented by an equivalent impermeable hydrodynamic sphere of radius R_h and then apply the Einstein, Flory-Fox or Mark-Houwink equations. [183] However, this approach is error prone especially for branched polymers. [183] A more sophisticated popular approach to calculate $[\eta]$ for dendrimers is in terms of a hydrodynamic tensor. [30] Mansfield and Klushin used this approach to defined both the upper bound and lower bound limits of $[\eta]$ for a dendrimer (the Zimm and Fixmann relations respectively). [30] Here, the dendrimer is described in terms of identical hydrodynamic beads representing segments of the dendrimer. After calculating the preaveraged hydrodynamic interaction tensor and $[\eta]$, the overall hydrodynamic radius of the dendrimer, R_η, is evaluated as follows:

$$[\eta] = \frac{10\pi}{3} \frac{R_\eta^3}{M} \tag{3.30}$$

where M is the molecular mass of the dendrimer and is often used in reverse, i.e., determine R_η from measured $[\eta]$ values. [120] This model is essentially the Rouse-Zimm or "bead per residue" approach. [185] Representing segments of the dendrimer as hydrodynamic beads is useful in that they radically reduce the complexity of the tensor. Additionally, the implementation of the Rotne-Prager tensor reduces inaccuracies of overlapping beads. [185] Mansfield and Klushin explicitly avoid overlapping beads by strictly enforcing excluded volume repulsions. [30] However, there are several disadvantages to this approach. The performance of the bead per residue approach to calculate the intrinsic viscosities is not well understood. [185] Further, by explicitly excluding overlapping beads, bias is introduced into the selection of the conformation of the dendrimer that is used in the calculation instead of using an average equilibrated conformation. In addition, the model

implements a single type of bead to describe every segment of the dendrimer. Therefore, the radius of this generic bead has to be carefully selected to adequately represent all types of segments within the dendrimer. Further, distortions of the shape of a bead depending on its unique environment is not considered in this model. The result is that the atomic detail of the polymer is lost. Finally, Cai and Cheng showed that the simplification of replacing the hydrodynamic tensor of each frame of the MD trajectory with the ensemble average leads to overestimation of $[\eta]$. [33] To avoid these difficulties and uncertainties associated with calculated the hydrodynamic radius, in this thesis, we employ a slightly different approach: the radius of hydration is calculated from the dendrimer's diffusion coefficient by employing the Stoke-Einstein relation (3.3).

In this thesis we make use of each analytical method detailed in this chapter to describe the structure and dynamics of each system in question. However, the true power of these techniques becomes evident when they are used conjunction with one another. This allows us to draw relationships between the structural and dynamical properties of the system. In the chapters that follow, we adopt this approach where possible, to enhance our understanding of each system modelled.

Chapter 4

Force Field Parameterization and Validation

4.1 Introduction

Computer simulations of solvated polymer systems are substantially more complex than the corresponding simulations in vacuum. The size of the solvated system (number of atoms) dwarfs that of the vacuum system. Complications arise when inaccuracies or small errors that may have gone undetected in the vacuum systems accumulate and increase proportional to the number of atoms in the solvated system thereby producing a significant source of error which will severely affect the accuracy of the system. Examples of such inaccuracies include small rounding errors, poorly selected convergence criteria and integration step size, inappropriate method for truncating long range interactions especially in charged systems or the use of an ineffective method for integrating the equations of motion. These can all contribute to the non-conservation of energy within the simulated system. [135] Additionally, there are complex issues arising from the competing forces at play in the solvated system, i.e., solvent-solvent and solute-solute interactions competing with the solvent-solute interactions. [128, 183] Hence, prior to simulating a solvated polymer system, it is essential that both the solvent and polymer models are valid and the combination of the solvent and dendrimer force fields used to describe the solution environment is also valid.

Solvent Parameterization There are a number of methods used to describe the solvent in macromolecular force field simulations. In dendrimer simulations, a common means of accounting for solvent effects is to represent the solvent implicitly, for example through a continuum solvent model. [44] A method to model an infinitely good solvent environment in a vacuum simulation is to apply a purely repulsive Lennard-Jones potential. [44,54] In addition, a frictional coefficient in combination with a stochastic interaction term can be added to the equations of motion. These terms can be manipulated to change the effective solvent quality without explicitly including solvent particles. This process is in essence replacing standard MD with Langevin MD. [44,135] Computer simulations of dendrimers in vacuum or in continuum solvent models have proved very popular because the computational requirements are significantly less than if the solvent is explicitly included. [135] However, the accuracy of continuum models are debatable. [135] The alternative approach is to explicitly include the solvent molecules, using either the unified atom or the all-atom approach (Section 2.2.1). Until recently, condensed phase polymer simulations have not been feasible without the use of super-computing facilities. Rapid increases in computational speed and capacity of data storage devices has moved the use of explicit solvent models in condensed phase computer simulations from the exotic to standard practice. While reliable water models are in routine use for the simulation of biopolymers, the development of equally reliable solvent models for the simulation of organic and inorganic solutions continues.

The aim of this thesis is to determine the behaviour of dendrimers in solution. This includes the folding of a dendrimer, which requires the simulation of dendrimers in an explicit poor solvent environment. Fréchet dendrimers are soluble in a range of solvents with varying degrees of solubility. [118,186] Four solvent environments are studied in this thesis: vacuum, water, chloroform and tetrahydrofuran (THF).

Vacuum simulations of Fréchet dendrimers [2] are representative of an implicitly poor solvent environment and in this thesis are used as the basis from which to compare existing work reported in literature. Water can be considered to be an explicitly poor solvent environment, on the basis of solubility parameters. A solute with a solubility parameter of δ_p is described as being insoluble in a solvent with a solubility parameter δ_s if $(\delta_s - \delta_p)^2 < 4$. [187] Jeong et al. suggested a Fréchet dendrimer has a δ_p between 18.2 and 18.4MPa$^{1/2}$. [118] Water has a δ_s of 47.9MPa$^{1/2}$. The difference of the solubility parameters of the Fréchet dendrimer and water far exceeds the limit stated above. In addition, polystyrene,

which is often used as to represent the linear analogue of Fréchet dendrimers, is extremely insoluble in water and further confirms that water is a poor solvent for Fréchet dendrimers. We selected Jorgensen's TIP3P model for our water simulations because the original force field from which our dendrimer force field was derived was specifically parameterized for TIP3P (see Chapter 2 for a discussion of the various water models available).

The selection of a good solvent suitable for the simulation of large macromolecular systems is based on several criteria:

1. The macromolecule must be readily soluble in the solvent.
2. It is preferable if the solvent is commonly used for analytical measurements.
3. A simple molecular mechanics force field should be able to accurately represent the solvent.
4. The solvent and polymer models should be of the same functional form.
5. Experimental data must be available to validate the solvent model.

Chloroform and THF represent good solvents as they both meet the criteria listed above; Fréchet dendrimers readily dissolve in chloroform and chloroform's deuterated isotopomer is the analytical solvent of choice for NMR measurements of these dendrimers; THF is used as a solvent medium in the synthesis [4] and viscosimetric measurements [118,120] of Fréchet dendrimers. However, from viscometric measurements it appears that the folded structure of Fréchet dendrimers in these two solvents differs significantly and the reason for this is not clearly understood. [118] It has been suggested that THF is a superior solvent to chloroform for Fréchet dendrimers and that these dendrimers remain unfolded in THF and fold in chloroform. [118] However, this seems unlikely considering the similarity of the chemical and physical properties of the chloroform and THF, particularly their solubility parameters (19.0 and 18.6 $MPa^{1/2}$ respectively). MD simulations of the dendrimers in these two solvents could provide clarity in this regard. However, it is important to first detail the characteristics of the chloroform and THF and establish any differences between the pure solvents. Any significant differences in the behaviour of the pure solvents could account for the differences in the behaviour of the dendrimer solvated in THF and chloroform. Therefore, this thesis begins with MD analysis of suitable chloroform and THF force field models in which to model Fréchet dendrimers.

There have been numerous computational studies of liquid chloroform, ranging from the Reference Interaction Site Model (RISM), [188] MD [189–196] and MC simulations, [197, 198] to hybrid QM/MC simulations. [199] As a result, there are numerous empirical models available, mostly variations of the five-site rigid model (where all five atoms are included) or of the fully relaxed four-site unified atom model (where the proton is absorbed into the carbon atom to form a new CH "atom"). However, some of these models do not compare favourably with experimental results [200] and the use of a rigid geometry or the use of a four-atom CH united atom model has limitations. [196] A detailed review of available literature yielded no appropriate model for a fully relaxed five-site representation of chloroform. Hence, we developed a fully relaxed all atom model for chloroform by combining several existing models which is described Section 4.2.2.

For THF there exist several simple force fields, including united-atom and all-atom models, along with limited experimental data. [201] Girard and Müller-Plathe recently applied the simplex optimization algorithm [202] to refine several popular THF models so that they more closely reproduced experimental data. [201] For our investigation we considered the best of the full atom and united atom models. The advantage of a united-atom model in this case was clear: the number of atoms would be halved which would result in a substantial reduction in the number of intramolecular bond stretch and angle bending calculations and intermolecular interactions resulting a significant gain in computational speed. In addition, the use of a CH_2 united atom in place of explicitly modelled hydrogen atoms does not significantly change the overall shape or dynamics of the molecule. We selected Girard and Müller-Plathe's modified Helfrich-Hentschke united atom model [127] to represent THF as it gave the closest overall match with experimental data, including the full atom models and is analysed in detail in Section 4.2.3.

Dendrimer Parameterization The majority of dendrimer computer simulations have been performed using course-grained models, with relatively few atomistic level simulations reported for dendrimers. [8] . A variety of force fields have been utilized in the atomistic simulations, including CHARMM, [133] AMBER, [130] MM3, [146] Dreiding [203] and CVFF [147]. The majority of these force fields were employed "as is" and were not specifically modified to ensure accurate representation of the dendrimer. We use a CHARMM-like force field developed in our laboratory specifically for accurate representation of poly (benzyl phenyl ether) dendrimers. [2, 10] This force field was derived

from the protein force field published by MacKerell and co-workers. [204] The advantage of basing the dendrimer model on an existing force field is that the parent force field has been through several iterations of development and testing and has been widely used. Therefore, the likelihood of such an extensively tested force field producing any abnormal or unrealistic behaviour is significantly reduced. Hughes et al. identified the ether linkage connecting the aromatic rings of the dendrimer as the most important factor affecting the rigidity and overall conformation of the dendrimer. [10] More specifically, they identified the central torsion angle of this ether linkage as the principle factor in determining the degree to which back-folding may occur in a dendrimer. Therefore, Hughes et al. focused their attention on this torsion angle and through extensive modelling obtained a good match with the equivalent *ab initio* profile. However, our investigations showed that further parameterization of the ether linkage was necessary and is the focus of Section 4.3 of this chapter.

Solution Parameterization Once the solvent and solute force fields have been independently tested and validated they are combined to produce the solute force field. When combining the two force fields it is necessary to ensure the interaction strengths between the most important structural elements in the molecular system (such as aromatic rings of the dendrimer and a methylene group of THF) are of comparable strength with the equivalent quantum mechanically or experimentally derived values. Benzene was selected as the representative functional group of the dendrimer. Since aryl rings comprise over 70% of the mass of the dendrimer, we are confident that benzene is a good representative of the dendrimer. An advantage of using benzene as the representative unit of the dendrimer as opposed to an alternative model unit (for example benzyl alcohol), is the wealth of related QM data that exists in literature for benzene. These include studies of the interactions of benzene with chloroform, methane, ethers and water. [205–207] Thus, we were able to source from literature independent, high level quantum mechanical interaction strengths involving benzene in our systems.

However, it is not only important that the interaction strengths in the force field are of the correct magnitude, it is important that the sequence of the interactions arranged according to their strengths (i.e., from weakest to strongest) are the same for MM and QM series. If the MM and QM series differ, the validity of the MM simulation is questionable. The following example illustrates the point: S_i and P_j represent the i^{th} solvent structural

entity (for example CH_2 of THF) and the j^{th} polymer structural entity (for example the aryl ring of the dendrimer) respectively. S_iS_i, P_jP_j and S_iP_j are the strengths of the solvent-solvent, polymer-polymer and solvent-polymer interactions respectively. If the QM-derived interaction strengths are in the following order, $P_jP_j > S_iS_i > P_jSi$, then it is likely that the folded conformation will be preferred as the homogeneous interactions (P_jP_j and S_iS_i) are stronger than the non-homogeneous interactions P_jS_i. However, if the equivalent MM interaction strengths were in the opposite order $P_jP_j < S_iS_i < P_jS_i$ then it is likely that the unfolded conformation will be preferred in the force field simulations because the homogeneous interactions (P_jP_j and S_iS_i) are weaker than the non-homogeneous interactions P_jS_i. Therefore, the outcome of the force field simulation will be invalid. Note that this is the *likely* outcome; only enthalpic contributions have been considered and entropic contributions, such as the number of possible arrangements, have not been accounted for. [183] Secondly, addition factors such as the shape of the minima (the breadth of the energy well) has not been considered. However, by considering the magnitudes and the order of the interaction strengths, it is possible to identify the most significant sources of error. This is discussed in more detail in Section 4.4.

Factors that are used to describe the simulation environment can also affect the outcome of the simulation. These include the temperature of the simulation, the method for treating long range non-bonded interactions and the ensemble sampled during the simulations. In Section 4.4.1 we investigate the effects that such factors have on the outcome of the simulation.

In this chapter we begin with a description of the development of a novel chloroform model suitable for our simulation requirements. This includes a brief discussion of both the intra- and intermolecular structural and dynamical details of chloroform and a review of existing force field models. This is followed by a description of the development of the new chloroform model and detailed structural (PDF, SDF and Voronoi analysis) and dynamical analysis (diffusion coefficients and rotational relaxation times) including comparisons with experimental data where possible. Thereafter, we discuss the THF model employed in this thesis. As we did not develop this model, we focus on the novel structural analysis of THF that we performed and compare with those of chloroform, in particular SDF and Voronoi analysis. Thereafter we discuss the parameterization of the dendrimer ether linkage. The analysis of the combination of the solvent and solute force fields follows. The chapter closes with a detailed look at simulation variables other than the force field that could affect the

overall conformation of the dendrimer, including factors such as temperature, ensemble sampling methods, integration time step, methods for handling long range interactions and periodic boundary conditions among others.

4.2 Solvent Parameterization

In this section we investigate the two good solvents used in this thesis, namely chloroform and THF. The MD simulation methods employed for both solvents were essentially identical, the details of which and the analytical methods employed are described in the following section:

4.2.1 Simulation conditions

The CHARMM program was used for all simulations. [133] Chloroform was simulated in a cubic box of 65.34 Å containing 2112 chloroform molecules positioned in a regular cubic lattice (density 1.489 g.cm^{-3}) that was minimized to reduce any unfavourable interactions. THF was simulated in a 46.1 Å cubic box containing 729 molecules at 293.15 K (density 0.899 g.cm^{-3}). Each system was heated to 293.15 K with 5 K increments every 10 ps by scaling the velocities and equilibrated at this temperature for the remainder of 200 ps. Data was collected over 1ns, performed using the micro-canonical ensemble (NVE). For all stages of the simulation, the Leapfrog integrator with a time step of 1fs was employed and periodic boundary conditions invoked. [134] The covalent bonds between hydrogen and carbon in chloroform were restrained with the SHAKE algorithm. [134] Non-bonded interactions were truncated using a switching function applied on a neutral group basis between 10.00 and 12.00 Å.

Analysis of each solvent's structure, in particular their coordination shells, and dynamics was conducted over the final 200 ps of each simulation. PDF, SDF and Voronoi analysis of each solvent were calculated with computer software packages written within our research group. [166, 175] The diffusion coefficient of each solvent was calculated for the average of the mean square displacement (MSD) of the centre of mass for all the solvent molecules using the Einstein relation (see Section 3.4, Equation (3.18)). Relaxation times ($\tau_{c,l}$) for chloroform were calculated using the C-H bond as the molecular reference vector (Section 3.4.2).

4.2.2 Chloroform

Chloroform is a simple yet versatile solvent and has been the topic of numerous studies detailing its inter- and intramolecular static, dynamic, chemical and physical properties. [189] Interest in this solvent is due not only to the synthetic applications of chloroform but also its wide use as an multi-purpose analytical solvent. Chloroform has a relatively small dipole moment (Table 4.1) and a belongs to the C_{3v} symmetry group. Together, these characteristics give chloroform the rare analytical property of approaching an Einstein sphere (a non-associating spherical solvent) which affords some unique structural and dynamical properties.

solvent	dipole moment, D
benzene	0.0
chloroform	1.15
THF	1.63
methanol	1.70
water	1.87

Table 4.1: Dipole moments of some common solvents

The structure of liquid chloroform has been extensively detailed in a series of small angle neutron and X-ray scattering experiments, published in the late 1970's and early 1980's by Bertagnolli, Zeidler, Leicht and Chieux. [208–212] Chloroform's molecular symmetry (termed a symmetric top) significantly simplified the experimental structure determination, since its scattering patterns are less complicated than similar molecules with lower symmetry. Chloroform's symmetry also makes the determination of chloroform's rotational correlation times simpler. [182] The scattering patterns are further simplified by the large difference in the coherent scattering lengths of the ^{35}Cl and ^{37}Cl isotopes, which result in appreciable differences between the neutron-diffraction patterns for isotopically enriched chloroform samples. [208] Bertagnolli and co-workers reported in detail the inter- and intramolecular structure of liquid chloroform, including molecular orientation and pair correlation functions. [208–212] The authors showed, among other results, that the head-to-tail ($HCCl_3 \cdots HCCl_3$), or parallel orientation of chloroform dimers is not favoured and that a series of head-to-head ($Cl_3CH \cdots HCCl_3$) and tail-to-tail orientations ($HCCl_3 \cdots Cl_3CH$) are preferred. More recently, Takahashi, Yano and Iijima performed

energy-dispersive X-ray diffraction studies of liquid chloroform and confirmed the lack of long range structure of chloroform. [213] They also suggested a nearest-neighbour distance (5.1 Å) slightly longer than reported by Bertagnolli and co-workers (4.8Å).

The dynamic behaviour of chloroform has been investigated via classic rheology and NMR-PFG SD measurements, [182,189,214] while the relaxation behaviour of chloroform has been studied in great detail by numerous spectroscopic techniques including infrared, Raman and Rayleigh scattering and NMR. [182,189,215]

The chloroform model that we required should be appropriate for investigating the solvated structural, dynamical and folding properties of neutral macromolecules (with negligible overall dipole moments), which require long simulation times (in the order of nanoseconds). Therefore, it is essential that not only does the model accurately represent the physical, dynamical and chemical properties of the solvent but is as simple as possible in order to maximize the sampling time. It has been shown that the local structure of chloroform is primarily a result of packing or steric effects. Thus it can be regarded as a normal non-associating liquid. [188] For this reason, it has been found that simple MM force fields are effective in modelling chloroform; features based primarily on quantum effects, such as electron donor-acceptor terms or polarization models, have been found to be unnecessary. Nevertheless, there have been models developed which include these effects. Examples include the hybrid QM/MM study by Luque et al. [199] (and their subsequent development of a self consistent reaction field model (SCRF) for chloroform) and the polarizable potential of Chang and Dang [192,193]. However, the contribution of the polarization energy to the total interaction energy was reported by Chang et al. to be relatively insignificant. The authors concluded that bulk properties of liquid $CHCl_3$ could be adequately reproduced by considering only Lennard-Jones interactions. They did suggest that the polarizable potential may be a significant factor in heterogeneous environments such as vapour-liquid interfaces. For charged solutes (with particular reference to ions) the authors noted the effect of polarization was appreciable. Luque et al. confirmed the polarization effect of chloroform on small solute molecules where they observed a small yet non-negligible increase in the dipole of a small solute molecule. [199]

Several simpler empirical models for chloroform exist of the same functional form used to describe the dendrimer model. [189,196,197] A summary of these models is listed in Table 4.2. However, in order to permit longer simulation times, these models are either rigid models or united atom models or both. The use of a rigid geometry or a united atom

Non-bonded terms									
Model	ϵ_C	ϵ_{Cl}	ϵ_H	q_C	q_{Cl}	q_H	σ_C	σ_{Cl}	σ_H
Evans [216]	0.087	0.300	0.023	0.131	-0.063	0.056	3.20	3.50	2.75
Kovacs et al. [191]	0.087	0.300	0.023	0.32	-0.14	0.10	3.20	3.50	2.75
Chang et al. [192]	0.137	0.275	0.020	0.5609	-0.1686	-0.0551	3.41	3.45	2.81
Gratias et al. [190]	0.080	0.300	-	0.420	-0.140	-	3.800	3.470	-
Dietz et al. [194]	0.102	0.299	0.0198	0.179	-0.087	-0.052	3.40	3.44	2.2

Bond terms				
Model	$K_{b(C-Cl)}$	$b_{0(C-Cl)}$	$K_{b(C-H)}$	$b_{0(C-H)}$
Evans [216]	-	1.758	-	1.100
Kovacs et al. [191]	-	1.758	-	1.100
Chang et al. [192]	-	1.76	-	1.07
Gratias et al. [190]	314.0	1.758	-	1.100
Dietz et al. [194]	-	1.758	-	1.100

Angle terms					
Model	$K_{\theta(H-C-Cl)}$	$\theta_{0(H-C-Cl)}$	$K_{\theta(Cl-C-Cl)}$	$\theta_{0(Cl-C-Cl)}$	Type
Evans [216]	-	107.47	-	111.3	A, R
Kovacs et al. [191]	-	107.47	-	111.3	A, R
Chang et al. [192]	-	107.6	-	111.2	A, R, P
Gratias et al. [190]	-	-	85.0	111.3	U, F
Dietz et al. [194]		107.47	-	111.3	A, R

Table 4.2: Bonded and non-bonded parameters for existing chloroform force fields. The three values reported in the Non-bonded terms section of the table are ϵ/kcal.mol^{-1}, R_{min}/Å and q/e. The Bond Terms section's values are K_b/kcal.mol^{-1}Å^2 and b_0/Å. The units in the Angle terms section of the table are K_θ/kcal.mol^{-1}deg^2 and θ_0/deg. The Type column denotes whether the model is rigid (R) or flexible (F), united atom (U) or all atom (A) model and includes polarizable (P) details. Only models that use a 6-12 Lennard-Jones potential (the same functional form as the dendrimer force field) are considered. Therefore, models such as Böhm and Ahlrichs' exp-6-1 model are not included.

model has limitations [196] and in order to obtain the most realistic behaviour possible for the solvent model, in particular one used in conjunction with a fully relaxed all atom polymer force field, it is desirable to remove as many constraints from the solvent model as possible. As no single chloroform model met our simulation requirements, we developed a fully relaxed all atom chloroform model by combining several existing models.

Description of the new chloroform model

From the available chloroform models, we selected the Dietz and Heinzinger's rigid five-site chloroform model [194] as the basis of our flexible model as it closely matches available experimental data, both static and dynamic properties, while employing a simple potential to model non-bonded interactions. [196] Their model employs partial charges centred on the atom positions and non-bonded interactions modelled by an effective pair potential consisting of 6-12 Lennard-Jones and Coulomb terms. Their non-bonded Lennard-Jones

and partial charge parameters were supplemented by intramolecular parameters for the relevant bond stretch and bond-angle bending interactions. These intramolecular parameters were obtained from existing chloroform force fields as well as from similar structural elements available in the CHARMM force field. [133, 190, 191, 194] Both the bonded and non-bonded parameters are listed in Table 4.2.2. Energies associated with distortions of improper dihedral angles were unnecessary since the symmetric top symmetry is easily maintained by the other parameters.

Non-bonded terms			
site	ϵ/kcal.mol^{-1}	R_{min}/Å	q/e
C	-0.102	1.908	0.32
Cl	-0.299	1.964	-0.14
H	-0.0198	1.543	0.10
Bonded terms			
bond	K_b/kcal.mol^{-1}Å^2		b_0/Å
C-Cl	314.0		1.758
C-H	340.0		1.100
angle	K_θ/kcal.mol^{-1}deg^2		θ_0/deg
H-C-Cl	46.0		107.47
Cl-C-Cl	100.0		111.30

Table 4.3: Bonded and non-bonded parameters for the new chloroform model. This is based on the Dietz and Heinzinger five-site rigid model, [194] modified by Kovacs et al. [191] We extended their model by including the relaxation constants derived from similar terms in other force fields. [133, 190]

Analysis of the new chloroform model

Despite the parameters being sourced from several different force fields including extended and united atom models, this model was independently tested by another group [217] who confirmed that our new model offers the closest match of available models to experimental values, including diffusion coefficients, density (1.46gcm^{-3}) and dielectric constant (4.3). Furthermore, the dipole moment of 1.10D is in good agreement with the gas-phase value of 1.01D (see Böhm [195] and the references there in). To fully characterise the structure

of the chloroform liquid we calculate the pair and spatial distribution functions to describe the arrangement of the solvent and compare with X-ray and neutron scattering data. We use Voronoi analysis to analytically describe the geometric characteristics of the solvent's structure. For the dynamical properties, we calculate the rotational correlation times and the diffusion coefficient of chloroform which we compare with NMR, infra-red and Raman spectroscopic data from literature. We found the following:

Structural Properties The calculated PDFs illustrated in Figure 4.1 correspond well with neutron scattering data. [210,212]. The slight differences between the computed and experimental data are within error limits attributable to both techniques. [194, 195] The PDFs quantitatively match those reported by Kovacs et al. [191] and Chang et al. [192] The first coordination shell represented by the $g_{C-C}(r)$ peak, centred at 5.45 Å, is larger than the experimental value of 4.8 Å reported by Bertagonolli and co-workers, [210] yet more closely matches the value of 5.1 Å reported by Takahashi et al. [213] This peak at 5.45 Å is very broad and includes a slight shoulder at 4.8 Å which was also observed by Kovacs and co-workers. [191] This shoulder suggests that at least 2 orientations are favourable in the first solvation shell. From a comparison of these PDFs it is possible to speculate on the relative orientation of the chloroform molecules in the first solvation shell. The two most important arrangements for a chloroform dimer are the parallel and anti-parallel arrangements (Figure 4.2).

In the chloroform PDFs it appears that the anti-parallel orientation is favoured. The first maximum of $g_{Cl-Cl}(r)$ (3.75 Å) in combination with that of $g_{H-H}(r)$ (5.1 Å) suggest that the tail-to-tail orientation ($HCCl_3 \cdots Cl_3CH$) is more likely than the head-to-head orientation ($Cl_3CH \cdots HCCl_3$). A small $g_{Cl-H}(r)$ peak at 3.2 Å suggests that the parallel orientation is possible although it is less favourable as the orientation associated with the second $g_{Cl-H}(r)$ peak (5.65 Å). Excluding $g_{C-C}(r)$, there is no long range ordering in the other PDF profiles. This is agreement with the findings of scattering data. [213]

Spatially averaged distributions functions (SDF) present a clearer representation of the solvent structure about a central solvent molecule (from here on referred to as the "solute" molecule). Bertagnolli, Goller and Zweier [197] calculated isodensity contours in their MC study of chloroform. However, this form of representation of the solvation of chloroform has not previously been reported for MD simulations. We interpret the position of the SDFs relative to the solute molecule using a spherical polar coordinate system (r, θ and

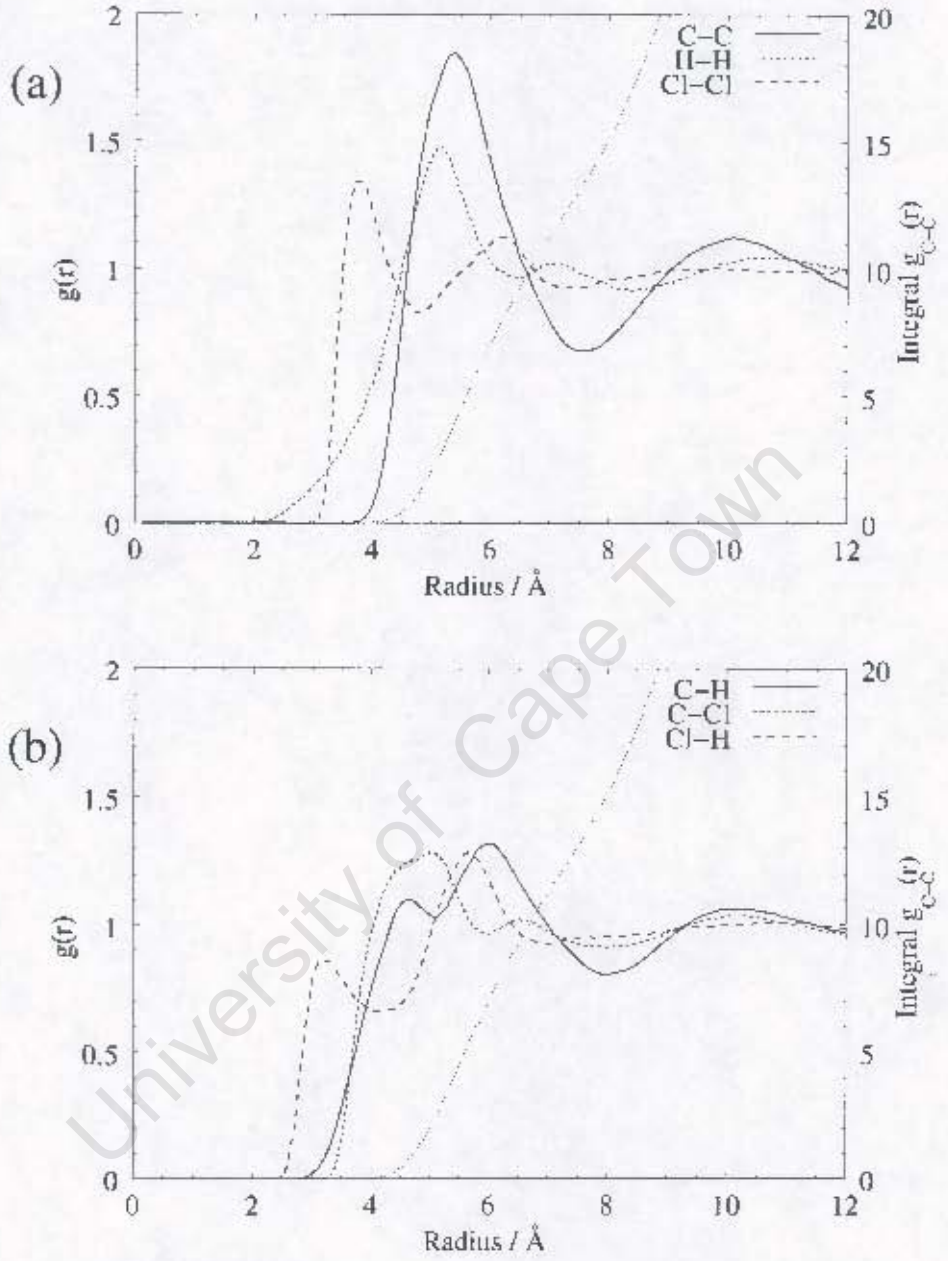

Figure 4.1: Pair correlations functions of the new chloroform model. The non-cross terms are represented in part (a) while the cross terms are shown in part (b). As the carbon atom in chloroform is a useful physical indicator of the approximate centre of mass of the molecule, the integral of $g_{C-C}(r)$, represented by the dotted line in both cases, indicates the average number of chloroform molecules that lie with their centre of mass within a shell of radius r from a central chloroform molecule.

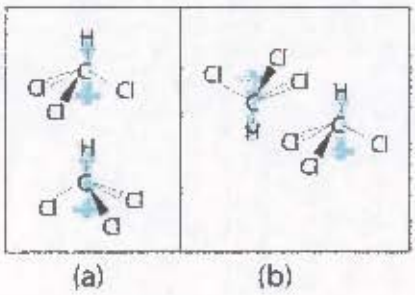

Figure 4.2: The two principal arrangements for a chloroform dimer are the (a) parallel and (b) anti-parallel arrangements. The terms parallel and anti-parallel refer to the relative alignment of the dipole moments of each molecule. Dipole moments are indicated by indicated by the watermark arrows.

ϕ) (Figure 4.3).

The results from our spatially averaged distributions of chloroform (Figure 4.4) are qualitatively similar to Bertagnolli's study. However, additional information is evident from our series of SDFs. In particular, there are two distinct components of the first solvation shell (Figure 4.4): a "strongly bound" shell visible at 50% above bulk density and a "weakly bound" shell visible at 25% above bulk density.

The "strongly bound" region of the first solvation shell encapsulates the solute chloroform molecule in a staggered conformation, bisecting the angle between the chlorine atoms, i.e., at $\phi = 60°, 180°$ and $240°$. Seven molecules form this strongly coordinated shell. This is in excellent agreement with experimental data suggesting the first solvation shell consists of between 6 and 8 nearest neighbours. [208, 213]

Three coordinating molecules form a plane at an acute angle of $\theta = 54°$, which lies above the solute hydrogen at r = 1.99Å. A further three molecules form a distorted plane with the solute chlorine atoms at r = 5.37Å and an average angle of $\theta = 115.5°$. The final coordinating molecule lies below the plane of the solute chlorine atoms at r = 4.81Å, slightly offset from the C_{3v} axis at $\theta = 170.0°$. In contrast, above the solute hydrogen atom ($\theta = 0°$) there is a notable void in the density distribution. This remains vacant even at very low probabilities, where the second solvation shell becomes visible (Figure 4.6). The result is a spherical asymmetrical solvent cage above and below the axis of symmetry. The asymmetry of the first solvation shell was also observed by Bertagnolli et al. [197] They concluded that the parallel orientation of $Cl_3CH \cdots Cl_3CH$ is not the preferred mode

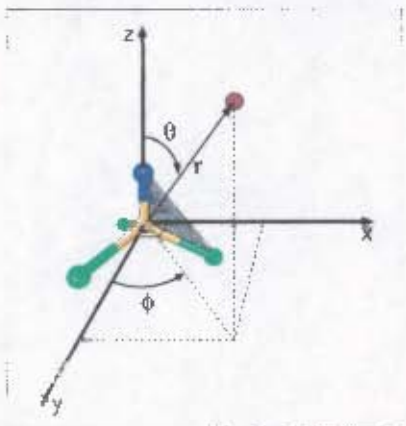

Figure 4.3: Coordinate system for orientation of neighbouring solvent molecules with respect to the solute chloroform. The C-H bond (and dipole moment) lies along the z-axis and one of the chlorine atoms lies in the XZ plane. The red sphere represents the carbon atom of the neighbouring chloroform molecule. r represents the distance between the two carbon atoms, θ is the angle formed between the proton and carbon of the reference molecule with the carbon atom of the neighbouring molecule and ϕ is the angle between the plane formed $H-C-C$ and the XZ plane, i.e., a quantitative measure of the degree to which the neighbouring molecule is in a staggered or eclipsed position relative to the reference molecule.

of association. Instead an anti-parallel orientation (Figure 4.5a) is more likely. Note that this is the strongest dipole-dipole interaction.

The orientation of the strongly bound solvent molecules relative to the solute becomes interpretable by including the hydrogen and chlorine isodensities (Figure 4.4b). In the case of the three molecules forming the acute plane with the solute C_{3v} axis, the chlorine isodensity surfaces line the interior of the carbon isodensities, with the hydrogen surfaces lining the exterior. Hence these solvent molecules are orientated with their dipole moments at an acute angle to that of the solute (Figure 4.5b). The orientation of the remaining four strongly bound molecules is less clear. The hydrogen and chlorine isodensities suggest there is no preferential alignment. Rather, a combination of orientations occurs; the enthalpically favoured anti-parallel orientation (Figure 4.5a) proposed by Bertagnolli [197] and a "diagonal orientation" (Figure 4.5b). In this diagonal arrangement, the symmetric top axis of a neighbouring chloroform molecule bisects the $Cl-C-H$ angle of the solute chloroform molecule. Idrisi recently showed similar results from MD simulations. [218] The author found that the anti-parallel conformation ($\theta = 170°$) is most probable at $r = 3.8$

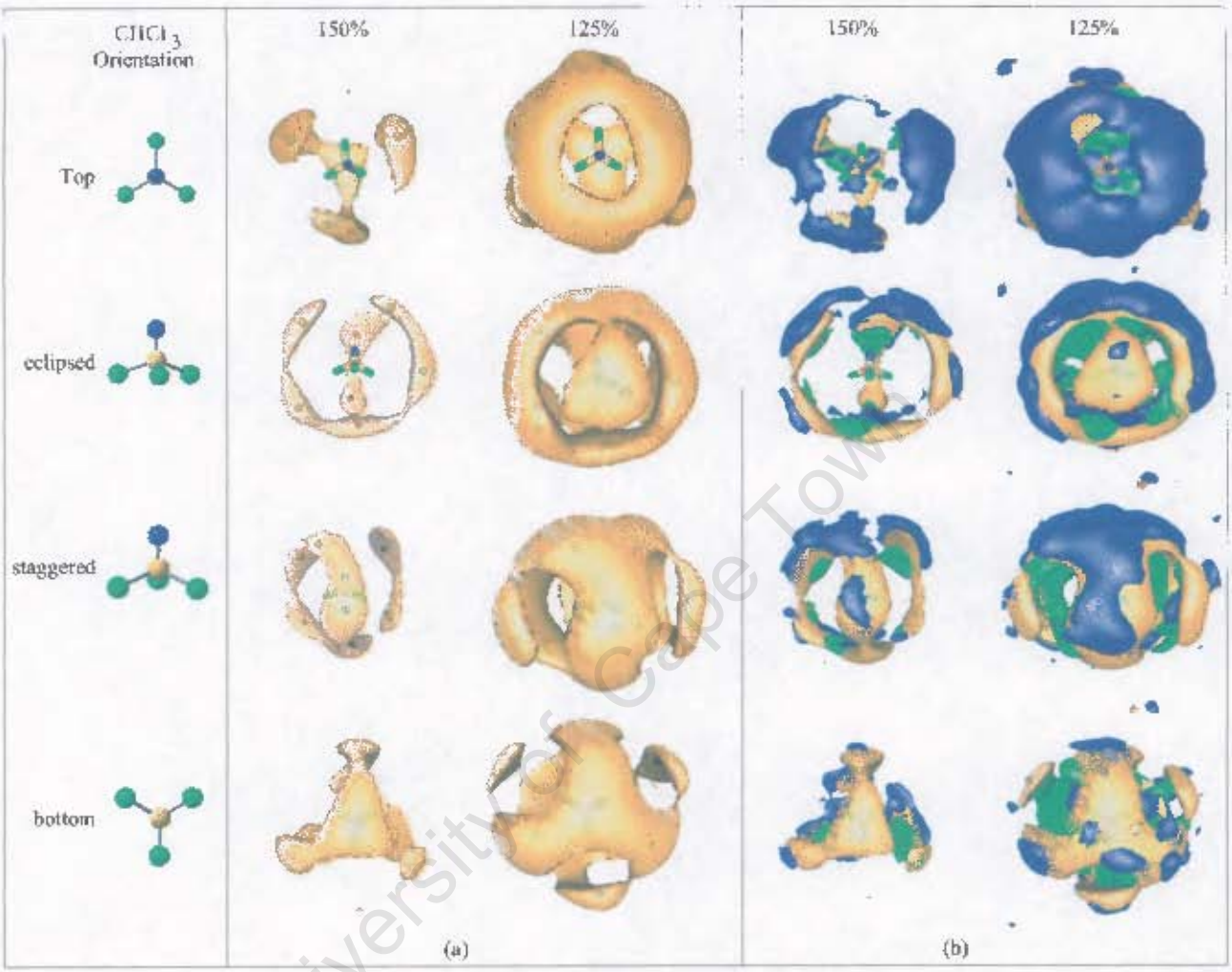

Figure 4.4: Spatially averaged density distributions for chloroform of (a) carbon only represent in yellow and (b) all atom types with chlorine represented in green and hydrogen in blue. For the carbon SDFs (a) black spheres representing the maxima within SDF (indicating the most likely position for a carbon atom) are included. "Top" ($\theta = 0°$) represents a view down the symmetry axis from the hydrogen atom, while "bottom" ($\theta = 180°$) is the view from chlorine atoms. The "staggered" view is perpendicular to the top axis ($\theta = 90°$), bisecting a $Cl - C - Cl$ angle ($\phi = 60°$) while the "eclipsed" view is directly in line with a chlorine atom ($\phi = 0°$). The probability level of each isodensity relative to bulk density is recorded above each column.

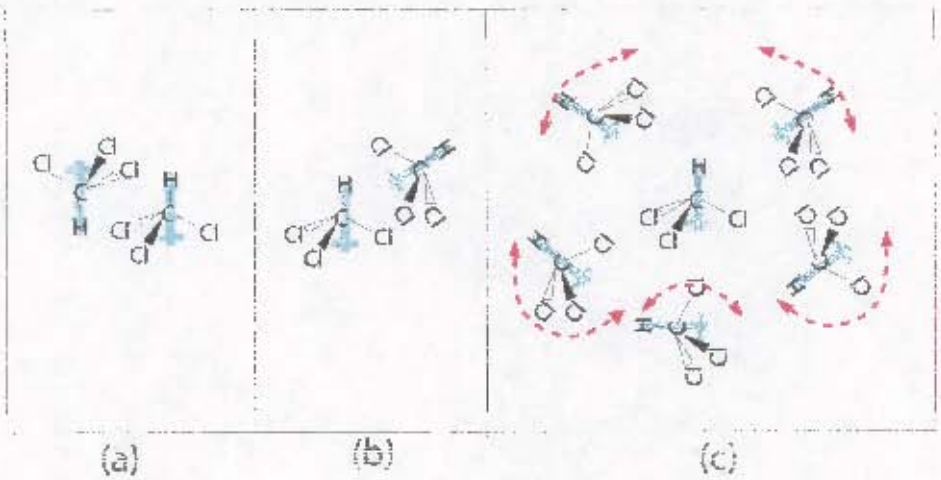

Figure 4.5: Orientation of the chloroform molecules.(a) represents Bertagnolli and co-workers most favourable anti-parallel configuration while (b) represents our proposed "diagonal alignment" and (c) represents the relative orientations of a slice through the strongly bound first solvation shell including suggested rotational modes of molecules to account for the isodensity distribution. Dipole moments are indicated by indicated by the watermark arrows.

and the 45° alignment up to 4.4 Å. [218] In this orientation the symmetric top axis through the solute chlorine atoms bisects the neighbouring chloroform's $Cl-C-H$ angle. This alignment seems likely considering the angular probability functions, $g(R,\Theta)$ reported by Bertagnolli, [197] where Θ represents the angle between two neighbouring molecule's C_{3v} axes. It was shown that the highest probability was found with Θ between 61° and 120°.

A suggested arrangement for a cluster of chloroform molecules representing a slice taken through the "strongly bound" region of the first solvation shell is illustrated in Figure 4.5(c). This arrangement is a combination of the "diagonal alignment" (Figure 4.5(b)) and the anti-parallel orientation proposed by Bertagnolli (Figure 4.5c). [197]

The "weakly bound" region of the first solvation shell comprises three chloroform molecules. These lie in eclipsed positions relative to the solute chlorine atoms at an average distance of $r = 6.33$ Å. These solvent molecules form a plane just below the solute carbon at $\theta = 100.3°$. The combination of the "strongly bound" and "weakly bound" shells account for the broad profile of the first solvation shell of $g_{C-C}(r)$. This is in good agreement with experimental data, which suggests a body centered cubic (BCC) arrangement of the first solvation shell at 6.24. [213] The "weakly bound" first solvation shell associates in a similar fashion to that seen for the strongly bound region. However,

in this case these profiles are not as well defined as the "strongly bound" regions, because the "weakly bound" molecules exhibit greater coordination freedom.

The second solvation shell (Figure 4.6) begins to appear at probabilities just above that of bulk. The average position of the maxima, at 10.14 Å, closely matches that of $g_{C-C}(r)$ (Figure 4.1). However, the second solvation shell clearly lacks significant order compared to that observed for the first solvation shell and no evidence of higher solvation shells was observed. This is in agreement with experimental observations. [213]

Figure 4.6: Chloroform's carbon isodensity surface at 10% above bulk density. (a) is a view down the symmetric axis from above the hydrogen atom while (b) is viewed perpendicular to the top axis bisecting one of $Cl-C-Cl$ angles.

Voronoi analysis is an additional analytical method used to geometrically characterise the solvent structure. [176] The size and shape of the polyhedra formed by the central molecule's nearest neighbours are indicative of the local intermolecular arrangement. From this purely geometrical approach, several properties of the polyhedra are available, including the volume (V), area (A), number of nearest neighbours (N), the local number density and asphericity (η, a quantitative measure of the distortion of the shape of a polyhedron from a sphere). Although this has been calculated for numerous solvents, [176] chloroform is a notable exception.

The values calculated for our chloroform model are detailed in Table 4.2.2 and in Figure 4.7 along with those of water, methanol, argon [176] which are included for comparative purposes. The similarities between argon (a reference non-associating liquid) and chloroform is striking. There is a distinct Gaussian distribution of the volumes of the polyhedra about the average. The relatively narrow distributions suggest only a single

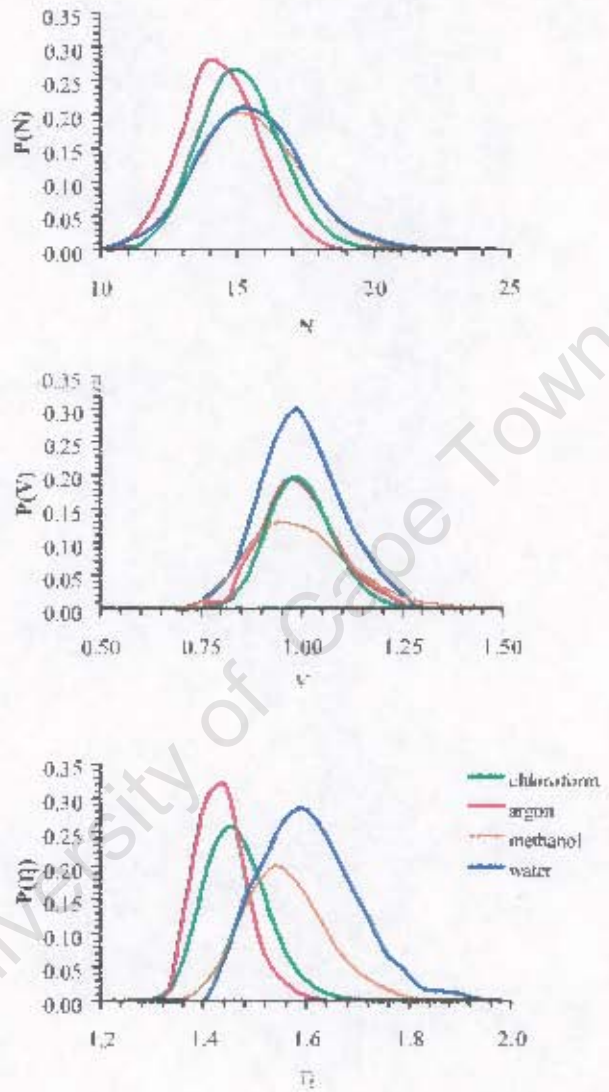

Figure 4.7: Probability distribution of the Voronoi properties for chloroform, argon, water and methanol. (A) Nearest neighbour, (B) polyhedra volume and (C) asphericity parameters. Values for chloroform were calculated from our MD simulations while argon, water and methanol are taken from Jedlovsky [176]

Solvent	η	N	V /Å^3
Chloroform	1.47 ± 0.06	14.61 ± 1.47	133.34 ± 10.87
Argon	1.44 ± 0.05	14.46 ± 1.34	47.58 ± 4.27
Water	1.61 ± 0.10	15.06 ± 1.81	27.80 ± 2.64
Methanol	1.74 ± 0.13	15.53 ± 1.97	66.23 ± 10.73

Table 4.4: Mean values and standard deviation of the averages of some of the properties of Voronoi polyhedra for chloroform and some comparative solvent systems.

type of polyhedron is present. In comparison, the hydrogen-bonded systems (water and methanol), where there are chain and branched-chain networks, have asymmetrical distributions. As η and number of nearest neighbours (N) are almost equal for chloroform and argon it suggests that the shape of the solvent structure about a central solvent molecule (or atom in the case of argon) for these systems are identical. This confirms that our model effectively behaves as a non-associating sphere, as is suggested from experimental evidence. [176]

Dynamic properties To test the dynamic behaviour of our new model, a comparison was made with reported self diffusion coefficients of chloroform obtained from NMR measurements and from existing computational models.

The diffusion coefficients for chloroform are listed in Table 4.5. There is some discrepancy within the literature, not only between the calculated values but also between the experimental values. The average of the NMR-PFGSD measurements suggest that the diffusion is of the order of 2.4 cm^2s^{-1}. [182, 195, 214, 219–221] In comparison to the other models, the value predicted by our model is close to the experimental values. Our model predicts a diffusion coefficient of 2.57 $cm^2.s^{-1}$ which differs from the average experimental value (2.44 $cm^2.s^{-1}$) by only 5.3%. This is within acceptable limits, especially when one considers the poor predictions of many models of other solvent systems. For example, some water models deviate from the experimental values by as much as 400% [153]

We further characterise the accuracy of our model through calculated reorientational behaviour in comparison with available experimental and computational data. Table 4.6 contains the relaxation times of our model in comparison to available experimental data and existing computational models. Evans has shown that, experimental data presented

Reference	T / K	D / $\times 10^{-9} m^2.s^{-1}$
Simulation		
Kovacs, Kowalewski and Laaksonen [191]	288	3.38
Evans [216]	293	4.00
Böhm and Alhrichs [195]	293	2.4
Chang and Dang [192]	298	3.5
Dietz and Heizinger [194]	295	2.6
Tironi et al. [196]	295	2.5
This work	**293**	**2.57**
Measured		
Kovacs, Kowalewski and Maliniak [182]	298	2.45
Böhm and Alhrichs [195]	293	2.37
Bender and Zeidler [219]	293	2.32
Bartusseck [220]	295	2.26
Sandhu [214]	295	2.8

Table 4.5: Comparison of self-diffusion coefficients (D) from both simulation and experimental methods at a variety of temperatures (T).

contradictory evidence about the nature of the relaxation modes and also highlighted the large differences of the reported data for both the first- and second-rank orientational autocorrelation functions. [189] However, the most recent experimental evidence suggests that the situation is no longer quite as unclear. [191] Our model lends support for a shorter tumbling relaxation than a spinning relaxation. More importantly, our model presented here offers the best overall agreement with the available experimental data. [182, 189, 215, 219]

4.2.3 Tetrahydrofuran (THF)

There are two principal conformations for THF: envelope and twist (Figure 4.8). [222, 223] The twist conformation is the lowest in energy. [222, 223] Due to ring puckering and subsequent conformational changes, the average structure of a THF molecule during MD or MC simulations is planar. [224] The result is that a C_{2v} symmetry axis is created through which the average dipole moment passes. This is illustrated in Figure 4.9, where we define

Simulation					
Reference	Temp / K	$\tau_1(z)$ / ps	$\tau_1(xy)$ / ps	$\tau_2(z)$ / ps	$\tau_2(xy)$ / ps
Böhm and Ahlrichs [195]	293	-	-	1.3	1.65
Evans [189]	293	3.6	-	1.3	1.5
Dietz and Heinzinger [194]	293	3.6	3.8	1.2	1.3
Kovacs et al. [196]	293	4.9	5.3	1.7	2.1
Jorgensen et al. [196]	293	3.1	3.6	1.1	1.4
This work	**293**	**3.498**	**3.612**	**1.274**	**1.395**
Experimental					
Reference	Temp / K	$\tau_1(z)$ / ps	$\tau_1(xy)$ / ps	$\tau_2(z)$ / ps	$\tau_2(xy)$ / ps
Huntress [215]	293	-	-	0.92	1.8
Kovacs et al. [182]	298	-	-	1.59	1.92
Evans [189]	$\sim$ 298	2.3 to 4.0	-	1.3 to 1.5	1.4 to 2.4

Table 4.6: Chloroform rotational relaxation data from simulation and physical measurements

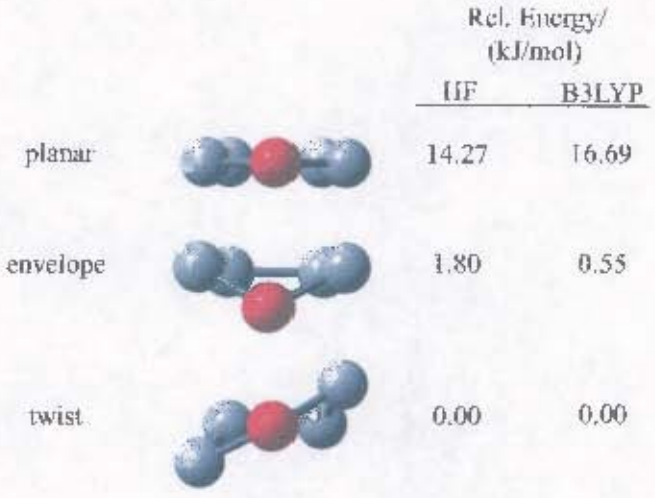

Figure 4.8: Conformations of THF and their relative energies from *ab initio* calculations with $HF/6-31G^{**}$ or $B3LYP/6-31G^{**}$. The planar minimum was obtained by constraining the ring to a planar conformation. (Figure 2 in reference [201])

a coordinate system for THF. This provides a useful frame of reference to describe the molecule's structure, and the relative arrangement and orientation of THF molecules in the condensed phase.

In comparison with chloroform, the amount of experimental data available for THF is limited. For example, the diffusion coefficient of THF has only been reported twice in literature [229, 230] and spectroscopic studies of THF, including Raman, infrared, NMR and X-ray and neutron scattering measurements [231–237] are not as extensive as the equivalent studies on chloroform. Several QM, [201, 222, 223, 234, 238, 239] MD [127, 201, 240, 241] and MC [225, 242, 243] studies have been performed on THF. As a result, several simple force fields exist of the same functional form as our dendrimer force field. These include fully relaxed united-atom and all-atom models. [201] A summary of these force fields' parameters are listed in Table 4.7. [201] The selection of an appropriate THF model that met our simulation requirements was simplified by the recent review article of THF models by Girard and Müller-Plathe who included improvements to these models to obtain a better match with experimental data. [202]

For our investigation we considered the best of the all-atom and united-atom models. The advantage of a united-atom model in this case was clear. The number of atomic interactions would be halved along with a substantial reduction in the number of intra- and intermolecular force field calculations. In addition, the use of a CH_2 united atom in

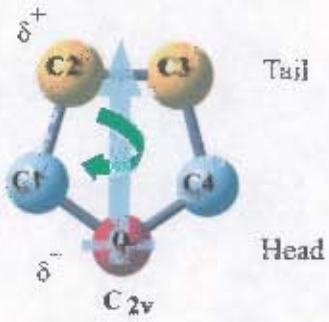

Figure 4.9: THF coordinate system scheme for the united atom model used in this work. The oxygen atom (charge -0.540) is shown in red, while the CH_2 united atoms C1 and C4 (charge +0.231), and C2 and C3 (charge +0.061) are represented in blue and yellow respectively. In all-atom THF models, hydrogen atoms H1, H2, H3 and H4 are bonded to carbon atoms C1, C2, C3 and C4 respectively. Rotation about the C_{2v} symmetry axis is indicated by the green arrow. The dipole moment is indicated by the watermark arrow.

place of explicitly modelled hydrogen atoms does not significantly change the overall shape of the molecule and is expected to interact in an equivalent manner with the dendrimer as an all-atom model. Girard and Müller-Plathe's modified Helfrich-Hentschke united-atom model [127] was selected as it gave the closest overall match with experimental data. The Helfrich-Hentschke force field [127] was based on parameters from the AMBER force field. [244] We fully characterise THF in comparison with chloroform by calculating the structural characteristics (including PDF, SDF and Voronoi polyhedra) and dynamical characteristics. Our findings are as follows:

Analysis of the Girard's modified Helfrich-Hentschke THF model

Structural properties Pair correlation functions have been reported for various THF models. [201, 224, 225, 240, 243] However, the Helfrich-Hentschke model has only been evaluated by the radial distribution of the centre of mass of the THF molecules in the system. Therefore we calculated the radial distribution for all possible combinations of atoms within this model (Figure 4.10) and the centre of mass of the THF molecules for completeness(Figure 4.11).

Presented in Figure 4.10 are the PDFs of each atomic combinations calculated in this thesis. These PDF profiles are qualitatively similar to those reported by Jorgensen and

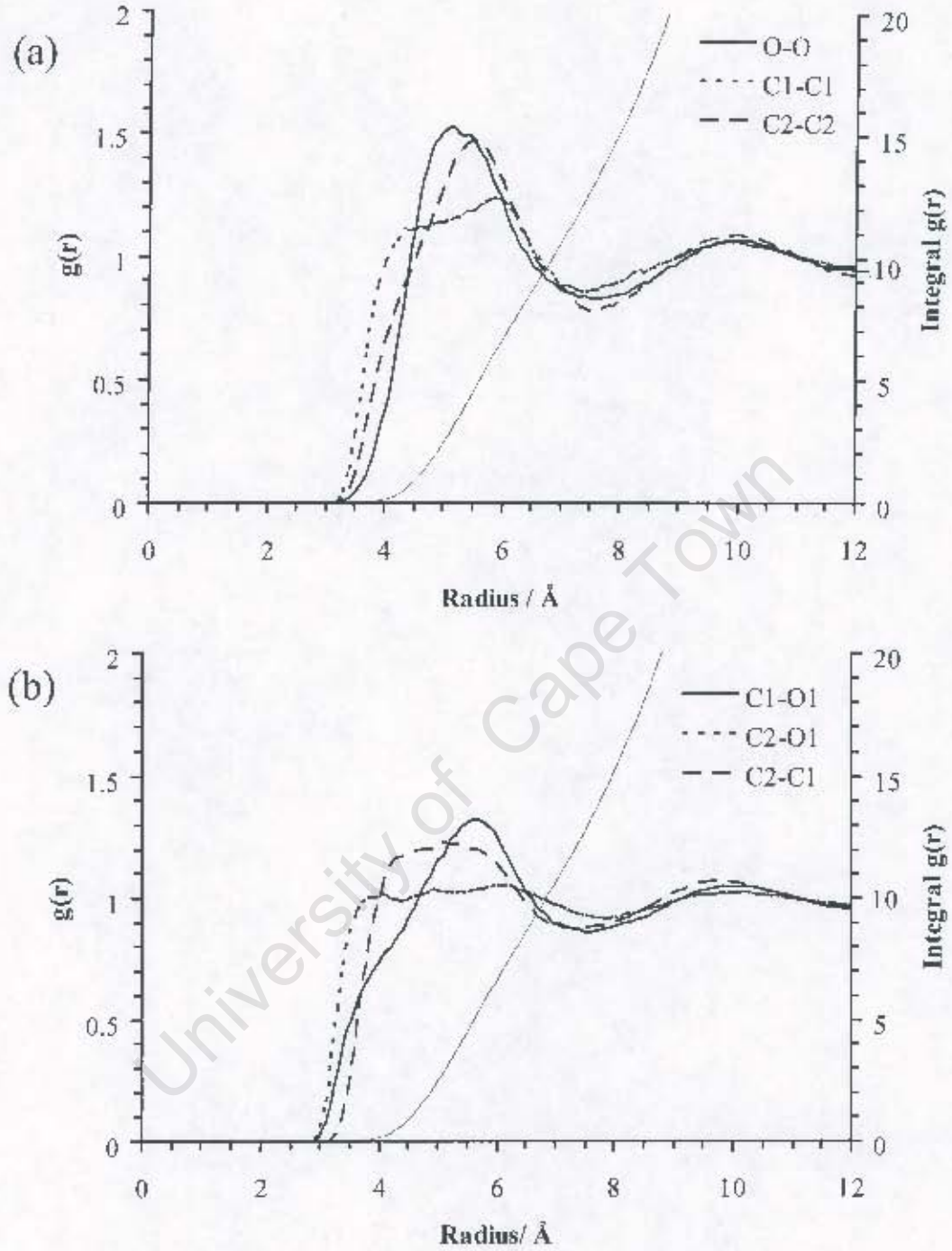

Figure 4.10: Pair correlations functions of THF. The non-cross terms are represented in part (a) while the cross terms are shown in part (b). The integral of g(r) of the centre of mass is represented by the dotted line in both cases. There are two types of carbon atoms in THF - here *C*1 refers to atoms C1 and C4 in Figure 4.9 and *C*2 refers to atoms C2 and C3 in Figure 4.9

	ϵ_C	ϵ_O	ϵ_H	σ_C	σ_O	σ_H	q_{C_1,C_4}	q_{C_2,C_3}	q_O	q_{H_1,H_4}	q_{H_2,H_3}
Fuller [202]	0.290	0.500	0.200	0.306	0.193	0.243	0.228	0.061	-0.577	0.000	0.000
Girard (FF 1) [201]	0.290	0.628	0.170	0.300	0.216	0.250	0.231	0.061	-0.584	0.000	0.000
Girard (FF 1*) [201]	0.290	0.628	0.170	0.295	0.300	0.240	0.231	0.061	-0.584	0.000	0.000
Girard (FF 2) [201]	0.230	0.510	0.200	0.306	0.200	0.246	0.231	0.061	-0.584	0.000	0.000
Briggs [225]	0.404	0.712	-	0.385	0.300	-	0.250	0.000	-0.500	-	-
Girard (FF 4) [201]	0.209	0.500	0.150	0.343	0.300	0.230	0.231	0.061	-0.584	0.000	0.080
Damm [226]	0.276	0.586	0.126	0.350	0.290	0.250	0.170	0.000	-0.400	0.015	0.000
Girard (FF 5) [201]	0.276	0.550	0.126	0.350	0.290	0.245	0.208	0.000	-0.528	0.028	0.000
Helfrich [127]	0.377	0.628	-	0.430	0.330	-	0.280	-0.010	-0.540	-	-
Girard (FF 6) [201]	0.450	0.890	-	0.395	0.300	-	0.231	0.061	-0.584	-	-
Rappé [227]	0.440	0.250	0.185	0.385	0.350	0.289					
Girard (FF 7) [201]	0.190	0.360	0.160	0.385	0.350	0.190	0.231	0.061	0.584	0.000	0.000
Verlinde [228]	0.184	0.209	0.107	0.380	0.348	0.300					
Girard (FF 8) [201]	0.340	0.490	0.390	0.230	0.220	0.240	0.231	0.061	-0.584	0.000	0.000

Table 4.7: Force fields for THF and variations thereof as reported by Girard and Müller-Plathe. [201] The units of the columns are: ϵ/kJmol^{-1}, σ/nm, q/e. Refer to Figure 4.9 for atom labels.

co-workers [225, 240, 243, 245] Jorgensen et al. report a $g_{OO}(r)$ peak height of approximately 1.36 centred at 5.0 Å. Drabowicz reports the same peak at 4.75 Å with a height of approximately 1.35. Our $g_{OO}(r)$ peak is centred at 5.0 Å but with a height of 1.53. This peak is broad, beginning at around 3.0 Å with the adjacent minimum centred at 7.7 Å. This is approximately 1 Å broader than the $g_{CC}(r)$ peak of chloroform. This suggests that the first solvation shell comprises a variety of conformations for THF. The other self-similar profiles ($g_{C1C1}(r)$ and $g_{C2C2}(r)$) concur in this regard; $g_{C1C1}(r)$ appears to be the combination of two peaks, the first centred at 4.40 Åand second at 6.00 Å, similarly with $g_{C2C2}(r)$ which has a large peak centred at 5.60 Å and a left shoulder centred at 4.30 Å. In each case, the two peaks making up the first solvation shell could be the result of the each of the CH_2 profiles comprising two methylene groups, i.e., C1 and C4 for $g_{C1C1}(r)$, and C2 and C3 for $g_{C2C2}(r)$. The two peaks of each of these profiles centre at around 5 Å. The cross-terms we identify the C2-O interaction as the most favoured interaction, i.e., a possible head to tail orientation.

The PDF for the centre of mass of chloroform and THF are remarkably similar; both the peak heights and positions are almost identical. However, there are slight differences between the chloroform and THF PDFs, such as the first solvation shell for THF being slightly more defined than that of chloroform, as its peak height and well depth are greater than those of chloroform. The centre of mass profile for THF suggests the first coordination

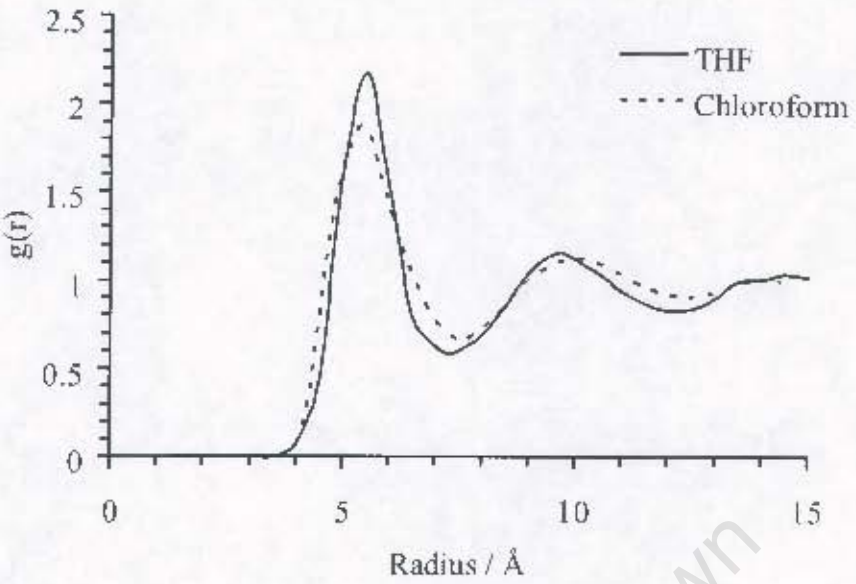

Figure 4.11: Pair correlations functions of the centre of mass of THF and chloroform.

shell is centred at 5.5 Å with a peak height of 2.18. This is very similar to the centre of mass peak of chloroform which is centred at 5.40 Å and a height of 1.88. THF appears to have slightly greater long-range order because the second solvation shell has a more pronounce minimum at approximately 12.5 Å in THF than chloroform. However, from the centre of mass PDF, there appears to be great similarity between the intermolecular solvent structure of chloroform and THF.

In Figure 4.12 the SDF of pure THF solvent orientated about a single THF molecule is present at 50% above bulk density. Here only the oxygen distribution has any observable structure. As a comparison, in chloroform all the atoms of the molecules forming the strongly bound region exhibit some ordering at this probability. This suggests that the THF molecules in the first solvation shell have greater flexibility compared with chloroform. The maxima of the SDF suggest that the methylene groups of the solute molecule are surrounded by six solvent THF molecules. Briggs et al. suggested from their calculated dimerization energy that there were four strongly associated neighbours. [225] However, we noted that if Briggs et al. had considered a slightly larger region of integration to include the full shoulder of THF's energy pair distributions (see Figure 15 in reference [225]), the number of neighbours for the complete shoulder is approximately six.

At 25% above bulk probability density, the complete structure of the first solvation shell becomes visible (Figure 4.13). Similar to chloroform, the solvation shell forms a sphere

Top Side

Figure 4.12: The spatial distribution of THF about a single solvent molecule at 50% above bulk density. Only the oxygen atoms show any significant order at this level. "Top" represents a view perpendicular to the five member ring while "Side" represents a view parallel to the ring.

around the solvated THF molecule rather than forming solvent chains similar to methanol. The isodensity surfaces of the methylene groups line the interior of the oxygen SDF near the head of the solute (at the oxygen atom) and conversely the exterior of the oxygen isodensity surfaces near the tail of the molecule (at the weakly charged methylene groups). The SDFs point to a combination of "head-to-tail" and "head-to-side" alignments of the dipole moments of neighbouring molecules as depicted in Figure 4.14. Unlike chloroform, at lower probability distributions the second solvation shell does not emerge. This appears to contradict the PDF of the centre of mass of THF and chloroform (Figure 4.11), where the second solvation shell of THF appears to be slightly more well defined than chloroform. One possible explanation is that although the second solvation shell in the centre of mass PDF is slightly more defined in THF than in chloroform, in THF the molecules forming this shell express greater rotational freedom in comparison with the molecules in the second solvation shell of chloroform. Hence the atomistic SDFs are not as well defined in THF as in chloroform.

Considering the similarities of the complete first solvation shells for THF and chloroform, it not surprising that the characteristics of the Voronoi polyhedra of THF are very similar to those of chloroform (see Figure 4.15 and Table 4.2.3). The differences between the VP of THF and chloroform are very small: the number of nearest neighbours differs by less than a single molecule (14.61 and 14.47 for chloroform and THF respectively) while

Figure 4.13: The spatial distribution of THF about a single solvent molecule at 25% above bulk density. The oxygen atom is shown in red, while the CH_2 united atoms C1 and C4, and C2 and C3, as identified in Figure 4.9, are represented in blue and yellow respectively . "Top" represents a view perpendicular to the five member ring while "Side" represents a view parallel to the ring.

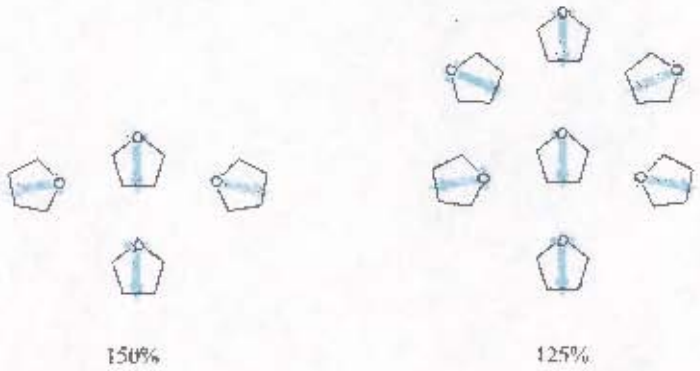

Figure 4.14: A schematic diagram of the arrangement of the molecules making up the first solvation shell of THF as suggested by the SDFs in Figures 4.12 and 4.13. The molecules forming this shell do not lie in the plane of the solvated molecule, rather they lie at acute angles out of the plane of the solvated THF molecule. This diagram presents only half of the molecules making up the solvation shell - a mirror image of these molecules is reflected below the plane of the solvated THF molecule.

the average volume of the VP differ by just over 1Å^3 - 133.34Å^3 and 134.39Å^3 for chloroform and THF respectively. Even the distributions about the mean values are almost identical. Therefore, the combination of the PDFs, SDFs and VP strongly suggest that the intermolecular structure of liquid chloroform and THF are very similar.

Dynamical properties In comparison with chloroform, only limited experimental data is available for THF. For example, only two experimental diffusion coefficients are available in literature and they differ by approximately 30% ($2.45 \times 10^{-5}\text{cm}^2\text{s}^{-1}$ and $3.40 \times 10^{-5}\text{cm}^2\text{s}^{-1}$). [201] Therefore, it is difficult to gauge the accuracy of the dynamics of the Girard and Müller-Plathe's modified Helfrich-Hentschke united-atom THF model employed in this thesis when compared to available independent experimental data. Girard et al. on the other hand, showed that this model accurately reproduced other physical and thermodynamic properties including density, heat of vaporization, isothermal compressibility and heat capacity at constant pressure. [201] We calculated a diffusion coefficient $2.65 \times 10^{-5}\text{cm}^2\text{s}^{-1}$ which is almost identical to the value reported by Girard et al. for this model. We are therefore confident that the Girard and Müller-Plathe's modified Helfrich-Hentschke united-atom model employed in this thesis sufficiently represents the structure and dynamics of liquid THF.

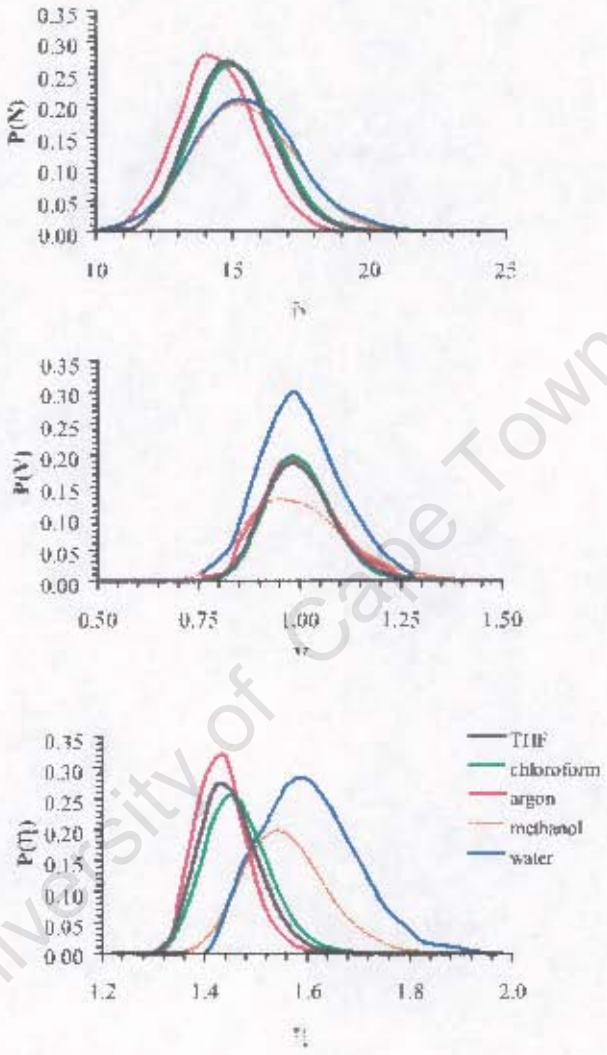

Figure 4.15: Probability distribution of the Voronoi properties for THF, chloroform, argon, water and methanol (an extension of Figure 4.7). (A) Nearest neighbour, (B) polyhedra volume and (C) asphericity parameters. Values for THF and chloroform were calculated from our MD simulations while argon, water and methanol are taken from Jedlovsky [176].

Solvent	η	N	V /Å^3
THF	1.45 ± 0.06	14.47 ± 1.46	134.39 ± 11.82
Chloroform	1.47 ± 0.06	14.61 ± 1.47	133.34 ± 10.87
Argon	1.44 ± 0.05	14.46 ± 1.34	47.58 ± 4.27
Water	1.61 ± 0.10	15.06 ± 1.81	27.80 ± 2.64
Methanol	1.74 ± 0.13	15.53 ± 1.97	66.23 ± 10.73

Table 4.8: Mean values and standard deviation of the averages of some of the properties of Voronoi polyhedra for chloroform, THF and some comparative solvent systems.This is an extension of Table 4.2.2

4.3 Dendrimer Parameterization

Figure 4.16: Benzyl phenyl ether used as the model "dimer" during parameterisation of the ether linkage.

The CHARMM-like poly (benzyl phenyl ether) dendrimer force field employed in this thesis was developed by Hughes et al. [10] in our laboratory to investigate whether Fréchet dendrimers are suitable catalytic supports. [2] Hughes et al. identified the ether linkage between the aromatic rings of the dendrimer as the most important factor affecting the rigidity and overall conformation of the dendrimer. [10] This ether linkage comprises three dihedral angles (Φ, Ψ and Ω), shown in Figure 4.16. Of these three dihedral angles, the authors identified Ψ as the most important parameter for predicting Fréchet dendrimer structure. [10] Hughes et al. used the model compound, benzyl phenyl ether (Figure 4.16) to model the dendrimer ether linkage. They fitted the empirical potential energy profile for rotating Ψ through 360° in this molecule to its corresponding *ab initio* (HF//6-31G(d)) profile (Figure 4.18). [10] Using a trial-and-error approach, Hughes et al. changed the torsion angle force constant (k_ψ) from an initial value of 0.27 kcalmol ^{1}rad ^{2} to 0.15 kcalmol ^{1}rad ^{2} to obtain the best match between the QM and MM profiles. [10]

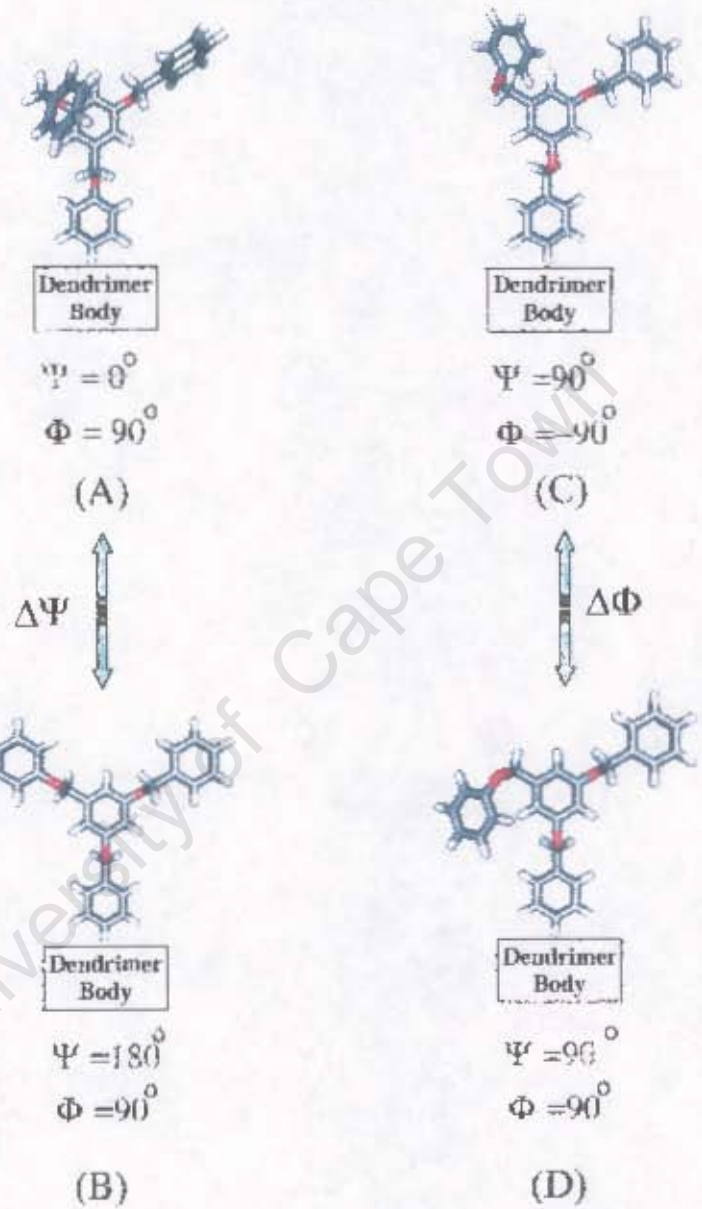

Figure 4.17: The effect of the torsion angle Φ on the structure of the dendrimer when Ψ is not 180°. Transition from conformation (A) to conformation (B) represents the effect of Ψ on the degree of extension of the dendrimer as modelled by Hughes et al. while the transition from conformation (C) to conformation (D) represents the effect of Φ on the degree of extension of the dendrimer.

Hughes et al. assumed that the torsional angles (Φ and Ω) would have little affect on the folding behaviour of the dendrimer. As a result, little attention was given to these parameters. However, if we consider the possible combinations of Ψ and Φ, as illustrated in Figure 4.17, it becomes evident that the torsion angle Φ can effect the overall conformation of the dendrimer. However, Φ only has an effect on the conformation of the ether linkage when $\Psi \neq 180^{\circ}$. For example, if we set Ψ to its global minimum of 180° (Figure 4.17(B)), regardless of what Φ is, the ether linkage will remain extended, i.e., the terminal rings will be at a maximum distance from the body of the dendrimer. However, if $\Psi = 90^{\circ}$ (a local minima, Figure 4.18), Φ can determine whether the terminal group folds out (Figure 4.17(B)) or folds in towards the parent layer (Figure 4.17(D)).

Visual inspection of the MD trajectory for a first generation wedge (WG1) suggested that rotations about Φ were not possible. This was confirmed from analysis of the time evolution of the dihedral angle Φ (shown in Figure 4.19A). No transitions about Φ occurred during the entire 500ps, indicating that the force field prohibits rotations about Φ. Since Φ and Ω had not been as carefully parameterized as Ψ and that it appeared rotation about Φ was prohibited, it was important to determine if Φ and Ω were parameterised correctly by comparing the force field and *ab initio* rotational energy profiles about these torsion angles and correcting if need be.

Parameterization of Ψ and Ω

We used the same model compound as Hughes et al. (benzyl phenyl ether, Figure 4.16) to calculate the potential energy profile of rotations about Φ and Ω, starting from 0° to 180° in 10° step sizes. Both the MM profile, using Hughes et al.'s force field, and the QM profile, using HF//6-31G+ level of theory and basis set combination, were calculated. The results are presented in Figure 4.18. For Ω, the MM and QM profiles are a very close match. The rotational energy barrier about Ω is essentially negligible in both instances, with the global maxima ($\Omega = \pm 100^{\circ}$) are slightly higher in the MM profile than the QM profile by less than 0.5 kcal.mol^{-1}. Therefore, Ω was not altered in any way.

The Φ torsion angle did not show as good a fit as Ω although the positions of the QM and MM minima and maxima corresponded well. However, Hughes et al.'s force field overestimates the rotational energy barrier for Φ by 100% in comparison with the *ab initio*-derived barrier height (Figure 4.18). We altered the energy barrier height of Φ by adding an additional parameter for this dihedral angle to the force field, the value of which

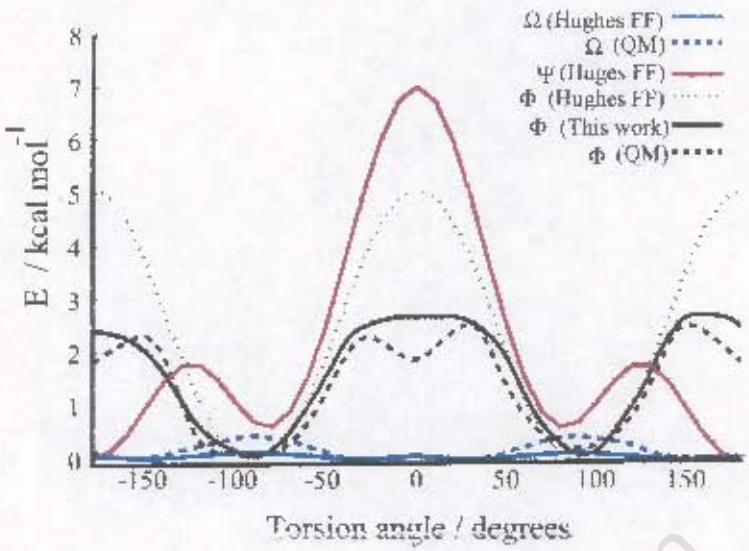

Figure 4.18: Φ, Ψ and Ω torsion rotation potential energy profiles for the force field of Hughes et al. (Hughes FF) and *ab initio* measurements (QM). The effect of our improvements to Φ torsion angle is represented as (Φ This Work).

was determined using a trial-and-error basis. The closest MM match with QM profile was obtained with a force constant -0.5360 kcal.mol^{-1}.rad^{-2} of periodicity 2 and a phase shift of 0°. The corrected rotational energy profile is included in Figure 4.18 and shows a close match between the new force field and QM profiles. Additionally, the time series of Φ for a first generation wedge (WG1) employing the corrected force field showed that rotations about Φ are now possible (Figure 4.19).

To test the effect of lowering the energy barrier on Φ, we performed two sets of experiments. First we conducted MD simulations of wedges WG1 to WG5 in vacuum over at least 1 ns using the Hughes et al.'s force field. We then repeated these calculations using the modified force field. The radius of gyration (R_g) time series for the two sets of simulations are illustrated in Figure 4.20 and the average R_g are listed in Table 4.9.[1] We observed no significant differences in the average structure or behaviour of the dendritic wedges with the modified force field. Wedges WG1 and WG2 show greater flexibility using the new force field than the old force field. It should be noted that in all cases the overall conformation of the dendrimer is not affected; wedge WG1 is extended while wedges WG2 to WG5 fold in vacuum. (The folding behaviour of the WG1 wedge is investigated in

[1] These simulations were performed on wedges rather than on full dendrimers in order to reduce the size of simulation (number of atoms) and allow a greater number of tests to be conducted.

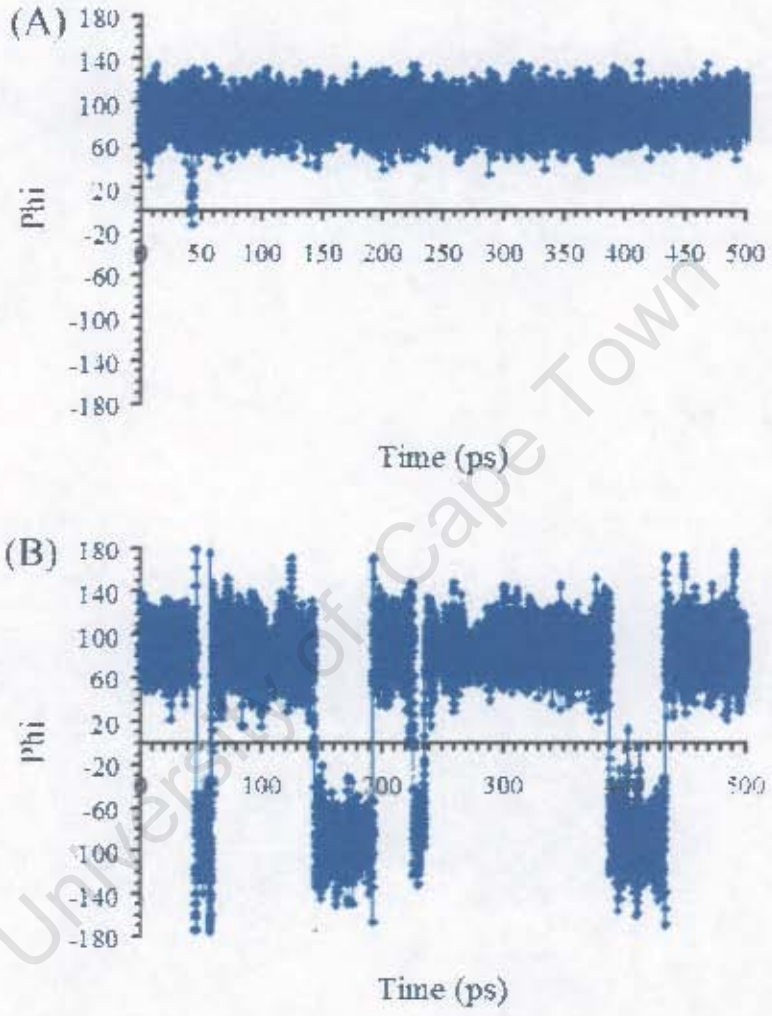

Figure 4.19: A comparison of the time series of Φ for an ether linkage of a terminal group of a G1 dendrimer in vacuum using the (A) Hughes et al.'s force field and (B) our modified force field

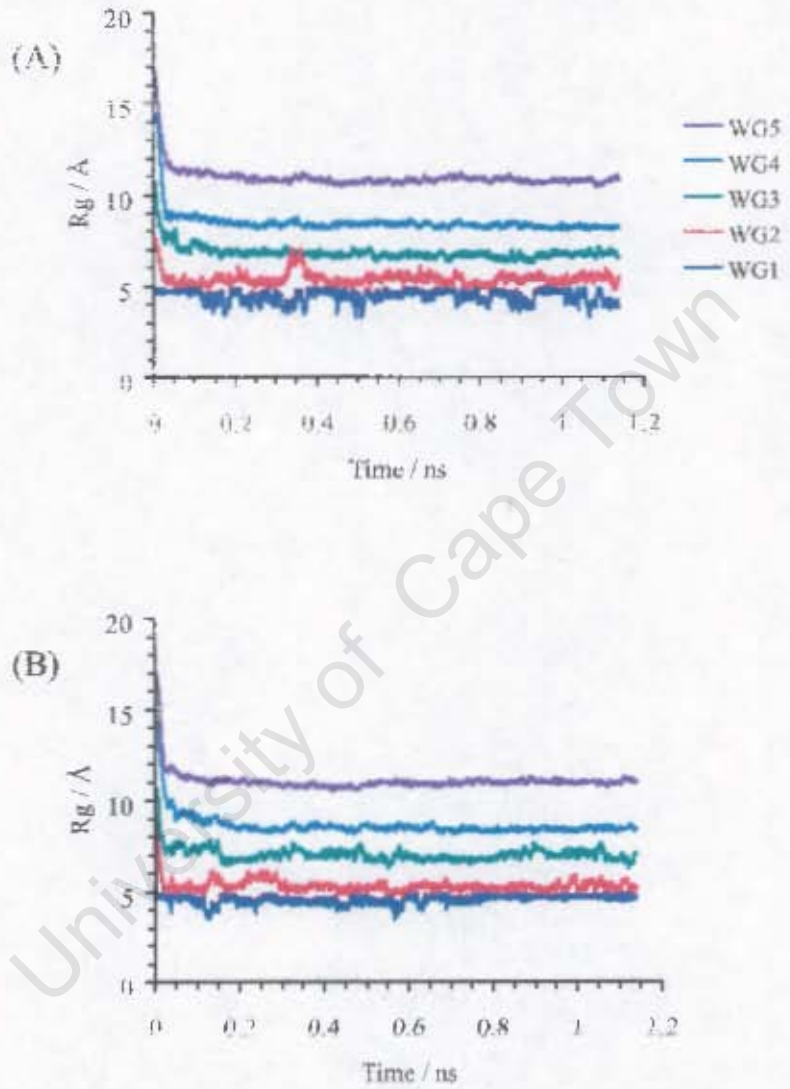

Figure 4.20: A comparison of the radius of gyration, R_g, time series for wedges WG1 to WG5 in vacuum using (A) the modified dendrimer force field and (B) Hughes et al.'s force field. The averages of these time series are listed in Table 4.9.

Wedge	Average R_g / Å		
Generation	Hughes et al.	This work	ΔR_g / Å
1	4.55	4.41	-0.14
2	5.33	5.41	0.08
3	7.03	6.84	-0.19
4	8.63	8.50	-0.07
5	11.05	10.96	-0.09

Table 4.9: The average R_g from the R_g time series for the wedges WG1 to WG5 as illustrated in Figure 4.20. The second column indicates the values calculated using Hughes et al.'s force field, while the third column has values calculated using our modified force field. The last column indicates the difference between the two models.

Wedge	Average R_g / Å		
Generation	Hughes et al.	This work	ΔR_g / Å
1	4.43	4.42	-0.01
2	7.36	7.32	-0.04
3	10.21	10.23	-0.02

Table 4.10: The average R_g of the R_g time series for the wedges WG1 to WG3 in vacuum as illustrated in Figure 4.21. The second column includes the values calculated using Hughes et al.'s force field, while the second column includes the values calculated using our modified force field. The last column shows the difference between the two models.

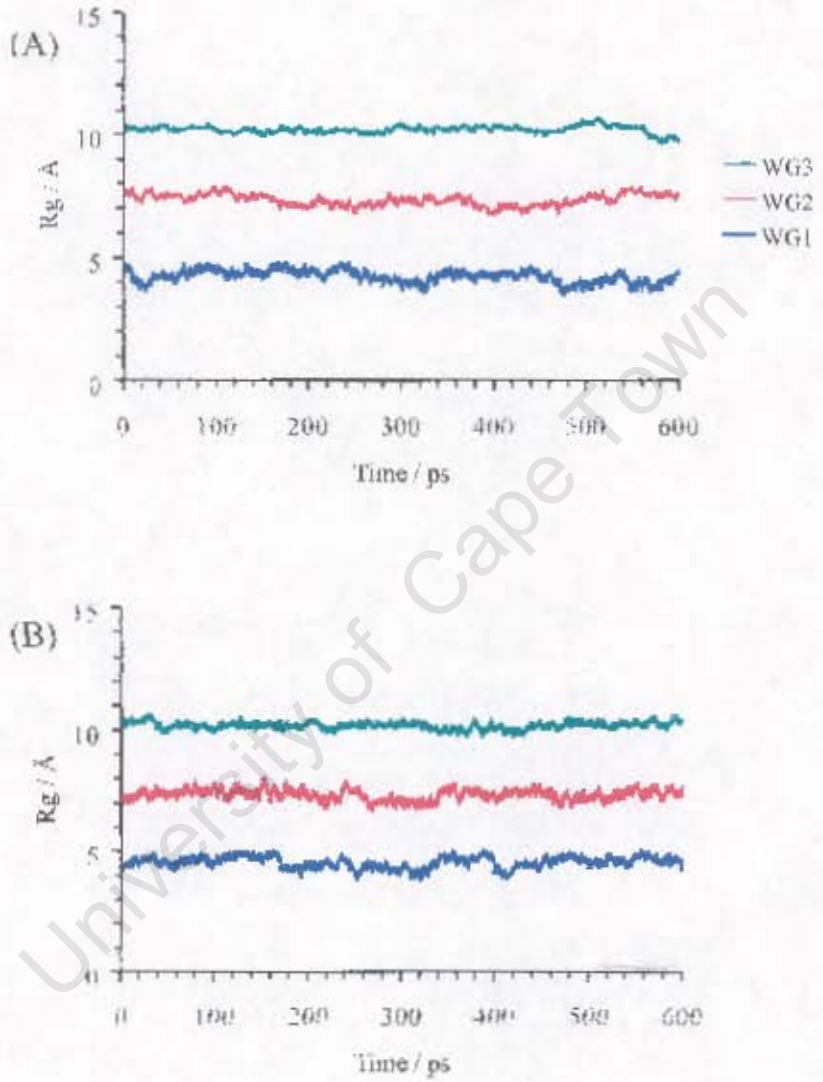

Figure 4.21: A comparison of the R_g time series for wedges WG1 to WG3 in chloroform using (A) the modified dendrimer force field and (B) Hughes et al.'s force field. The averages of these time series are listed in Table 4.10.

detail in Chapter 6). There is a slight difference in the average R_g (Table 4.9) between the force fields, with the new force field producing slightly lower R_g.

The second test was to investigate the effect of lowering the barrier height of Φ in an explicit solvent environment. Therefore, an additional preliminary test was conducted using wedges WG1 to WG3 in chloroform (Figure 4.21 and Table 4.10). Again, no significant differences were observed in the overall structure or radius of gyration in the two sets of simulations. The effect of reducing the rotational energy barrier of Φ was to increase the frequency of rotations of the ether linkage (as is shown in the time series of Φ in Figure 4.18). However, this greater flexibility did not affect the relative position of the aryl rings.

4.4 Solution Parameterization

With the individual components of the solution system successfully parameterised, it is important to ensure that no strange anomalies occur with the combination of the dendrimer and solvent force fields. As discussed in the introduction to this chapter, one way to ensure that the combination of the force fields is valid is to ensure that relative strengths of the most common monomer-monomer interactions are valid. Monomer-monomer interactions that we considered to be most important are listed in Table 4.11. As mentioned in the introduction of this chapter, benzene is employed as the representative functional group for the dendrimer. An additional simplification was made for THF-benzene QM interaction. Because there is no suitable THF-benzene *ab initio* study available in literature, we modelled the THF interactions using the closest analogue - the interaction of a methylene monomer of an alkyl chain perpendicular to the benzene ring. [206] The dendrimer in vacuum is the basis of this study and as the benzene-benzene dimer interaction represents the dendrimer-dendrimer interaction, this interaction energy is used as the basis to rank the strengths of the other interactions. In other words, all the interaction strengths are normalised according to the benzene-benzene interaction. This is indicated in Table 4.11. While there are clearly a great number of alternative interactions and orientations that we could test, it is practically impossible to test all possibilities. Our aim is not to test every possible combination and orientation but to identify the most significant potential sources of error and correct if required.

We consider each solvent-dendrimer system separately, and rank the interactions strengths of each system with respect to the strength of the benzene-benzene interaction (Table

	Interaction Type	MM (kcal.mol^{-1})	Relative strength	QM (kcal.mol^{-1})	Relative strength
Benzene dimer	D-D	-2.48	1.00	-2.30^{a}	1.00
Chloroform dimer	S-S	-2.39	0.96	-2.66^{c}	1.16
THF dimer	S-S	-3.10	1.25	-3.20^{d}	1.39
Water dimer	S-S	-5.84	2.35	-5.00^{e}	2.17
Benzene - chloroform	S-D	-3.96	1.60	-5.10^{e}	2.22
Benzene - THF	S-D	-2.76	1.11	-2.10^{e}	0.91
Benzene - Water	S-D	-3.20	1.29	-3.15^{b}	1.37

Table 4.11: Global minima for each interaction type (dendrimer-dendrimer (D-D), solvent-solvent (S-S) and solvent-dendrimer (S-D)), and normalized with respect to the benzene dimer global minimum. Equivalent QM values are included for comparative purposes.(a) Hobza et al. [205], (b) Jorgensen et al. [246], (c) Chang et al. [192], (d) Briggs et al. [225], (e) Tsuzuki et al. [206]

4.11). For each solvent system, the solvent-solvent interaction is referred to as the S-S, solvent-dendrimer interaction (THF-benzene, water-benzene and chloroform-benzene) as S-D and the dendrimer-dendrimer interaction is refer to as D-D.

We begin with the dendrimer-THF system. In this system, the largest discrepancy between our MM calculations and QM literature results occurs for the SD interaction (an overestimation of 31%). The sequence of the interaction strengths differs between the minima of our MM calculations ($S - S(1.25) > S - D(1.11) > D - D(1.0)$) and QM values ($S - S(1.39) > D - D(1.0) > S - D(0.91)$). From QM calculations, the SD interaction is the weakest interaction, while in the force field the D-D interaction is the weakest. Therefore, our force field overestimates the dendrimer-solvent interaction in the THF system and could show bias toward the extended conformation of the dendrimer in THF.

In the dendrimer-chloroform system, the order of the interactions for our MM calculations ($S - D(1.6) > D - D(1.0) > S - S(0.96)$) also differs from the QM literature values ($S - D(2.22) > S - S(1.16) > D - D(1.0)$). However, this is expected to have little impact, as the interaction strengths are only marginally different and the order differs among the homogeneous interactions and should not have a significant effect on the folding the dendrimer. The greatest difference between the QM and MM results is the relative strength

of the S-D interaction. In the QM calculations the S-D strength is 220% of the D-D interaction while in the MM calculation, the S-D strength is only 160% of the S-D interaction. This is most likely because of the lack of polarizable features in the CHARMM force field which is the source of the substantial chloroform-benzene interaction strength. Therefore, in comparison with the QM S-D interaction, the MM S-D interaction would show less favour toward the folded conformation of the dendrimer.

In the dendrimer-water system, the sequence of the interaction strengths is the same for our MM calculations ($S - S(2.35) > S - D(1.29) > D - D(1.0)$) and QM literature values ($S - S(2.17) > S - D(1.37) > D - D(1.0)$). However, the water dimer interaction (S-S) is slightly stronger in our MM calculations compared to the QM literature values. This could result in the dendrimer folding slightly faster during the MD simulations.

In the literature it has been suggested that chloroform is a poor solvent for Fréchet dendrimers. [118] Therefore, it was surprising to discover from a thorough review of the literature that the interaction between chloroform with benzene is extremely strong. [206] As detailed in Table 4.11, this interaction is in fact slightly stronger than the strength of a hydrogen bond interaction in water (-5.1 kcal.mol^{-1} and 5.0 kcal.mol^{-1} for chloroform-benzene and water-water interactions respectively) (Table 4.11). [206] This is a result of an induced dipole moment within the highly polarizable chloroform molecule (8.53Å^3) [192] interacting with the delocalised cloud of electrons of the aromatic ring. It was also surprising that the THF-benzene interaction is relatively weak when compared to water-benzene and chloroform-benzene interactions since THF is reported to be a very good solvent for Fréchet dendrimers. [118] From the QM interactions reported in Table 4.11, it suggests that chloroform is a better solvent than THF. This is contrary to the findings of Jeong et al. who suggested that in chloroform Fréchet dendrimers fold by as much as 50% of the extended conformation, while in THF, these dendrimers remain fully extended. [118] Our simulations of Fréchet dendrimers in chloroform (Figure 4.21 and Chapter 5) indicate that the dendrimer remains extended in chloroform. Initially, it was suspected that the dendrimer-chloroform interactions in our force field where unrealistically strong. However, as was demonstrated above, our force field underestimates the chloroform-dendrimer interaction and therefore is already biased towards the folded conformation of the dendrimer and should underestimate the extent of unfolding of the dendrimer in chloroform.

Nevertheless, in order to build further confidence in our force field and ensure that additional factors had been considered, we attempted to force the dendrimer to fold in

chloroform by altering the force field. In the CHARMM force field there are four parameters used to specify non-bonded interactions; the atomic charge, the NONBond (van der Waal) parameters, the NBFIX parameters (to manipulate interactions between specific atom pairs), and HBOND (hydrogen bond) parameters. We do not explicitly include hydrogen bond parameters in this force field as they are implicitly included in the CHARMM parameter set in the electrostatic and van der Waal interactions. [133]. We reduced the charges on the dendrimer aryl ring by 30%, increased the strength of the van der Waal interactions by increasing the well depth by 30% and heavily penalized the dendrimer-chloroform interaction by introducing specific terms to set these interaction energies to zero. In this way, we had some success forcing the dendrimers to fold in chloroform. However, such a force field is unacceptable for the following reasons. Firstly, the dendrimer force field originates from a force field which has been refined over several iterations and has been thoroughly tried and tested by numerous independent research groups. Secondly, earlier in this chapter (Section 4.2.2), the chloroform force field was shown to replicate the physical measurements of chloroform. Thirdly, as discussed in this section, the force field is already biased toward the dendrimer folding in chloroform in comparison with the QM interactions. Fourthly, the changes to non-bonded parameters to force the dendrimer to fold in chloroform had to be selectively applied to the chloroform-dendrimer systems and would not be suitable for the water-dendrimer and THF-dendrimer systems. Hence, two separate force fields would be necessary, one force field specifically for the dendrimer-chloroform simulations and another for dendrimer-water and dendrimer-THF simulations. The use of a non-transferable force field is a poor strategy. Further, we are unable to substantiate why these large artificial constraints were selectively required for the chloroform-dendrimer parameters. Finally, a solute with a solubility parameter of δ_p is described as being insoluble in a solvent with a solubility parameter δ_s if $(\delta_s - \delta_p)^2 < 4$. [247] Jeong it et al. suggested a Fréchet dendrimer has a δ_p between 18.2 and 18.4 $MPa^{1/2}$. [118] The solubility parameter of chloroform and THF are 19.0 $MPa^{1/2}$ and 18.6 $MPa^{1/2}$ respectively. [118] The difference between the δ_s of chloroform and the dendrimer suggests that chloroform is a very good solvent.

After due consideration, it was decided for the reasons mentioned above not to apply any modifications to the force field. Therefore, the force field selected for the MD simulations was the same force field developed by Hughes et al. with only the Φ dihedral angle parameter modified. No alterations were made to the charges or Lennard-Jones parame-

ters. Therefore, we sought an alternative source to account for the difference between the results of the viscosity studies of Jeong et al. and our MD simulations.

4.4.1 Other factors affecting the conformation of dendrimers

The simulation environment can also affect the outcome of the simulation. Factors to consider include the following:

- Temperature ($15 - 45°C$ at 5° intervals) .
- The ensemble used to sample phase space (NVE, NVT or NPT).
- Method of integration (Verlet or Leap-frog) and integration step size (1fs or 2fs).
- Size and shape of the periodic cell (truncated octahedron or cube).
- Truncating methods for long range interactions (group-based versus atom-based cut-offs).
- Long range interactions (evaluated using Ewald summations).
- Dynamics of a wedge versus the dynamics of full dendrimer.
- Starting conformation of the dendrimer (folded versus extended).

A series of MD simulations were run to test each of these factors. As this was a preliminary investigation to identify any significant errors, only limited analysis was performed using the radius of gyration time series. If there was a notable change in this time series due to a single variable change, further analysis would be applied. The radius of gyration time series for each set of MD simulations are included in Appendix A. For specifics of the computational details, such as cut-off lengths, please refer to Section 5.2. Any change in the simulation environment for a series of simulations is specified accordingly.

To test the effect of temperature on the overall behaviour of the dendrimer, we simulated wedges WG1 to WG3 in chloroform for 500ps after an initial 100ps equilibration phase to obtain the desired temperature. A total of seven sets of simulations were conducted from ($15 - 45$°C at 5° intervals, Figure A.1). There was notable change in the average R_g within this temperature range. In each case, the dendritic wedge remained fully extended. To test the effect of the type of ensemble used, we ran a further 500ps on wedges WG1 to WG3 in chloroform at 20°C after an initial 100ps equilibration phase

(Figure A.2), sampling from each one of the ensembles (NVE, NVT, NPT). Extensive use of the NVE and NPT ensembles starting from both extended and contracted conformations respectively led to essentially equivalent structures (Chapters 5 and 6). Therefore, the equilibrated conformation of a dendrimer was deemed to be independent of these variables. Various size and shape periodic boundary conditions were applied to the overall dynamics of the dendrimer (see Chapter 5). No significant difference was observed between the different simulation cells. Atom-based cut-offs resulted in non-conservation of energy within the system with the overall energy of the system gradually decreasing. Therefore, group-based cut-offs were applied uniformly throughout this thesis. The effect of including Ewald summations, was limited to slightly increasing the rate at which the dendrimer unfolded in comparison to the simulation without Ewald summations (Figure A.3).

A significant difference between Jeong et al.'s measurements and our dendrimer simulations is that the viscosimetric measurements were conducted on wedges while our simulations are performed on complete dendrimers. However, MD simulation of wedges WG1 to WG3 in chloroform (Figure 4.21) and dendrimers G1 to G5 (Figure 5.2) indicates that in chloroform, both Fréchet dendrimers and dendritic wedges are fully extended.

The effect of the starting configuration of the dendrimer is also likely to have a considerable effect on the equilibrium conformation of the dendrimer. From a series of MD simulations of dendrimers G1 to G5 in chloroform, it was observed that the dendrimers remained unfolded when initiated from an extended conformation and unfold when starting from a contracted conformation. Therefore, although the initial conformations of the dendrimer were of opposite extremes, the equilibrium conformations were both extended. The folding of dendrimers is discussed in detail in Chapter 6.

Finally, physical stresses and strains that are inherent to an experimental environment such as the viscosity measurements, are not accounted for in standard MD simulations. These external forces may assist the dendrimer to overcome high conformational energy barriers and explore conformations inaccessible in MD simulations. Calculating the potential of mean force for a number of model dendrimer molecules, one can simulate the effects of pulling terminal groups in to the core of the dendrimer. This is discussed in detail in Chapter 6.

4.5 Conclusion

In this chapter we have prepared a simulation environment suitable for performing nanosecond MD simulations of Fréchet dendrimers in explicitly modelled chloroform and THF solvents.

A new fully relaxed five-site chloroform model was developed, which improves on existing models, offering closer correspondence with experimental data. Therefore, it is the preferred choice over the existing chloroform models for the use in the simulation of explicitly solvated dendritic systems. There are few differences between the structure and dynamics of THF and chloroform. This was surprising considering the substantial difference in the behaviour of Fréchet dendrimers in these solvents. [118] The similar traits of the pure solvents suggests that the interaction between the solvent and the solute is the determining factor in the differences in their behaviour.

For the dendrimer force field, a correction was made to the Φ dihedral angle of the ether linkage. However, this had little effect on the overall behaviour of the dendrimer. The parameterization of the combined solvents-dendrimer force field to describe the solution force field showed that the dendrimer-chloroform interaction biases a folded conformation while the dendrimer-THF interaction biases the unfolded conformation. After considering the relative strengths of the interactions in the dendrimer-solvent systems, we were unable to identify the cause for the difference in behaviour of Fréchet dendrimers in THF and chloroform. Further tests to investigate the effect of simulation conditions showed that the equilibrated conformation of the dendrimer in chloroform is not affected by the temperature, ensemble, integration step size, method of integration, starting conformation or the size and shape of the periodic cell.

Therefore, after extensive testing of the force field we are confident that this force field accurately represents the behaviour of dendrimers in chloroform, THF and water. In the following chapter we investigate the structural and dynamical properties of Fréchet dendrimers in chloroform and THF and investigate the origin of their unique viscosity characteristics.

Chapter 5

Dendrimer structure and dynamics in good solvents

5.1 Introduction

Attempts to conclusively resolve the debate over the structure of dendrimers, particularly the location of the terminal groups, the existence of internal voids and the overall density distribution within the dendrimer have proved challenging, both experimentally and computationally. Numerous comparisons have been made between experimental measurements and simulation results. However, in the majority of cases the comparisons were made between measurements performed on dendrimers in good solvents and simulations conducted in vacuum (i.e., a poor solvent). Some simulations have attempted to account for solvent effects by applying effective potentials within the dendrimer. Most notable is Murat and Grest's attempt to mimic the quality of the solvent. [44] Some investigations have used the results of Murat et al. to infer that vacuum simulations are valid for all solvent conditions. However, Murat and Grest's investigation employed a coarse grain model in vacuum and did not explicitly take into account atomic detail within the dendrimer model nor did it explicitly include the solvent. Therefore, there are aspects of solvation which cannot be realistically represented in their vacuum simulations. Hence there is a need for explicitly solvated dendrimer simulations, in particular, to test the findings of Murat and Grest. There is a growing number of dendrimer simulations that include explicit solvent models. [60, 62, 65, 68, 70–72, 75] However, all of these simulations have been limited to a few hundred picoseconds at most. This is partly due to the shear

size (number of atoms) of the simulation and complexities inherent to explicitly solvated large polymeric systems. The computational resources required for such a study have, until recently, only been available through super-computing facilities.

Despite the widespread commercial and academic use of Fréchet dendrimers, only explicit solvated simulations of PAMAM, PPI and glycodendrimers have been reported. [60, 62, 65, 68, 70–72, 75] However, detailed analyses of vacuum simulations have been reported. [2, 77] Hughes et al. conducted a series of MD simulations of organic and organometallic-terminated Fréchet dendrimers (G1 to G5) in vacuum. Their aim was to investigate whether dendrimers were suitable catalytic supports. Hughes showed that from the time evolution of the radius of gyration, in vacuum the dendrimers fold rapidly (in the order of tens of picoseconds) and remain contracted for the duration of the simulation. From radial distribution profiles, the authors showed that all the dendrimers adopted a "dense core" conformation. In addition, they suggested backfolding was equally prevalent in the organic and organochromium dendrimers in the smaller generations (G1 to G3) while in the larger generations (G4 and G5) the terminal groups of the organochromium terminal groups do not penetrate to the core as readily as the organic terminal groups. The authors concluded that despite the compact nature of the dendrimers, the terminal groups were readily accessible to act as catalysts in a chemical reaction. Ortiz and co-workers essentially repeated the simulations conducted by Hughes (G1 to G4). [77] However they used the PCCF force field which allowed for the flexibility to treat electron delocalization in aromatic rings. [77–79] Ortiz et al. observed similar radial distribution profiles to Hughes et al. although the average radius of gyration calculated by Ortiz et al. were slightly larger than those reported by Hughes et al. and reported significant backfolding especially in the larger generations. From donor/acceptor distances and Förster energy-transfer rates calculated as a function of dendrimer generation, Ortiz and co-workers demonstrated the wrapping of peripheral groups to the core of the dendrimer was comparatively rare, yet dominates the rate constant of energy transfer and leads to very short donor/acceptor distances.

This chapter is an extension of Hughes and co-worker's study of Fréchet dendrimers. Here we present a detailed analysis of MD simulations of a series of explicitly solvated organic Fréchet dendrimers (G1 to G5). Chloroform and THF were selected as the solvents of choice for this study and have been discussed in detail in Chapter 4. Where appropriate, the results of the explicit solvent simulations are discussed in relation to previously

Figure 5.1: The coordinate system employed in this thesis to describe the view of the dendrimer. The core group has been identified in yellow, while the methyl group is purple and the central ethylene atom is coloured purple. The "Top" of the dendrimer is defined as view from the methyl group (purple) down the alkyl bond to the central core atom (blue), perpendicular to the plane of the three aryl rings of the core, while the "Side" is a view parallel to the plane of the core, and "Below" is the view from the central core atom down the bond to the core methyl group.

reported studies of the same series of dendrimers in vacuum. [2, 77] This Chapter begins with a description of the simulation details. This is followed by a detailed analysis of the structural properties including traditional analytical methods, such as radius of gyration, moments of inertia and radial distribution functions. This is followed by the spatially averaged analysis of the dendrimers. An analysis of the dynamics of the dendrimer follows and are discussed in relation with measured experimental results reported in the literature. This chapter closes with an analysis of the solvent structure and diffusion in and around the dendrimer. To assist with the description of the dendrimer and solvent structure in the spatially averaged analysis, we define a simple coordinate system for a dendrimer, centred at its core and detailed in Figure 5.1

5.2 Computational details

All simulations in this chapter were performed using the CHARMM molecular modelling program. [133] The force fields used to describe the dendrimer and solvents are discussed in Chapter 4. Group-based cut-offs were applied for long range interactions with a switching function applied between 10 Å to 12 Å. A list of the nearest neighbours up to 14 Å was

Chloroform			
Generation	Solvent residues	Dendrimer atoms	Cell size /Å
1	2081	164	65.54
2	2053	332	65.54
3	1994	668	65.54
4	2964	1340	93.88
5	2850	2684	93.88
THF			
1	711	164	46.1
2	851	332	62.00
3	1324	668	72.00
4	1909	1340	82.00
5	2605	2684	92.00

Table 5.1: Simulation details of dendrimers G1 to G5 in chloroform and THF

maintained and updated every 10 steps of the simulation. Bonds between hydrogen and heavy atoms were restrained using the SHAKE algorithm with a convergence tolerance of 10^{-10}. [134] The equations of motion were integrated using the Leap-Frog method. Periodic boundary conditions were invoked for the explicitly solvated systems and were not invoked for the vacuum simulations. [134] For the solvated systems, dendrimers G1 to G3 were simulated using cubic periodic cells while dendrimers G4 and G5 were simulated using truncated octahedron periodic cells. The details of the solvated systems are presented in Table 6.1).

Starting conformations An initial coordinate set for each dendrimer was created using an iterative CHARMM script to create extended conformations of the dendrimers. [248] Each dendrimer was then minimized first using the steepest descent algorithm for 1000 steps, followed by further minimization using the Newton-Raphson algorithm until convergence was achieved. This was used as the starting conformation for the vacuum simulations.

In the solvated system, the primary periodic cell containing only the solvent was equilibrated for 500 ps. The dendrimer was included by placing it at the centre of the primary periodic cell and removing all solvent molecules that overlapped with the dendrimer

(overlap was defined as when a solvent and solute atom are within 2.0 Å). Thereafter, the system was briefly minimized using the Newton-Raphson algorithm to remove any remaining solute-solvent steric clashes. To avoid regions within the solvent approaching unrealistic solid-like configurations, complete convergence of the minimisation procedure was prevented.

Simulation conditions For the vacuum simulations, we used the protocol of Hughes et al. [2] This entailed an initial heating phase of 15 ps (from 10C K - 293.15 K) followed by a further 600 ps where the velocities were periodically rescaled to maintain the correct temperature of 300 K, effectively resulting in a canonical ensemble. [2]

After deriving a starting configuration for the solvated system, this was followed by an initial NVT heating phase where the temperature was raised incrementally from 100 K to 293.15 K by 5 K every 5 ps by periodically rescaling the velocities. Thereafter the temperature was held constant (within 5 K of 293.15 K) for the remainder of the heating phase (a total of 200 ps) and a further 200 ps of equilibration. Finally this was followed by five nanoseconds of simulation performed using a microcanonical ensemble (NVE).

Representative conformations of the average equilibrium structure of the dendrimer were derived by calculating a coordinate set of the average position for every atom over a selected period of the simulation, typically the final 200 ps. This coordinate set did not necessarily represent a feasible conformation due to atoms overlapping or even superimposed on top of one another. Therefore, each frame of the trajectory was compared to this average structure. Using a least squares criterion, the trajectory frame that offered the closest match to the average structure was selected as the representative equilibrium conformation.

Analysis specific details All analysis (excluding T_1 relaxation rates) was done with computer software packages written by the author and within our research group. [166,175] Longitudinal relaxation rates were calculated employing the Charmm NMR analytical tools. [133]

Analysis of vacuum simulations was performed over the last 30C ps of the simulation. For the solvated systems, the same analysis was carried out over the last 1 ns of the simulation. For reasons of clarity, only the aromatic carbon atoms are considered in the spatially average distributions. In the T1 analysis, the overall rotational correlation time was approximated using the Stokes-Einstein relation and the atomistic relaxation rates

	R_g/ Å		
Generation	Vacuum	THF	Chloroform
1	6.53 ± 0.35	10.21 ± 0.35	9.85 ± 0.45
2	8.35 ± 0.31	13.38 ± 0.48	13.48 ± 0.39
3	10.08 ± 0.25	16.45 ± 0.50	16.74 ± 0.42
4	13.15 ± 0.12	19.75 ± 0.32	19.84 ± 0.21
5	15.62 ± 0.12	22.19 ± 0.20	22.20 ± 0.13

Table 5.2: The average R_g values calculated from the last 200 ps for the vacuum simulation and for the last 1 ns from the solvated systems (THF and chloroform)

calculated over the final 500 ps.

5.3 Results and discussion

5.3.1 Dendrimer size and shape

This section opens with a discussion of the methods commonly used to analyse the shape and size of dendrimers, in particular the time evolution of the radius of gyration and the ratios of the principle moments of inertia. We discuss the radially averaged distribution functions and consider various forms in which the data can be presented and the different perceptions that can result from such analysis. This section closes with the 3D characterisation of the density distribution about the dendrimer.

Radius of Gyration

In Figure 5.2, the time evolution of R_g of the dendrimers in vacuum is compared with the time series for the explicitly solvated dendrimers. Although the vacuum system rapidly folds in less than 50 ps, after more than 5 ns, the dendrimers in THF and chloroform remain extended. The average R_g are detailed in Table 5.2

A comparison of the average equilibrium conformation (Figure 5.3 using G5 as an example) for each simulation confirms that the dendrimers remain extended in THF and chloroform. For the chloroform system, this apparently contradicts the conclusions drawn by Jeong et al. from their intrinsic viscosity measurements of Fréchet dendritic wedges. [118] (The viscosity measurements of dendrimers are discussed in detail in Section 5.4.1) Fur-

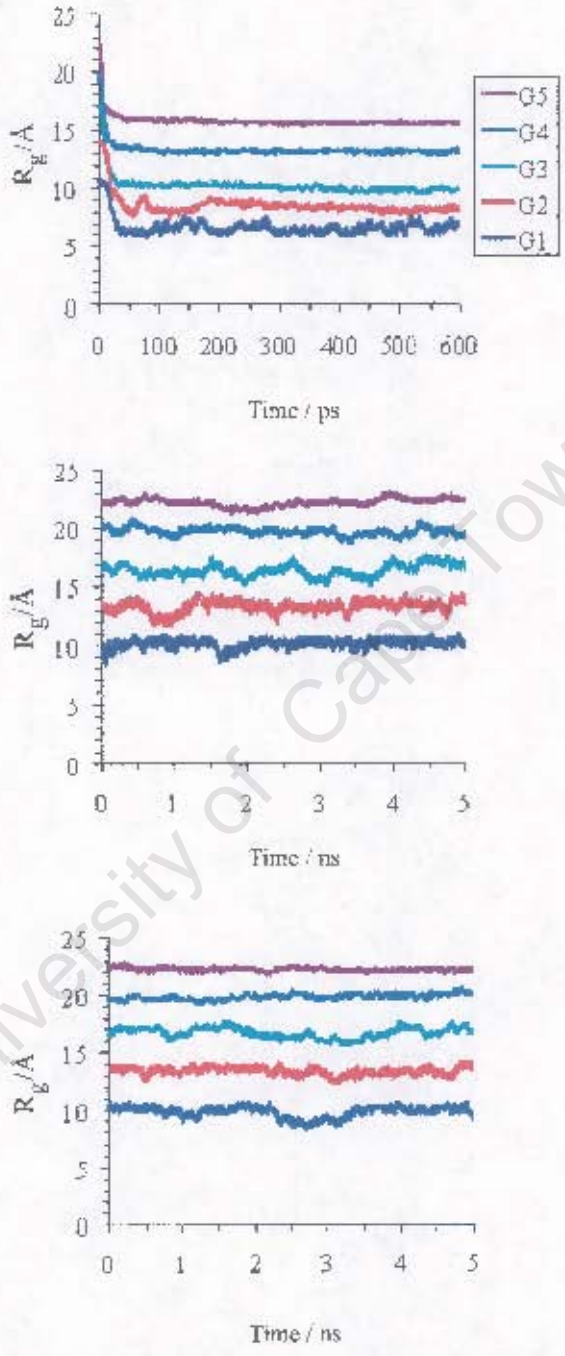

Figure 5.2: The time evolution of the radius of gyration (R_g) for the (A) vacuum (B) THF and (C) chloroform dendritic systems.

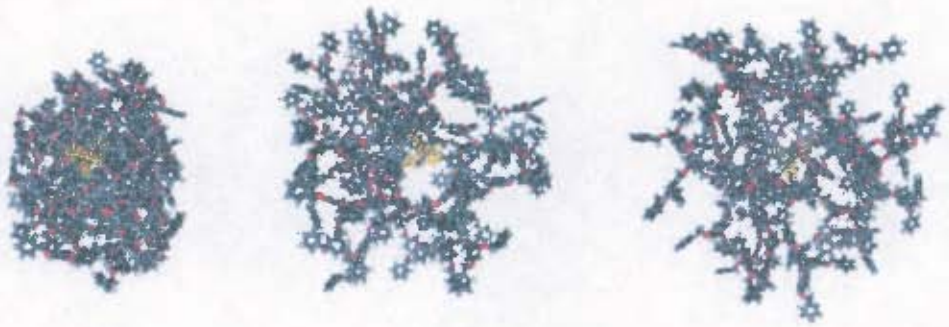

(A) (B) (C)

Figure 5.3: The average equilibrium conformations of G5 dendrimer in (A) vacuum, (B) THF and (C) chloroform systems.

ther, our R_g results contradict the findings of Murat and Grest, who predicted from their coarse grain model that the dendrimer would have a compact structure for all solvent conditions. [44] This strongly suggests that the inclusion of solvent in simulations of Fréchet dendrimers makes a large contribution to the conformation and dynamics of the system. Comparisons with experimental results in solution, presented later, support the results obtained with explicit solvent simulations. However, vacuum simulations implicitly modelling a good solvent (such as considering only repulsive nonbonded interactions) can produce conformations that approximate a dendrimer in an explicit good solvent. Throughout this chapter, we note further differences between the good solvent and vacuum simulations.

Moments of inertia

In order to assess the shape of the dendrimer system, the ratios of the principle moments of inertia of the dendrimers in vacuum, THF and chloroform are shown in Figure 5.4. There is a similar trend exhibited by the dendrimers in chloroform and THF, and vacuum, with the notable exception of dendrimer G4 in vacuum. In general, the ratios of the principal moment of inertia decreases and approach unity as the size of the dendrimer increases. Dendrimer G4 in vacuum is a notable exception to the trend and this suggests that this dendrimer folds in an anisotropic fashion. This is discussed later in this Chapter using spatially averaged methods (Section 5.3.2). There are some small differences between the THF and chloroform simulations, the most notable difference visible at G2, where the

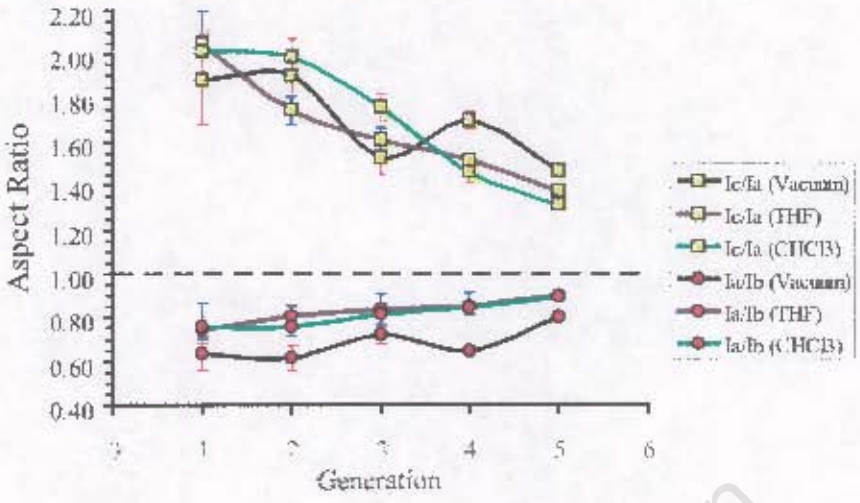

Figure 5.4: The ratios of the principle moments of inertia (aspect ratio) for the dendrimers vacuum, chloroform and THF dendrimer systems. The error bars represent the standard deviation of each of the time series.

dendrimer in THF is more spherical than the dendrimer in chloroform (1.75 and 1.99 respectively). In general, the smaller dendrimers adopt more spherical conformations in THF than in chloroform, while in the larger dendrimers (G4 and G5), the dendrimers are marginally more spherical in chloroform than in THF. However, it is difficult to gain a clear understanding of the overall structure of the dendrimer from an analysis of the principle moments of inertia alone. Hence, in the following section, we analyse the distribution of groups within the dendrimer.

5.3.2 Dendrimer intramolecular distribution profiles

This section begins with a discussion of the methods commonly used to analyse the distribution of the various topological layers within the dendrimer and the radial density distribution. In particular, the usefulness of the terminology of "hard shell" and "dense core" density profiles is explored by consider the effect of the method used for normalising these distributions and the various ways in which the data can be presented creating significantly different perceptions. This section closes with the 3D characterisation of the density distribution within the dendrimer.

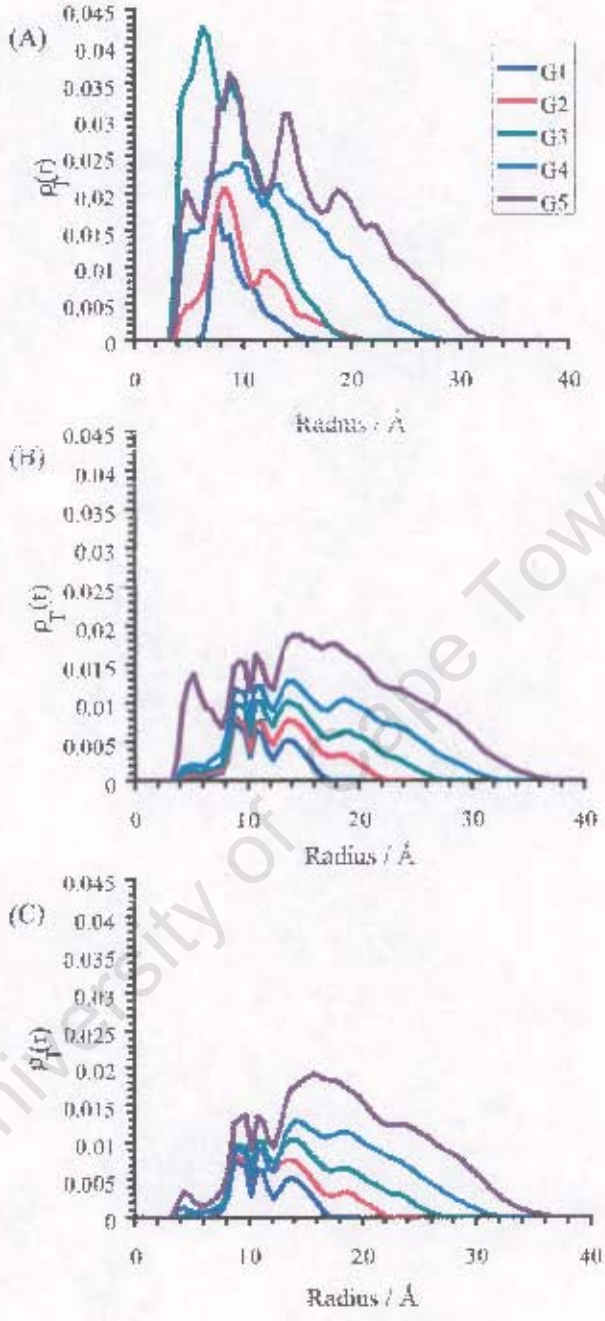

Figure 5.5: Radially averaged distributions of the total density ($\rho_T(r)$) of dendrimers G1-G5 in (A) vacuum, (B) THF and (C) chloroform. These distribution profiles represent the sum of the density contributions from each topological layer within the dendrimers, but exclude the contribution of the density of the core group to avoid obscuring the effect of backfolding from the other topological layers to the core. See Figure 5.7 and Appendix B for the density profiles of the topological layers the dendrimers.

Radially averaged analysis

First we consider the total radial density distributions of the dendrimers (the sum of the contributions from each topological layer) for the three series of simulations. We refer to the total density distribution as $\rho_T(r)$ and an individual topological layer's density distribution as $\rho_l(r)$ where r is the distance from the selected atom to the centre of the core of the dendrimer. Illustrated in Figure 5.5 are $\rho_T(r)$ of the dendrimers in vacuum, THF and chloroform. $\rho_T(r)$ of the vacuum simulations (Figure 5.5A) have been discussed previously. [248] Nevertheless, it is useful to briefly mention some of the important features for comparative purposes. The vacuum $\rho_T(r)$ are characteristically "dense core" (as defined in the introduction of this thesis) which is most prominent in dendrimer G3. This suggests that the greatest degree of backfolding occurs in this dendrimer. $\rho_T(r)$ decreases from the "dense core" out toward the periphery of the dendrimers. In dendrimers G4 and G5, $\rho_T(r)$ does not decrease monotonically as suggested from equilibrium self-consistent mean field calculations of model dendrimer systems. [37] Instead, in these large dendrimers we observe several local minima, the deepest minimum centred at 11.8 Å, with a ρ_{min}/ρ_{max} ratio of 75% and 55.6% for dendrimers G4 and G5 respectively. These ratios indicate regions of lower density, such as cavities or channels within the dendrimer. These ratios are smaller than those reported for other dendritic systems, especially for G5. [38] This suggests that Fréchet dendrimers G4 and G5 are capable for hosting guest molecules even in their folded conformations.

In contrast, the THF and chloroform solvated systems (Figures 5.5 B and C respectively), exhibit a far more evenly distributed density profile, exhibiting "hollow core" characteristics with a "dense shell" centred at approximately 15 Å. The density profiles for the dendrimers in THF and chloroform are almost identical, with the exception of the prominent peak at 5.25 Å in the G5 dendrimer in THF, which is significantly smaller for the same dendrimer in chloroform. This suggests that a higher degree of backfolding occurs in THF than in chloroform. In both these solvents, there are minima in $\rho_T(r)$ of all the dendrimers, most notably at 10.25 Å, 17.25 Å and 22.35 Å, with points of inflection centred at 27.25 Å and 32.25Å. Because these minima (and points of inflection) are at regular intervals, and coincide with the end of the terminal layer of the smaller generation dendrimer, these minima indicate the position of the junction (or ether linkage) between two topological layers. As these minima are regularly dispersed, they also strongly suggest that the topological layers of the dendrimers form concentric shells as assumed by de

Gennes and Hervet. [9] The substantial difference between the $\rho_T(r)$ of the vacuum and solvated dendrimers further highlights the differences between vacuum and explicit solvent simulations of Fréchet dendrimers.

However, radial *density* distributions profiles ($\rho(r)$) should be interpreted with care, as their results may be misleading. $\rho_l(r) = N_l(r)/V(r)$, where $V(r)$ represents the volume of the shell (of width $\Delta r - 1$Å) used to normalise $N_l(r)$, the sample of the population of layer l, that lies within the shell at distance r from the core. $V(r)$ increase from the core out to the periphery. Therefore, a higher density near the core ($\rho_l(r)$) does not indicate a greater number of groups within this region (i.e., larger $N_l(r)$) in comparison with a low density region at a greater distance from the core. $\rho(r)$ does not indicate *how many* groups contribute to a particular region of density. For example, in Figure 5.6, we compare the various radially averaged distributions ($\rho_l(r)$, $N_l(r)$ and $P_l(r)$) for each layer of the G5 dendrimer in vacuum. (The complete set of radially averaged distribution functions for all dendrimers G1 to G5 in vacuum, THF and chloroform is included in Appendix B). From $\rho_l(r)$ (Figure 5.6A), it is generally agreed that the dendrimer undergoes substantial backfolding. [2] For example, $\rho_l(r)$ of the terminal layer has a large peak from 3.5 Å spanning 4.5 Å from which one could be tempted to assume that there is a substantial degree of backfolding of terminal groups in to the core and as a result, the majority of the terminal groups are located near the core. However, $N_l(r)$ (Figure 5.6B) presents a significantly different picture of the distribution of the topological layers within the dendrimer; $N_l(r)$ of the terminal layer indicates that in the $\rho_l(r)$, the large peak near the core comprises only a small sample of the total terminal group population. In the integration of $P_l(r)$ (Figure 5.6C) this peak accounts for approximately 10% of the total population of terminal groups. Nonetheless, this is notably more backfolding than in the explicit solvent systems. The use of number density functions is not novel. Gorman et al. showed similar trends in their NDF and RDF analysis of Fréchet related dendrimers. [73] Of particular interest is the similarity in the NDFs and RDFs of Gorman et al.'s stiff repeat unit dendrimers with the our equivalent profiles in THF and chloroform. This suggests that in an explicit good solvent, the dendrimer is extended and the groups of each layer are suspended in the solvent in such a way as to constrain them to specific regions and give the equivalent effect of stiff repeat units.

In general density distribution profiles are described qualitatively, i.e., whether $\rho(r)$ fits a "dense core" or "dense shell" profile. In order to determine whether additional back-

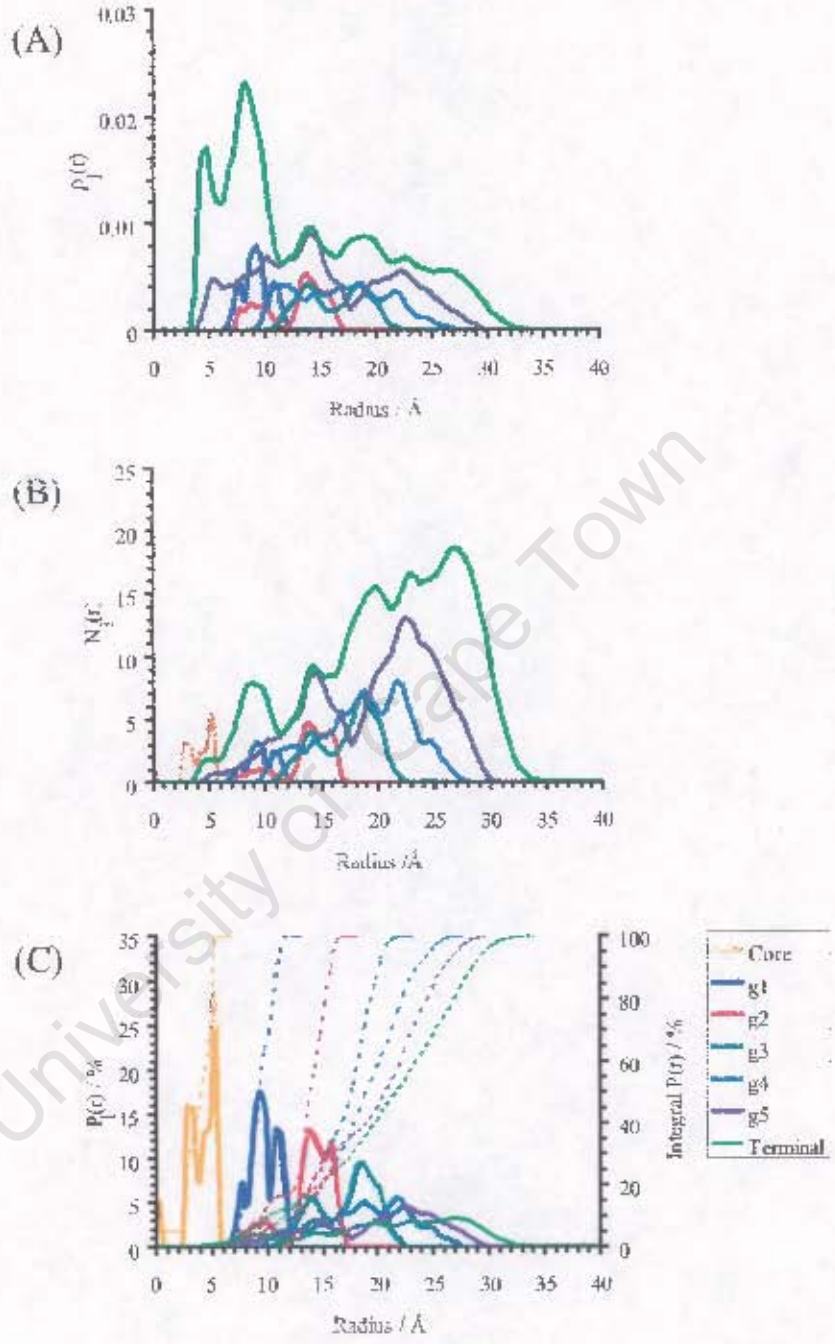

Figure 5.6: Radially averaged distributions for the topological layers of a G5 dendrimer in vacuum, (A) normalised by the shell volume ($\rho_l(r)$), (B) non-normalised or number density ($N_l(r)$) and (C) percentage of the population of each layer ($P_l(r)$).

folding may occur or if host molecules could be accommodated within the high density regions, it would be useful if there was a quantitative limit available to indicate the density beyond which no additional groups could be accommodated within the dendrimer. Currently, it is unclear what this backfolding limiting density is, i.e., what is the maximum number of terminal groups that the internal generations can accommodate. We suggest the following simple method to approximate the density limit: compare the density the dendrimer with density of the liquid which most closely represents the repeat units of the dendrimer, as if the repeat units were able to freely disperse within the volume of the dendrimer and were not constrained by the linkages between the dendrimer's monomers. For example, we define the density limit of Fréchet dendrimers as the density of benzyl alcohol ($1.043 g.mol^{-1}$). [249] For the G5 dendrimer in vacuum, the highest density occurs within the g1 layer, up to 11.75 Å (Figure 5.6A). The density, calculated from the sum of all groups from all topological layers that lie within this region, is $0.55 g.mol^{-1}$. Therefore, this high density region within the dendrimer is approximately only 52% of the density of benzyl alcohol. Therefore, the "dense core" description does not indicate the existence of an impenetrable shell surrounding core. This is somewhat surprising considering the compact structure of the average conformation of this dendrimer in the vacuum simulation. In Section 5.3.2, the 3D representation of the distribution of the layers of this dendrimer gives a clearer picture of the distribution of the groups about the core.

Continuing with the radially averaged analysis, we make a comparison of the various radially averaged distributions of the vacuum and solvated systems, focusing on the contribution of each internal layer of the dendrimer to the total density of the dendrimer, as illustrated in Figure 5.7 for dendrimer G5. In vacuum, the "dense core" in $\rho_T(r)$ is almost completely due to the terminal layer backfolding into the core which is most clearly visible for dendrimers G2 to G5 (Figure B.7). The $\rho_l(r)$ of the internal layers becomes more evenly distributed throughout the dendrimer for the outermost layers of the dendrimer. This results in significant intermixing of layers within the dendrimer in vacuum. In the solvated systems, $\rho_l(r)$ of the inner layers are localised within concentric shells, particularly layers g1 and g2 of the larger dendrimers G4 and G5. In contrast, $\rho_l(r)$ of the topological layers closer to the periphery of the dendrimer (g3 to the terminal layer) become broader and $\rho_l(r)$ is evenly distributed throughout the dendrimer. These well defined layers or concentric shells are particularly visible in $N_l(r)$ (Figure 5.8) and $P_l(r)$ (Figure 5.9) of the dendrimers in THF and chloroform. Although there appears to be

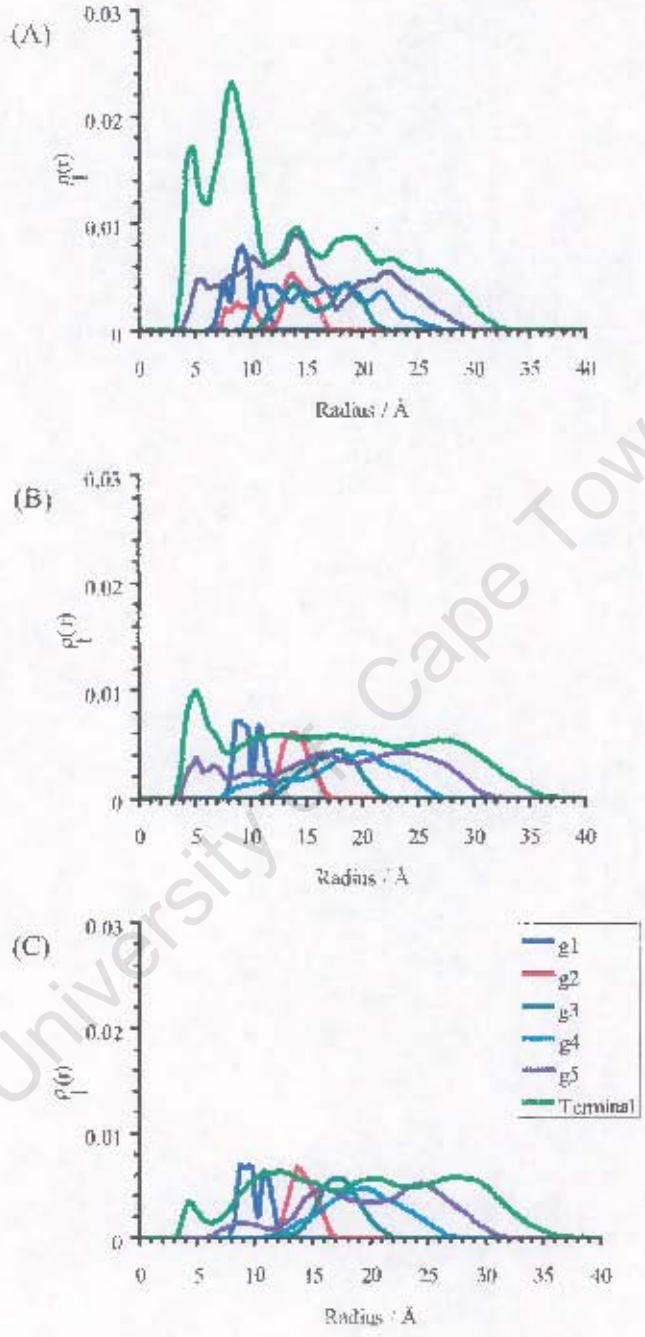

Figure 5.7: $\rho_l(r)$ of each topological layer of the G5 dendrimer in (A) vacuum, (B) THF and (C) chloroform

a degree of backfolding in the solvated systems, the plateau of constant density in $\rho_t(r)$ that suggests an even distribution of these groups throughout the dendrimer, is in fact shown in $N_t(r)$ to be a proportional increase in the number of these groups to the distance from the core. The majority of terminal groups of a dendrimer in THF and chloroform are located at the periphery ranging from approximately 100% in G1 to 50% in G5. In THF and chloroform, the dendrimer typically has a maximum of not more than 5% of the terminal groups within the first topological layer, even the large peak visible in $\rho_t(r)$ of G5 in THF. This may be interpreted as a small amount of backfolding, where the terminal groups diffuse into the body of the dendrimer. However, Gorman and Smith showed that the close association of terminal groups with the core could be accounted for by "hyper-branching effects" (Figure 5.10) - the successive branching in large stiff-chain dendrons results in the terminal groups being brought near to the core. [73] Therefore, we suggest that internal layers of the dendrimer in a good solvent behave as if the repeat units are confined to specific regions and are prevented from substantial overall displacements due to the interactions with the surrounding solvent and the connections with the groups' parent and child layers. This hypothesis is revisited later in this chapter. Additionally, the clear difference between the vacuum and solvated $\rho_t(r)$ is in disagreement with the findings of Murat and Grest. [44] They suggest, using implicit solvent models, that the difference in a dendrimer's structure between a "good" and "poor" solvent was that the intensity of the constant density region decreased as the quality of the solvent increased. The need for an explicit solvent environment seems unavoidable.

There are two assumptions inherent to radially averaged methods. Firstly, the radial distribution profiles are all relative to the position of the core of the dendrimer. In other words, it is assumed that the core is at the geometric centre of the dendrimer, which coincides with its centre of mass. Secondly, it is assumed that the dendrimers are radially symmetrical. These assumptions may be valid for dendrimers with highly coordinated cores, such as the fully substituted benzene-core dendrimers of Hecht and Fréchet [17]. However, it is doubtful that dendrimers with tri-substituted cores, such as those typical of Fréchet dendrimers and the tertiary amine core of the PAMAM dendrimers, are spherically symmetrical. The lower the degree of symmetry at the core, the less likely the dendrimer will be spatially symmetrical. It is certain that these assumptions are not valid for dendritic wedges. However numerous experimental measurements are based on these assumptions, including scattering measurements, NMR measurements and viscosimetric

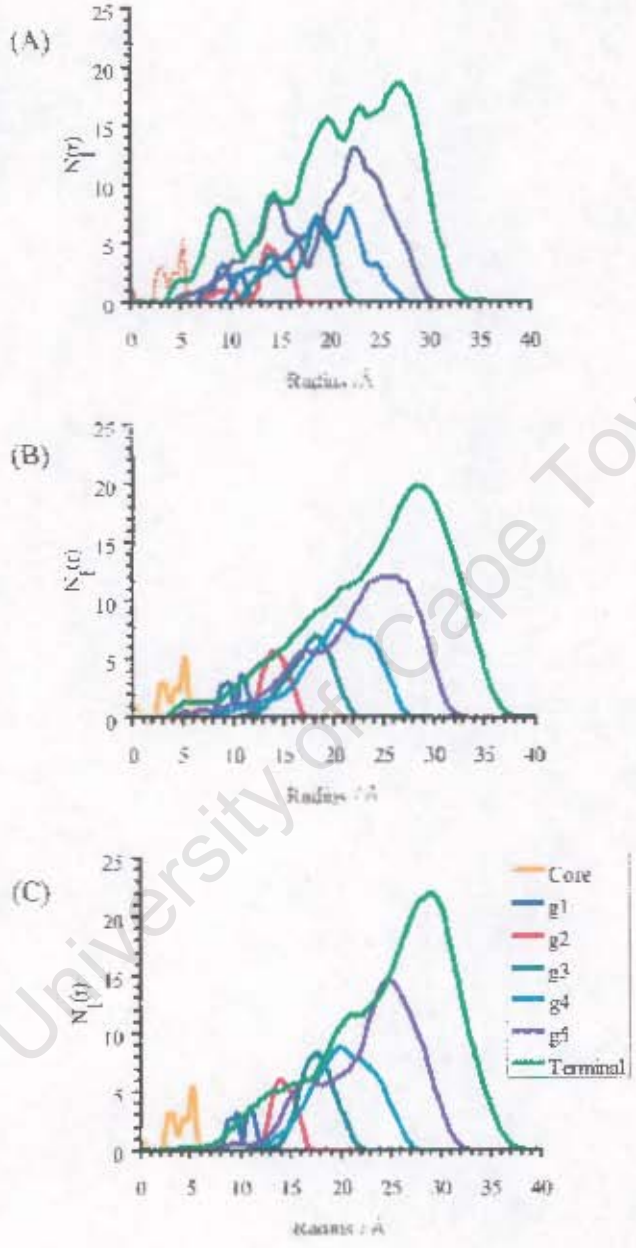

Figure 5.8: $N_l(r)$ of the topological layers of G5 dendrimer in (A) vacuum, (B) THF and (C) chloroform.

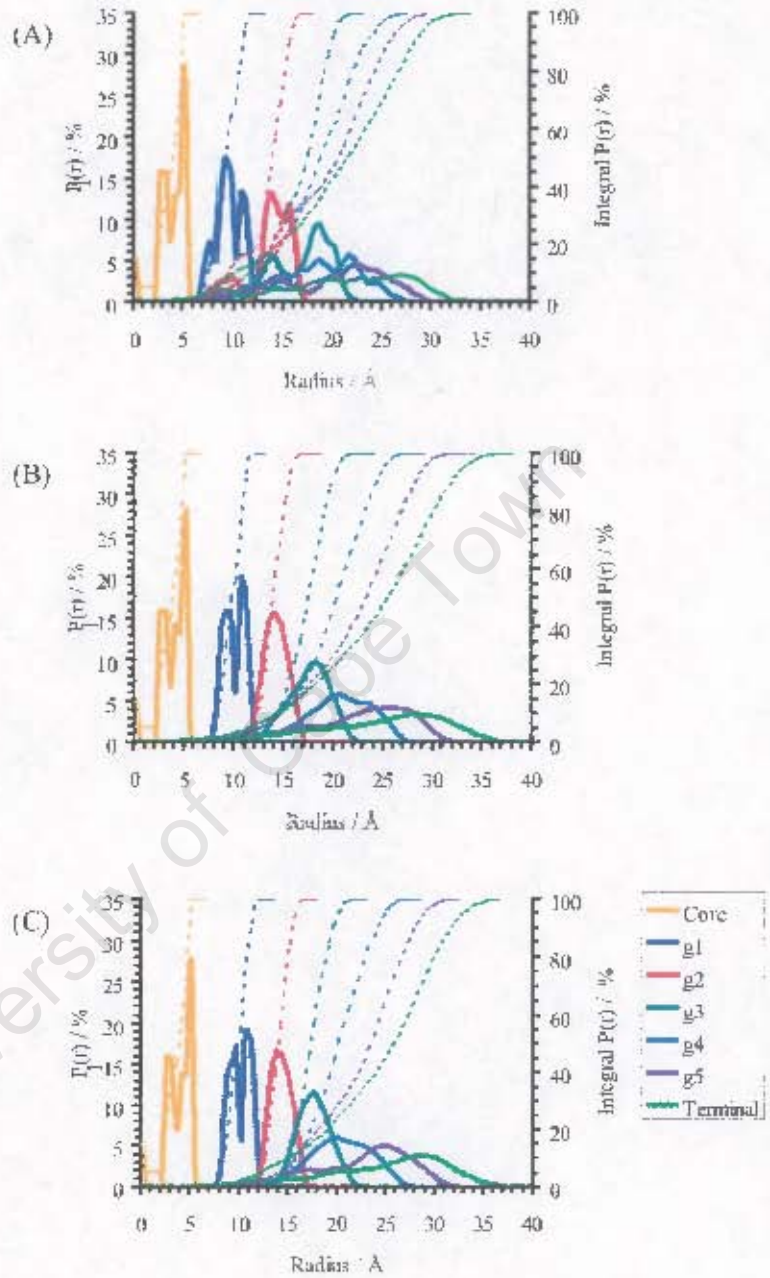

Figure 5.9: $P(r)$, the radial distribution of the percentage of the population of groups of each layer in the (A) vacuum, (B) THF and (C) chloroform systems. Included is the integration of these distributions, showing the accumulation of each group within the dendrimer as one progresses to the dendrimer's periphery.

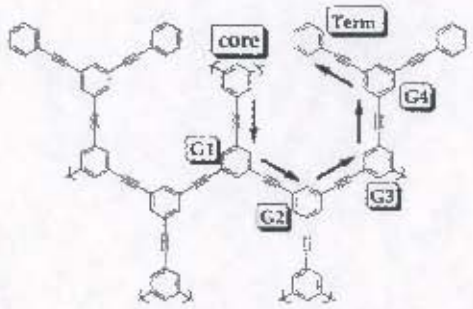

Figure 5.10: Schematic diagram depicting the inward folding of stiff-chain dendrons via a rigid branching angle that forces repeat units in toward the molecular core (Gorman et al. in Figure 6 of reference [73])

measurements. Therefore, it is still useful to describe the structure of dendrimers in terms of radially averaged methods, as long as these assumptions are kept in mind. For a better understanding of the structural nature of dendrimers, including the position of the core group, their radial symmetry and the general location of their various topological layers, spatially average representations are the next obvious step.

Spatially averaged analysis

Spatially averaged distribution functions of the solute provide a description of the 3D structure of dendrimers. An example SDF is shown in Figure 5.11 of a G3 dendrimer in chloroform (solvent molecules are not shown). For reasons of clarity only aryl carbon atoms (which make up approximately 70% of the dendrimer by mass) were considered. All isodensities presented in this chapter are at bulk density (as defined in Section 3.2.4) unless otherwise stated.

Simultaneously viewing of the entire collection of SDF's of the topological layers of a dendrimer can prove extremely challenging even when using modelling software (such as gOpenmol) that is capable of easily rotating the SDF of the dendrimer in three dimensions in real time. [173,174] Analysing these 3D SDFs in a 2D diagram is even more challenging (see Figure 5.11 as an example). Therefore, before considering any specific details, we discuss the overall size and shape of the dendrimer as depicted by the SDFs. This is followed by a description of the internal layers of the dendrimer and how each layer contributes to the overall structure of the dendrimer. However, the size of the collection of SDFs poses a significant challenge; each layer, of every dendrimer, in each solvent environment, was

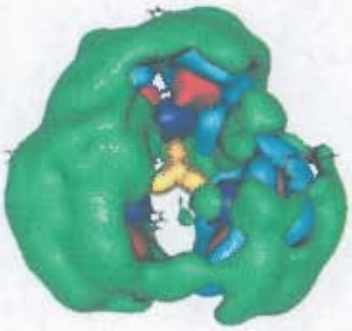

Figure 5.11: The complete set of SDF's of the topological layers of a G3 dendrimer solvated in chloroform (the solvent residues are not shown). For reasons of clarity, only aryl carbon atoms were considered. The colour coding for the topological layers used in the radially averaged methods is employed here: the core is always indicated in yellow and the terminal groups in light green, while the inner generations are coded accordingly; g1 navy blue, g2 red, g3 dark green, g4 light blue and g5 purple. All isodensities are at bulk density as defined in Section 3.2.4.

rendered at three different density distributions (50%, 100% and 200% of bulk density of each layer) from three different angles (above the core, side on to the core, and below the core). The total number of SDF's rendered is represented by a collection of over 500 figures. To describe each figure individually distracts from the general trends that exist between the dendrimers. Therefore, we select the average sized dendrimer (G3) to discuss in detail and to illustrate the general trends observed for all the dendrimers. Any significant differences in these trends for a dendrimer are also discussed. For the complete collection of SDFs, the reader is referred to Appendices C - F.

Overall size and shape of the dendrimer from the SDFs The complete set of SDFs of each of the dendrimers (G1 to G5) in vacuum, THF and chloroform are illustrated in Figures 5.12 and 5.13. From these SDFs it is clear that in vacuum, the dendrimers are completely folded, while in THF and chloroform, the dendrimers are fully extended. The vacuum SDFs highlight the asymmetrical conformation adopted by the dendrimer in vacuum. Instead of the wedges folding such that the groups are evenly distributed about the core, in vacuum the wedges of the dendrimer tend to fold under the core. This is

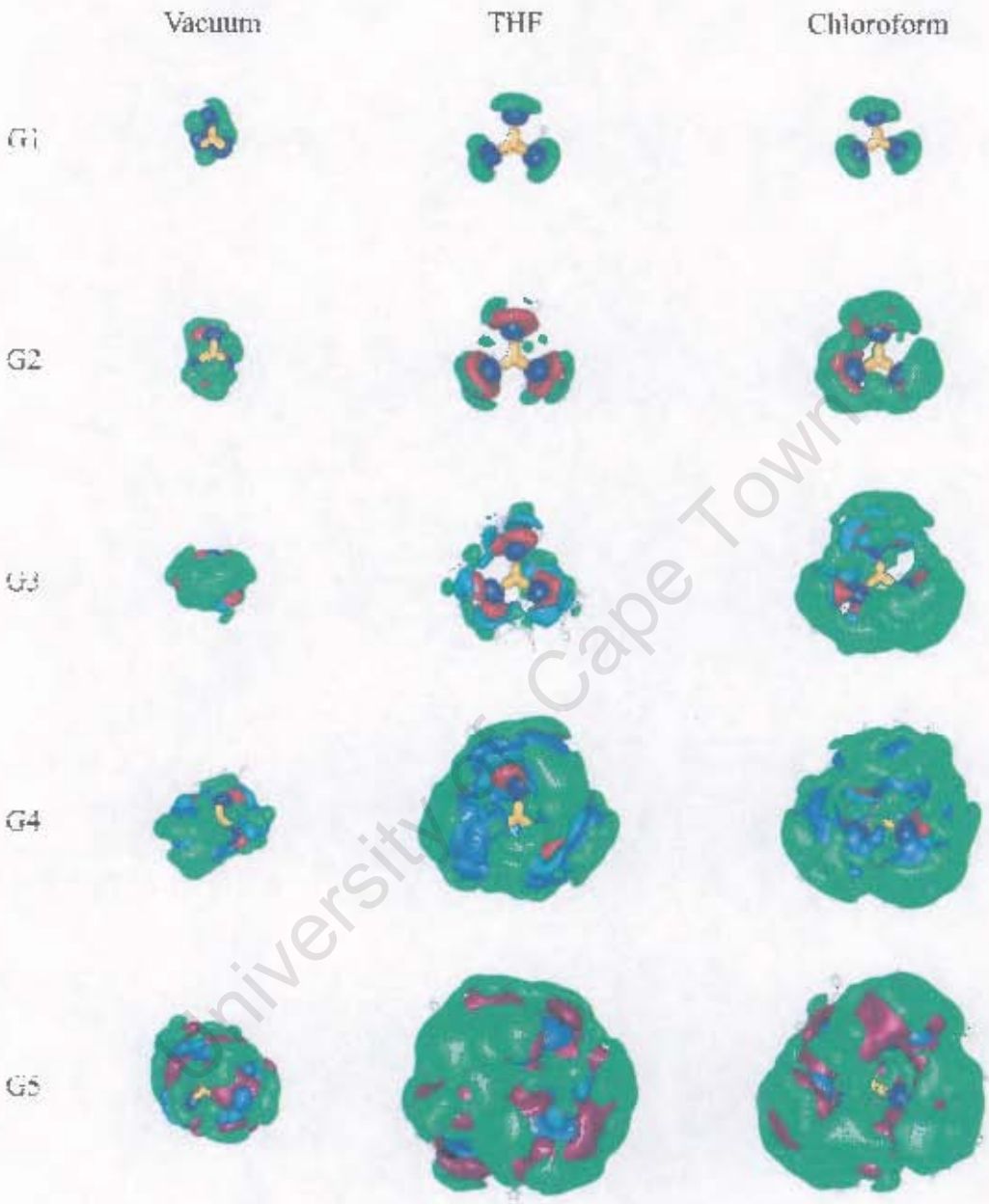

Figure 5.12: A view from above the SDFs of dendrimers G1 to G5 in vacuum, THF and chloroform at bulk density. SDFs of the dendrimers at half bulk density, bulk density and twice bulk density are included in Appendix C

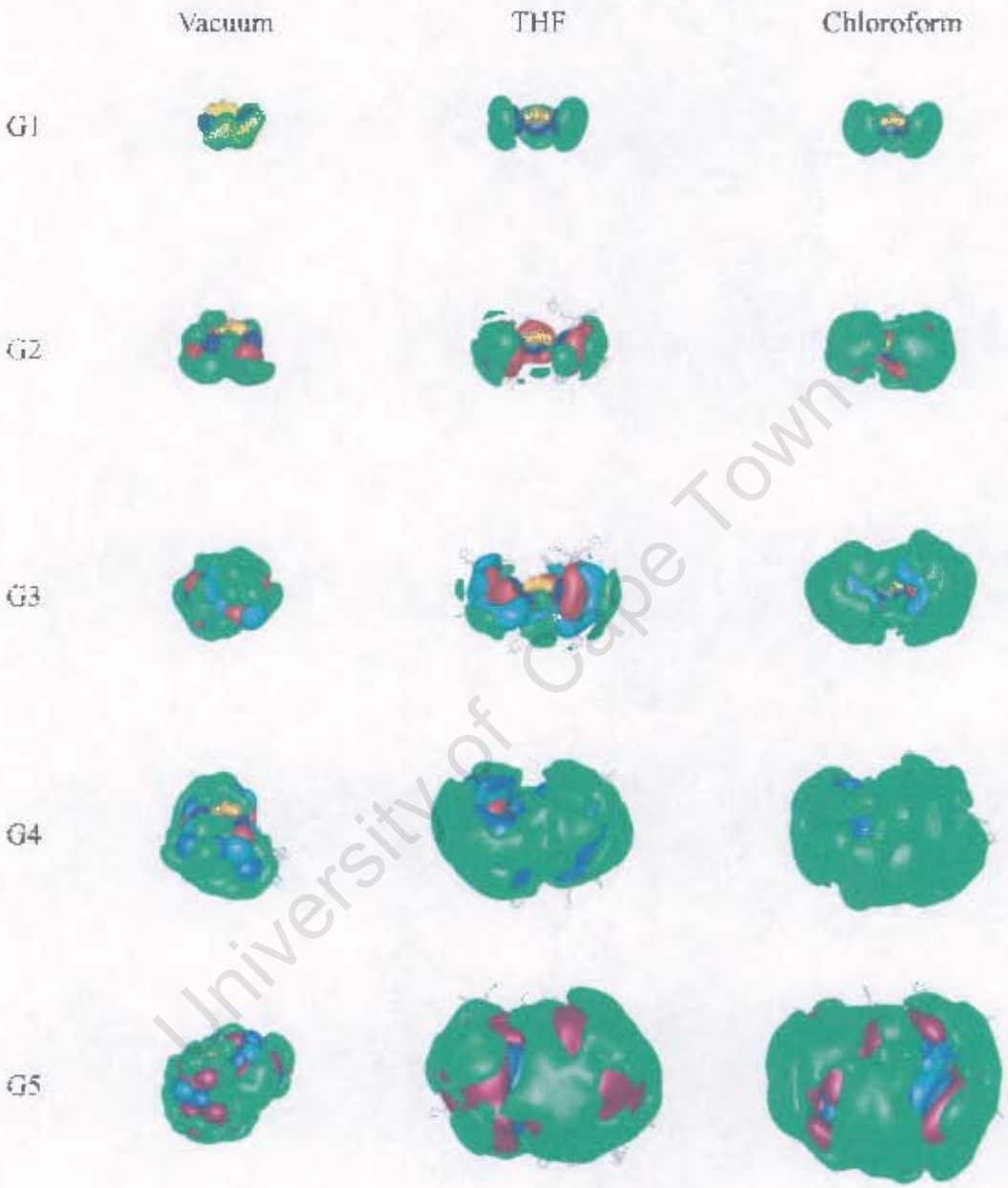

Figure 5.13: Side view of the SDFs at bulk density of dendrimers G1 to G5 in vacuum, THF and chloroform. SDFs of the dendrimers at half bulk density, bulk density and twice bulk density are included in Appendix C

most clearly visible in Figure 5.13. Dendrimer G4 represents an extreme instance of this asymmetrical folding. From the aspect ratios discussed earlier in this chapter (see Figure 5.4), the equilibrium conformation of the G4 dendrimer is not spherical. The SDFs of this dendrimer in vacuum show that a prolate, or cigar-shaped conformation is adopted. The reason for G4 dendrimer acquiring this folded conformation is not absolutely clear. A side view of the SDFs (Figure 5.13) suggests that because of the rapid folding of the wedges under the core, these wedges become entangled which results in the dendrimer's aspherical shape. This entanglement does not occur to the same extent in either the G3 (or smaller dendrimers) and the G5 dendrimer. One possible explanation is that in the smaller dendrimers the wedges are smaller and have significantly greater steric freedom than in the G4 dendrimer thus making it less likely for the wedges to become excessively entangled. In the larger G5 dendrimer, the opposite is the case - the wedges are so large that the steric crowding prevents the initial mixing of the dendritic wedges thus maintaining a more spherical shape. The asymmetrical folding prevalent in the dendrimer in vacuum results in the displacement of the geometric centre of the dendrimer away from the core. In the 2D methods, the core is assumed to represent the geometric centre of the dendrimer. The result is that instead of the core being encapsulated deep in the body of the dendrimer inaccessible to the reaction medium, the core is at or near the surface of the dendrimer. This is even the case for the large dendrimers (G4 and G5). The radially averaged distributions suggest that the core is surrounded by a densely packed shell and is inaccessible to the reaction medium. The SDFs show that the conformation of the dendrimer in vacuum suggested by the radially averaged methods (i.e., the "dense core" description) is inaccurate. Further, the fact that the core group is not at the geometric centre of the dendrimer accounts for the low value calculated for the density of the "dense core" region of G5 dendrimer as calculated earlier in this chapter.

In THF and chloroform, the groups of the dendrimer are approximately symmetrically distributed about the core, both radially, and above and below the plane of the core. However, the dendrimer is not spherically symmetrical in either solvent. The core of the dendrimer is accessible to the reaction medium in generations G1-G3, but in the larger dendrimers (particularly G5 in THF) the core is encapsulated by the terminal groups. The SDFs of the dendrimer are more well-defined in chloroform than in THF which is most clearly visible in G3. At twice bulk probability density (Appendix C), the SDFs of all the layers of the dendrimer are visible in chloroform, yet in THF, only the structure of the

internal layers is evident. This suggests that the dendrimer exhibits greater flexibility in its outer layers in THF than in chloroform.

SDFs of the topological layers of the dendrimer Here the the SDFs of each layer of the dendrimer in the three solvent environments are compared to establish how the structure of the dendrimer differs in these solvent environments as one progresses from the core out to the periphery. For this detailed analysis of the SDFs of each topological layer of the dendrimer we use the average sized G3 dendrimer as our example from which we highlight characteristics common to the full range of dendrimers (G1 - G5). The SDFs of each layer of the G3 dendrimer simulated in vacuum, chloroform and THF are illustrated in Figure 5.14. For the complete set of SDFs the reader is referred to Appendices D, F, E

In all three solvents, the SDF of the first topological layer (g1 in Figure 5.14) consists of three well defined spheroids, each representing one of the three residues making up this layer. These three spheroids form the first generation shell. The SDF of the g1 layer, is almost identical across all three environments and all sizes of dendrimers (G1 to G5) due to linkage constraints.

The SDF of the second topological layer (g2 in Figure 5.14) consists of six well defined spheroids, each representing one of the aryl rings making up this layer. In vacuum, the dendrimer adopts a folded conformation where the g2 layer is not evenly distributed about a spherical shell. Instead this layer lies beneath the core and overlaps with the shell created by the first topological layer. In THF and chloroform, these high density spheroids lie at approximately equal distance from the core, forming the second generation shell.

In the SDF of the pre-terminal layer (g3 in Figure 5.14) of the dendrimer in vacuum, there is evidence of backfolding; the pre-terminal SDF intermixes with the SDFs of the inner layers (g1 and g2 in Figure 5.14) such that some of the pre-terminal groups are in direct contact with the core group. The SDFs of the pre-terminal topological layer overlap so that the SDF does not comprise separate spheroids, as in the case of the g1 and g2 topological layers. However it is still possible to identify the most likely position of an individual ring in the pre-terminal layer. For the dendrimer in THF and chloroform, the SDFs of the pre-terminal layer differ substantially from their vacuum counterparts. In THF and chloroform, the SDF of the pre-terminal layer is located near the periphery of the dendrimer and does not consist of a collection of individual spheroids. Instead the high density regions form surfaces where it is no longer possible to associate a particular

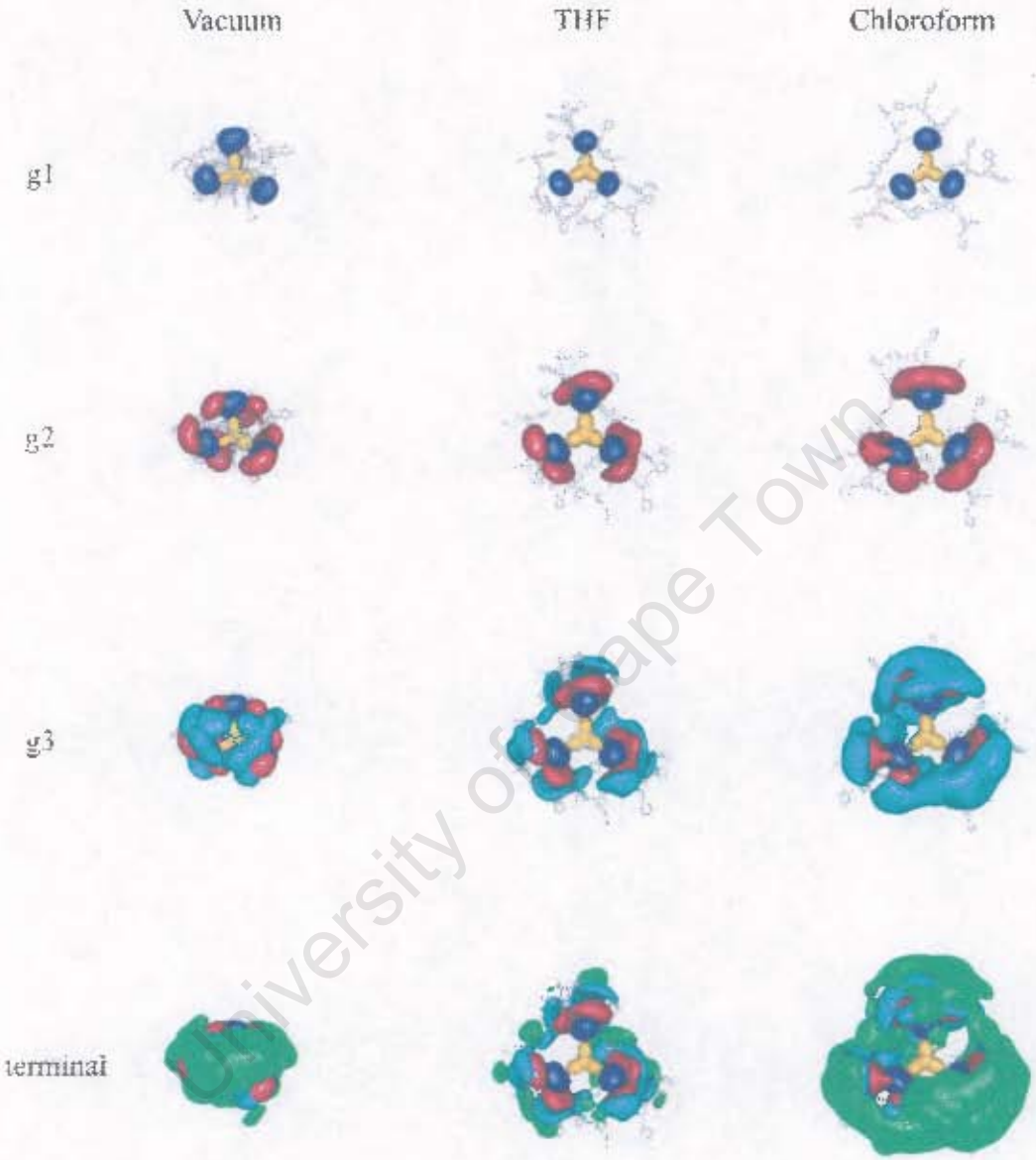

Figure 5.14: A comparison of the distribution of the topological layers of a G3 dendrimer in vacuum, THF and chloroform. The SDFs are represented at bulk density. The average conformation of the dendrimer is included to place the SDFs in perspective.

Figure 5.15: A side view of the SDFs of the G3 dendrimer in Figure 5.14.

region (or surface) of the SDF with a particular aryl ring of the dendrimer. The SDF of the pre-terminal layer is more defined in chloroform than in THF.

The terminal groups of the G3 dendrimer (labelled "terminal" in Figure 5.14)in vacuum are located at the periphery of the dendrimer and distributed throughout the body of the dendrimer, resulting in some groups coming into direct contact with the core. This is due to the dendrimer adopting a folded conformation. Although the dendrimer is in an extended conformation in THF and chloroform, some of the terminal groups are located close to the core. However, the outermost surface of the dendrimer is populated completely by the terminal groups.

The full range of dendrimers share several of the characteristics detailed for the G3 dendrimer of which some characteristics are are common to the dendrimers irrespective of the solvent environment. In all the dendrimers the SDFs of the innermost layers of the dendrimer show that the groups that make up each layer are located in clearly defined regions, even at twice bulk density. Topological layers that are closer to the periphery have less well defined SDFs and it is difficult to associate a particular region of the SDF with an individual ring. The fact that the groups of the internal topological layers are located in well defined specific regions that become less well defined as we progress to the outer topological layers, suggests that the location and diffusion of the groups making up each layer are constrained by the position and dynamics of that layer's parent and child layers. For example, in the G3 dendrimer, the region sampled by the terminal layer is dependent on the location of its parent layer (the pre-terminal or g3 layer) while the region accessible by the pre-terminal layer will be dependent on the location of the terminal and its parent layer (g2 in our example dendrimer G3). In order for a group of the pre-terminal layer to sample a significantly larger region, it would not only require its child terminal groups to also be displaced but also its parent layer to a lesser degree. Similarly, even more effort would be required to displace a group from the g2 or g1 layers. The flexibility of each layer is discussed quantitatively in Section 5.4.1.

There are some of the characteristics which the full range of dendrimers share but not across all solvents. For the dendrimers in vacuum, with the exception of the first topological layer the internal layers of these dendrimers do not lie in a spherical shell as assumed by de Gennes and Hervet. Instead, as a result of backfolding the groups of one layer mix with its parent layers. This mixing is most prominent in the outermost layers of each dendrimer, particularly the pre-terminal layer. Further, the dendrimers fold in

vacuum such that the groups are not evenly distributed about the core because the the wedges fold underneath the core. This is most clearly visible from the side profiles, as illustrated in Figure 5.15. The result is that the core of the smaller dendrimers (G1 and G2) is completely exposed to the reaction medium while in the larger dendrimers (G3 to G5), the core is less exposed as the terminal groups fold around to encapsulate the core which is most clearly visible in dendrimer G3. Finally, the structure of the vacuum SDFs are virtually independent of the probability density used to render the figure and are identical from half of bulk density to twice bulk density. This suggests that once the dendrimers have assumed a folded conformation, there are no significant conformational changes for the remainder of the simulation.

In chloroform and THF, the internal layers of the dendrimers form concentric shells up to the forth topological layer in an analogous fashion as assumed by de Gennes and Hervet. [9] From the forth topological layer onwards the effect of the hyperbranching of the dendrimer becomes visible. This is the hyperbranching effect first suggested by Gorman et al and is illistrated Figure 5.10. This results in the terminal groups of the larger generation dendrimers coming into close proximity of the core by virtue of the branching inherent to dendrimers. However, the close association of some of the terminal groups with the core should not be confused with the backfolding of these groups as observed in vacuum. In vacuum, the dendrimer folds in on itself to maximise the dendrimer-dendrimer interactions, while in a good solvent, terminal groups lying close to the core are due to the branching of the dendrimer. The SDF at half bulk density (Appendix C) illustrates the complete surface that is sampled by the dendrimer during the simulation. From these SDFs and from the R_g time series (Figure 5.2) it is clear that a dendrimer is equally extended in THF and chloroform. However, the SDFs of the pre-terminal and terminal layers at bulk density are more clearly defined in chloroform than in THF. The fact that the dendrimers are equally extended in THF and chloroform yet the SDFs of their terminal layer differ significantly in these two solvents suggests that the solvent in which the terminal and pre-terminal layer SDFs are less clearly defined, indicates the solvent in which these layers exhibit the greatest flexibility. For example, in dendrimer G3 (Figure 5.14), the terminal and pre-terminal layers are more clearly defined in chloroform than in THF suggesting that the dendrimer exhibits greater flexibility in THF than in chloroform.

There is experimental and synthetic evidence supporting the open structure of dendrimers and the accessibility of their cores to the reaction medium. The accessibility of

the internal layers of the dendrimers have been exploited chemically and functionalised with other organic or metallic derivatives and even dendrimers within dendrimers, where new dendritic wedges are attached to the internal layers of the dendrimers. [23] Similarly the accessibility of the core by the reaction medium is well documented, including the numerous accounts of dendrimers with functionalised cores [17, 102, 106, 107, 124, 250–252] (as opposed to a functionalised periphery) and reports where the core itself has been completely removed from the dendrimer [22, 253].

Location of the terminal groups As mentioned previously, including the complete set of SDFs of all the layers of a dendrimer is difficult to establish the extent to which the terminal groups diffuse into the body of the dendrimer. To overcome this difficulty and analyse the location of the terminal groups in relation to the core, we compare cutplanes through the SDFs of the G5 dendrimer in the three solvent environments. To readily establish the position of the terminal groups, these cutplanes are simplified and only include the terminal layer and core group. (For the full series of SDFs and cutplanes, the reader is referred to Figures G.1 to G.3 in Appendix G.) In vacuum, the cutplanes are very similar among the different sized dendrimers in vacuum, with the greatest density lying beneath the core. The result is that the core is afforded very little protection from the reaction medium by the terminal groups which appear to be evenly distributed throughout the dendrimer. In THF and chloroform, the terminal groups are located primarily at the periphery of the dendrimer forming what resembles a dense shell. From the top view of the cutplane, it can be seen that the terminal groups diffuse into the core. However, the terminal groups are not evenly distributed through out the dendrimer, but are concentrated in specific regions giving the effect of spokes on a wagon wheel. This is most clearly visible in G5 in THF. From the side view, the terminal groups are located in a dense shell at the periphery of the dendrimer, yet there is a significant probability of locating a terminal group near the core.

The conventional argument that the distribution of the terminal groups throughout the dendrimer is due to backfolding as a result of congestion at the periphery, is a possible explanation for the structure observed in the SDFs and cutplanes. However, the low densities observed for the terminal groups in the SDFs suggest an alternative explanation, namely Gorman's "hyperbranching" effect. From the SDFs and cutplanes we propose that the structure of the dendrimer can be described in terms of the schematic representation

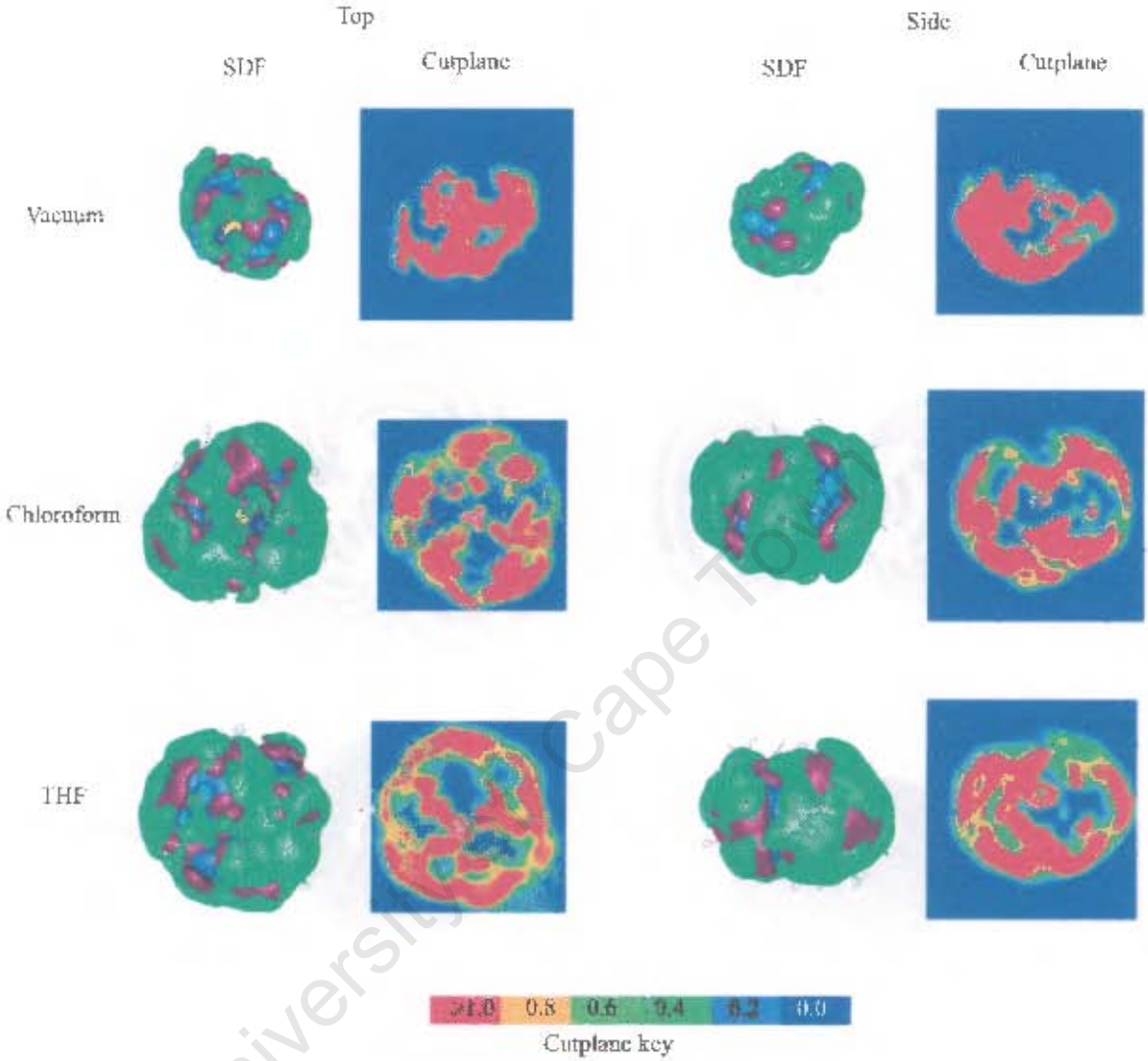

Figure 5.16: A comparison of the top and side view of the cutplanes through the SDF of dendrimer G5 at bulk density in vacuum, THF and chloroform. (The full SDFs are included as a point of reference.) The cutplanes only include the terminal layer and core group so that the location of the terminal groups relative to the core can be more easily identified without the added complexity of the internal layers. The key represents the density distribution within each cutplane, red represents areas where the density of the terminal or core group is equal to or greater than bulk density and blue represents zero probability. The complete series of cutplanes is illustrated in Appendix C.

in Figure 5.17. This schematic representation of the layered structure of the dendrimer accounts for the conflicting results that show that on the one hand the terminal groups are at the surface of the dendrimer, while on the other hand the terminal groups are in close proximity to the core. [57, 96]

5.4 Solute dynamics

In the previous section, we showed that the dendrimers are equally extended in chloroform and THF. This is contrary to conclusions drawn from experimental measurements of dendrimers and dendritic wedges in THF and chloroform, which suggests that dendrimers in chloroform should be half as extended if the dendrimer was solvated in THF. [118] Further, the SDFs suggest that a Fréchet dendrimer is more flexible in THF than in chloroform. In this section we investigate the dynamics of the dendrimers in THF and chloroform in an attempt to provide a suitable alternative explanation as to why these dendrimers behave so differently in the THF and chloroform. We begin by calculating the overall diffusion coefficients which is followed by a discussion of intrinsic viscosity calculations. This section closes by characterising the dynamics of the internal layers of the dendrimer by calculating the rate of diffusion for each topological layer and the longitudinal relaxation rates of important atomic components within each layer.

5.4.1 Overall dendrimer dynamics

Diffusion Coefficients

In Figure 5.19 we present a comparison of our calculated translational diffusion coefficients of Fréchet dendrimers in chloroform and THF with measured diffusion coefficients of several other dendritic systems reported in literature. Although none of the dendrimer-solvent systems used as comparisons are identical to our simulated dendrimer-solvent systems, they afford a degree of confidence in our simulations - the variety of types of dendrimers in different solvents, pHs and temperatures have diffusion coefficients within the same order of magnitude as our calculated values which suggests that this is the typical range in which most dendrimers diffuse. The diffusion coefficients calculated from our simulations fall comfortably into this range. A summary of our calculated diffusion coefficients is listed in Table 5.3.

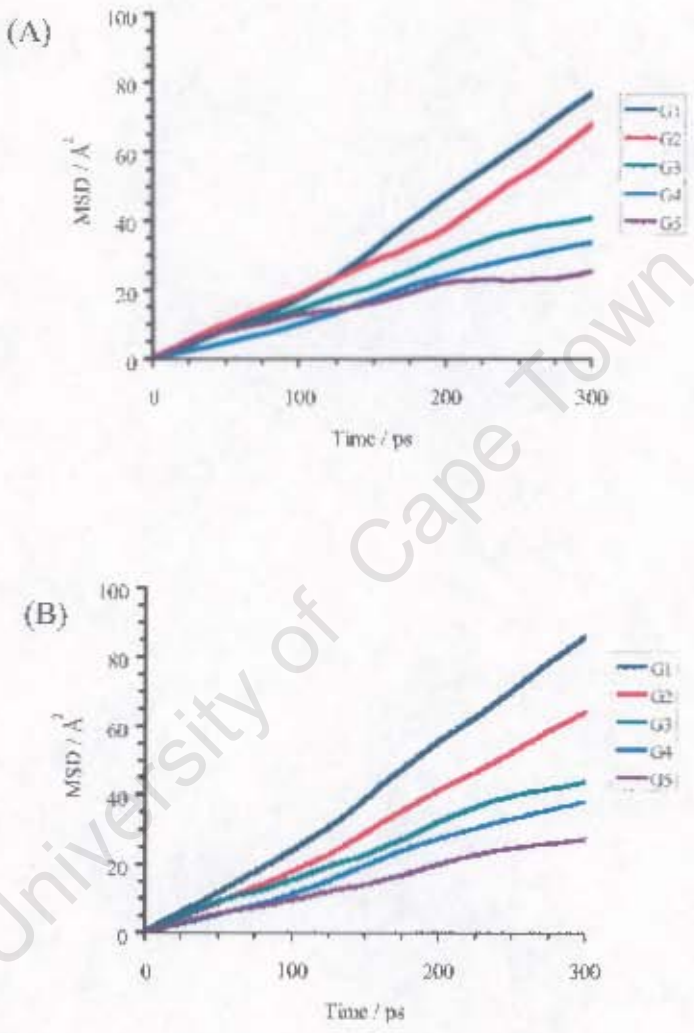

Figure 5.18: Mean squared displacement (MSD) of dendrimers G1 to G5 in (A) THF and (B) chloroform. From this Figure 5.19 was generated.

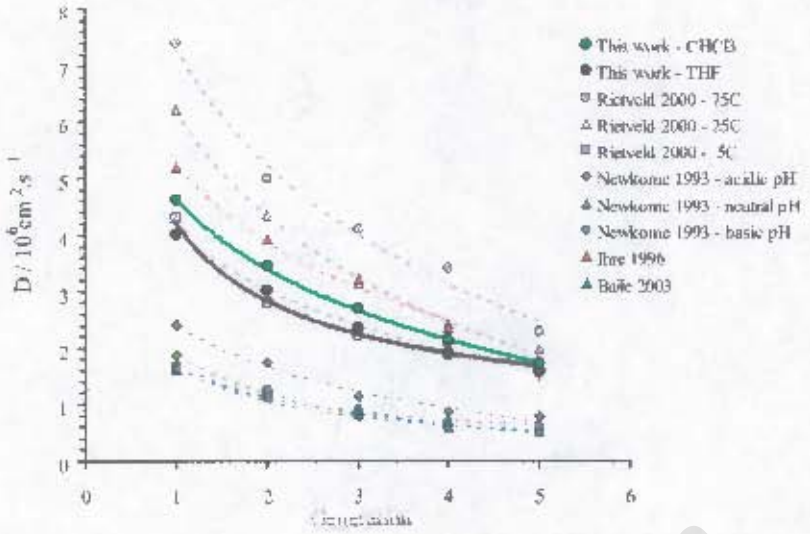

Figure 5.19: The calculated translational diffusion coefficient of Fréchet dendrimers in THF and chloroform in comparison with a selection of diffusion coefficient profiles for other dendritic systems where the lines represent the exponential fit for each series (see Figure 5.18 for MSD profiles). Rietveld 2000 - PFGSE NMR measurements on PPI dendrimers in methanol; [114] Newkome 1993 - DOSY NMR measurements of a selection of a variety of PAMAM-type dendrimers in D_2O under different pHs; [111, 112] Baille 2003 - PFG NMR measurements on PPI dendrimers in D_2O [105]

In general the rate of diffusion has an inverse exponential relation with the size of the dendrimer, in both THF and chloroform. Surprisingly, the dendrimers diffuse faster in chloroform than in THF. One would expect the opposite to occur as chloroform is almost twice as dense as THF (although the viscosities of THF and chloroform are identical). The radius of hydration (R_h) was calculated via the Stokes-Einstein relation (Equation (3.3)). In both chloroform and THF, particularly in the smaller dendrimers, R_h is smaller than R_g. This is most likely due to the fact that the Stokes-Einstein relation is valid for large Brownian particles in a continuous flow, i.e., this relation is employed based on the assumptions that the dendrimer is a non-draining sphere and that it is significantly larger than the solvent molecules - as if the dendrimer was diffusing in a continuous medium. It was shown from the aspect ratios of the dendrimers (Section 5.3.1) that the dendrimers are not spherical (particularly the smaller dendrimers) and from the SDFs (Section 5.3.2) that the dendrimers are completely extended in both solvents, with cavities and channels readily accessible by the reaction medium. However, R_h in THF shows an excellent fit

	Chloroform			THF		
G	D/ $\times 10^{-6}$cm^2/s	R_h/Å	R_g/Å	D/ $\times 10^{-6}$cm^2/s	R_h/Å[a]	R_g/Å
1	4.62 ± 0.08	8.58 ± 0.29	10.21	$4.01 + 0.01$	9.88 ± 0.03 (10)	9.85
2	3.45 ± 0.04	11.48 ± 0.30	13.38	3.02 ± 0.01	13.12 ± 0.16 (13)	13.48
3	2.71 ± 0.01	14.67 ± 0.12	16.45	2.36 ± 0.02	16.79 ± 0.34 (17)	16.74
4	2.15 ± 0.06	18.43 ± 0.92	19.75	$1.9 \perp 0.04$	$20.85 = 1.46$ (21)	19.84
5	1.69 ± 0.06	23.30 ± 1.63	22.19	1.59 ± 0.05	24.92 ± 2.25 (25)	22.20

Table 5.3: The diffusion coefficients (D) and hydrodynamic radii (R_h) calculated from our dendrimer simulations. R_g is the average radius of gyration (R_g) calculated for a dendrimer earlier in this chapter. [a] Also included is the hydrodynamic radius (Å) in the parentheses reported by Mourey et al. for these dendrimers in THF. [120]

with the measurements of Mourey et al. [120] In THF, the hydration shell of a dendrimer is larger than in chloroform, despite the R_g being essentially identical for a dendrimer in the two solvents. This suggest that in THF, the diffusion of the dendrimer is impeded by a significantly larger solvation shell that in chloroform. From the SDFs of the terminal layer, it has been suggested that a Fréchet dendrimer is more flexible in THF than in chloroform. Hence, for two dendrimers of equal size and shape, the dendrimer that it most flexible will offer the greatest resistance to diffusion. We return to this point in Section 5.4.2.

Intrinsic Viscosity of Dendrimers

From R_h, the intrinsic viscosity ($[\eta]$) of each dendrimer was calculated using the method employed by Mourey et al. (i.e., Equation 3.30) and are illustrated in Figure 5.20. Experimental data for $[\eta]$ is only available for Fréchet dendrimers in THF, [120] for which a close match was obtained between the calculated $[\eta]$ and measured results. No experimental data is available in the literature for Fréchet dendrimers in chloroform. However, experimental data is available for Fréchet dendritic wedges. [118] Jeong et al. showed that the dendritic wedges WG3-WG5 in chloroform do not exhibit a maximum in $[\eta]$ as is observed in THF. Similarly, no maximum is obtained in the calculated $[\eta]$ of dendrimers G3 to G5 in our chloroform simulations. However, there is an increase in $[\eta]$ from dendrimer G1 to G3. This trend, where $[\eta]$ increases from G1 to G3 and remains constant from G3 to G5 is qualitatively similar to the trend reported by Scherrenberg et al. for two sets of PPI

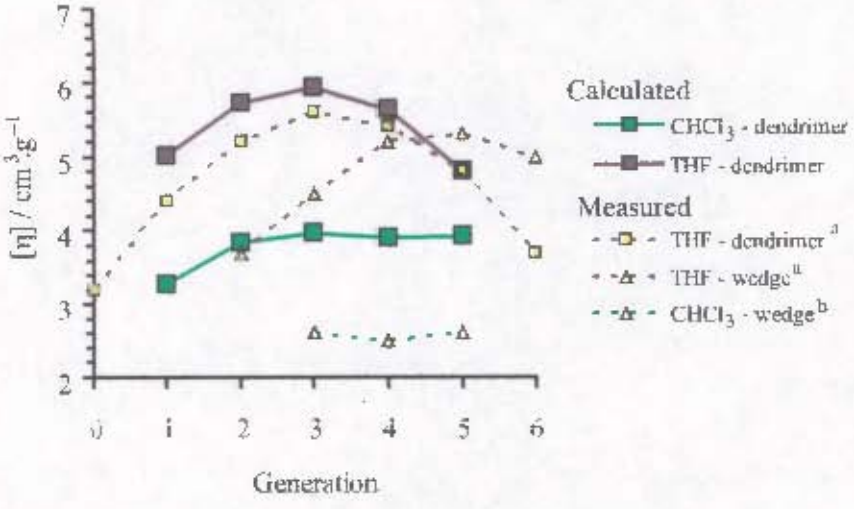

Figure 5.20: The calculated intrinsic viscosity, $[\eta]$, of Fréchet dendrimers in THF and chloroform, presented in Table 5.4 . [a] Also included are the measured intrinsic viscosity in THF reported by Mourey et al. [120] and [b] Jeong et al. [118]

dendrimers comprised different end groups in D_2O and acetone. [29]

The data presented thus far in this chapter suggests that the difference in the transport properties of a Fréchet dendrimer in THF and chloroform (i.e., diffusion coefficient and intrinsic viscosity) is not a function of the average conformation of the dendrimer but depends strongly on the dynamic behaviour of the dendrimer in solution.

5.4.2 Dynamics of the layers of a dendrimer

We have suggested that the difference in behaviour of the dendrimer in THF and chloroform could originate from the flexibility of the dendrimer in the solvents rather than the degree to which the dendrimer is unfolded. Therefore, we examine the dynamics of the individual topological layers to identify any notable differences in the behaviour of the dendrimers in chloroform and THF. We begin by describing the relative diffusion of the aryl rings of each layer, followed by a more detailed look at the atomic relaxation rates of each layer.

Average mean square displacement of the topological layers

The average mean square displacement (MSD) of each topological layer relative to the core (i.e., the rotational and translational motion of the dendrimer has been removed),

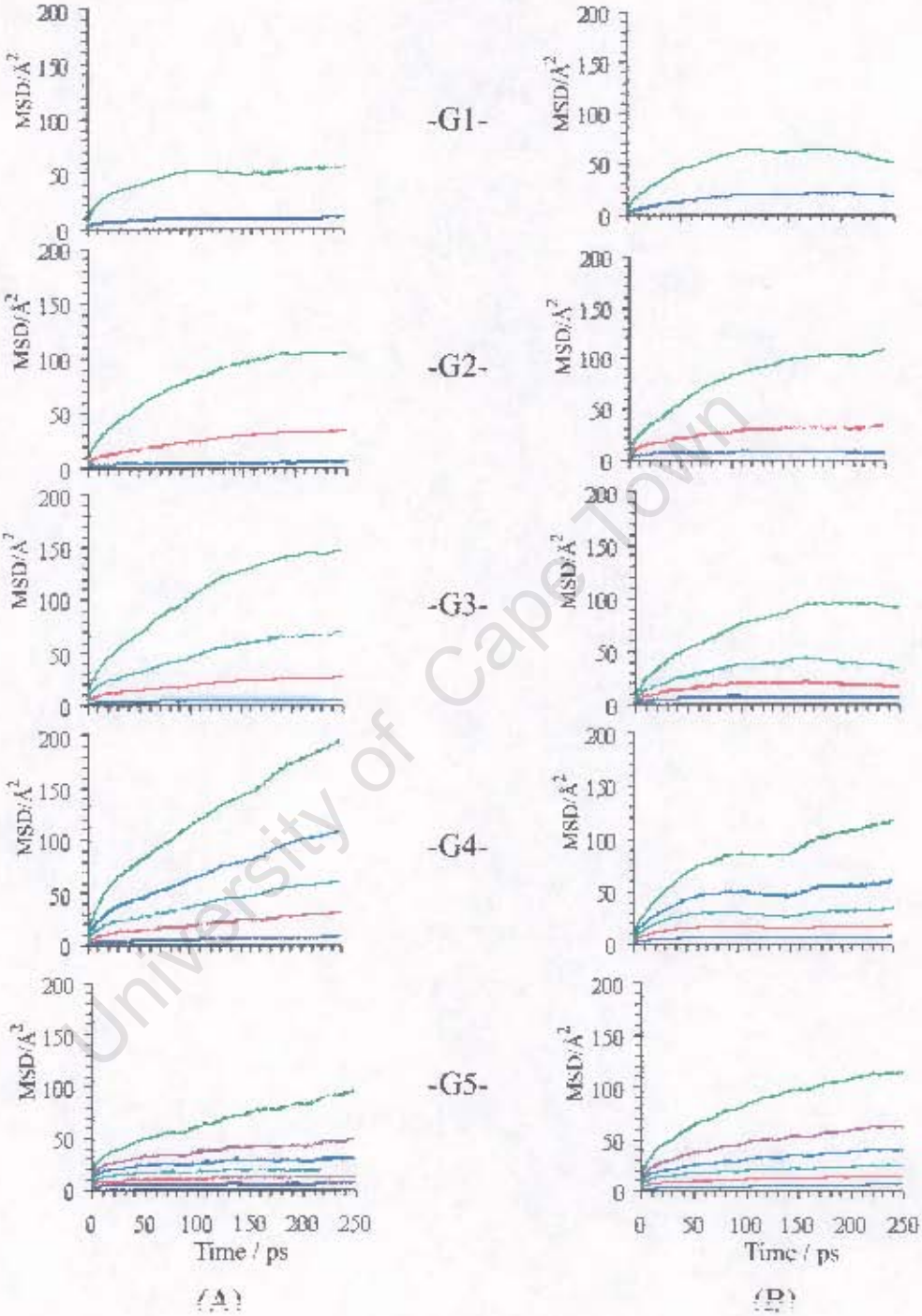

Figure 5.21: Mean square displacement time series for each layer of the (A) THF and (B) chloroform solvated dendritic systems.

	$[\eta]/cm^2.g^{-1}$	
Generation	Chloroform	THF[a]
1	3.28 ± 0.17	$5.02 = 0.02$ (4.4)
2	$3.84 = 0.15$	5.73 ± 0.11 (5.2)
3	$3.96 = 0.05$	5.93 ± 0.18 (5.6)
4	3.90 ± 0.29	5.64 ± 0.60 (5.4)
5	3.93 ± 0.41	4.81 ± 0.65 (4.8)

Table 5.4: The calculated intrinsic viscosity, $[\eta]$, of Fréchet dendrimers in THF and chloroform presented in Figure 5.20. [a] Also included in parentheses are the measured intrinsic viscosities in THF reported by Mourey et al. [120]

was calculated for the last 500ps of each simulation (Figure 5.21). The MSD time series reveal a significant difference in the behaviour of the terminal layer compared with the internal layers. The terminal layer exhibits typical *liquid-like* behaviour, while the internal layers exhibit *solid-like* behaviour (Section 3.4.1). The first topological layer is the most constrained layer and each successive layer is progressively less constrained than its parent layer. *Liquid-like* behaviour is characterised by a steady increase in the MSD and indicates less restricted motion. Gorman and Smith noted a similar trend in their dendritic systems and accounted for the difference in the mobility of the terminal groups as being due to the decreased steric congestion at the surface of the dendrimer, in comparison to the interior. [73] Although this is likely to be a contributing factor, we suggest that the *liquid-like* behaviour of the terminal groups is because the dynamics of the terminal group are only constrained by its parent layer, whereas all other layers of the dendrimer are constrained by the dynamics of its parent and child layers.

In general, there are consistent trends within MSDs of the layers of the dendrimers of each solvent system. Firstly, the terminal groups clearly have a unique motion in comparison to the other topological layers. Secondly, the MSD of the consecutive layers of a single dendrimer increase incrementally. This incremental increase is a result of the branching in the dendrimer where its internal motion is coupled to its child and parent layers. For example, if the inner-most layer, g1, is displaced by a magnitude dx_{g1}, then its children, layer g2, would be displaced by $dx_{g1} - dx_{g2}$. Similarly for the latter layers, with each layer expressing a slightly greater degree of mobility than its parent, i.e., $dx_{gn} > dx_{gn-1}$. The terminal layer shows the greatest mobility because its displacement is

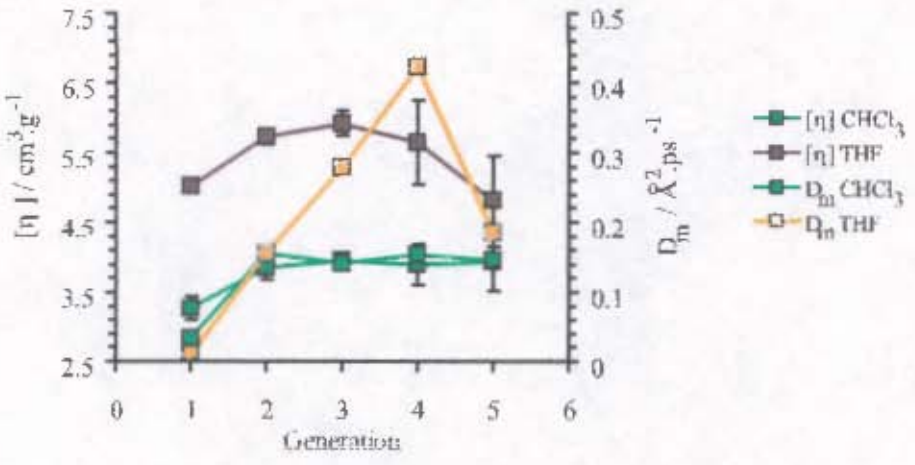

Figure 5.22: A comparison of the average diffusion coefficients for all the aryl rings (or monomers) of the solvated dendrimers, D_M, and intrinsic viscosities, $[\eta]$, of the dendrimers G1 to G5, presented in Figure 5.20

a sum of the displacements of all the ancestral layers and more importantly, the mobility of this layer is not constrained by a child layer as all the internal layers are. While the dendrimers in THF and chloroform exhibit similar overall characteristics of the dynamics of the topological layers, the internal layers of a dendrimer solvated in THF exhibit more liquid-like trends than the same layers for the same size dendrimer solvated in chloroform. This suggests the dendrimers have greater conformational freedom and are more flexible in THF than in chloroform.

Employing the Einstein relation (Equation (3.18)), we calculate the average diffusion coefficient of the aryl rings (or monomers) of each dendrimer, D_m. These diffusion coefficients are presented in Figure 5.22. D_m is dominated by dynamics of the terminal groups because these groups comprise half of the mass of the dendrimer, exhibit the least constrained dynamics and, in comparison to the internal topological layers, dominate the interaction with the reaction medium. In Figure 5.22, a comparison is made with the intrinsic viscosities calculated in the previous section (see Figure 5.20) The similarity between the trends in D_m and the calculated viscosities is striking. In THF, D_m and $[\eta]$ both exhibit an increase from G1 to G3, however, D_m has a maximum at G4 followed by a sudden decrease at G5 while $[\eta]$ has a maximum at G3 followed by more gradual decrease in G4 and G5. In chloroform, there is an even closer match between D_M and $[\eta]$. The similarity of the overall trends in D_m and $[\eta]$ strongly suggests that there is a correlation between the flexibility of the dendrimer and $[\eta]$. Therefore, the following heuristic expres-

sion is proposed for intrinsic viscosity as a function of the size, shape and flexibility of the dendrimer:

$$[\eta] = [\eta]\left(R_g, \bar{\mathbf{I}}\right) - P.D_m \tag{5.1}$$

where $[\eta]\left(R_g, \bar{\mathbf{I}}\right)$ is the contribution to the intrinsic viscosity dependent on the size (R_g) and shape ($\bar{\mathbf{I}}$, the principal moments of inertia tensor) of the dendrimer, while $P.D_m$ represents the contribution of the flexibility of the dendrimer to the overall intrinsic viscosity. Here, P is a proportionality constant. An example of $[\eta]\left(R_g, \bar{\mathbf{I}}\right)$ is $[\eta] = C.V$ derived by Brenner [254] where C is a nonnegative function of the aspect ratio (i.e., the shape of the dendrimer) and V is the volume of the dendrimer.

A means of verifying this hypothesis is to measure the viscosity of several Buckminster fullerenes of various sizes (for example, C_{60}, C_{70} and C_{78}). These molecules closely represent the ideal hydrodynamic particle, i.e., spherically symmetrical, non-draining rigid molecules. With the exception of their size, these molecules are essentially chemically and physically identical, including their flexibility.

Atomic relaxation rates

The dynamics of the dendrimer at an atomic level are described in terms of the longitudinal relaxation times calculated for all C-H vectors of the dendrimers simulated in THF and chloroform. A summary of the relaxation times is illustrated in Figure 5.23. In both solvents, the relaxation rates of the terminal groups are substantially longer than the relaxation rates for the internal layers by a factor of 4.90 on average in chloroform and by a factor of 6.41 on average in THF. This supports the suggestions made during SDF analysis of the dendrimers, that the terminal groups are substantially more flexible than the internal generations. The longer relaxation rate of the terminal layer protons in comparison to the interior protons is in agreement with experimental measurements. [17]

Additionally, in both solvents the relaxation rate of the terminal groups decreases as the size of the dendrimer increases. This suggests greater steric congestion in the terminal layer of the larger generation dendrimers and matches the trend in T_1 measurements of the terminal layer of dendrimers. [100, 101, 105, 255] The internal layers do not display this trend and there is no variation in the relaxation rates within the dendrimer as a function of the size of the dendrimer. This suggests that the effect of steric congestion is localised to the terminal groups.

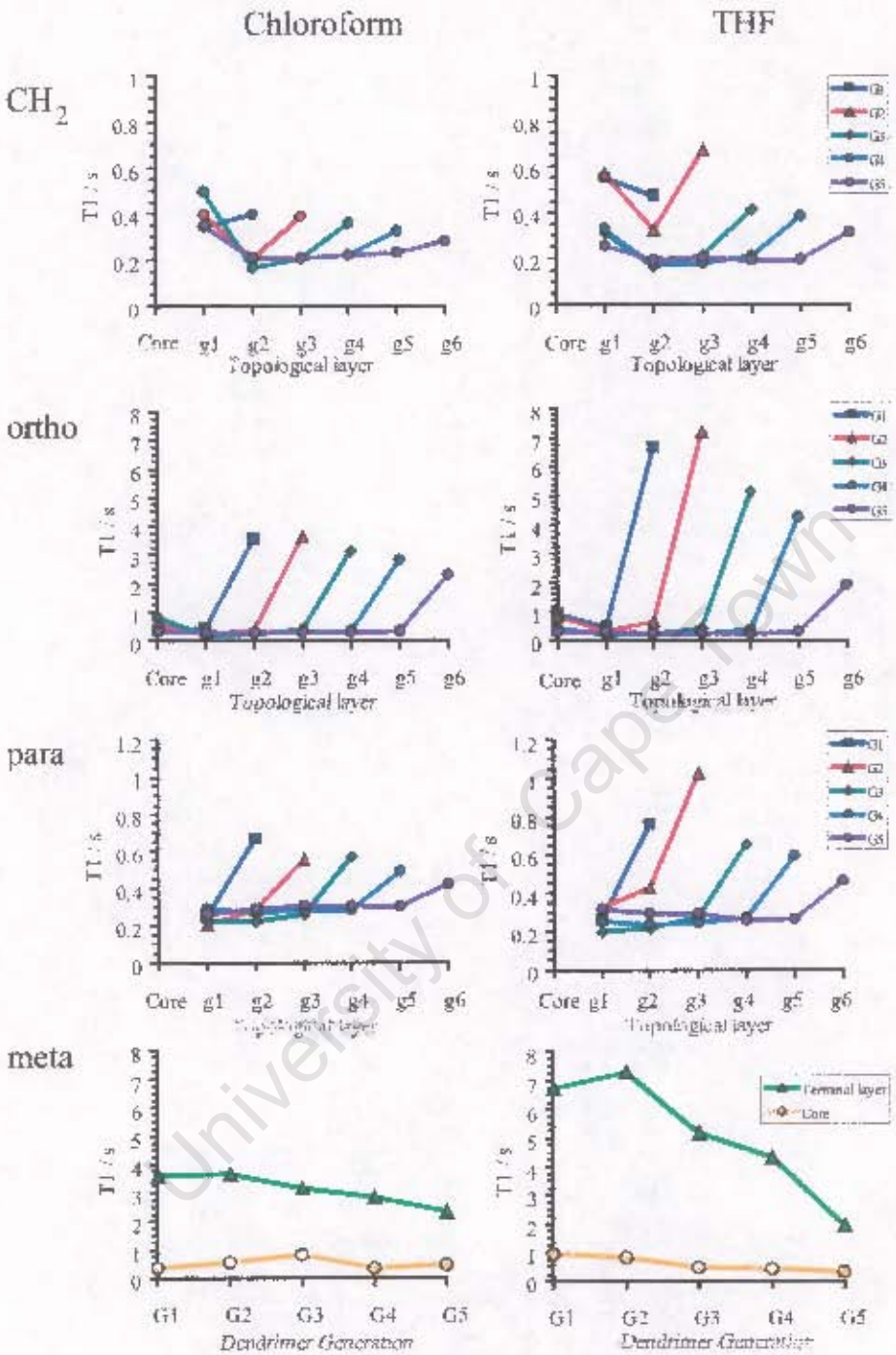

Figure 5.23: Calculated longitudinal relaxation rates of the dendrimers simulated in chloroform and THF. The CH_2 row refers to the relaxation rates of the benzyl protons in the ether linkage of each layer a dendrimer. The *ortho*, *meta* and *para* rows refer to the relaxation rates of the aromatic protons. The *ipso* position is that carbon which is coordinated via the ether linkage to the previous topological layer. Only the core and terminal layers are protonated at the meta position.

The most notable difference between the relaxation times of the dendrimers in THF and chloroform is that the relaxation rates of the terminal groups in THF are on average a factor of 1.43 longer than the equivalent rate in chloroform. This supports the findings in the SDF analysis that the terminal layer in THF is more flexible than in chloroform. The difference in relaxation times of the terminal layers is most prevalent in the smaller dendrimers. We were unable to identify a trend in the relaxation times analogous to those of D_m in Figure 5.22. However, the difference in the relaxation times of the terminal groups in chloroform and THF generally decreases as the size of the dendrimer increases. This trend is not consistent in the relaxation across all proton environments and is most prevalent in the ortho and meta terminal protons.

The relaxation rate of the protons at the para position in the terminal layer have a relaxation rate substantially faster than the protons at the ortho and meta positions, by a factor of 5.74 and 7.02 in chloroform and THF respectively. The cause of this difference is unclear at this stage, but preliminary T_1 measurements of Fréchet dendrimers in our laboratory show a similar trend and we are confident that this is not an anomaly of the simulation or calculation of the relaxation rates. [256] One possible explanation to account for the longer relaxation rates of the protons at the ortho and meta positions is due to librations about the axis of the terminal ring - oscillations about the 1-4 axis (the axis formed by the carbon atoms at the ipso and para positions) would tend to only affect the protons at the ortho and meta positions. In comparison, this would have little effect on the relaxation of the proton in the para position. This effect would only be noticeable in the terminal groups which have the greatest degree of flexibility. This hypothesis is supported by the fact that the relaxation rates of the protons of the internal layers at all three positions are of comparable magnitudes. Librations about the 1-4 axis of the aryl rings of the internal layers would be significantly hindered due to the rings coordination with its parent and child layers. This is the topic of continued investigation and forms the basis of future work.

A number of NMR relaxation studies have been reported in literature documenting the relaxation times of a variety of dendrimers. [17, 86, 100–103, 103–107, 110, 255, 257] In all of these reports, where the authors include details of the relaxation times of both the internal and terminal layers, the terminal layer relaxation times are typically at least two fold longer than those of the internal layers. Some examples are illustrated in Figure 5.24. This lends support to our calculations, particularly the study by Hecht and Fréchet where

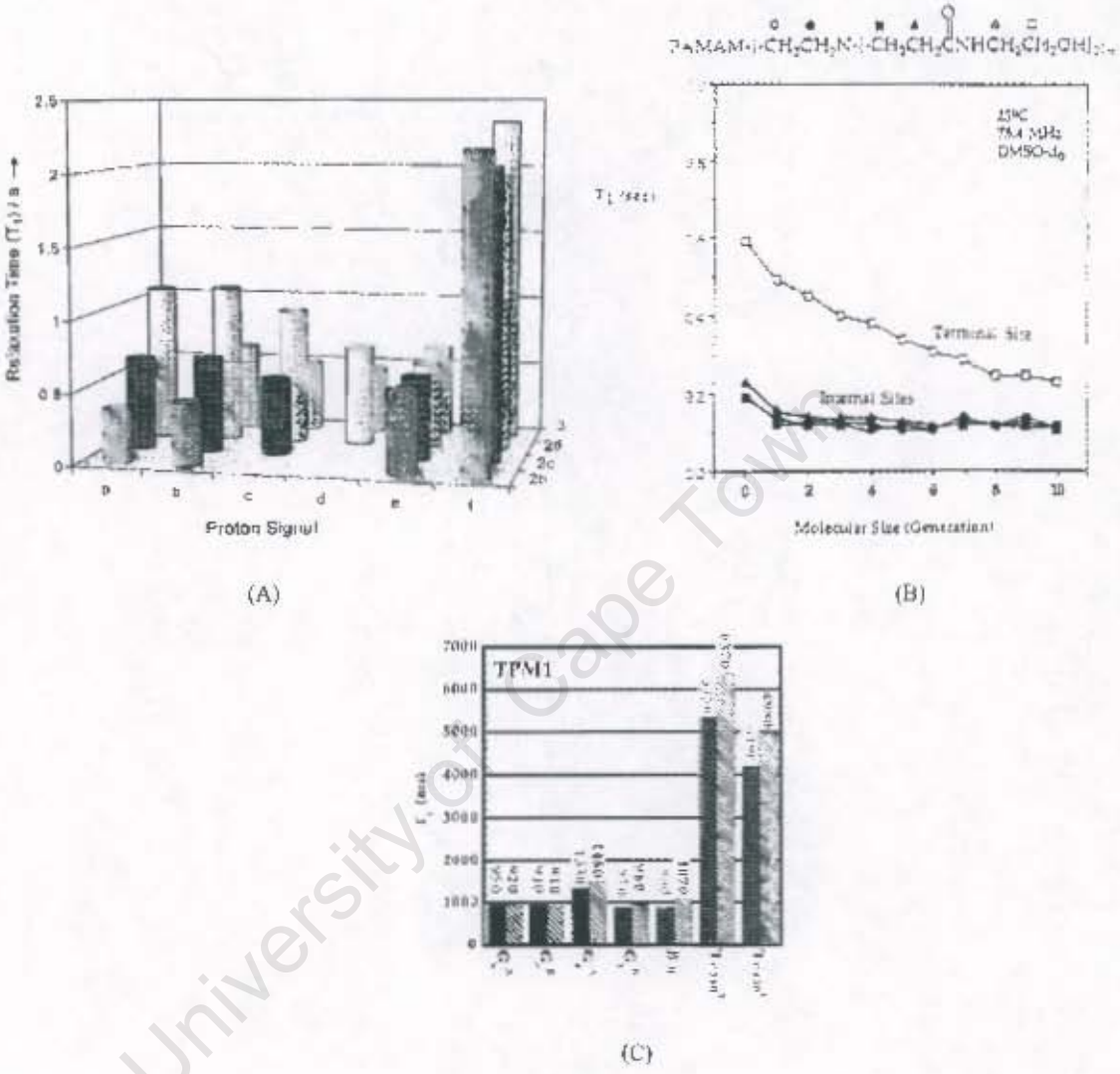

Figure 5.24: Some examples of the relaxation times of dendrimers as reported in literature. (A) Proton relaxation rates of the aromatic rings of Fréchet dendrimers (row 3) and fully coordinated benzene-core Fréchet dendrimers (2b-2d), a-e representing internal relaxation and f the terminal layers. [17] (B) ^{13}C Relaxation PAMAM dendrimers. [100] (C) Proton relaxation rates for Fréchet dendrimers with paramagnetic cores (the solid and dashed bars are for relaxation rates at 25°C and 40°C respectively).

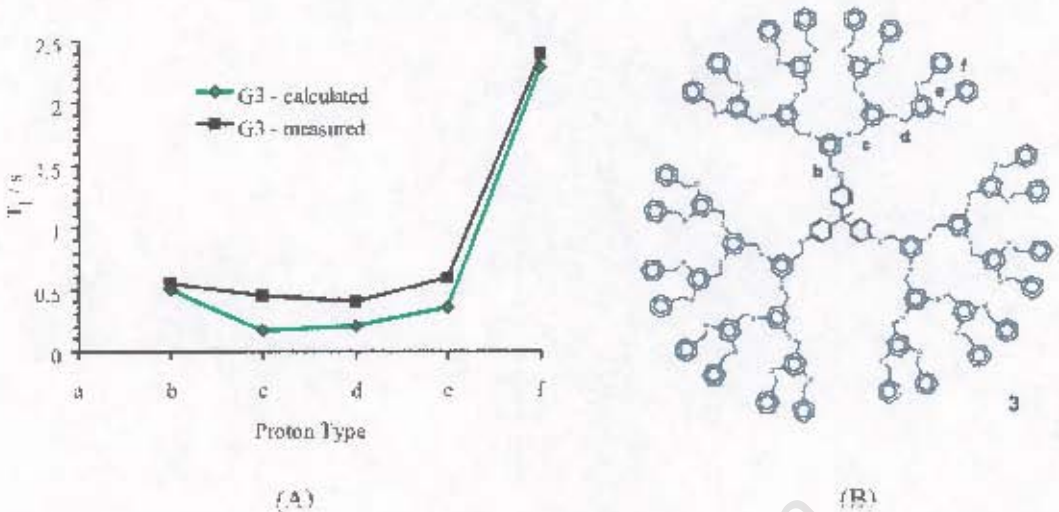

Figure 5.25: (A) A comparison of the relaxation times of a G3 dendrimer in chloroform as calculated from our simulations and measured by Hecht and Fréchet. [17] (B) The scheme of G3 indicating the position of the proton types (Scheme 3, Figure 2 in Reference [17]).

they measured the relaxation rates of a G3 dendrimer in chloroform (row 3 in Figure 5.24A) in addition to the relaxation rates of a similar fully coordinated benzene-core dendrimer. In Figure 5.25 we compare the measured relaxation rates reported by Hecht and Fréchet with our calculated relaxation rates for the C3 dendrimer in chloroform. This close match between independently measured values and our calculated values lends further confidence in our simulations.

In Figure 5.26, the effect of the flexibility of a dendrimer on its diffusion through the system is illustrated. This can give the impression of a larger hydrodynamic volume. If the dendrimer is rigid, it can diffuse through the system as a single hydrodynamic entity. However, if the dendrimer is flexible it cannot be described as a single rigid particle and is comprised several dynamic units. In dendrimers, these dynamic units would most likely comprise wedges or sub-wedges. This could account for the difference in the viscosimetric measurements as reported in literature. Further, if the dendrimer is dynamic on the time scale of diffusion, then the approximation of a rigid body is not valid and the situation is more complex.

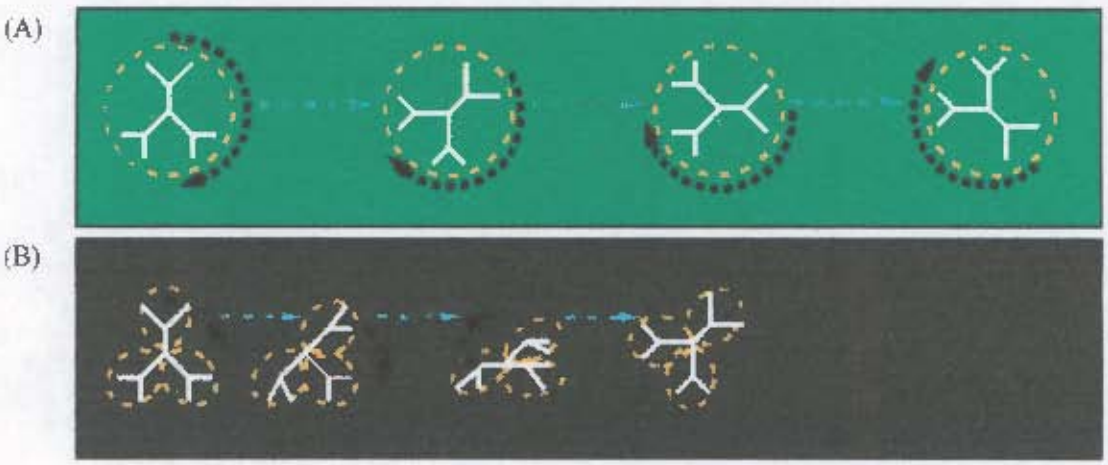

Figure 5.26: Schematic diagram of (A) a dendrimer in chloroform diffusing as a single hydrodynamic element and (B) the same dendrimer in THF diffusing as a flexible molecule where the wedges act as the hydrodynamic elements. The yellow rings indicate the hydrodynamic elements and the black arrows indicate the rotation or displacement of these elements. The cyan arrows indicate the displacement of the dendrimer over equal time periods of Δt. The result is the flexible dendrimer diffuses slower than the rigid dendrimer.

5.5 Solvent structure in and around the dendrimer

The difference in the dynamics of identical dendrimers simulated in THF and chloroform under identical simulation conditions point to a difference in the interaction and arrangement of the solvent in and about the dendrimer. The spatial arrangement of the solvent about the dendrimer is a qualitative means of identifying any significant differences in the distribution of the solvent within the dendrimers. The SDFs of the solvents at 50% above bulk density of the solvent are illustrated in Figures 5.27 and 5.28. These SDFs indicate where the solvent has a 50% higher probability of been found in comparison with the bulk solvent probability distribution. It is clear that both solvents penetrate into the core of the dendrimer. Further, the SDFs suggest that as the dendrimer diffuses through the solvent, the solvent near the core diffuses together with the dendrimer. However, the similarity in the solvent SDFs indicates that the arrangement of the solvent within the dendrimer is approximately equal in THF and chloroform. Considering the similarity of the PDFs and SDFs of the pure solvents (see Section 4.2) it is not surprising the spatial arrangement of the solvent within the dendrimer is similar across the solvents. In THF, there are additional pockets of high density regions on the periphery of the dendrimer.

However this only indicates that solvent is likely to be found in this region and does not necessarily indicate that the same solvent molecules comprise these regions (i.e., these regions do not reflect the diffusion of the solvent within the polymer).

The spatial representation of the diffusion profile of the solvents in and about the dendrimer indicates the greatest resistance to diffusion or flow of the solvent within the dendrimer. Figures 5.29 and 5.30 detail the diffusion profile of the solvents at half the diffusion rate of the bulk solvent. Although these diffusion profiles are also very similar, chloroform's diffusion profiles show greater detail within the dendrimer than in the THF diffusion profiles. This is most clearly visible in dendrimers G3 and G4 and indicates that the while the solvent may diffuse in to the body of the dendrimer, the flow of the solvent close to the dendrimer itself is more impeded in chloroform than in THF. This could account for lower mobility of the terminal layer in chloroform than in THF, while at the same time accounting for the essentially equal probability of locating solvent within the body of the polymer.

5.6 Conclusion

In this chapter, it has been shown that while a dendrimer folds in vacuum, in an explicitly modelled good solvent dendrimers remain extended. It can be concluded that vacuum simulations (without any implicit solvent model) do not adequately represent the behaviour of a dendrimer in solution as some empirical simulations have suggested. In addition, it has been shown that particularly in the folded state the core of the dendrimer is not at the geometric centre of the dendrimer and the overall distribution of groups about the core is asymmetrical. Additionally, depending on the method used for normalising the radial distribution a completely different perception can be created of the distribution of the topological layers of the dendrimer about the core. Hence, the results from radially averaged methods must be interpreted with care. Further, it was illustrated using a simple comparison between the density of benzyl alcohol and that of the "dense core" region that the "dense core" analogy did not indicate that the core was surrounded by an impenetrable shell that could not accommodate any additional groups such as terminal groups due to backfolding or guest molecules. It was shown that spatially averaged distribution functions more clearly illustrate the structure of a dendrimer in three dimensions. With such 3D methods, it is not only possible to gain a clear picture of the overall shape and size of

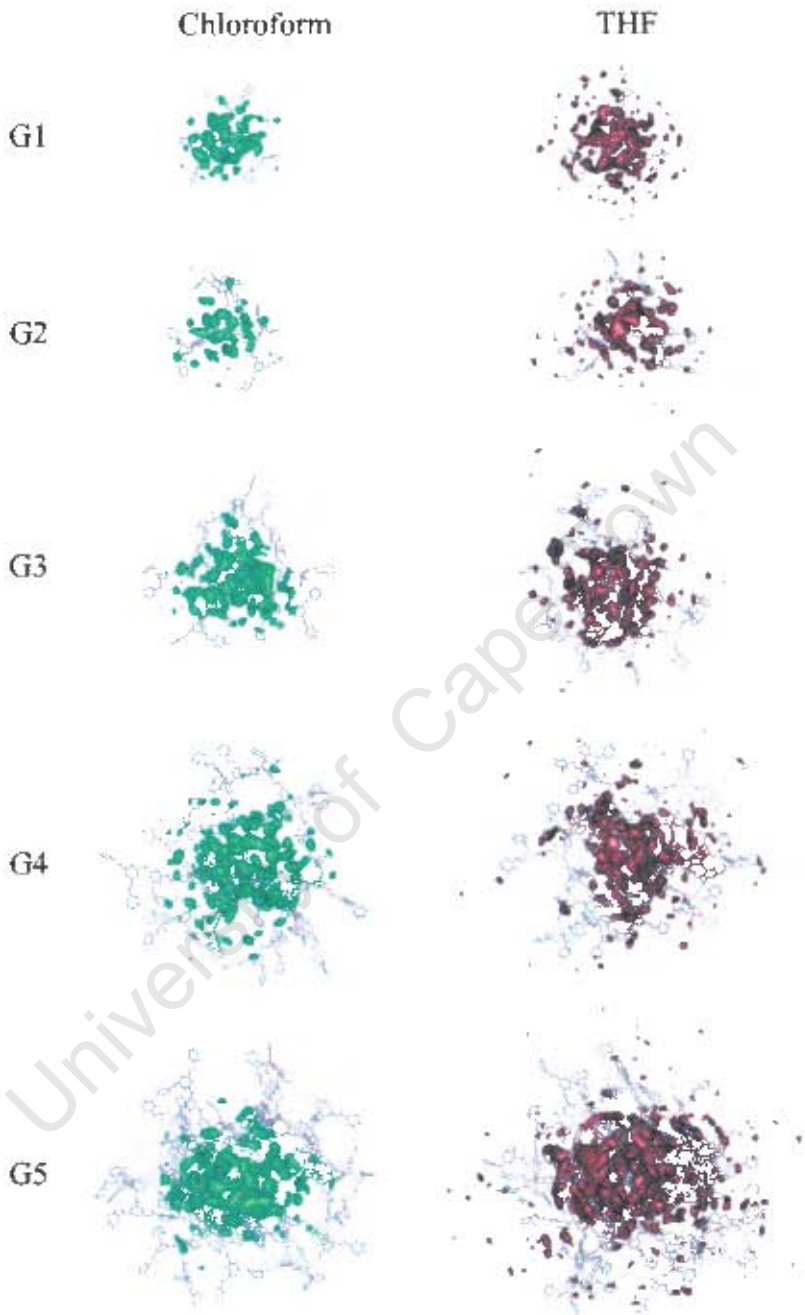

Figure 5.27: Solvent SDF at 50% above bulk density of each solvent illustrating the distribution of the solvent about the dendrimer. The SDFs were calculated from the centre of mass of each solvent molecule.

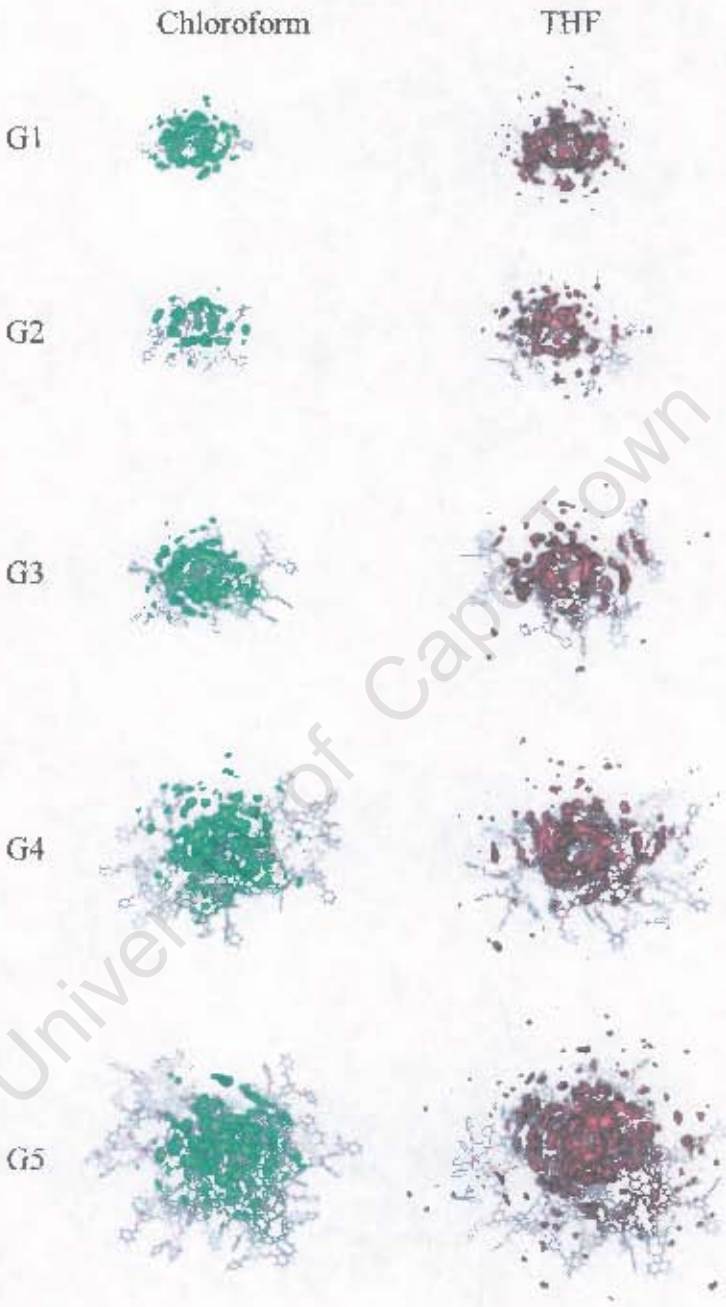

Figure 5.28: A side view of the solvent SDF at 150% of bulk density of each solvent illustrating the distribution of the solvent about the dendrimer.

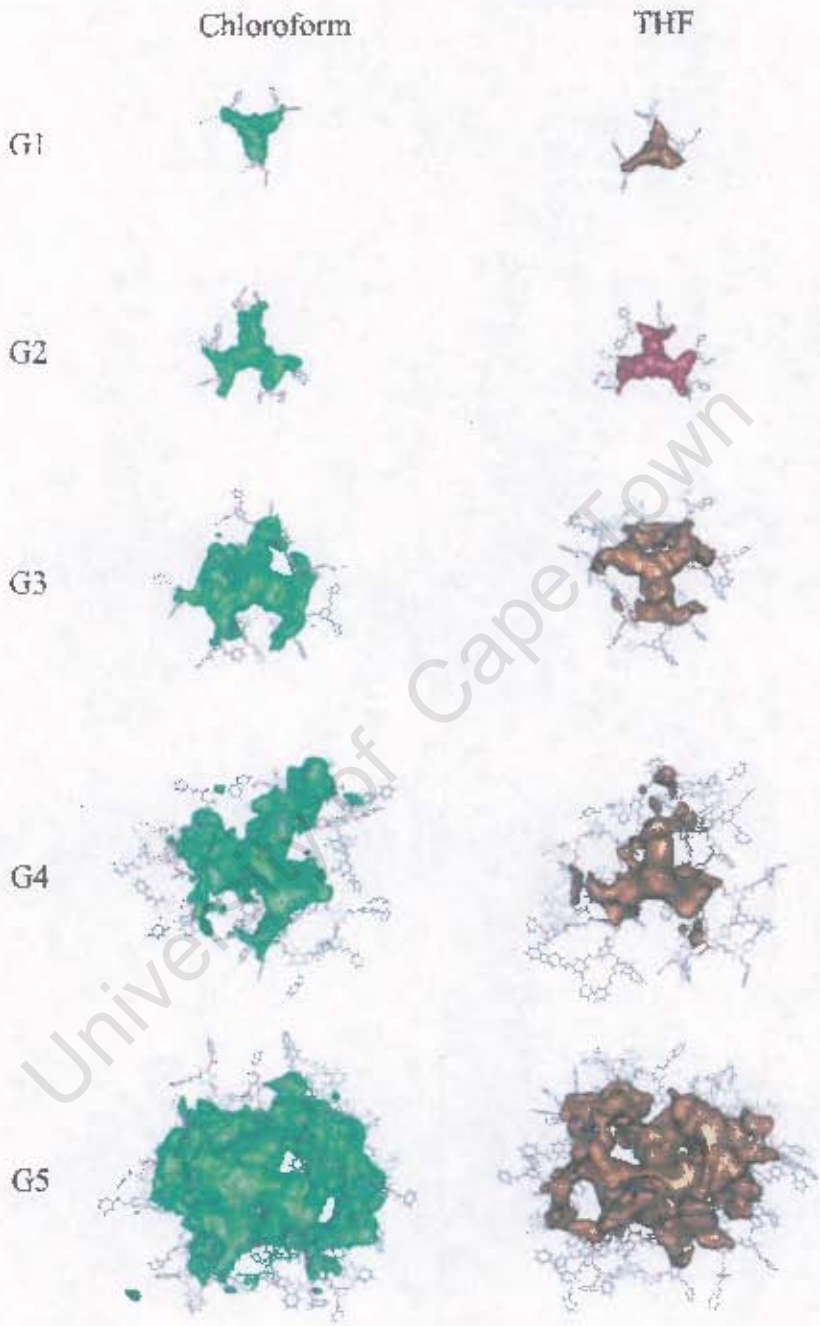

Figure 5.29: Spatial representation of the diffusion profile of the solvents in and about the dendrimer at half the diffusion rate of the bulk solvent.

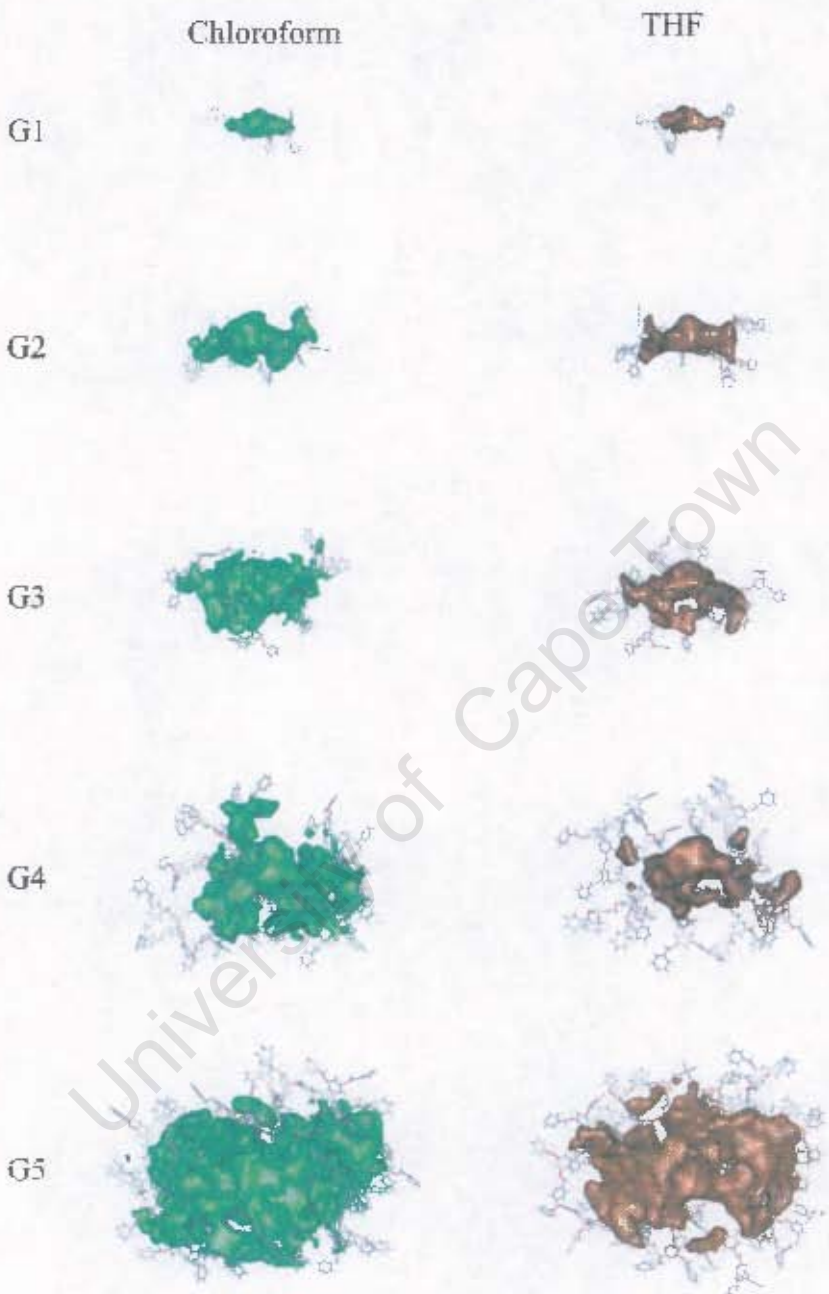

Figure 5.30: A side view of spatial representation of the diffusion profile of the solvents in and about the dendrimer at half the diffusion rate of the bulk solvent.

the dendrimers, but it is also possible to analyse the internal structure of the dendrimer. It was also illustrated that the hyperbranching inherent to dendrimers can account for the distribution of the layers of the dendrimer as observed in both the spatially and radially averaged methods. However, the contribution of backfolding in the classical sense (where the terminal groups diffuse into the body of the dendrimer) to the distribution of the terminal groups close to the core cannot be ruled out completely.

Analysis of the dynamics of the dendrimer revealed that the internal structure of the dendrimer is rigid and the internal motion of the dendrimer is isolated to the terminal groups. It was observed that the terminal layer of a dendrimer in chloroform expresses far less mobility than in THF. The flexibility of the dendrimer in a solvent has been shown to be a major contributing factor to the overall dynamic behaviour of the dendrimer in solution. A new relation for the intrinsic viscosity was proposed which includes contributions of the size and shape of the dendrimer along with the flexibility of the dendrimer in a particular solvent. The flexibility of the dendrimer accounts for the difference in the measured intrinsic viscosities of Fréchet dendritic wedges in chloroform and THF. Confidence in the simulations is provided by the close match between our calculated T_1 relaxation rates and available experimental data in the literature.

The spatial arrangement of the solvent about the dendrimers and the spatially averaged diffusion profiles of THF and chloroform within the dendrimers indicate that while the arrangement of the solvent within the dendrimer is approximately equal in THF and chloroform, chloroform experiences the greatest resistance to diffusion close to the internal surface of the dendrimer. This could account for the decrease in flexibility of the dendrimer in chloroform in comparison with the flexibility of the dendrimer in THF.

Recently in literature, it was suggested that dendrimers in good solvents were characterised as ultrasoft flexible molecules with dense cores and all other models should be ignored. [26, 57] This conclusion was derived from a comparison of scattering data with computer simulations of dendrimers in vacuum. The results from our simulations contradict this viewpoint. Considering the significant number of opposing views of the structure of dendrimers available in literature, it is most likely that it will be sometime before the debate over the structure of dendrimers is conclusively resolved. In this chapter we have suggested tests to validate our simulations which would help in this end.

Chapter 6

Dendrimer Folding Dynamics

6.1 Introduction

In the final chapter of this thesis we investigate dendrimer folding dynamics. The aim of this chapter is two-fold: to validate the solvent simulations presented in the previous chapter and to gain insight into the folding dynamics of the dendrimer. Note that a complete study of the folding dynamics of dendrimers is beyond the scope of a single chapter in a thesis; the aim of this study is to prepare the foundation for future work.

Before proceeding, it is useful to reiterate our definition of whether a dendrimer's conformation is classified as folded or unfolded (Chapter 1). We use the radius of gyration (R_g) as a quick method to quantitatively identify when the dendrimer is folded or unfolded. In this thesis we define the dendrimer to be completely folded, or contracted, when its R_g is equal to that of the average equilibrium conformation of the dendrimer in the vacuum molecular dynamics simulations. The dendrimer is said to be completely unfolded when the dendrimer has a R_g equal to the energy minimized conformation of the dendrimer in vacuum. The dendrimer in vacuum is used as the basis of our definition as it is only dependent on the dendrimer force field and independent of solvent effects.

In the previous chapter of this thesis, analysis of nanosecond MD simulations of Fréchet dendrimers in chloroform and THF established that the dendrimers remain equally extended in both solvents. Confidence in these results was given by the analysis of the solution force field in Chapter 4 and the close match of the simulated results with experimental data reported in literature. However, the outcome of MD simulations using standard Boltzmann sampling can be dependent on the starting structure of the solute

molecule. [128,135] Therefore, it is possible that the dendrimer remains unfolded in chloroform MD simulations because using an extended conformation as the starting conformation could bias the outcome of the simulation to favour an extended state. This bias could be the result of significant resistance to conformational changes which would hinder greater dendrimer-dendrimer interactions, thus preventing the dendrimer from folding. Therefore, it could be argued that for the dendrimer to overcome such resistance to conformational change would require simulations in the order of hundreds of nanoseconds or even milliseconds, i.e., the simulations in previous chapter were simply not long enough for folding to occur. However, simulations of this magnitude are beyond the capabilities of our computational resources. As an alternative, we run a series of simulations of dendrimers (G1 to G5) in chloroform, with the dendrimers starting in folded conformations. In addition we run a series of dendrimers (G1 to G3) in water, starting from the unfolded conformation to test if the dendrimer will fold in an explicit poor solvent environment. The choice of water as the poor solvent was based on solubility parameters; a solute with a solubility parameter of δ_p is described as being insoluble in a solvent with a solubility parameter δ_s if $(\delta_s - \delta_p)^2 < 4$. [187] Jeong et al. suggested a Fréchet dendrimer has a δ_p between 18.2 and 18.4 $MPa^{1/2}$. [118] Water has a δ_s of 47.9 $MPa^{1/2}$. Additionally, polystyrene, which is often referred to as a linear analogue of Fréchet dendrimers, [118] is extremely insoluble in water which supports the use of water as a suitable poor solvent for Fréchet dendrimers. From these two series of simulations we compare the folding and unfolding mechanisms. This forms the first part of this chapter.

The second part of this chapter focuses on calculating the free energy of folding for various important structural groups within the dendrimer (Figure 6.1). The aim is threefold:

- To identify the smallest component of the dendrimer which is likely to fold.
- To establish how differing solvent conditions modify the vacuum free energy profile.
- To determine if there are any significant differences between the free energy profiles of the dendritic systems in chloroform and THF that could account for the difference in the dendrimer dynamics as observed in Chapter 5.

The potential of mean force (PMF) of folding for a series of structural elements of the Fréchet dendrimer was calculated in four solvent environments: vacuum, water, chloroform and THF. The vacuum free energy profiles are the foundation of this investigation -

all solvent effects are removed and the free energy profile is solely a function of the characteristics of the polymer. Vacuum simulations represent a poor solvent because there are no solute-solvent interactions to compete with the solute-solute interactions. [2] Therefore, the PMF in vacuum will be a function of the dendrimer's intramolecular forces only and the difference in the PMF in an explicit poor solvent and vacuum establishes the effect of an explicit poor solvent.

The difference in the flexibility of the dendrimers in THF and chloroform can be analyzed quantitatively using free energy calculations. The models used in our PMF calculations are illustrated in Figure 6.1. The benzene-benzene dimer interactions (Figure 6.1A) represent the simplest and most common type of intramolecular interaction in a Fréchet dendrimer which is the interaction of terminal groups of neighbouring wedges. There have been several PMF calculations performed on the benzene dimer in a variety of solvents, including water, chloroform and pure benzene. [246, 258–261] These PMF profiles were computed using several different methods, with a combination of statistical perturbation theory and umbrella sampling in the context of both MD and MC simulations. The PMFs were defined as the distance between the centre of mass of the benzene rings for the stacking and T-Shape arrangements, as well as the conversion between the two, [258,261] and the orientationally averaged conformations where the two benzene molecules were allowed to rotate freely depending on the torques acting on them. [246, 259, 260]. Despite the diverse methods used to calculate the PMFs, all the PMFs have a global minimum between 4.3Å and 5.5Å (the distance from the centre of mass of the benzene rings as the reaction coordinate), usually accompanied by local minima at further separation distances. Therefore, if this global minimum is significantly different in the PMF of our model systems, it is due to the connectivity of the dendrimer - the branching that connects the aryl rings.

As the benzene dimer interactions have been thoroughly studied we computed the PMFs for a series of Fréchet dendrimer related compounds as illustrated in Figures 6.1B to D. The first model (Figure 6.1B) represents the basic repeat unit found throughout the dendrimer and represents the smallest unit capable of folding (the backfolding of one topological layer). For this PMF, we define the reaction coordinate as the distance between the centre of a terminal phenyl ring and the parent benzyl ring. We used this PMF as the starting point of our investigation - what is the PMF energy profile of the terminal group folding back toward the parent generation?

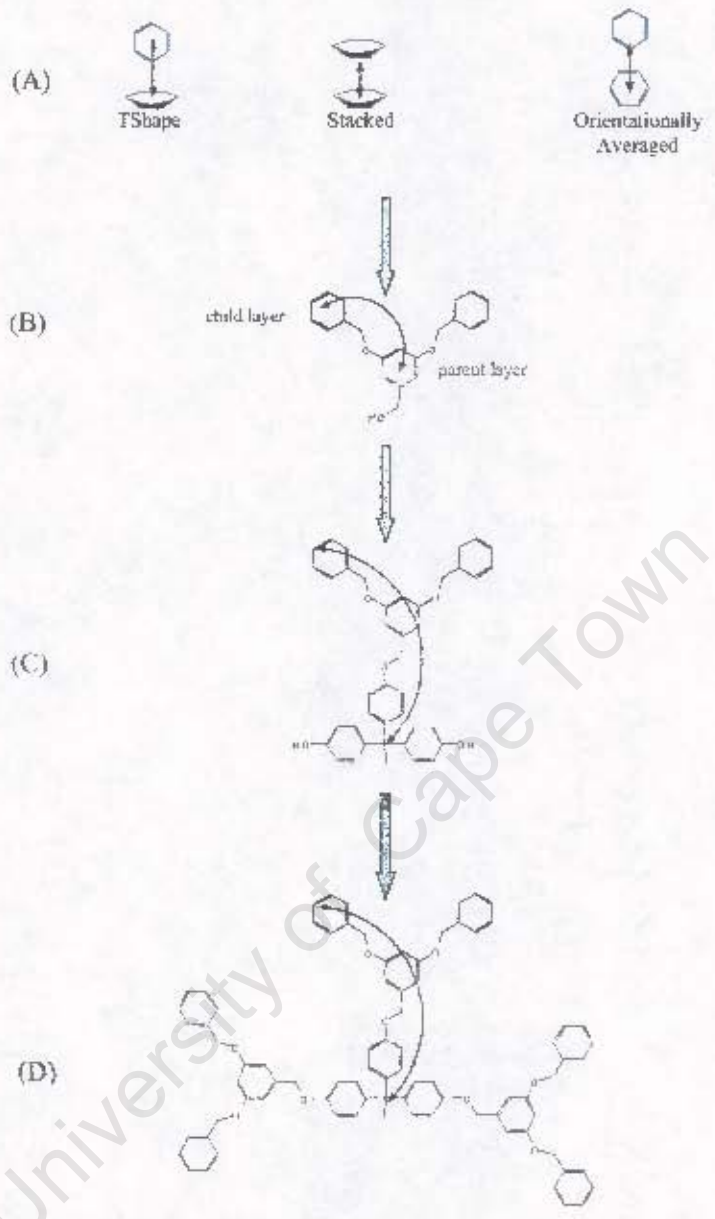

Figure 6.1: The model systems representing the important structural components of the dendrimer, starting from the simplest, (A) benzene dimer. Each model contains additional complexity and size; (B) The PMF of the first generation wedge takes into account the effect of the ether linkage and characterises the folding back of 1 topological layer. (C) Attaching the first generation wedge to a Fréchet core group, we calculate the PMF of folding back two topological layers to the core of the dendrimer. (D) Finally, all three wedges are included in the model (a full G1 dendrimer) to quantify the effect (if any) of a coordinated folding between the three wedges. The arrows indicate the increase in complexity of the each model.

For the second model (Figure 6.1C), we extended the first model by attaching a first generation wedge to a Fréchet dendrimer core group (1,1,1-tris(4'-hydroxyphenyl)-ethane). On the core, the two remaining sites that are usually coordinated to wedges are instead coordinated with hydroxyl groups. This makes the PMF calculation far simpler and removes the added complication of the influence of neighbouring wedges of the full dendrimer. Using this PMF we investigated the folding of the terminal group of the first generation terminal group in to the central core atom. The reaction coordinate is defined as the distance between the para carbon atom of a terminal phenyl ring and the central core atom. This is also equivalent to the folding back of two dendritic layers.

A third model (Figure 6.1D) was also investigated which once again builds on the previous model, this time all three wedges are coordinated to the core. The same reaction coordinate was used in the second model. With this model the aim was to determine if the three wedges exhibit some cooperative behaviour in their folding dynamics to create a synergistic effect, i.e., do the three wedges collectively aid each other in folding, thereby lowering the total energy of a dendrimer's folded conformation? A further aim was to identify and differences in chloroform and THF systems. Despite more than 600 ns of sampling from the vacuum system, this PMF showed no signs of converging as the sampling over the whole of the reaction coordinate was extremely erratic. Hence we abandoned this attempt as it was computationally too expensive for the PMF to converge with the resources currently available. An alternative PMF to investigate is the PMF of pulling together the terminal groups of two neighbouring wedges. However, this is also beyond our computational resources at this time and is the topic for future work.

6.2 Computational Details

All simulations in this chapter were performed using the CHARMM molecular modelling program.[1] The force fields used to describe the dendrimer and solvents are discussed in Chapter 4. Group-based cut-offs were applied for long range interactions with a switching function applied between 10 Å to 12 Å. A list of the nearest neighbours up to 14 Å was maintained and updated every 10 steps of the simulation. Bonds between hydrogen

[1]The general simulation details such as cut-off distances, temperature, method of integration, update frequencies and the method for equilibrating the systems are the same as those specified in Chapter 5.

and heavy atoms were restrained using the SHAKE algorithm. [134] The equations of motion were integrated using the Leap-Frog method. [134] The general simulation procedure involved first equilibrating the pure solvent cell for 500 ps after which a solute molecule (either a dendrimer or a model dendrimer unit) was included by placing the solute molecule at the centre of the primary periodic cell and removing all solvent molecules that overlapped with the solute. Thereafter, the system was briefly minimized using the Newton-Raphson algorithm to remove any remaining solute-solvent steric clashes. This was followed by an initial NVT heating phase for 200 ps before commencing with NPT sampling in the folding simulations or the 500 ps NVE equilibration before beginning the iterative procedure in the PMF calculations.

Folding dynamics simulation details The starting conformation of the dendrimers for the unfolding simulations (i.e., dendrimers in chloroform) were those of the lowest energy conformation in the vacuum dynamics while in the folding simulations (i.e., dendrimers in water), the energy minimized conformation of the dendrimer in vacuum was used as the starting conformation (i.e., the same starting conformation as the simulations in the previous chapter). The folding and unfolding simulations sampled from an NPT ensemble. This was to avoid the possibility of a sudden increase in local density at the site where a dendrimer would undergo a significant conformational change such as the unfolding of a dendritic wedge. In a constant volume ensemble, a sudden increase in local density resulting from a substantial conformation change could prevent the dendrimer from undergoing such a transformation. An NPT ensemble allows the volume of the simulation cell to adjust slightly, to reduce such regions of high density. We use Andersen's method [161] as implemented in CHARMM, with the pressure of 1 atm and the temperature of 293.15 K maintained with pressure and thermal pistons masses of 500 amu and 1000 kcal.mol^{-1}ps^2 respectively, both with a collision frequency of 5 ps^{-1}. All water simulations were conducted using truncated octahedron periodic cells. The size of the truncated octahedrons were based on the size of the cubic simulation cells used for the chloroform simulations. Only dendrimers G1 to G3 were investigated. The G3 dendrimer in water represents the limit of our computational resources. The number of atoms required for G4 and G5 simulations would have far exceed this limit. In the chloroform simulations, dendrimers G1 to G3 were conducted using cubic periodic cells while dendrimers G4 and G5 were simulated using truncated octahedron periodic cells (see Table 6.1) In the unfolding sim-

ulations, to accommodate the longer simulation times necessary for the larger dendrimers (G4 and G5), the simulations of the smaller dendrimers (G1 to G3) were stopped after the dendrimer had not expanded for at least 1 ns.

Representative conformations of the average equilibrium structure of the dendrimer were derived by calculating a coordinate set of the average position for every atom over a selected period of the simulation, typically the final 200 ps. This coordinate set did not necessarily represent a feasible conformation because of atoms overlapping or even superimposed on top of one another. Therefore, each frame of the trajectory was compared to this average structure. Using a chi-squared test, the trajectory frame that offered the closest match to the average structure was selected as the representative equilibrium conformation.

PMF Calculation details For the PMF calculations we implemented adaptive umbrella sampling (Section 2.3.1) with a histogram bin size of 0.1 Å. After the 200 ps NVT heating phase after adding the solute molecule to the solvent cell, 500 ps of NVE sampling was run to ensure the system was equilibrated before commencing with the PMF calculations. The first iteration of the simulation applied a completely flat potential (the simulation was unbiased). Successive iterations applied the umbrella potential calculated from the previous iterations which were combined using the WHAM algorithm (Section 2.3.1). The starting conformation for each iteration was that of the final conformation of the previous iteration. The iterative procedure to generate the free energy profile followed and comprised a series of 10ns NVT simulations. This iterative procedure continued until the entire reaction coordinate was evenly sampled during a 10ns simulation.

The WHAM algorithm and calculation of the umbrella potential were determined using custom software written within our research group. [166,262] The umbrella sampling was performed by modifying the USERE subroutine in CHARMM. This was modified in such a way that the energy from the umbrella potential was added to the energy of the specified atoms. For the first model, the first generation wedge (Figure 6.1B), this energy was applied to the centre of mass of the aryl ring and was evenly distributed among the ring carbon atoms. The range of the separation distance (r) was dependent on the steric clashes at short ranges and the maximum stretching distances of the groups as was possible, the latter governed by the connectivity of the dendrimer. The simulation, binning, WHAM and smoothing procedure were automated.

Dendrimer folding - chloroform			
Generation	Solvent residues	Dendrimer atoms	Cell size /Å
1	2081	164	65.54
2	2053	332	65.54
3	1994	668	65.54
4	2964	1340	93.88
5	2850	2684	93.88
Dendrimer folding - water			
1	2630	164	55.1
2	3726	332	62.00
3	5842	668	72.00
PMF - First generation wedge			
Water	1110	42	41.0
Chloroform	262	42	41.0
THF	249	44	41.0
PMF - Second generation wedge			
Water	1520	82	45.1
Chloroform	335	82	45.1
THF	380	82	45.1

Table 6.1: Simulation details of folding and PMF calculations

For the first two model systems (Figures 6.1B and C) in the vacuum simulation, more than 140 iterations each of 10ns were conducted for each model resulting in a combined simulation time of over 1.4 ms. The large number of iterations were performed in order to test the long term sampling and convergence of the free energy surface. In general, after approximately 10 iterations a near perfect distribution of the sampling was achieved and no significant change in the energy surface was observed. In the explicit solvent simulations, typically between 10 and 30 iterations (100 to 300ns) were required before uniform sampling of the reaction coordinate was achieved. In the case of the third model system (the full first generation dendrimer) only 20 iterations were conducted. This system showed no signs of convergence and no further simulations were conducted.

6.3 Results and Discussion

6.3.1 Folding Dynamics

We begin by investigating the overall folding dynamics of dendrimers. Specifically we investigate how Fréchet dendrimers fold in water (an explicit poor solvent environment) and how their equilibrium conformation in water compare with their equilibrium conformation in vacuum.

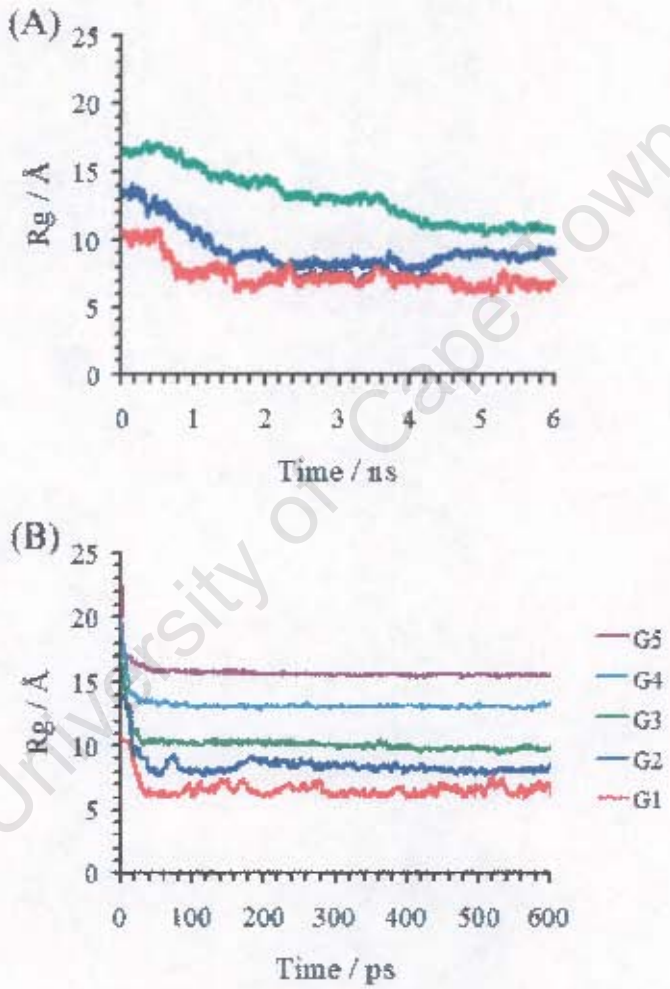

Figure 6.2: Radius of gyration (R_g) time series of (A) G1 to G3 in explicit water and (B) G1 to G5 in vacuum. [2] In vacuum, the dendrimers take less than 46 ps to fold while in water, the dendrimers take in the order of nanoseconds to fold to the same extent as the dendrimers in vacuum.

The time series of the radius of gyration (R_g) of dendrimers G1 to G3 in water (Figure

	Vacuum		TIP3P	
Generation	R_g / Å	t / ps	R_g / Å	t / ps
1	6.66	94	6.70	780
2	8.52	84	8.90	1275
3	10.22	33	10.83	4088

Table 6.2: A comparison of the average equilibrium radius of gyration (R_g) for dendrimers G1 to G3 in vacuum (calculated over the final 500 ps) and water (calculated over the final 1ns), including the time taken to reach the equilibrium R_g. While the R_g values are very similar for each generation (the R_g in water is slightly larger), the time taken to reach this equilibrium value is significantly slower in water (in the order of nanoseconds) than in vacuum (in the order of tens of picoseconds).

6.2A) is compared to that of the dendrimers G1 to G5 in vacuum (Figure 6.2B). From this time series, it is clear that the dendrimers fold to approximately the same extent in water as in vacuum, although in water the dendrimers fold at a much slower rate than in vacuum (Table 6.2). The slow rate of folding is likely a combination of effects which are all present in the water simulations but absent in the vacuum simulations. These include solvent and solute frictional forces, the disruption of solvent shells surrounding the various groups of the dendrimer and the formation of partially folded intermediate equilibrium structures. In the water time series, initially the dendrimer does not undergo any folding and requires a few hundred picoseconds before the dendrimer begins to fold. This is most clearly visible in dendrimer G1. No folding occurs in this dendrimer over the first 555 ps. However, over of the next 220 ps, the dendrimer rapidly folds. This time series (Figure 6.2A) suggests that a specific arrangement of the solvent around the dendrimer has to be achieved or that the dendrimer has to attain a specific conformation before the overall folding may begin. Once this conformation has been attained, the dendrimer folds and, within a few hundred picoseconds, assumes a completely folded state (i.e., the equilibrium conformation of the vacuum simulation). In the larger generations there are stable intermediates which hinder the immediate progression to a completely folded conformation.

A comparison of the average R_g for the water and vacuum simulations (Table 6.2) reveals the dendrimers fold to the same extent in water as in vacuum; the R_g of the dendrimers in vacuum are only marginally smaller than the R_g in water. The differences in R_g of the vacuum and water simulations are a result of the dendrimers assuming slightly

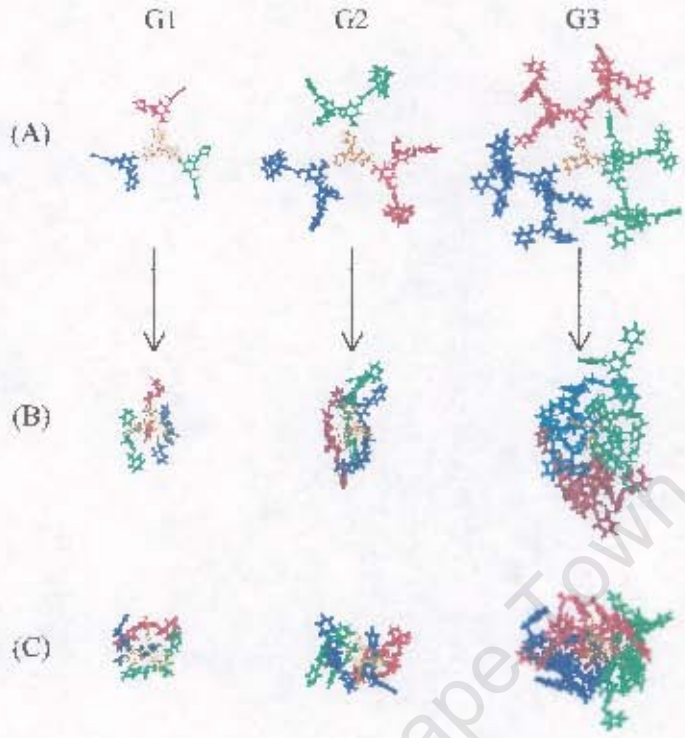

Figure 6.3: The folding of dendrimers G1 to G3 in water starting from (A) the energy minimized extended structures (the common starting conformations for both the water and vacuum simulations) to (B) the representative equilibrium folded structure for the last 1ns of the simulation. For comparative purposes (C), the vacuum representative equilibrium folded structure of these dendrimers is included. The choice of colour coding for the wedges has no significance other than ease of identification of the individual wedges.

more elongated conformations in water as compared with the vacuum simulations where the dendrimers are more spherical. (This is illustrated in Figure 6.3, where the average conformations of the dendrimers in water and vacuum are compared.) The rate at which a dendrimer folds (Table 6.2) in vacuum is inversely related to its size, while in water the converse is the case. Inspection of the MD trajectories reveals that initially the dynamics of the dendrimer are very similar to that of the dendrimer in the chloroform and THF simulations; the dynamics of the internal layers of the dendrimer are constrained with no overall motion while the terminal groups exhibit a greater degree of freedom of mobility. We observed the terminal groups frequently fold back to their parent layer and rapidly fold

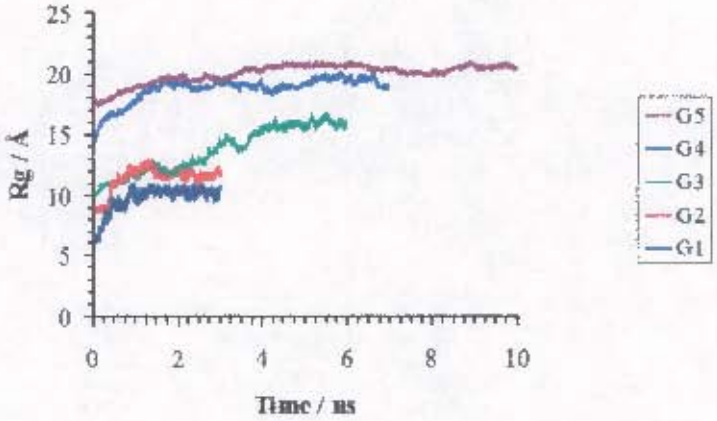

Figure 6.4: Time series of the R_g for dendrimers G1 to G5 unfolding in chloroform after starting from a folded conformation. To accommodate the longer simulation times necessary for the larger dendrimers (G4 and G5), the simulations of the smaller dendrimers (G1 to G3) were stopped after the dendrimer had not expanded for at least 1 ns.

back out again. The folding of each terminal group is random and is not coordinated with terminal groups of neighbouring wedges which has little effect on the overall conformation of the dendrimer. In addition, we observed what appears to be the cooperative interaction of neighbouring wedges, as suggested earlier in from the R_g time series. A single wedge is unlikely to fold in to the core on its own. However, if the wedge interacts with the neighbouring wedges, the entire dendrimer rapidly folds up on itself. The result is a pincer-like effect, where two wedges entrap the third wedge. This is most clearly visible in G1 and G2 in water (Figure 6.3). Further, in the water simulations we observed that the wedges exchange positions by the dendrimer expanding slightly and adopting a more unfolded conformation, allowing the wedges to reorientate such that one of the outer wedges becomes locked in middle. The result is a constant interchange between conformations and no one specific folded conformation is preferred. However, in the vacuum simulation we did not observe this exchange in position among the wedges. The dendrimers remained in their tightly folded conformation.

To examine the unfolding process of the dendrimer, we performed the opposite experiment in chloroform - start the dendrimers from a folded conformation and observed them unfolding. The radius of gyration time series (Figure 6.4) clearly shows that the dendrimers begin to unfold almost instantaneously and continue to expand throughout the simulation, until they are fully extended. For example, dendrimer G1 remains con-

	R_g / Å	
Generation	(A)	(B)
1	9.96	10.77
2	13.51	12.16
3	16.94	16.02
4	19.68	19.32
5	22.30	20.58

Table 6.3: A comparison of the average equilibrated R_g of the dendrimer in chloroform starting from (A) an extended conformation (i.e., the simulations in Chapter 5) and (B) a folded conformation. The dendrimers either completely unfold or are slightly folded (the difference in R_g marginally greater than 1 Å at the most).

tracted for the first 200ps, thereafter it rapidly expands over the next 550ps and is fully extended for the remainder of the simulation. A comparison of the average average R_g (Table 6.3) for the final 1ns of the unfolding simulations with the average equilibrium R_g of the simulations in Chapter 5 shows that only G1 unfolds completely. G2 to G5 adopt slightly folded conformations. However, it is unlikely that these are the final conformations in the unfolding process. It is expected that with additional simulation time, the G2 to G5 dendrimers would unfold to the same extent as the dendrimers in the simulations that start from an extended conformation. Figure 6.5 compares the average conformation of the dendrimer unfolded in chloroform for the last nanosecond of the simulation with the average structure of the dendrimer in chloroform but simulated initially from an extended conformation (Chapter 5). From the average conformations (Figure 6.5) and the time series of R_g (Figure 6.4), there is little doubt that the dendrimers unfold in chloroform.

In the simulations in the previous chapter we observed no folding of the dendrimers during the 5ns simulations. Given sufficient simulation time, we are confident that dendrimers G2 to G5 would completely unfold in a similar fashion to G1 and that once the dendrimers have fully unfolded in chloroform, they do not fold at all - the equilibrium conformation of Fréchet dendrimers in chloroform is completely unfolded. However, for the practical applications of Fréchet dendrimers it is not essential that the dendrimer completely unfolds; even in a partially unfolded state, all layers of the dendrimer are easily accessible by the reaction medium, as is visible in Figure 6.5.

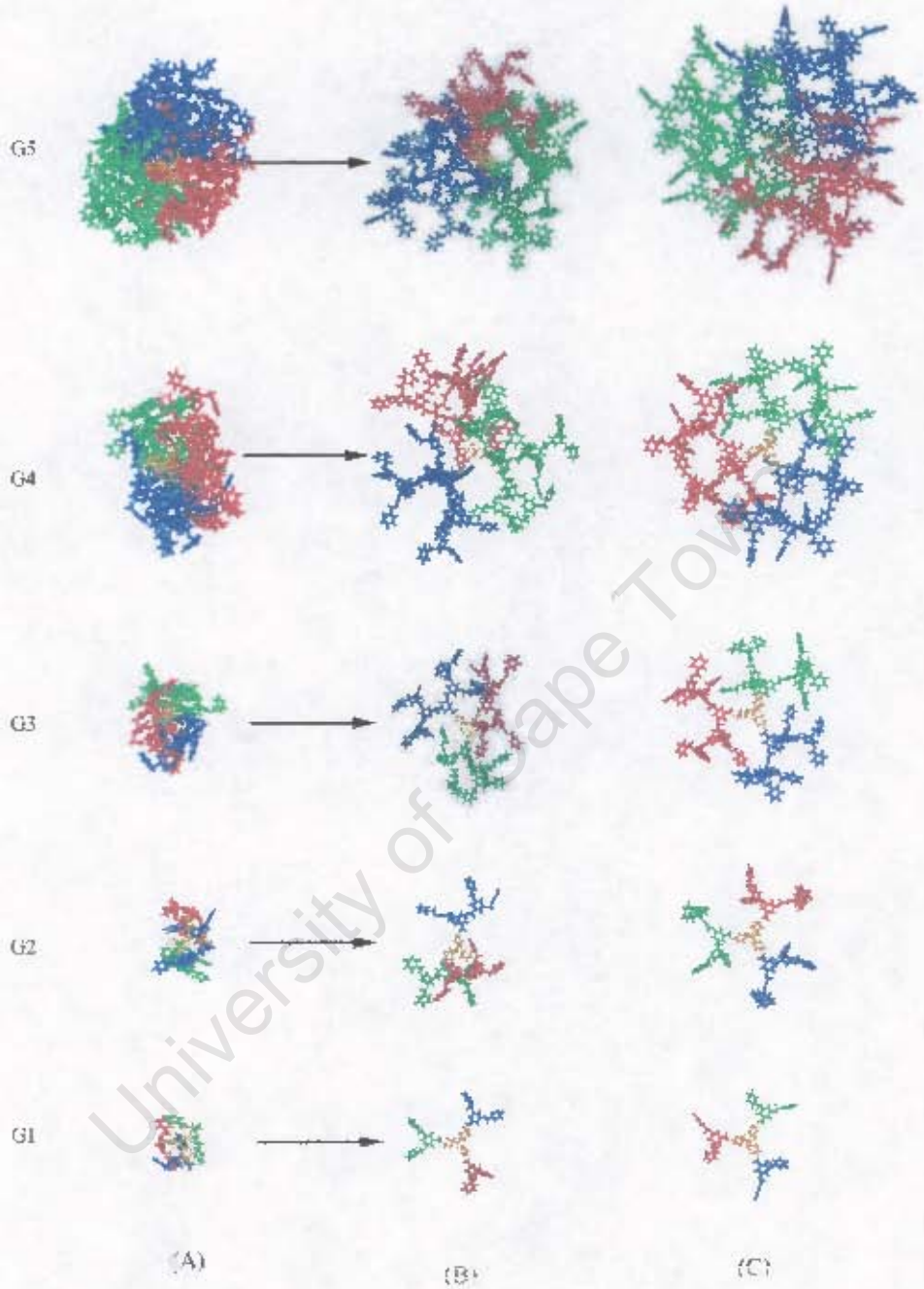

Figure 6.5: The unfolding of dendrimers G1 to G5 starting from (A) the folded conformation to (B) the representative equilibrium unfolded structure for the dendrimers in chloroform. For comparative purposes, (C) the representative equilibrium structure from the simulations of these dendrimers in chloroform starting from a unfolded conformation is included. As in Figure 6.3, the choice of colour coding for the wedges has no significance other than case of identification of the individual wedges.

	Rate (ps)	
Generation	Folding	Unfolding
1	780	435
2	1275	1116
3	4088	3880

Table 6.4: A comparison of the rate at which the dendrimers fold and unfold. The rates are in the same order of magnitude with the dendrimer unfolding faster in chloroform (a good solvent) than it folds in an water (an explicit poor solvent).

In Table 6.4, we make a comparison of the folding and unfolding rates of dendrimers G1 to G3. The rate of unfolding was anticipated to be far slower than that of the folding process (by an order of magnitude or more) because the solvent has to diffuse into the polymer and effectively pry the dendrimer open by disrupting the dendrimer-dendrimer interactions. In the folding simulations, the hydrophobic effect would result in the water pushing the dendrimer in onto itself. However, from Table 6.4, it is clear that this assumption was incorrect; both the unfolding and folding processes occur at similar rates, with the unfolding process marginally faster than the folding process. Because the rates are similar, this implies that the dendrimer can rapidly fold and unfold at approximately the same rate depending on specific environmental conditions.

6.3.2 Free Energy of Folding

In the previous section, the folding and unfolding simulations indicate that our dendrimer-solvent systems readily undergo conformational changes resulting from a change in solvent quality. In this section we investigate the free energy profiles of some model systems (Figure 6.7) which represent important structural components of Fréchet dendrimers. We describe the PMFs in terms of the energy required to pull the two rings together. The solvent PMFs are described in terms of general solvation principles by defining the two rings as two separate solute particles and assuming that the ether linkage has a small to negligible effect on the solvation shells, as illustrated in Figure 6.6.

(A) (B) (C)

Figure 6.6: A schematic diagram of the change in the solvation shells about the two aryl rings (black spheres) as they are pulled together. The red and blue rings in (A) represent the solvent shells of each ring in a solvent separated arrangement which merge to form a solvent shared arrangement (B) with a common solvent shell represented in purple. (C) represents the contact pair minimum where the shared solvent shell between the rings has been removed.

First generation wedge PMF

Our smallest folding model is the a first generation wedge (Figure 6.7A), which represents the smallest unit in a Fréchet dendrimer that is capable of backfolding, in this case one topological layer deep. We define the parent ring as the benzyl ring to which the two phenyl rings (child rings) are coordinated; in a full first generation dendrimer, the parent ring would be the first topological layer and the child rings would be the terminal layer. First we describe the poor solvent PMF, where it is expected for backfolding to predominate.

The PMF of the first generation wedge in vacuum and water exhibit only a single minimum, when the two rings are 11.0 Å apart. Therefore, the extended conformation of the wedge is preferred in both poor solvent environments. In vacuum, the plateau between 9.5 Å and 6.5 Å below 1 kcal.mol^{-1} suggests that folded conformations are possible. However, the steric clashes between the methyl protons of the ether linkage and the protons the parent benzyl ring make these folded conformations less favourable than unfolded conformations. The effect of the explicit poor solvent on the folded state is quantified by the differences between the water and vacuum profiles. In water, at 11.0 Å the two rings each have their own solvation shells. As the rings draw closer, these shells interact and repel each other resulting in a steady increase in energy as they draw closer. Between 7.0 Å and 5.8 Å, the shells merge to form a single solvent shared system. Note that in the vacuum system the energy rises over the same range (7.0 Å to 5.8 Å), suggesting that the formation of a single, shared solvent shell compensates for the increase energy in the intramolecular steric clashes as discussed earlier. Between 5.8 Å and 4.0 Å, the

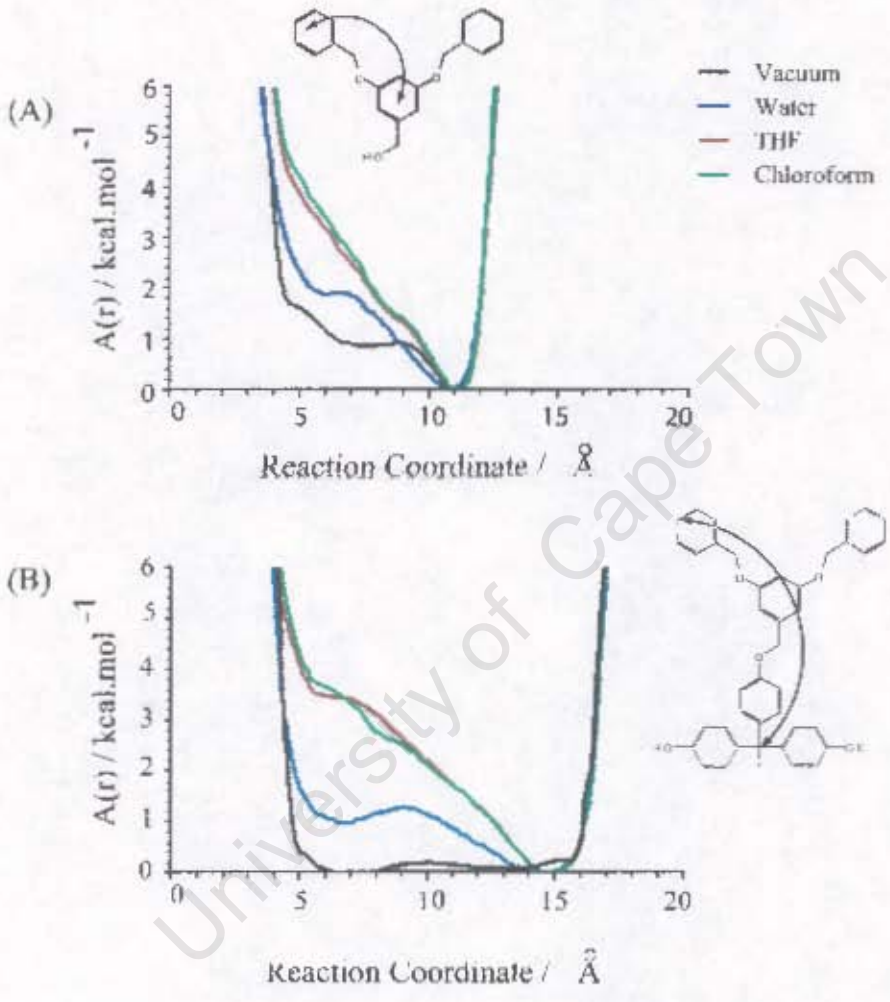

Figure 6.7: (A) The PMF the terminal group of a first generation wedge folding back to the parent layer in vacuum (black), water (blue), THF (brown) and chloroform (green). (B) The PMF of the terminal group of a first generation wedge folding back to the core of the dendrimer (B).

energy increases as the rings are pulled together, as the solvent shell system transforms to a contact pair minimum with no solvent shell between them. This increase in energy is interpreted as a combination of disruption of the shared solvent shell and the steric clashes within the molecule because the vacuum PMF (which is independent of solvent effects) also increases over this range. The formation of solvent shells and contact pairs have also been observed for the benzene dimer in water. Jorgensen and Severance reported a solvent shared local minimum at 7.5 Å for the benzene dimer in water PMF and a contact minimum centred at 5.5 Å, which was the global minimum. [246]

From the vacuum and water PMFs, we conclude that even in poor solvent conditions the first generation wedge favours an extended conformation. Therefore, the first generation wedge is not the smallest component of the dendrimer capable of folding. Backfolding of one topological is possible, however this folded conformation is not the most energetically favoured and this folded state is unlikely to persist longer than a few picoseconds and will not contribute to the sustainable overall folding of the dendrimer. This was confirmed during testing of the dendrimer force field in Chapter 4 (Figure 4.20) where the first generation wedge did not assume a folded conformation for longer than a few picoseconds during vacuum MD simulations.

The PMFs of the first generation wedge in the good solvents (chloroform and THF) are almost identical. The PMFs share the same global minimum with the vacuum and water PMFs at 11.0 Å and the PMFs increase at a similar rate to the water PMFs as the rings are drawn together. However in the THF and chloroform PMFs, there is no plateau due to the formation of solvent shared or contact pair arrangements. There is an almost perfect inverse linear relation between the free energy and the distance between the two aryl rings. The only observable difference between the THF and chloroform systems is between 7.5 Å and 4.5 Å, where the interaction free energy in THF is fractionally lower than that in chloroform (by 0.3kcal.mol^{-1} at maximum). It is unlikely that this small difference in energy is the cause for the substantial difference of the dynamics of the full dendrimer in THF and chloroform (Chapter 5).

The second generation PMF

From the PMF of the first generation wedge it has been established that the dendrimer is unlikely to fold back one topological layer. However, the G1 dendrimer folds in vacuum and water (Figure 6.2). Therefore, we investigate a slightly larger system to the first generation

wedge, by attaching a first generation wedge to a Fréchet dendrimer core (Figure 6.1C). The free energy surface for this model is shown in Figure 6.7B. As with the first generation wedge PMF, we begin by discussing the poor solvent PMFs.

In vacuum, the global minimum in the free energy profile is at 6.9 Å, i.e., a folded conformation is energetically favoured in vacuum. This global minimum is separated from a shallow and broad local minimum at 13 Å (an unfolded conformation) by a small barrier of 0.2 kcal.mol^{-1}. Therefore a terminal group of a Fréchet dendrimer in vacuum is capable of folding back two internal generations without the assistance of a neighbouring wedge and a folded conformation is the lowest energy conformation. For the water PMF a minimum representing the folded state also at 6.5 Å is not the global minimum. Instead the global minimum is the unfolded state at 14.5 Å. This is surprising as the first generation dendrimer folds in both vacuum and water (Figure 6.2). However, the barrier height between the global and local minima in water is only 1.3 kcal.mol^{-1}. Therefore it is possible that the complete first generation dendrimer folds in water (despite a single wedge preferring an unfolded conformation) because the three wedges fold in a collaborative manner, thereby lowering the overall energy of the folded conformation.

The PMFs of the two good solvents (chloroform and THF) are very similar; they share the same global minimum at 15.0 Å (an unfolded conformation) and the only noticeable difference between the PMFs is that the relative energies of the PMFs interchange between 11.0 Å and 5.5 Å, i.e., from 11.0 Å and 6.9 Å the free energy in chloroform is slightly lower than that for THF (a maximum difference of 0.3kcal.mol^{-1} at 8.2 Å) and between 6.8 Å and 5.5 Å the THF PMF is lower in energy than chloroform PMF. However, considering each PMF independently reveals subtle characteristics in the profile. The THF PMF increases linearly from 15.0 Å to 7.5 Å where it reaches a plateau. We identify this plateau as the formation of a contact pair as this plateau falls over the same distance as the vacuum global minimum. The linear increase in the THF PMF up to the formation of the contact pair (at 7.5 Å) suggests that in THF there is no stable intermediate, such as a solvent shared arrangement. The chloroform PMF is essentially identical to the THF PMF up to approximately 9.5 Å (the chloroform PMF is marginally lower than the THF PMF from 11 Å). Thereafter, two distinct regions in the chloroform PMF are visible. The first is a flattening of the PMF from 9.5 Å to 8.2 Å after which the PMF rapidly increases again to 6.5 Å, at which point the PMF flattens slightly until 5.5 Å. The first region (9.5 Å to 8.2 Å) is likely to be a result of the formation of a solvent shared system between the core

and the terminal groups while the second region (6.5 Å to 5.5 Å) is the formation of the contact pair. These subtle differences in the PMF of chloroform and THF are unlikely to be the sole reason for the difference in the dynamics of the dendrimer in solution. However, these PMFs do suggest that a Fréchet dendrimer is more likely to form solvent shells in chloroform than in THF which is not surprising when one considers the strong chloroform-benzene ring interaction as described in Chapter 4. The formation of solvent shells in chloroform could restrict the dynamics of the dendrimer terminal groups whereas in THF the terminal rings do not form solvent shells as readily as chloroform and therefore the solvent does not impede the dynamics of the dendrimer to the same extent.

6.4 Conclusion

From the unfolding simulations of Fréchet dendrimers in chloroform we have shown the preferred equilibrium conformation of a Fréchet dendrimer in chloroform is an unfolded conformation and this is independent of whether the dendrimer is initiated from a folded or unfolded state. We have shown that the dendrimer folds in water (an explicit poor solvent) and the equilibrium conformation of the dendrimer is comparable with that of the vacuum equilibrium conformation. Therefore, vacuum simulations of dendrimers best represent dendrimers in poor solvents and do not adequately represent the dendrimer in a good solvent environment. Hence, drawing conclusions from comparisons between vacuum simulations and experimental measurements conducted in a good solvent, such as those that have recently appeared in the literature, [57] should be done so with great care.

We have shown that a dendrimer folds and unfolds at approximately the same rate and is typically the order of several nanoseconds. The rapid (un)folding of the dendrimer could have numerous useful applications. These includes catalysis, where a sensitive catalytic group could be shielded from the reaction medium when placed within the body of the dendrimer which remains folded until a specific step in the reaction process at which point the dendrimer could unfold and expose the catalyst. Thereafter a change in the solvent quality of the reaction medium could trigger the dendrimer to collapse around the catalyst to continue to shield it. In drug delivery it is desirable that the guest molecule to be released from the dendrimer host molecule as close to the target site as possible. The more rapidly the dendrimer responds to folding and unfolding triggers (such as pH changes), the more accurately specific regions in the body can be targeted. Alternatively,

dendrimers could be used to mop up specific pharmacological toxins; if the specifically designed dendrimer came into contact with the target toxin, the dendrimer would have to fold around the toxin to encapsulate it before the toxin diffused away. The quicker the encapsulating process is performed, the greater the chance of entrapping the toxin.

From the PMFs calculated for our first dendrimer model (the first generation wedge), we have shown that the first generation wedge is not the primary source of folding within the dendrimer, i.e., the sustainable folded conformation is not generated from the back-folding of one topological layer. Secondly the folding back of the terminal group to the parent layer in THF and chloroform is identical and cannot account for the difference in the dynamics of a Fréchet dendrimer in THF and chloroform. From the PMFs of our second model (the first generation wedge attached to a core group), we showed that the dendrimer is capable of folding back over two topological layers. More importantly, a subtle difference between the PMFs of this model in THF and chloroform suggest that the difference in the behaviour of the dendrimer in THF and chloroform is a result of the formation of a solvent shells in chloroform which are absent in THF.

With the advances in computational power keeping pace with Moore's Law (the complexity of integrated circuits doubles every 18 months) [263], it is likely in the very near future that it will be possible to achieve convergence of the third model (a terminal group of a full first generation folding back into the core) and even more complex models may be investigated. This is a topic for future work.

Chapter 7

Final Conclusions and Future Work

In this thesis, the structure and dynamics of dendrimers in solution have been studied through nanosecond atomistic MD simulations of explicitly solvated Fréchet dendrimers. The properties of these dendrimers have been investigated in four solvent environments: vacuum and water (representatives of poor solvents), and tetrahydrofuran (THF) and chloroform (representatives of good solvents). To establish the effect of the quality of the solvent on the conformation of the dendrimer, additional nanosecond MD simulations were performed, with the dendrimers starting from both initially folded and unfolded conformations. Free energy calculations of model dendritic units were employed to provide an energetic rational for the folding behaviour of these dendrimers.

To ensure these simulations were as accurate as possible, the dendrimer and solvent force fields were scrutinised in detail. A detailed review of available literature yielded no appropriate model for a fully relaxed five-site representation of chloroform. Hence, we developed a fully relaxed all atom model for chloroform by combining several existing models. The radially and spatially averaged distribution functions of liquid chloroform were fully characterised using the new chloroform model developed in this thesis. The SDFs revealed a first solvation shell comprised two parts; a strongly bound and a weakly bound region. At lower probabilities, the second solvation shell could be observed. Dynamic properties calculated for the new chloroform model, including diffusion coefficients and rotational correlation times gave an excellent fit with experimental data. For THF a suitable force field was selected from several models available in literature. This THF

force field was not modified in this thesis, however the calculation of the spatially averaged distributions and Voronoi polyhedra for the THF solvent were novel. A comparison of the RDFs, SDFs and Voronoi polyhedra suggest that the intermolecular structure of chloroform and THF are very similar. The dendrimer force field was obtained by modifying an existing force field developed in our laboratory. This modification involved the lowering of the rotational energy of the ether linkage. The ether linkage is the most important factor affecting the rigidity and overall conformation of a Fréchet dendrimer. Lowering this rotational energy barrier allowed for greater flexibility of the dendrimer but did not impact its overall conformation. The dendrimer and solvent force fields were combined without further modification to produce the solution force field employed in this thesis. Analysis of simulation conditions, such as the temperature and ensemble sampling, revealed that none of the factors investigated had any significant effect on the equilibrium conformation of the dendrimer. Therefore, we are confident that the MD simulations of dendrimers in solution presented in this thesis accurately represent the behaviour of Fréchet dendrimers in solution.

The effect of solution on Fréchet dendrimers was explored through MD simulations in vacuum, THF and chloroform. In literature it has be shown that dendrimers fold in vacuum. However, we showed that in an explicitly modelled good solvent (THF and chloroform), the dendrimers remain fully extended. It was concluded that vacuum simulations do not adequately represent the behaviour of a dendrimer in solution as some early coarse grain simulations have suggested. In addition, particularly in the folded state, the core of the dendrimer is not at the geometric centre of the dendrimer and the distribution of the groups of the dendrimer about the core is asymmetrical. Further, interpretation of radially averaged distributions was shown to be dependent on the method of normalisation employed. Hence, the results from radially averaged methods must be interpreted with care. Radially averaged analysis is commonly used to describe the structure of dendrimers as "dense core" or "dense shell". However, a simple comparison between the density of benzyl alcohol and that of the "dense core" region of a dendrimer, showed that the "dense core" analogy did not indicate that the core was surrounded by an impenetrable shell. Rather the "dense core" region can accommodate additional groups, whether these groups are from the terminal layer due to backfolding, or guest molecules. Spatially averaged distribution functions more clearly illustrate the structure of a dendrimer in three dimensions. Employing SDFs it is not only possible to gain a clear picture of the overall

shape and size of the dendrimers, but it is also possible to analyse the internal structure of the dendrimer. The distribution of the layers of the dendrimer as observed in both the spatially and radially averaged methods can be accounted for by the hyperbranching inherent to dendrimers. However, the contribution of backfolding in the classical sense (where the terminal groups diffuse into the body of the dendrimer) to the distribution of the terminal groups close to the core cannot be ruled out completely.

Analysis of the dynamics of the dendrimer, revealed the internal structure of the solvated dendrimer to be inflexible. The flexibility of the dendrimer is isolated to the terminal groups. In this thesis a close correlation was observed between the flexibility of a dendrimer in a particular solvent and its dynamics in that solvent. The terminal layer of a dendrimer in chloroform is notably less flexibility than in THF. This difference in flexibility of the dendrimer in THF and chloroform accounts for the difference between the measured intrinsic viscosities of Fréchet dendritic wedges in chloroform and THF as reported in the literature. As a result, a new expression for the intrinsic viscosity was proposed. This expression is a function of the standard contributions of the size and shape of the dendrimer and is also a function of the flexibility of the dendrimer in a particular solvent. The dendrimer simulations in this thesis were verified through a close match between independently measured longitudinal relaxation rates reported in literature and the relaxation rates calculated in this thesis. The relaxation rates of the terminal groups of the dendrimer are substantially longer in comparison with the relaxation rates of the internal layers. Further, the relaxation rates in THF were longer than those in chloroform. Hence, these relaxation rates support the conclusions that the terminal groups are substantially more flexible than the internal generations and that the dendrimer has greater flexibility in THF than in chloroform. The increase flexibility of the dendrimer in THF in comparison with chloroform can be accounted for from the spatial arrangement of the solvent about the dendrimers and the spatially averaged diffusion profiles of the THF and chloroform solvents within the dendrimers. These profiles indicates that while the arrangement of the solvent within the dendrimer in THF and chloroform is very similar, chloroform experiences the greatest resistance to diffusion close to the internal surface of the dendrimer, thereby reducing the flexibility of the dendrimer.

The unfolding simulations of Fréchet dendrimers in chloroform showed that the preferred equilibrium conformation of a Fréchet dendrimer in chloroform is an unfolded conformation and this is independent of whether the dendrimer is initiated from a folded

or unfolded state. Further, the dendrimer folds in water (an explicit poor solvent) with an equilibrium conformation of the dendrimer comparable with that of the vacuum equilibrium conformation. Therefore, vacuum simulations of dendrimers best represent dendrimers in poor solvents and do not adequately represent the dendrimer in a good solvent environment. Hence, drawing conclusions from comparisons between vacuum simulations and experimental measurements conducted in a good solvent, should be done so with care. In addition, in this thesis it was shown that a dendrimer folds and unfolds at approximately the same rate and is typically the order of several nanoseconds. The rapid (un)folding of the dendrimer could have numerous useful applications. An example is using dendrimers as catalytic scaffolds - a sensitive catalytic group could be shielded from the reaction medium when placed within the body of the dendrimer which remains folded until a specific step in the reaction process. At this point the dendrimer could unfold in response to a environmental change (such as solvent quality) and expose the catalyst to the reaction medium. Thereafter, a change in the solvent quality of the reaction medium could trigger the dendrimer to collapse around the catalyst to once again protect the catalyst. An additional example is in drug delivery. It is desirable that the guest molecule is released from the dendrimer host molecule as close to the target site as possible. The more rapidly the dendrimer responds to folding and unfolding triggers (such as ionic strength or pH changes), the more accurately specific regions in the body can be targeted. Alternatively, dendrimers could be used to mop up specific pharmacological toxins; if the "designer" dendrimer came into contact with the target toxin, the dendrimer would have to fold around the toxin to encapsulate it before the toxin diffused away. The quicker the encapsulating process is performed, the greater the chance of entrapping the toxin.

The folding simulations provided a qualitative description of how the dendrimer conformational changes occur. A quantitative analysis of the folding of the dendrimer is obtained from free energy calculations of model dendritic units. These provide an energetic rational for the folding behaviour of the dendrimers. One dimensional PMFs of the model dendritic systems show that sustainable backfolding was unlikely to occur one generation deep, even in vacuum or in an explicit poor solvent. Backfolding of the terminal groups is only energetically favoured in vacuum when folding back over two generations. However, this is not the case for the dendrimer in water, THF or chloroform (although in water the local and global minimum are separated by a small energy barrier). The PMFs of terminal groups folding back in chloroform and THF are almost identical. However, the

subtle difference between the PMFs of the terminal group folding back two generations in THF and chloroform suggest that the difference in the behaviour of the dendrimer in THF and chloroform is a result of the formation of more strongly bound solvent shells in chloroform than in THF. The knowledge of the free energy surfaces of additional dendritic models is key to understanding the micro- and macroscopic properties of dendrimers. Free energy calculations provide valuable insight into the molecular details of the dynamics and dendrimer properties. In this thesis, the PMF of a third model (the folding back of a terminal group of a complete G1 dendrimer in to the core of the dendrimer) which included the effect of the neighbouring wedges was attempted but showed no signs of converging in a reasonable period with existing computational resources. However, with the rapid developments in computer hardware the calculation of this PMF could be feasible in the near future. This PMF would enable the quantitative measure of the effect of the neighbouring wedges on the folding of the dendrimer. An alternative PMF to calculate is the free energy profile of drawing together two terminal groups from neighbouring wedges within the same dendrimer. This could highlight the difference in the behaviour of the dendrimer in chloroform and THF.

In our laboratory, preliminary NMR investigations are underway on dendrimers G1 to G3 in d_8-THF and $CDCl_3$. These measurements include ^2H T_1 relaxation rates and diffusion coefficients employing the inversion recovery pulse sequence and DOSY NMR respectively. However, these measurements present significant challenges to overcome, in particular isolating the various resonances of the internal generations of the dendrimer. Further, the effect the concentration of the dendrimer solution and impurities from incomplete and side reactions during the synthetic process have yet to be established. The initial results, although preliminary, are encouraging - the relative diffusion rates of the dendrimers indicate that the dendrimers diffuse faster in chloroform than in THF. Further, T_1 analysis of the terminal aromatic protons indicates that the protons in the para position have a relaxation rate of approximately a third of that of the protons in the ortho or meta positions. Furthermore, the relaxation rates for the protons in THF are approximately twice that for the same proton in chloroform. These measurements correspond well with the trends observed in the calculated results presented in this thesis. However, it is too early to draw final conclusions from these preliminary measurements which remain the focus of future work.

The progress of computational studies of dendrimers will largely be dependent on the

availability of sufficiently large parallel computing systems. Such systems will enable large complex dendrimer simulations to be routinely investigated. The obvious extension of this thesis is to study other dendrimer-solvent systems, to calculate the free energy profiles of more complex dendrimer fragments and to study how two or more dendrimers interact in solution. However, more exotic studies include non-equilibrium MD simulations of solvated dendrimers, for example dendrimers under flow. This will enable the behaviour of the dendrimers to be established under more realistic environments; dendrimers acting as catalytic supports are under constant mixing in a reaction medium, while dendrimers acting as pharmaceutical delivery agents are under constant flow within the human body. Therefore, it is crucial that we understand how dendrimers behave under such conditions and how their behaviour differs from the systems discussed in this thesis. However, the practical applications of dendrimers are likely to be the driving force for the direction of future simulations of solvated dendrimers. A greater understanding of the behaviour of dendrimers in solution may ultimately enable "designer" dendrimer systems to be produced with specifically crafted characteristics for applications of these hyperbranched polymers in new and exciting fields.

Bibliography

[1] F. Aulenta, W. Hayes, and S. Rannard. Dendrimers: a new class of nanoscopic containers and delivery devices. *Eur. Polym. J.*, 39:1741–1771, 2003.

[2] K. J. Naidoo, S. J. Hughes, and J. R. Moss. Computational investigations into the potential use of poly(benzyl phenyl ether) dendrimers as supports for organometallic catalysts. *Macromolecules*, 32(2):331–341, 1999.

[3] D. A. Tomalia, H. Baker, J. Dewald, M. Hall, G. Kallos, S. Martin, J. Ryder, and P. Smith. A new class of polymers: starburst-dendritic macromolecules. *Polym. J.*, 17:117–132, 1985.

[4] C. J. Hawker and J. M. J. Fréchet. Preparation of polymers with controlled molecular architecture. A a new convergent approach to dendritic macromolecules. *J. Am. Chem. Soc.*, 112:7638–7647, 1990.

[5] E. M. M. de Brabander and E. W. Meijer. Poly(propylene imine) dendrimers: large-scale synthesis via heterogeneously catalyzed hydrogenation. *Angew. Chem. Int. Ed. Engl.*, 32:1308–1311, 1993.

[6] H. Uchida, Y. Kabe, K. Yoshino, T. Tsumuraya, and S. Masamune. General strategy for the systematic synthesis of oligosiloxanes. silicone dendrimers. *J. Am. Chem. Soc.*, 112:7077–7079, 1990.

[7] C. J. Hawker, E. E. Malmström, C. W. Frank, and J. P. Kampf. Exact linear analogs of dendritic polyether macromolecules: design, synthesis, and unique properties. *J. Am. Chem. Soc.*, 119:9903–9904, 1997.

[8] G. R. Newkome, C. N. Moorefield, and F. Vögtle. *Dendrimers and dendrons: concepts, syntheses, applications.* Wiley-VCH, Wienheim, 2001.

[9] P. G. de Gennes and H. Hervet. Statistics of starburst polymers. *J. Phys. Lett.*, 44:351–360, 1983.

[10] S. J. Hughes, J. R. Moss, K. J. Naidoo, J. F. Kelly, and A. S. Batsanov. Force-field parameterisation, synthesis and crystal structure of a novel tricarbonylchromium arene complex. *J. Organomet. Chem.*, 588:176–185, 1999.

[11] E. Buhleier, W. Wehner, and F. Vögtle. Cascade and nonskid-chain-like syntheses of molecular cavity topologies. *Synthesis*, pages 155–158, 1978.

[12] D. Zanini and R. Roy. Practical synthesis of starburst PAMAM-thiosialodendrimers for probing multivalent carbohydrate-lectin binding properties. *J. Org. Chem*, 63:3486–3491, 1998.

[13] A. Adronov and J. M. J. Fréchet. Light-harvesting dendrimers. *Chem. Commun.*, 18:1701–1710, 2000.

[14] R. van Heerbeek, P. C. J. Kamer, P. W. N. M. van Leeuwen, and J. N. H. Reek. Dendrimers as support for recoverable catalysts and reagents. *Chem. Rev.*, 102:3717–3756, 2002.

[15] R. Esfand and D. A. Tomalia. Poly(amidoamine) (pamam) dendrimers: from biomimicry to drug delivery and biomedical applications. *Drug Discovery Today*, 6(8):427–436, 2001.

[16] S. M. Grayson and J. M. J. Fréchet. Convergent dendrons and dendrimers: from synthesis to applications. *Chem. Rev.*, 101:3819–3867, 2001.

[17] S. Hecht and J. M. J. Fréchet. An alternative synthetic approach toward dendritic macromolecules: novel benzene-core dendrimers via alkyne cyclotrimerization. *J. Am. Chem. Soc.*, 121(16):4084–4085, 1999.

[18] C. Valério, J.-L. Fillaut, J. Ruiz, J. Guittard, J-C. Blais, and D. Astruc. The dendritic effect in molecular recognition: Ferrocene dendrimers and their use as supramolecular redox sensors for the recognition of small inorganic anions. *J. Am. Chem. Soc.*, 119:2588–2589, 1997.

[19] U. Boas and P. M. H. Heegaard. Dendrimers in drug research. *Chem. Soc. Rev.*, 33:43–63, 2004.

[20] L. J. Twyman, A. S. H. King, and I. K. Martin. Catalysis inside dendrimers. *Chem. Soc. Rev.*, 31:69–82, 2002.

[21] A. W. Bosman, H. M. Janssen, and E. W. Meijer. About dendrimers: structure, physical properties, and applications. *Chem. Rev.*, 99:1665–1688, 1999.

[22] M. S. Wendland and S. C. Zimmerman. Synthesis of cored dendrimers. *J. Am. Chem. Soc.*, 121:1389–1390, 1999.

[23] J.-P. Majoral, C. Larré, R. Laurent, and A.-M. Caminade. Chemisty of the internal voids of dendrimers. *Coord. Chem. Rev.*, 190-192:3–18, 1999.

[24] A. M. Naylor, W. A. Goddard III, G. E. Kiefer, and D. A. Tomalia. Starburst dendrimers. 5. Molecular shape control. *J. Am. Chem. Soc.*, 111:2339–2341, 1989.

[25] R. L. Lescanec and M. Muthukumar. Configurational characteristics and scaling behavior of starburst molecules: a computational study. *Macromolecules*, 23:2280–2288, 1990.

[26] S. Rosenfeldt, N. Dingenouts, D. Pötschke, M. Ballauff, A. J. Berresheim, K. Müllen, and P. Linder. Analysis of the spatial dimensions of fully aromatic dendrimers. *Angew. Chem. Int. Ed.*, 43:109–112, 2004.

[27] J. C. Smith and C. B. Gorman. Dendrimer shape and internal organisation as related to molecular size and repeat unit flexibilty - a Molecular Dynamics investigation. *ACS PMSE Proc.*, 78:226–227, 1998.

[28] L. Cavallo and F. Fraternali. A Molecular Dynamics study of the first five generations of poly(propylene imine) dendrimers modified with n-tboc-L-phenylalanine. *Chem. Eur. J.*, 4:927–934, 1998.

[29] R. Scherrenberg, B. Coussens, P. van Vliet, G. Edouard, J. Brackamn, and E. de Brabander. The molecular characteristics of poly(propyleneimine) dendrimers as studied with small-angle neutron scattering, viscosimetry and Molecular Dynamics. *Macromolecules*, 31:456–461, 1998.

[30] M. L. Mansfield and L. I. Klushin. Intrinsic viscosity of model starburst dendrimers. *J. Phys. Chem.*, 96:3994–3998, 1992.

[31] C. Cai and Z. Y. Chen. Rouse dynamics of a dendrimer model in the Θ condition. *Macromolecules*, 30:5104–5117, 1997.

[32] J. Aerts. Prediction of intrinsic viscosities of dendritic, hyperbranched and branched polymers. *Comput. Theor. Polym. Sci.*, 8(1-2):49–54, 1998.

[33] C. Cai and Z. Y. Chen. Intrinsic viscosity of starburst dendrimers. *Macromolecules*, 31:6393–6396, 1998.

[34] A. H. Widmann and G. R. Davies. Simulation of the intrinsic viscosity of hyperbranched polymers with varying topology. 1. Dendritic polymers built by sequential addition. *Comput. Theor. Polym. Sci.*, 8:191–199, 1998.

[35] B. Hammouda. Structure factor for starburst dendrimers. *J. Polym. Sci., Part B: Polym. Phys.*, 30:1387–1390, 1992.

[36] M. L. Mansfield. Dendron segregation in model dendrimers. *Polymer*, 35:1827–1830, 1994.

[37] D. Boris and M. Rubinstein. A self-consistent mean field model of a starburst dendrimer: dense core vs dense shell. *Macromolecules*, 29:7251–7260, 1996.

[38] M. L. Mansfield and L. I. Klushin. Monte Carlo studies of dendrimer macromolecules. *Macromolecules*, 26:4262–4268, 1993.

[39] W. Carl. A monte carlo study of model dendrimers. *J. Chem. Soc., Faraday Trans.*, 92:4151–4154, 1996.

[40] Z. Y. Chen and S.-M. Cui. Monte Carlo simulations of star-burst dendrimers. *Macromolecules*, 29:7943–7952, 1996.

[41] R. la Ferla. Conformations and dynamics of dendrimers and cascade macromolecules. *J. Chem. Phys.*, 106(2):686–700, 1997.

[42] L. Lue and J. M. Pausnitz. Structure and thermodynamics of homogeneous-dendritic-polymer solutions: computer simulation, integral-equation, and lattice-cluster theory. *Macromolecules*, 30:6650–6657, 1997.

[43] Z. Y. Chen and C. Cai. Pattern formation in a dendrimer model. *Phys. Rev. E: Stat*, 57(3):3652–3655, 1998.

[44] M. Murat and G. S. Grest. Molecular Dynamics study of dendrimer molecules in solvents of varying quality. *Macromolecules*, 29:1278–1285, 1996.

[45] P. Welch and M. Muthukumar. Tuning the density profile of dendritic polyelectrolytes. *Macromolecules*, 31:5892–5897, 1998.

[46] M. A. Mazo, P. A. Zhilin, E. B. Gusarova, S. S. Sheiko, and N. K. Balabev. Computer simulation of intramolecular mobility of dendrimers. *J. Mol. Liq.*, 82:105–116, 1999.

[47] Z. Y. Chen and C. Cai. Dynamics of starburst dendrimers. *Macromolecules*, 32:5423–5434, 1999.

[48] A. V. Lyulin, G. R. Davies, and D. B. Adolf. Brownian dynamics simulations of dendrimers under shear flow. *Macromolecules*, 33:3294 – 3304, 2000.

[49] F. Ganazzoli, R. La Ferla, and G. Terragni. Conformational properties and intrisic viscosity of dendrimers under excluded-volume conditions. *Macromolecules*, 33:6611–6620, 2000.

[50] K. Karatasos, D. B. Adolf, and G. R. Davies. Statics and dynamics of model dendrimers as studied by Molecular Dynamics simulations. *J. Chem. Phys.*, 115(11):5311–5319, 2001.

[51] F. Ganazzoli, R. La Ferla, and G. Terragni. Intramolecular dynamics of dendrimers under excluded-volume conditions. *Macromolecules*, 34:4222–4228, 2001.

[52] Y.-J. Sheng, S. Jiang, and H.-K. Tsao. Radial size of a startburst dendrimer in solvents of varying quality. *Macromolecules*, 35:7865–7868, 2002.

[53] E. G. Timoshenko, Y. A. Kuznetsov, and R. Connolly. Conformations of dendrimers in dilute solution. *J. Chem. Phys.*, 117(19):9051–9062, 2002.

[54] H. M. Harreis, C. N. Likos, and M. Ballauff. Can dendrimers be viewed as compact colloids? A simulation study of the fluctuation in a dendrimer of fourth generation. *J. Chem. Phys.*, 118:1979–1988, 2003.

[55] S. V. Lyulin, L. J. Evers, P. van der Schoot, A. A. Darinskii, A. V. Lyulin, and M. A. J. Michels. Effect of solvent quality and electrostatic interactions on size and structure of dendrimers. brownian dynamics simulations and Mean-Field theory. *Macromolecules*, 37:3049–3063, 2004.

[56] A. V. Lyulin, G. R. Davies, and D. B. Adolf. Location of terminal groups of dendrimers: Brownian dynamics simulations. *Macromolecules*, 33:6899–6900, 2000.

[57] M. Ballauf and C. N. Likos. Dendrimers in solution: insight from theory and simulation. *Angew. Chem. Int. Ed.*, 43(23):2998–3020, 2004.

[58] M. K. Bhalgat and J. C. Roberts. Molecular modelling of polyamidoamine (PAMAM) starburst dendrimers. *Eur. Polym. J.*, 36:647–651, 2000.

[59] T. Cagin, G. Wang, R. Martin, N. Breen, and W. A. Goddard III. Molecular modelling of dendrimers for nanoscale applications. *Nanotechnology*, 11:77–84, 2000.

[60] T. Cagin, G. Wang, R. Martin, G. Zamanakos, N. Vaidehi, D. T. Mainz, and W. A. Goddard III. Multiscale modeling and simulation methods with applications to dendritic polymers. *Comput. Theor. Polym. Sci.*, 11:345–356, 2001.

[61] M. Elshakre, A. S. Atallah, S. Santos, and S. Grigoras. A structural study of carbosilane dendrimers versus polyamidoamine. *Comput. Theor. Polym. Sci.*, 10:21–28, 2000.

[62] I. Lee, B. D. Athey, A. W. Wetzel, W. Meixner, and J. R. Baker Jr. Structural Molecular Dynamics studies on polyamidoamine dendrimers for a therapeutic application: effects of pH and generation. *Macromolecules*, 35:4510–4520, 2002.

[63] P. K. Maiti, T. Cagin, G. Wang, and W. A. Goddard III. Structure of PAMAM dendrimers: generations 1 through 11. *Macromolecules*, 37:6236–6254, 2004.

[64] E. Canetta and G. Maino. Molecular dynamic analysis of the structure of dendrimers. *Nucl. Instr. and Meth. in Phys. Res. B*, 213:71–74, 2004.

[65] P. K. Maiti, T. Cuagin, S.-T. Lin, and W. A. Goddard III. Effect of solvent and pH on the structure of PAMAM dendrimers. *Macromolecules*, 38:979–991, 2005.

[66] E. Blasizza, M. Fermeglia, and S. Pricl. Dendrimers as functional materials. A molecular simulation study of poly(propylene) imine starburst molecules. *Mol. Sim.*, 24:167–189, 2000.

[67] N. Zacharopoulos and I. G. Economou. Morphology and organization of poly(propylene imine) dendrimers in the melt from Molecular Dynamics simulation. *Macromolecules*, 35:1814–1821, 2002.

[68] G. Teobaldi and F. Zerbetto. Molecular Dynamics of a dendrimer-dye guest-host system. *J. Am. Chem. Soc.*, 125(24):7388–7393, 2003.

[69] Z. Zhang, K. J. Haxton, L. Ropartz, D. J. Cole-Hamilton, and R. E. Morris. Synthesis and computer modelling of hydroxy-derivatised carbosilane dendrimers based on polyhedral silsequioxane cores. *J. Chem. Soc., Dalton Trans.*, 22:3261–3268, 2001.

[70] M. A. Mazo, M. Y. Shamaev, N. K. Balabaev, A. A. Darinskii, and I. M. Neelov. Conformational mobility of carbosilane dendrimer: Molecular Dynamics simulation. *Phys. Chem. Chem. Phys.*, 6:1285–1289, 2004.

[71] S. Pricl and M. Fermeglia. Molecular simulation of host-guest inclusion compounds: an approach to the lactodendrimers case. *Carbohydr. Polym.*, 45:23–33, 2001.

[72] C.-W. von der Lieth, M. Frank, and T. K. Lindhorst. Molecular Dynamics simulations of glycoclusters and glycodendrimers. *Reviews in Molecular Biotechnology*, 90:311–337, 2002.

[73] C. B. Gorman and J. C. Smith. Effect of repeat unit flexibility on dendrimer conformation as studied by atomistic molecular dynamics simulations. *Polymer*, 41:675–683, 2000.

[74] J. G. Jang and Y. C. Bae. Phase behaviours of dendrimer/solvent systems: molecular thermodynamics approach. *J. Chem. Phys.*, 116(8):3484–3492, 2002.

[75] M. Fermeglia, M. Ferrone, and S. Pricl. Computer-aided simulation of a dendrimer with a protoporphyrinic core as a potential, novel hemoprotein mimic. *Bioorg. Med. Chem.*, 10:2471–2478, 2002.

[76] S. Pricl, M. Ferrone, M. Fermeglia, and A. Asquini. Shape persistent polyphenylene-based dendrimers: a computational approach. *Polym. Mater. Sci. Eng.*, 88:407, 2003.

[77] W. Ortiz, A. E. Roitberg, and J. L. Krause. Molecular Dynamics of poly(benzylphenyl ether) dendrimers: effects of backfolding on Förster energy-transfer rates. *J. Phys. Chem. B*, 108:8218–8225, 2004.

[78] M. J. Hwang, T. P. Stockfisch, and A. T. Hagler. Derivation of class II force fields. 2. Derivation and characterization of a class II force field, CFF93, for the alkyl functional group and alkane molecules. *J. Am. Chem. Soc.*, 116:2515–2525, 1994.

[79] H. Sun. Ab initio calculations and force field development for computer simulation of polysilanes. *Macromolecules*, 28:701–712, 1995.

[80] D. Seyferth, D. Y. Son, A. L. Rheingold, and R. L. Ostrander. Synthesis of an organosilicon dendrimer containing 324 Si-H bonds. *Organometallics*, 13:2682–2690, 1994.

[81] A. W. Bosman, M. J. Bruining, H. Kooijman, A. L. Spek, R. A. J. Janssen, and E. W. Meijer. Concerning the localization of end groups in dendrimers. *J. Am. Chem. Soc.*, 120:8547–8548, 1998.

[82] R. Moors and F. Vögtle. *Cascade molecules: building blocks, multiple functionalization, complexing units, photoswitches in Advances in dendritic macromolecules*, pages 41–71. JAI, Greenwich, Conn., 1995.

[83] H. Suzuki, Y. Kimata, S. Satoh, and A. Kuriyama. Polysilane dendrimer. synthesis and characterization of $[2,2-(Me_3Si)_2Si_3Me_5]_3SiMe$. *Chem. Lett.*, 24:293–294, 1995.

[84] P.-A. Jaffres and R. E. Morris. Synthesis of highly functionalised dendrimers based on polyhedral silsesquioxane cores. *J. Chem. Soc., Dalton Trans.*, 16:2767–2770, 1998.

[85] M. Chai, Z. Pi, C. Tessier, and P. L. Rinaldi. Preparation of carbosilane dendrimers and their characterization using $^{1}H/^{13}C/^{29}Si$ triple resonance 3D NMR methods. *J. Am. Chem. Soc.*, 121:273–279, 1999.

[86] M. Chai, Y. Niu, W. J. Youngs, and P. L. Rinaldi. Structure and conformation of DAB dendrimers in solution via multidimensional NMR techniques. *J. Am. Chem. Soc.*, 123:4670–4678, 2001.

[87] D. Banerjee, M. A. C. Broeren, M. H. P. van Genderen, E. W. Meijer, and P. L. Rinaldi. An NMR study of the supramolecular chemistry of modified poly(propyleneimine) dendrimers. *Macromolecules*, 37:8313–8318, 2004.

[88] B. J. Bauer, R. M. Briber, B. Hammounda, and D. A. Tomalia. *ACS PMSE Proc.*, 67:340, 1992.

[89] T. J. Prosa, B. J. Bauer, E. J. Amis, D. A. Tomalia, and R. Scherrenberg. A SAXS study of the internal structure of dendritic polymer systems. *J. Polym. Sci., Part B: Polym. Phys.*, 35:2913, 1997.

[90] A. Ramzi, R. Scherrenberg, J. Brackman, J. Joosten, and K. Mortensen. Intermolecular interactions between dendrimer molecules in solution studied by small-angle neutron scattering. *Macromolecules*, 31:1621–1626, 1998.

[91] A. Ramzi, B. J. Bauer, R. Scherrenberg, P. Froehling, J. Joosten, and E. J. Amis. Fatty acid modified dendrimers in bulk and solution: single-chain neutron scattering from dendrimer core and fatty acide shell. *Macromolecules*, 32:4983–4988, 1999.

[92] D. Pötschke, M. Ballauff, P. Linder, M. Fischer, and F. Vögtle. Analysis of the structure of dendrimers in solution by small-angle neutron scatttering including contrast variation. *Macromolecules*, 32:4079–4087, 1999.

[93] D. Pötschke, M. Ballauff, P. Linder, M. Fischer, and F. Vögtle. The structure of dendritic molecules in solution as investigated by small-angle neutron scattering. *Macromol. Chem. Phys.*, 201:330–339, 2000.

[94] C. N. Likos, M. Schmidt, H. Löwen, M. Ballauff, D. Pöschke, and P. Linder. Soft interactions between dissolved and flexible dendrimers: theory and experiment. *Macromolecules*, 34:2914–2920, 2001.

[95] M. Ballauff. Structure of dendrimers in dilute solution. *Top. Curr. Chem.*, 212:177–194, 2001.

[96] A. Topp, B. J. Bauer, J. W. Klimash, R. Spindler, D. A. Tomalia, and E. J. Amis. Probing the location of the terminal groups of dendrimers in dilute solution. *Macromolecules*, 32:7226–7231, 1999.

[97] A. Topp, B. J. Bauer, D. A. Tomalia, and E. J. Amis. Effect of solvent quality on the molecular dimensions of PAMAM dendrimers. *Macromolecules*, 32:7232–7237, 1999.

[98] A. Topp, B. J. Bauer, T. J. Prosa, R. Scherrenberg, and E. J. Amis. Size change of dendrimers in concentrated solution. *Macromolecules*, 32:8923–8931, 1999.

[99] K. Funayama and T. Imae. Structural analysis of spheircal water-soluble dendrimer by SANS. *J. Phys. Chem. Solids*, 60:1355–1357, 1999.

[100] A. D. Meltzer, D. A. Tirrell, A. A. Jones, P. T. Inglefield, D. M. Hedstrand, and D. A. Tomalia. Chain dynamics in poly(amido amine) dendrimers. A study of ^{13}C NMR relaxation parameters. *Macromolecules*, 25:4541–4548, 1992.

[101] A. D. Meltzer, D. A. Tirrell, A. A. Jones, P. T. Inglefield, D. M. Hedstrand, and D. A. Tomalia. Chain dynamics in poly(amido amine) dendrimers. a study of ^{2}H NMR relaxation parameters. *Macromolecules*, 25:4549–4552, 1992.

[102] C. B. Gorman, M. W. Hager, B. L. Parkhurst, and J. C. Smith. Use of a paramagnetic core to affect longitudinal nuclear relaxation in dendrimers - a tool for probing dendrimer conformation. *Macromolecules*, 31:815–822, 1998.

[103] Y. Pan and W. T. Ford. Dendrimers with both hydrophilic and hydrophobic chain at every end. *Macromolecules*, 32:5468–5470, 1999.

[104] J. W. Lee, Y. H. Ko, S.-H. Park, K. Yamaguchi, and K. Kim. Novel pseudorotaxane-terminated dendrimers: Supramolecular modification of dendrimer periphery. *Angew. Chem. Int. Ed.*, 40(4):746–748, 2001.

[105] W. E. Baille, C. Malveau, X. X. Zhu, Y. H. Kim, and W. T. Ford. Self-diffusion of hydrophilic poly(propyleneimine) dendrimers in poly(vinyl alcohol) solutions and gels by pulsed field gradient NMR spectroscopy. *Macromolecules*, 36:839–847, 2003.

[106] Y. Tomoyose, D.-L. Jiang, R.-H. Jin, T. Aida, T. Yamashita, and K. Horie. Aryl ether dendrimers with an interior metalloporphyrin functionality as a spectroscopic probe: interpenetrating interaction with dendritic imidazoles. *Macromolecules*, 29:5236–5238, 1996.

[107] D.-L. Jiang and T. Aida. Morphology-dependent photochemical events in aryl ether dendrimer porphyrins: cooperation of dendron subunits for singlet energy transduction. *J. Am. Chem. Soc.*, 120:10895–10901, 1998.

[108] K. L. Wooley, C. A. Klug, K. Tasaki, and J. Schaefer. Shapes of dendrimers from rotational-echo double-resonance NMR. *J. Am. Chem. Soc.*, 119:53–58, 1997.

[109] H.-M. Kao, A. D. Stefanescu, K. L. Wooley, and J. Scheafer. Location of terminal groups of dendrimers in the solid state by rotational-echo double-resonance NMR. *Macromolecules*, 33:6214–6216, 2000.

[110] J. D. Epperson, L.-J. Ming, G. R. Baker, and G. R. Newkome. Paramagnetic cobalt(II) as an NMR probe of dendrimer structure: Mobility and cooperativity of dendritic arms. *J. Am. Chem. Soc.*, 123:8583–8592, 2001.

[111] G. R. Newkome, J. K. Young, G. R. Baker, R. L. Potter, L. Audoly, D. Cooper, and C. D. Weis. Cascade polymers. pH dependence of hydrodynamic radii of acid terminated dendrimers. *Macromolecules*, 26:2394–2396, 1993.

[112] J. K. Young, G. R. Baker, and G. R. Newkome. "Smart" cascade polymers. modular synthesis of four-directional dendritic macromolecules with acidic neutral or basic terminal groups and the effect of pH changes on their hydrodynamic radii. *Macromolecules*, 27:3464–3471, 1994.

[113] H. Ihre, A. Hult, and E. Söderlind. Synthesis, characterization, and ^{1}H NMR self-diffusion studies of dendritic aliphatic polyesters based on 2,2-bis(hydroxymethyl)propionic acid and 1,1,1-tris(hydroxyphenyl)ethane. *J. Am. Chem. Soc.*, 118:6388–6395, 1996.

[114] I. B. Rietveld and D. Bedeaux. Self-diffusion of poly(propylene imine) dendrimers in methanol. *Macromolecules*, 33:7912–7917, 2000.

[115] S. Wong, D. Appelhans, B. Voit, and U. Scheler. Effect of branching on the scaling behaviour of poly(ether amide) dendrons and dendrimers. *Macromolecules*, 34:678–680, 2001.

[116] C. J. Hawker, P. J. Farrington, M. E. Mackay, K. L. Wooley, and J. M. J. Fréchet. Molecular ball bearings : the unsual melt viscosity behavior of dendritic macromolecules. *J. Am. Chem. Soc.*, 117:4409, 1995.

[117] P. R. Dvornic. A decade of rheology : what have we learned? *ACS PMSE Proc.*, 84:84–85, 2001.

[118] M. Jeong, M. E. Mackay, and R. Vesterberg C. J. Hawker. Intrinsic viscosity variation in different solvents for dendrimers and their hybrid copolymers with linear polymers. *Macromolecules*, 34:4927–4936, 2001.

[119] L. J. Hobson and W. J. Feast. Dendritic solution viscosity behaviour in core terminated hyperbranched poly(amidoamine)s. *Chem. Commum.*, 21:2067–2068, 1997.

[120] T. H. Mourey, S. R. Turner, M. Rubenstein, J. M. J. Fréchet, C. J. Hawker, and K. L. Wooley. Unique behaviour of dendritic macromolecules: Intrinsic viscosity of polyether dendrimers. *Macromolecules*, 25:2401, 1992.

[121] B. M. Tande, N. J. Wagner, M. E. Mackay, C. J. Hawker, and M. Jeong. Viscosimetric, hydrodynamic, and conformational properties of dendrimers and dendrons. *Macromolecules*, 34:8580–8585, 2001.

[122] M. E. Mackay, G. Camezini, B. B. Sauer, W. G. Kampert, E. Malmström, and J. Englund. Surface properties of dendritic polymers. *ACS PMSE Proc.*, 84:86–87, 2001.

[123] I. B. Rietveld and J. A. M. Smit. Colligative and viscosity properties of poly(propylene imine) dendrimers in methanol. *Macromolecules*, 32:4608–4614, 1999.

[124] M. S. Matos, J. Hofkens, W. Verheijen, F. C. De Schryver, S. Hechet, K. W. Pollak, J. M. J. Fréchet, B. Forier, and W. Dehaen. Effect of core structures on photophysical and hydrodynamic properties of porphyrin dendrimers. *Macromolecules*, 33:2967–2973, 2000.

[125] G. Evmenenko, B.J. Bauer, N. Mischenko, B. Forier, and W. Dehaen. SANS study of poly(benzyl ether) dendrimers. *Physica B*, 276-278:349–350, 2000.

[126] M. L. Mansfield. Monte Carlo studies of dendrimers. Additional results for the diamond lattice model. *Macromolecules*, 33:8043–8049, 2000.

[127] J. Helfrich and R. Hentschke. Molecular Dynamics simulation of macromolecular interactions in solution: poly(γ-benzyl glutamate) in dimethylformamide and tetrahydrofuran. *Macromolecules*, 28:3831–3841, 1995.

[128] A. R. Leach. *Molecular modelling principles and applications.* Addison Wesley Longman Limited, Edinburgh Gate, Harlow, 1996.

[129] W. R. P. Scott, P. H. Hunenberger, I. G. Tironi, A. E. Mark, S. R. Billeter, J. Fennen, A. E. Torda, T. Huber, P. Kruger, and W. F. van Gunsteren. The GROMOS biomolecular simulation program package. *J. Phys. Chem. A.*, 103:3596–3607, 2001.

[130] S. J. Weiner, P. A. Kollman, D. A. Case, U. C. Singh, C. Ghio, G. Alagona, S. Profeta, and P. Weiner. A new force field for molecular mechanical simulation of nucleic acids and proteins. *J. Am. Chem. Soc.*, 106:765–784, 1984.

[131] W. Smith and T. R. Forester. DL_POLY 2.0 A general purpose parallel Molecular Dynamics package. *J. Mol. Graphics*, 14:136–151, 1996.

[132] L. Kalé, R. Skeel, M. Bhandarkar, R. Brunner, A. Gursoy, N. Krawetz, J. Phillips, A. Shinozaki, K. Varadarajan, and K. Schulten. NAMD2: Greater scalability for parallel Molecular Dynamics. *J. Comp. Phys.*, 151:283–312, 1999.

[133] B. R. Brooks, R. E. Bruccoleri, B. D. Olafson, D. J. States, S. Swaminathan, and M. Karplus. CHARMM: A program for macromolecular energy, minimization, and dynamics calculations. *J. Comput. Chem.*, 4(2):187–217, 1983.

[134] M. P. Allen and D. J. Tildesley. *Computational simulations of liquids.* Claredon Press, Oxford, 1987.

[135] J. M. Haile. *Molecular Dynamics simulation: elementary methods.* John Wiley & Sons, Inc., New York, 1992.

[136] L. Verlet. Computer experiments on classical fluids. I. Thermodynamical properties of Lennard-Jones molecules. *Phys. Rev.*, 159:98–103, 1967.

[137] R. W. Hockney. *The potential calculation and some applications*, volume 9, pages 136–211. 1970.

[138] W. C. Swope, H. C. Anderson, P. H. Berens, and K. R. Wilson. A computer simulation method for the calculation of equilibrium constants of formation of physical clusters: application to small water clusters. *J. Chem. Phys.*, 76:637–649, 1982.

[139] D. Beeman. Some multistep methods for use in Molecular Dynamics calculations. *J. Comp. Phys.*, 20:130–139, 1976.

[140] C. W. Gear. *Numerical initial value problems in ordinary differential equations*, chapter 9. Prentice-Hall, Englewood Cliffs, NJ, 1971.

[141] S. Nosé. A Molecular Dynamics method for simulations in the canonical ensemble. *Mol. Phys.*, 53:255–268, 1984.

[142] W. G. Hoover. Canonical dynamics: equilibrium phase-space distributions. *Phys. Rev. A: At. Mol. Opt. Phys.*, 31:1695–1697, 1985.

[143] J. P. Ryckaert, G. Cicotti, and H. J. C. Berendsen. Numerical integration of the Cartesian equations of motion of a system with constaints: Molecular Dynamics of n-alkanes. *J. Comp. Phys.*, 23:327–341, 1977.

[144] R. Car and M. Parrinello. Unified approach for Molecular Dynamics and Density-Functional Theory. *Phys. Rev. Lett.*, 55:2471–2474, 1985.

[145] C. J. Mundy, J. Hutter, and M. Parrinello. Microsolvation and chemical reactivity of sodium and water clusters. *J. Am. Chem. Soc.*, 122:4837–4838, 2000.

[146] N. L. Allinger, Y. H. Yuh, and J.-H. Lii. Molecular mechanics: The MM3 force field for hydrocarbons I. *J. Am. Chem. Soc.*, 111:8551–8556, 1989.

[147] A. T. Hagler, E. Huler, and S. Lifson. Energy functions for peptides and proteins. Derivation of a consistent force-field including hydrogen bond for amide crystals. *J. Am. Chem. Soc.*, 96:5316–5327, 1974.

[148] H. J. C. Berendsen, J. P. M. Postma, W. F. van Gunsteren, and J. Hermans. *Intermolecular Forces*, chapter Interaction models for water in relation to proteins hydration, pages 331–342. Reidel, Dordrecht, 1981.

[149] H. J. C. Berendsen, J. R. Grigera, and T. P. Straatsma. The missing term in effective pair potentials. *J. Phys. Chem.*, 91:6269–6271, 1987.

[150] W. L. Jorgensen, J. Chandrasekhar, J. D. Madura, R. W. Limpey, and M. L. Klein. Comparison of simple potential functions for simulations of liquid water. *J. Chem. Phys*, 79:926–935, 1983.

[151] W. L. Jorgensen and J. D. Madura. Temperature and size dependence for Monte Carlo simulations in TIP4P water. *Mol. Phys.*, 56:1381–1392, 1985.

[152] M. W. Mahoney and W. L. Jorgensen. A five-site model for liquid water and the reproduction of the density anomaly by rigid, nonpolarizable potential functions. *J. Chem. Phys.*, 112(20):8910–8922, 2000.

[153] M. W. Mahoney and W. L. Jorgensen. Diffusion constant of the TIP5P model of liquid water. *J. Chem. Phys.*, 114(1):363–366, 2001.

[154] J.J. Nicolas, K. E. Gubbins, W. B. Streett, and D. J. Tildesley. Equation of state for the Lennard-Jones fluid. *Mol. Phys.*, 37:1429–1454, 1979.

[155] P. H. Hünenberger and W. F. van Gunsteren. Alternative schemes for the inclusion of a reaction-field correction into Molecular Dynamics simulations: Influence on the simulated energetic, structural, and dielectric properties of liquid water. *J. Chem. Phys.*, 108(15):6117–6134, 1998.

[156] P. Ewald. Due berechnung optischer und elektrostatischer gitterpotentiale. *Ann. Phys.*, 64:253–287, 1921.

[157] H. L. Friedman. Image approximation to the reaction field. *Mol. Phys.*, 29:1533–1543, 1975.

[158] H.-Q. Ding, N. Karasawa, and W. A. Goddard III. Atomic level simulations on a million particles: the cell multipole method for Coulomb and London nonbonding interactions. *J. Chem. Phys.*, 97:4309–4315, 1992.

[159] H.-Q. Ding, N. Karasawa, and W. A. Goddard III. The reduced cell multipole method for Coulomb interactions in periodic systems with million-atom unit cells. *Chem. Phys. Let.*, 196:6–10, 1992.

[160] L. Greengard and V. I. Roklin. A fast algorithm for particle simulations. *J. Comp. Phys.*, 73:325–348, 1987.

[161] H. C. Andersen. Molecular Dynamics simulations at constant pressure and/or temperature. *J. Chem. Phys.*, 72(4):2384–2393, 1980.

[162] G.A. Patey and J. P. Valleau. A Monte Carlo method for obtaining the interionic potential of mean force in ionic solution. *J. Chem. Phys.*, 63:2334–2339, 1975.

[163] G. M. Torrie and J. P. Valleau. Non-physical sampling distributions in Monte Carlo free-energy estimation: umbrella sampling. *J. Comp. Phys.*, 23:187–199, 1977.

[164] M. Mezei. Adaptive umbrella sampling: self-consistent determination of the non-Boltzmann bias. *J. Comp. Phys.*, 68:237–248, 1987.

[165] G. H. Paine and H. A. Scheraga. Prediction of the native conformation of a polypeptide by a statistical-mechanical procedure. I. Backbone structure of enkephalin. *Biopolymers*, 24:1391–1436, 1985.

[166] M. Kuttel, J. W. Brady, and K. J. Naidoo. Carbohydrate solution simulations: producing a force field with experimentally-consistent hydroxyl rotational frequencies and populations. *J. Comput. Chem.*, 23(13):1236–1243, 2002.

[167] C. Bartel and M. Karplus. Probability distributions for complex systems: adaptive umbrella sampling of the potential energy. *J. Phys. Chem.*, 102:865–880, 1998.

[168] C. Bartel and M. Karplus. Multidimensional adaptive umbrella sampling: applications to main-chain and side-chain peptide conformations. *J. Comput. Chem.*, 18:1450–1462, 1997.

[169] A. Guinier and G. Fournet. *Small Angle scattering of X-rays.* Wiley, New York, 1955.

[170] F. Mallamace, E. Canetta, D. Lombardo, A. Mazzaglia, A. Romeo, L. Monsù Scolaro, and G. Maino. Scaling properties in the internal structure of dendrimer systems. *Physica A*, 304:235–243, 2002.

[171] J. Foote and A. Raman. A relation between the principal axes of inertia and ligand binding. *Proc. Natl. Acad. Sci. USA*, 97(3):978–983, 2000.

[172] Q. Liu and J. W. Brady. Anisotropic solvent structuring in aqueous sugar solutions. *J. Am. Chem. Soc*, 118:12276–12286, 1996.

[173] L. Laaksonen. A graphics program for the analysis and display of Molecular Dynamics trajectories. *J. Mol. Graph.*, 10:33–34, 1992.

[174] D. L. Bergman, L. Laaksonen, and A. Laaksonen. Visualization of solvation structures in liquid mixtures. *J. Mol. Graph. Model.*, 15:301–306, 1997.

[175] R. B. Best, G. E. Jackson, and K. J. Naidoo. Modelling the $\alpha(1-6)$ branch point of amylopectin in solution. *J. Phys. Chem. B*, 106:5091–5098, 2002.

[176] P. Jedlovszky. The local structure of various hydrogen bonded liquids: Voronoi polyhedra analysis of water, methanol and HF. *J. Chem. Phys.*, 113(20):9113–9121, 2000.

[177] L. Zaninetti. The Vornoi tessellation generated from different distributions of seeds. *Phys. Lett. A.*, 165:143–147, 1992.

[178] R. W. Pastor. Time correlation functions. In P. von Ragué Schleyer, P. R. Schreiner, N. L. Allinger, T. Clark, J. Gasteiger, P. A. Kollman, and H. F. Schaefer III, editors, *Encyclopedia of Computational Chemistry*, volume 3, pages 3003–3011. John Wiley & Son, Chichester, 1998.

[179] C. S. Johnson Jr. Diffusion ordered Nuclear Magnetic Resonance spectroscopy: principles and applications. *Prog. Nucl. Magn. Reson. Spectrosc.*, 12:203–256, 1999.

[180] M. J. Thrippleton, N. M. Loening, and J. Keeler. A fast method for the measurement of diffusion coefficients: one-dimensional DOSY. *Mag. Reson. Chem.*, 41:441–447, 2003.

[181] R. Huo, R. Wehrens, J. van Duynhoven, and L. M. C. Buydens. Assessment of techniques for DOSY NMR data processing. *Anal. Chim. Acta*, 490:231–251, 2003.

[182] H. Kovacs, J. Kowalewski, and A. Maliniak. Multinuclear relaxation and NMR self-diffusion study of the Molecular Dynamics in acetonitrile-chloroform liquid mixtures. *J. Phys. Chem.*, 93:962–969, 1989.

[183] R. J. Young and P. A. Lovell. *Introduction to Polymers.* CRC Press, Florida, 2 edition, 1991.

[184] K. A. Dill and B. H. Zimm. Dynamics of polymer solutions I. Theory for an instrument. *Macromolecules*, 13:426–432, 1980.

[185] J. Garcia de la Torre, M. L. Huertas, and B. Carrasco. Calculation of hydrodynamic properties of globular proteins from their atomic-level structure. *Biophys. J.*, 78:719–730, 2000.

[186] C. J. Hawker, K. L. Wooley, and J. M. Fréchet. Solvatochromisim as a probe of the microenvironment in dendritic polyethers: transition from an extended to a globular structure. *J. Am. Chem. Soc.*, 115:4375–4376, 1993.

[187] D.W. Van Krevelen. *Properties of Polymers.* Elsevier Science Pub Co, Amsterdam, 1990.

[188] C. S. Hsu and D. Chandler. RISM calculation of the structure of liquid chloroform. *Mol. Phys.*, 37(1):299–301, 1979.

[189] M. W. Evans. A review and computer simulation of the structure and dynamics of liquid chloroform. *J. Mol. Liq.*, 25:211–260, 1983.

[190] R. Gratias and H. Kessler. Molecular Dynamics study on microheterogeneity and preferential solvation in methanol/chloroform mixtures. *J. Phys. Chem. B*, 102:2027–2031, 1998.

[191] H. Kovacs, J. Kowalewski, and A. Laaksonen. Molecular Dynamics simulations of liquid mixtures of acetonitrile and chloroform. *J. Phys. Chem.*, 94:7378–7385, 1990.

[192] T.-M. Chang and L. X. Dang. Computer simulation of chloroform with a polarizable potential model. *J. Phys. Chem. B*, 101:3413–3419, 1997.

[193] T.-M. Chang and L. X. Dang. Ion solvation in polarizable chloroform: a molecular dynamics study. *J. Phys. Chem.*, 101:10518–10526, 1997.

[194] W. Dietz and K. Heinzinger. A Molecular Dynamics study of liquid chloroform. *Ber. Bunzenges. Phys. Chem.*, 89:968–977, 1985.

[195] H. J. Böhm and R. Ahlrichs. Molecular Dynamics simulations of liquid CH_2Cl_2 and $CHCl_3$ with new pair potentials. *Mol. Phys.*, 54(6):1261–1274, 1985.

[196] I. G. Tironi and W. F. van Gunsteren. A Molecular Dynamics simulation study of chloroform. *Mol. Phys.*, 83(2):381–403, 1994.

[197] H. Bertagnolli, K. Goller, and H. Zweier. Structure investigations of liquid chloroform by statistical-mechanical calculations and reverse Monte Carlo simulation. *Ber. Bunsenges. Phys. Chem.*, 99:1168–1178, 1995.

[198] W. L. Jorgensen, J. M. Briggs, and M. L. Contreras. Relative partition coefficients for organic solutes from fluid simulation. *J. Phys. Chem.*, 94:1683–1686, 1990.

[199] F. J. Luque, Y. Zhang, C. Alemán, M. Bachs, J. Gao, and M. Orozco. Solvent effects in chloroform solution: Parametrization of the MST/SCRF continuum model. *J. Phys. Chem.*, 100:4269–4276, 1996.

[200] H. Bertagnolli and M. D. Zeidler. Comparison of neutron scattering and Molecular Dynamics studies on liquid chloroform. *J. Mol. Liq.*, 25:277–280, 1983.

[201] S. Girard and F. Müller-Plathe. Molecular Dynamics simulations of liquid tetrahydrofuran: on the uniqueness of force fields. *Mol. Phys.*, 101(6):779–787, 2003.

[202] R. Faller, H. Schmitz, O. Biermann, and F. Müller-Plathe. Automatic parameterization of force fields for liquids by simplex optimization. *J. Comp. Chem.*, 20(10):1009–1017, 1999.

[203] S. L. Mayo, B. D. Olafson, and W. A. Goddard III. DREIDING: A generic force field for molecular simulations. *J. Phys. Chem.*, 94:8897–8909, 1990.

[204] J. MacKerell, A. D. Bashford, M. Bellott, R. L. Dunbrack Jr., J. D. Evanseck, M. J. Field, S. Fischer, J. Gao, H. Guo, S. Ha, D. Joseph-McCarthy, L. Kuchnir, k. Kuczera, F. T. K. Lau, C. Mattos, S. Michnick, T. Ngo, D. T. Nguyen, B. Prodhom, I. Reiher, W. E. B. Roux, M. Schlenkrich, J. C. Smith, R. Stote, J. Straub, M. Watanabe, J. Wiorkiewicz-Kuczera, D. Yin, and M. Karplus. All-atom empirical potential for molecular modeling and dynamics studies of proteins. *J. Phys. Chem. B*, 102:3586–3616, 1998.

[205] P. Hobza, H. L. Selzle, and E. W. Schlag. Potential energy surface of the benzene dimer: *ab initio* theoretical study. *J. Am. Chem. Soc.*, 116:3500–3506, 1994.

[206] S. Tsuzuki, K. Honda, T. Uchimaru, M. Mikami, and K. Tanabe. The interaction of benzene with chloro- and fluoromethanes: effects of halogenation on CH/π interaction. *J. Phys. Chem. A.*, 106:4423–4428, 2002.

[207] B. V. Cheney, M. W. Schulz, J. Cheney, and W. G. Richards. Hydrogen-bonded complexes involving benzene as an h acceptor. *J. Am. Chem. Soc.*, 110:4195–4198, 1988.

[208] H. Bertagnolli, D. O. Leicht, and M. D. Zeidler. X-ray diffraction study of liquid chloroform. *Mol. Phys.*, 35(1):193–197, 1978.

[209] H. Bertagnolli, D. O. Leicht, M. D. Zeidler, and P. Chieux. A neutron-diffraction study of liquid chloroforom I. $CDCl_3$. *Mol. Phys.*, 35(1):199–203, 1978.

[210] H. Bertagnolli, D. O. Leicht, M. D. Zeidler, and P. Chieux. A neutron-diffraction study of liquid chloroforom II. $CD^{35}Cl_3$ and $CD^{37}Cl_3$. *Mol. Phys.*, 36(6):1769–1777, 1978.

[211] H. Bertagnolli and P. Chieux. A neutron diffraction study of a hydrogen containing organic liquid $CHCl_3$ as an example. *Ber. Busenges. Phys. Chem.*, 84:1225–1231, 1980.

[212] H. Bertagnolli and P. Chieux. The complete set of atom pair correlation functions of liquid chloroform as obtained from a final neutron scattering experiment with H/D isotopic substitution. *Mol. Phys.*, 51(3):617–631, 1984.

[213] A. Takahashi, Y. F. Yano, and T. Iijima. Structure of liquid chloroform as investigated by energy-dispersive X-ray diffraction. *Bull. Chem. Soc. Jpn.*, 71:2081–2086, 1998.

[214] H. S. Sandhu. Coefficient of self-diffusion in liquids using pulsed NMR techniques. *J. Magn. Res.*, 17:34–40, 1975.

[215] W. T. Huntress Jr. A Nuclear Magnetic Resonnance study of anisotropic molecular rotation in liquid chloroform and in chloroform-benzene solution. *J. Phys. Chem.*, 73(1):103–111, 1969.

[216] M. W. Evans. Molecular Dynamics simulation of liquid chloroform. *Adv. Mol. Relax. Int. Pr.*, 24:123–138, 1982.

[217] R. Venable. Personal communication. 6 January 2003.

[218] A. Idrissi. Effect of the local anisotropy on the structural and dynamic properties in liquid chloroform: a Molecular Dynamics analysis. *J. Mol. Liq.*, 107(1-3):29–39, 2003.

[219] H. J. Bender and M. D. Zeidler. Translation and anisotropic rotation difusion in liquid chloroform as studied by nmr relaxation. *Ber. Bunsenges. Phys. Chem.*, 75(141):236–242, 1971.

[220] I. Bartusseck. Personal communication. 4 June 2002.

[221] W. Dietz and K. Heinzinger. A Molecular Dynamics study of liquid chloroform. *Ber. Bunzenges. Phys. Chem.*, 88:543, 1985.

[222] D. Cremmer and J. A. Pople. General definition of ring puckering coordinates. *J. Am. Chem. Soc.*, 97:1354–1358, 1975.

[223] D. Cremmer and J. A. Pople. Molecular orbital theory of the electronic structure of organic compounds. XXIII. Pseudorotation in saturated five-membered ring compounds. *J. Am. Chem. Soc.*, 97:1358–1367, 1975.

[224] J. Chandrasekhar and W. L. Jorgensen. Monte Carlo simulations of liquid tetrahydrofuran including pseudorotation. *J. Chem. Phys.*, 77(10):5073–5079, 1982.

[225] J. M. Briggs, T. Matsui, and W. L. Jorgensen. Monte Carlo simulations of liquid alkyl ethers with the OPLS potential functions. *J. Comp. Chem.*, 11(8):958–971, 1990.

[226] W. Damm, A. Frontera, J. Tirado-Rives, and W. L. Jorgensen. OPLS all-atom force field for carbohydrates. *J. Comput. Chem.*, 18:1955–1970, 1997.

[227] A. K. Rappe, C. J. Casewit, K. S. Colwell, W. A. Goddard III, and W. M. Skiff. UFF, a full periodic table force field for molecular mechanics and Molecular Dynamics simulations. *J. Am. Chem. Soc.*, 114:10024–10035, 1992.

[228] C. L. Verlinde, C. J. De Ranter, N. M. Blaton, and O. M. Peeters. Static disorder in (-)-(1R,5R,9R,13S)-2'-hydroxy-5,9-dimethyl-2-(2-methyl-tetrahydrofurfuryl)-6,7-benzomorphan, $C_{20}H_{29}NO_2$. Crystal structure and MM2 pucker analysis of the tetrahydrofuran ring. *Acta Cryst. B*, 45:107–112, 1989.

[229] E. von Goldammer and M. D. Zeidler. Molecular motion in aqueous mixtures with organic liquids by NMR relaxation measurements. *Ber. Bunsenges. Phys. Chem.*, 73:4–15, 1969.

[230] D. J. Gisser, B. S. Johnson, M. D. Ediger, and E. D. von Meerwall. Comparison of various measurements of microscopic friction in polymer solutions. *Macromolecules*, 26:512–519, 1993.

[231] S. Pignataro and G. Disefano. n-σ mixing in pentatomic heterocyclic compounds of sixth group by photoelectron spectroscopy. *Chem. Phys. Lett.*, 26:356–360, 1974.

[232] E. Von Goldammer, H.-D Lüdemann, and O. Röder. ^{13}C spin-lattice relaxation behaviour of pyridine and tetrahydrofurane. *Chem. Phys. Lett.*, 26:387–391, 1974.

[233] M. Strajbl, V. Baumruk, and J. Florian. Scaled quantum mechanical force filds and vibrational spectra of nucleic acid constituents. 9. Tetrahydrofuran. *J. Phys. Chem. B*, 102:1314–1319, 1999.

[234] E. Gallinella, B. Cadioli, J. P. Flament, and G. Berthier. A scaled force field for tetrahydrofuran and its isotopomers from quantum mechanical calculations and infrared and Raman spectra. *J. Mol. Struct.*, 315:137–148, 1994.

[235] C. Coulombeau and H. Jobic. Contribution to the vibrational normal modes analysis of d_8 – THF by neutron inelastic scattering. *J. Mol. Struct.*, 330:127–130, 1995.

[236] T. Takamuku, A. Nakamizo, M. Tabata, K. Yoshida, T. Yamaguchi, and T. Otomo. Large-angle X-ray scattering , small-angle neutron scattering and NMR relaxation studies of mixing states of 1,4-dioxane-water, 1,3-dioxane-water and tetrahydrofuran-water mixtures. *J. Mol. Liq.*, 103-105:143–159, 2003.

[237] C. Y. Jones, S. L. Marshall, B. C. Chakoumakos, C. J. Rawn, and Y. Ishii. Structure and thermal expansivity of tetrahydrofuran deuterate determined by neutron powder diffraction. *J. Phys. Chem. B*, 107:6026–6031, 2003.

[238] B. Cadioli, E. Gallinella, C. Coulombeau, H. Jobic, and G. Berthier. Geometric structure and vibrational spectrum of tetrahydrofuran. *J. Phys. Chem.*, 97:7844–7856, 1993.

[239] J. A. Dobado, J. Molina Molina, and M. Rodriguez Espinosa. A comparative molecular mechanics, semiempirical and *ab initio* study of saturated five-member rings. *J. Mol. Struct.*, 303:205–212, 1994.

[240] W. Dradowicz. Molecular Dynamics study of the structural and dynamical properties of liquid tetrahydrofuran. *Z. Naturforsch.*, pages 1342–1344, 1990.

[241] J. P. Bareman, R. I. Reid, A. N. Hrymak, and T. A. Kavassalis. Estimation of solvent diffusion coefficients using Molecular Dynamics simulations. *Mol. Sim.*, 11:243–250, 1993.

[242] L. C. G. Frietas and J. M. M. Cordeiro. Monte Carlo simulation of water-tetrahydrofuran mixtures. *J. Mol. Struct.*, 335:189–195, 1995.

[243] J. Chandrasekhar and W. L. Jorgensen. The nature of dilute solutions of sodium ion in water, methanol, and tetrahydrofuran. *J. Chem. Phys.*, 77(10):5080–5089, 1982.

[244] S. J. Weiner, P. A. Kollman, D. T. Nguyen, and D. A. Case. An all atom force field for simulations of proteins and nucleic acids. *J. Comput. Chem.*, 7:230–252, 1986.

[245] J. Chandrasekhar and W. L. Jorgensen. Monte Carlo simulations of liquid tetrahydrofuran including pseudorotation. *J. Chem. Phys.*, 77(10):5073–5079, 1982.

[246] W. L. Jorgensen and D. L. Severance. Aromatic-aromatic interactions: free energy profiles for the benzene dimer in water, chloroform, and liquid benzene. *J. Am. Chem. Soc.*, 112:4768–4774, 1990.

[247] P. J. Flory. *Principles of Polymer Chemistry.* Cornell University Press, Ithaca, NY, 1953.

[248] S. J. Hughes. A computational and synthetic study of poly(benzyl phenyl ether) dendrimers. Master's thesis, Univesity of Cape Town, 1998.

[249] R. H.Perry and D. Green. *Perry's chemical engineers' handbook.* McGraw-Hill Book Company, Singapore, 6 edition, 1984.

[250] S. De Backer, Y. Prinzie, W. Verheijen, M. Smet, K. Desmedt, W. Dehaen, and F. C. Shryver. Solvent dependence of the hydrodynamic volume of dendrimers with a rubicene core. *J. Phys. Chem. A.*, 102:5451–5455, 1998.

[251] J. Hofkens, W. Verheijen, R. Shukla, W. Dehaen, and F. C. De Schryver. Detection of a single dendrimer macromolecule with a fluorescent dihydopyrrolopyrroledione (DPP) core embedded in a thin polystyrene polymer film. *Macromolecules*, 31:4493–4497, 1998.

[252] R-. H. Jin, T. Aida, and S. Inoue. 'caged' porphyrin: the first dendritic molecule having a core photochemical functionality. *J. Chem. Soc., Chem. Commun.*, 16:1260–1262, 1993.

[253] L. G. Schultz, Y. Zhao, and S. C. Zimmerman. Synthesis of cored dendrimers with internal cross-links. *Angew. Che. Int. Ed.*, 40(10):1962–1966, 2001.

[254] H. Brenner. Rheology of a dilute suspension of axisymmetric brownian particles. *Int. J. Multiphase Flow*, 1:195–341, 1974.

[255] D. A. Tomalia, A. M. Naylor, and W. A. Goddard III. Starburst dendrimers: molecular-level control of size, shape, surface chemistry, topology, and flexibility from atoms to macroscopic matter. *Angew. Chemie. Int. Ed. Engl.*, 29:138–175, 1990.

[256] M. A. Hearshaw, S. C. Simpson, J. McKenzie, J. R. Moss, and K. J. Naidoo. An NMR study of the Fréchet dendrimers in solution. 2005.

[257] J. D. Epperson, L.-J. Ming, B. D. Woosley, G. R. Baker, and G. R. Newkome. NMR study of dendrimer structures using paramagnetic cobalt(II) as a probe. *Inorg. Chem.*, 38:4498–4502, 1999.

[258] P. Linse. Stacked or T-shaped benzene dimer in aqueous solution? A molecular dynamic study. *J. Am. Chem. Soc.*, 114:4366–4373, 1992.

[259] P. Linse. Orientation-averaged benzene-benzene potential of mean force in aqueous solution. *J. Am. Chem. Soc.*, 115:8793–8797, 1993.

[260] J. Gao. Supercritical hydration of organic compounds. The potential of mean force for benzene dimer in supercritical water. *J. Am. Chem. Soc.*, 115:6893–6895, 1993.

[261] G. Ravishanker and D. L. Beveridge. Potential of mean force for the stacking of phenyl rings in aqueous solution. *J. Am. Chem. Soc.*, 107:2565–2566, 1985.

[262] M. Kuttel. *Simulations of Carbohydrate Conformational Dynamics and Thermodynamics.* PhD thesis, University of Cape Town, 2003.

[263] G. E. Moore. Cramming more components onto integrated circuits. *Electronics*, 38(8):114–117, 1965.

Appendix A

Auxiliary Parameterization Results

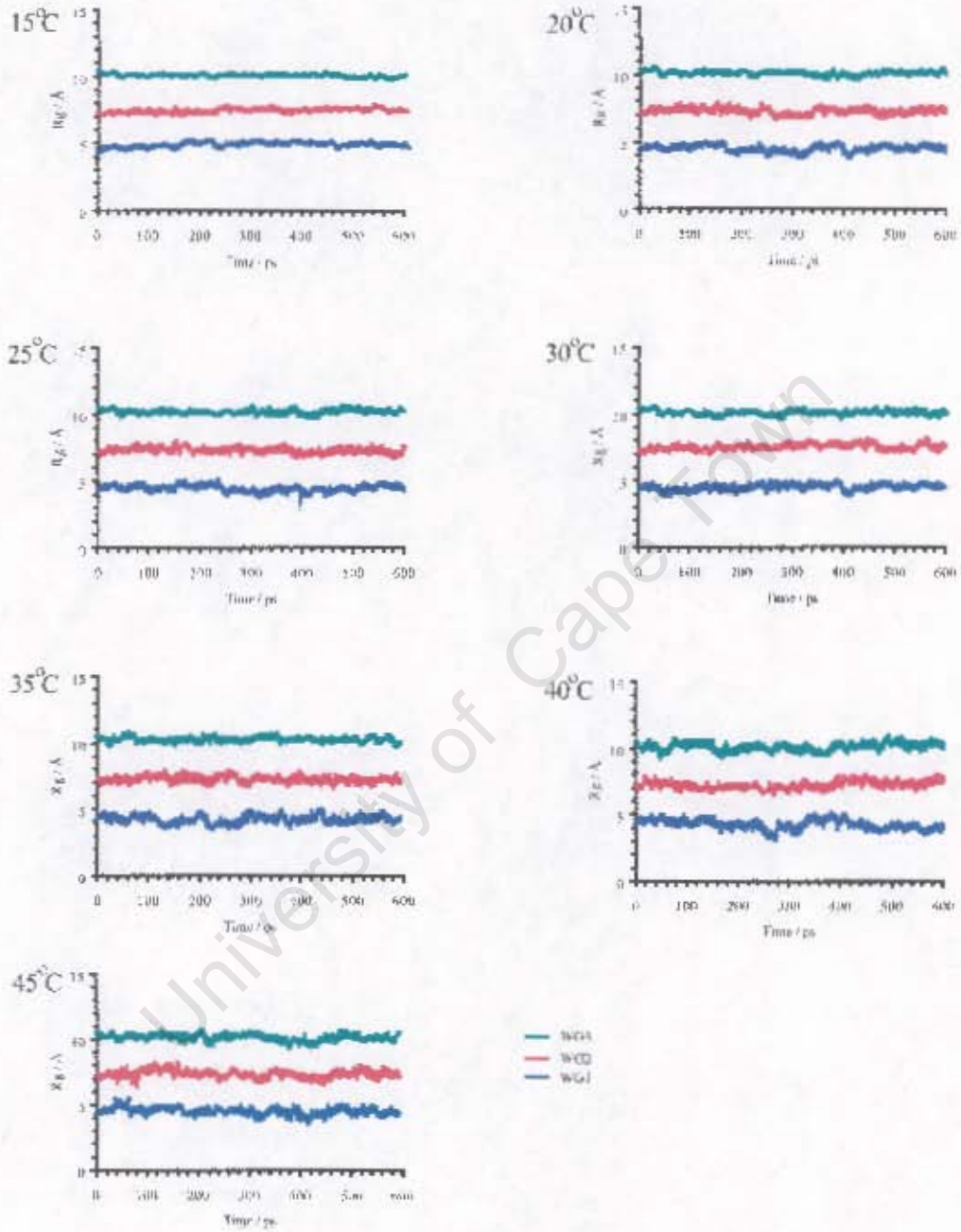

Figure A.1: Effect of the temperature on the time evolution of R_g of wedges WG1 to WG3 in chloroform.

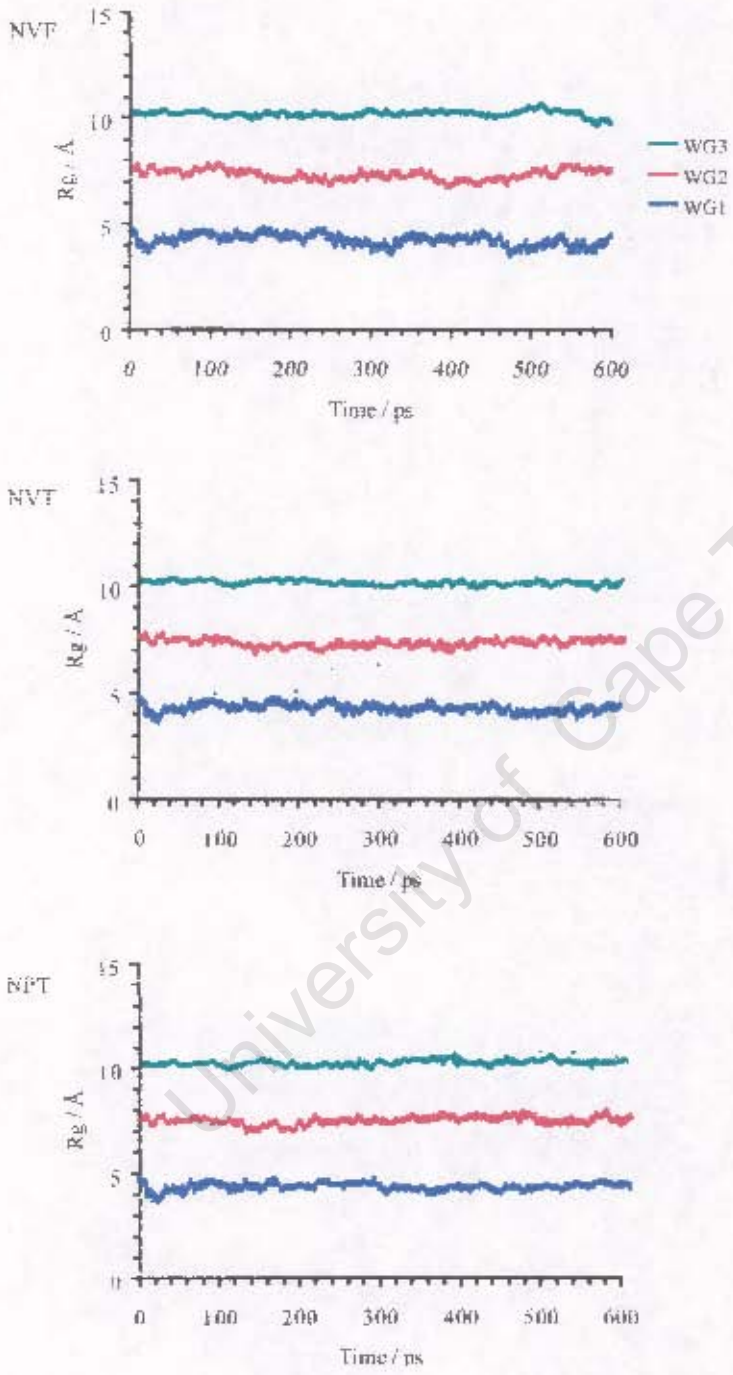

Figure A.2: Effect of the ensemble sampled during the MD simulation on the time evolution of R_g of wedges WG1 to WG3 in chloroform

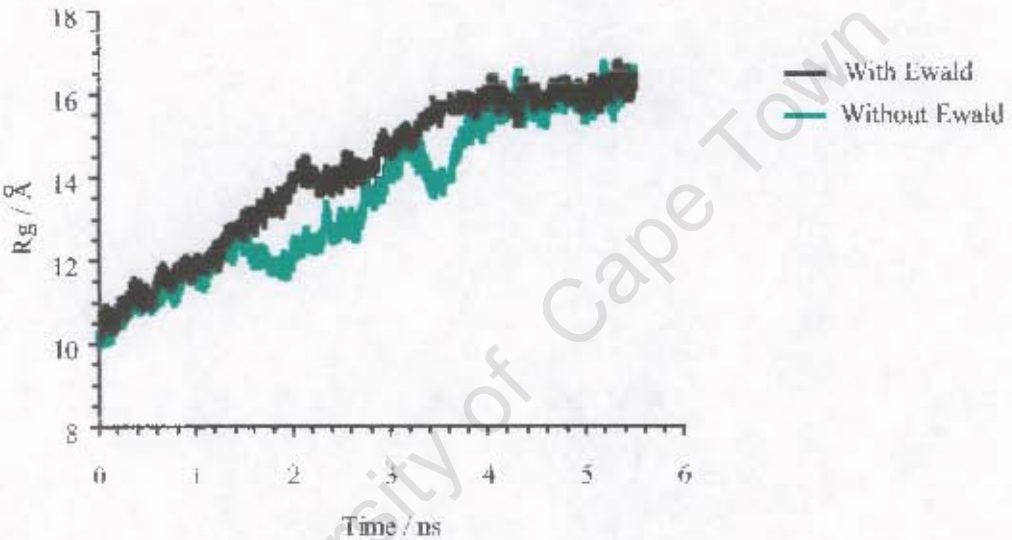

Figure A.3: A comparison between the time evolution of dendrimer G3 unfolding in chloroform with and without Ewald summations employed.

Appendix B

Auxiliary Radial distribution profiles

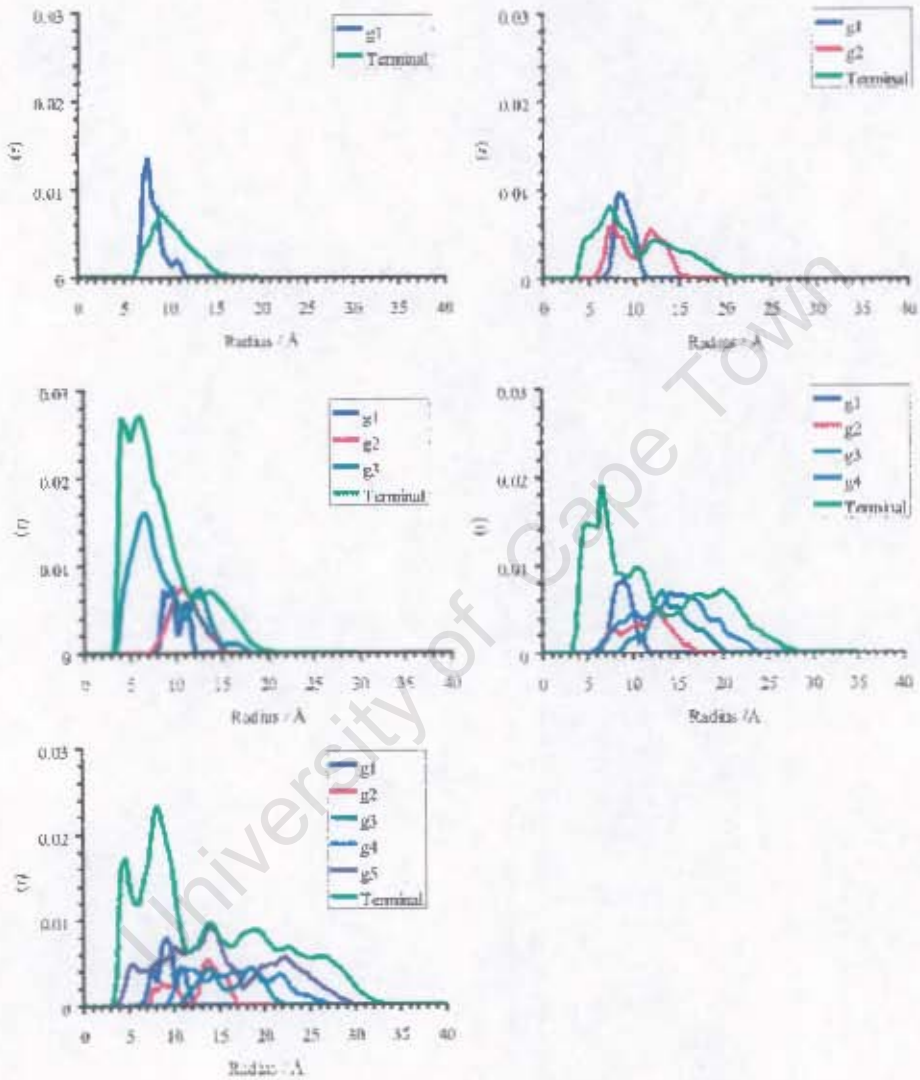

Figure B.1: $p_i(r)$ of the topological layers of dendrimers G1 to G5 in vacuum.

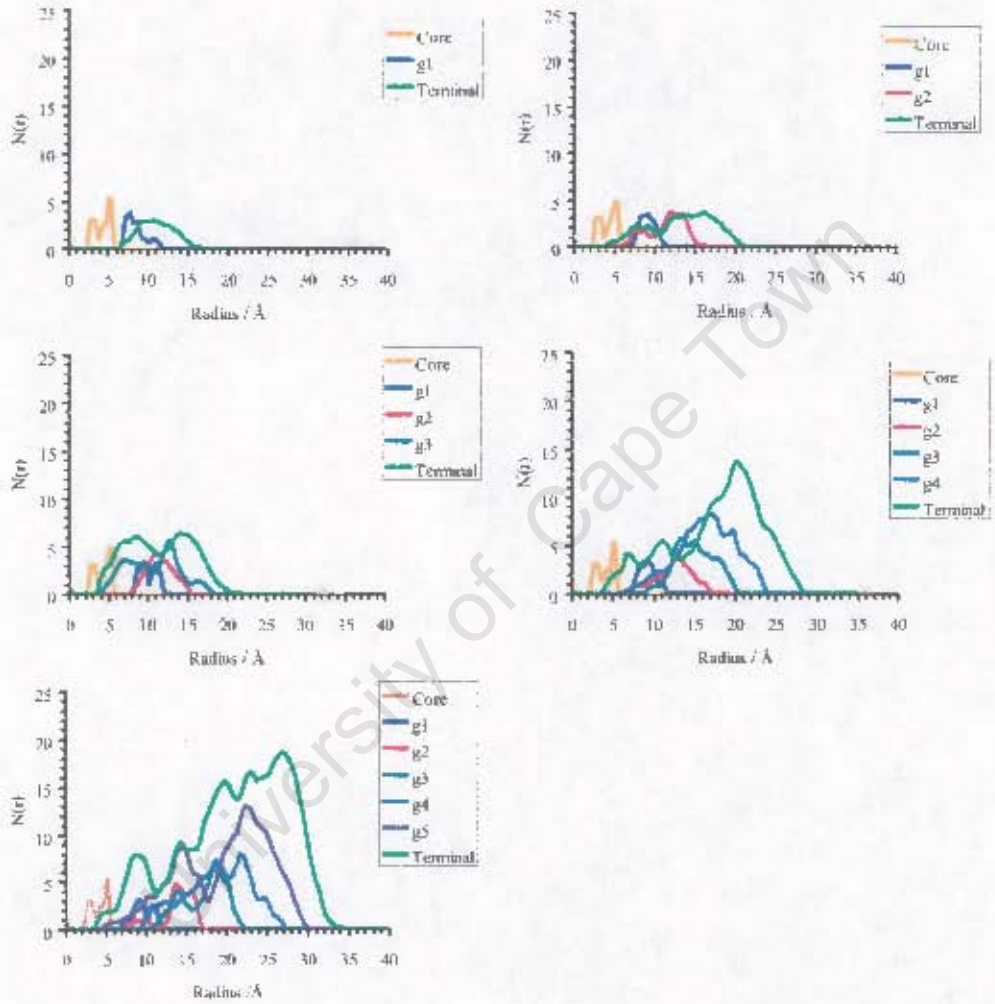

Figure B.2: $N_T(r)$ of the topological layers of dendrimers G1 to G5 in vacuum.

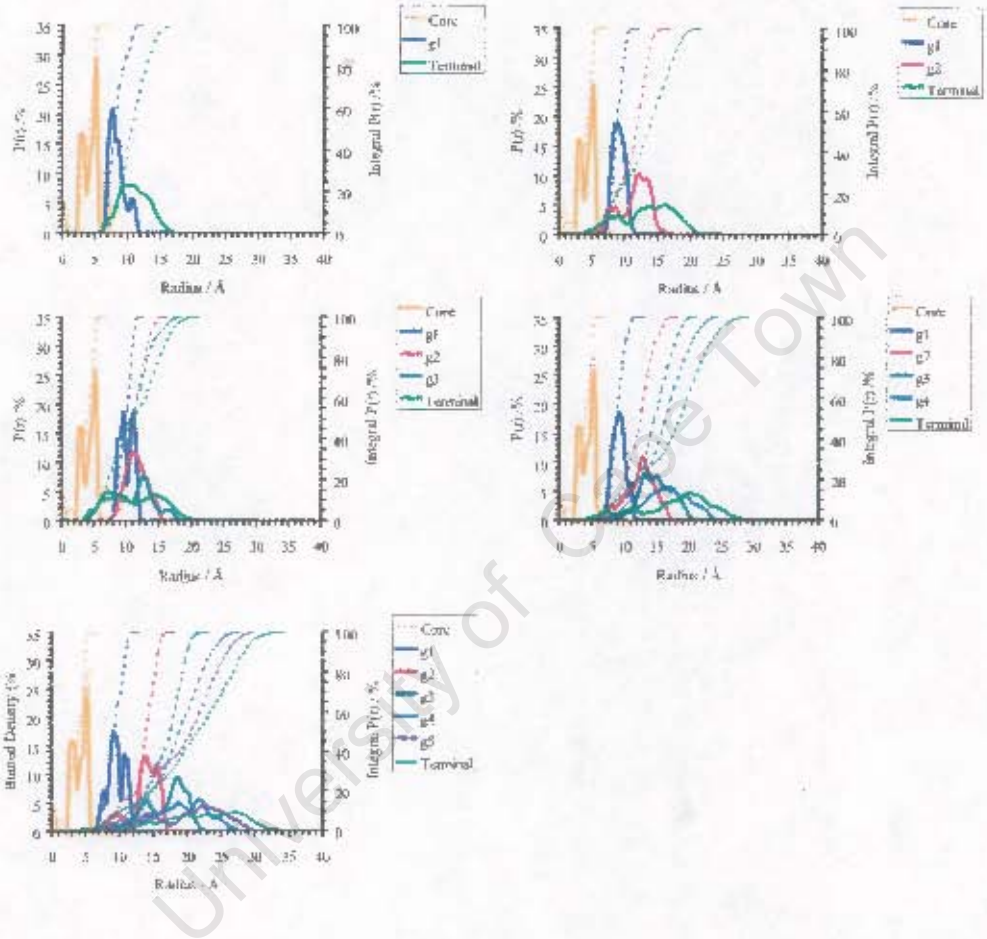

Figure B.3: $P_i(r)$ each layer of dendrimers G1 to G5 in vacuum. This includes the integration of these distributions showing their accumulation within the dendrimer as one progresses to its periphery.

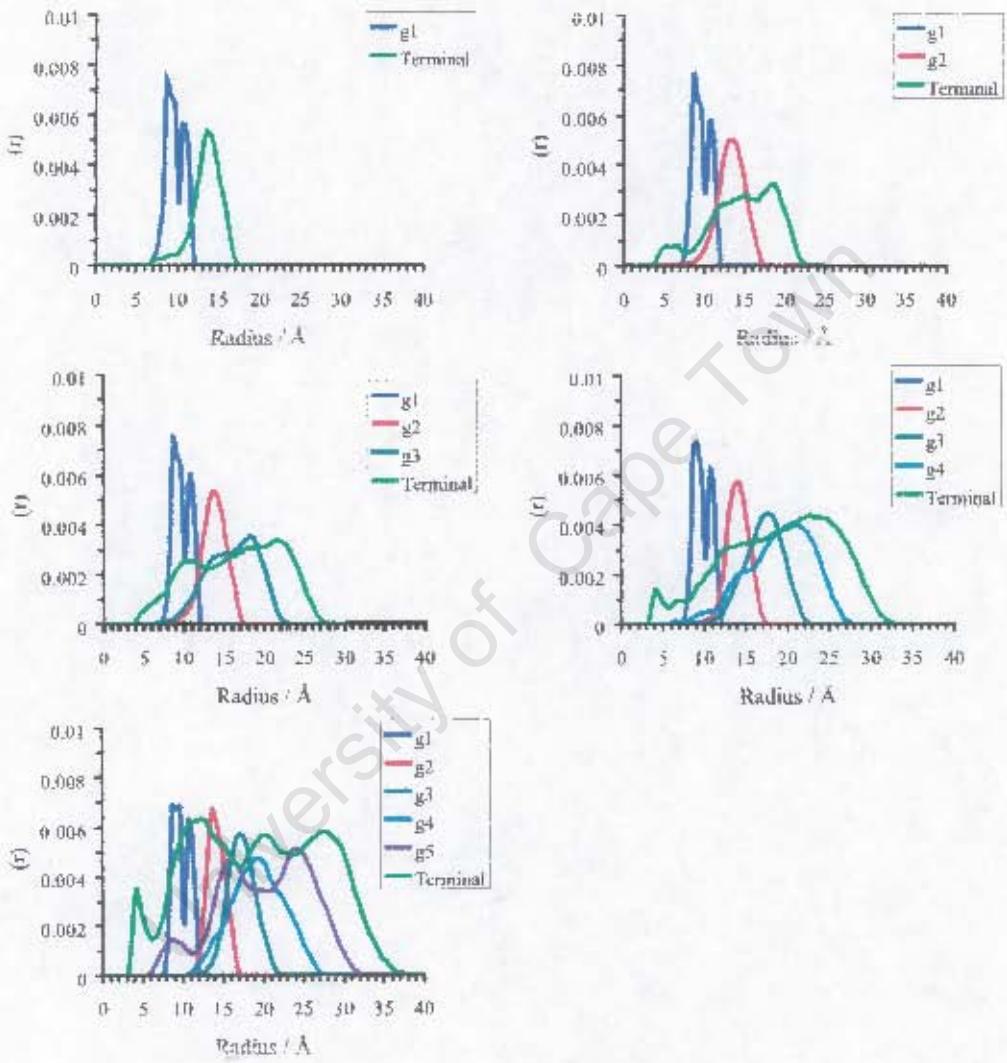

Figure B.4: $\rho_t(r)$ of the topological layers of dendrimers G1 to G5 in chloroform.

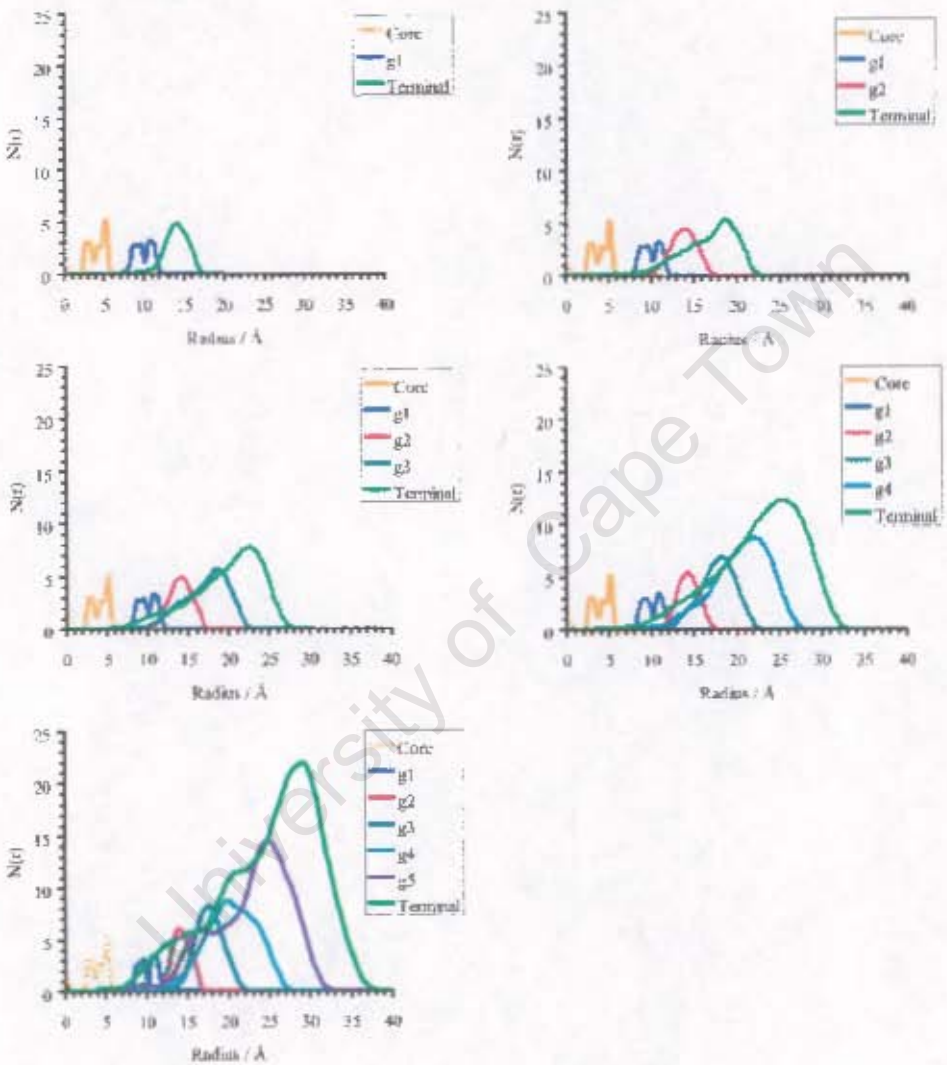

Figure B.5: $N_l(r)$ of the topological layers of dendrimers G1 to G5 in chloroform.

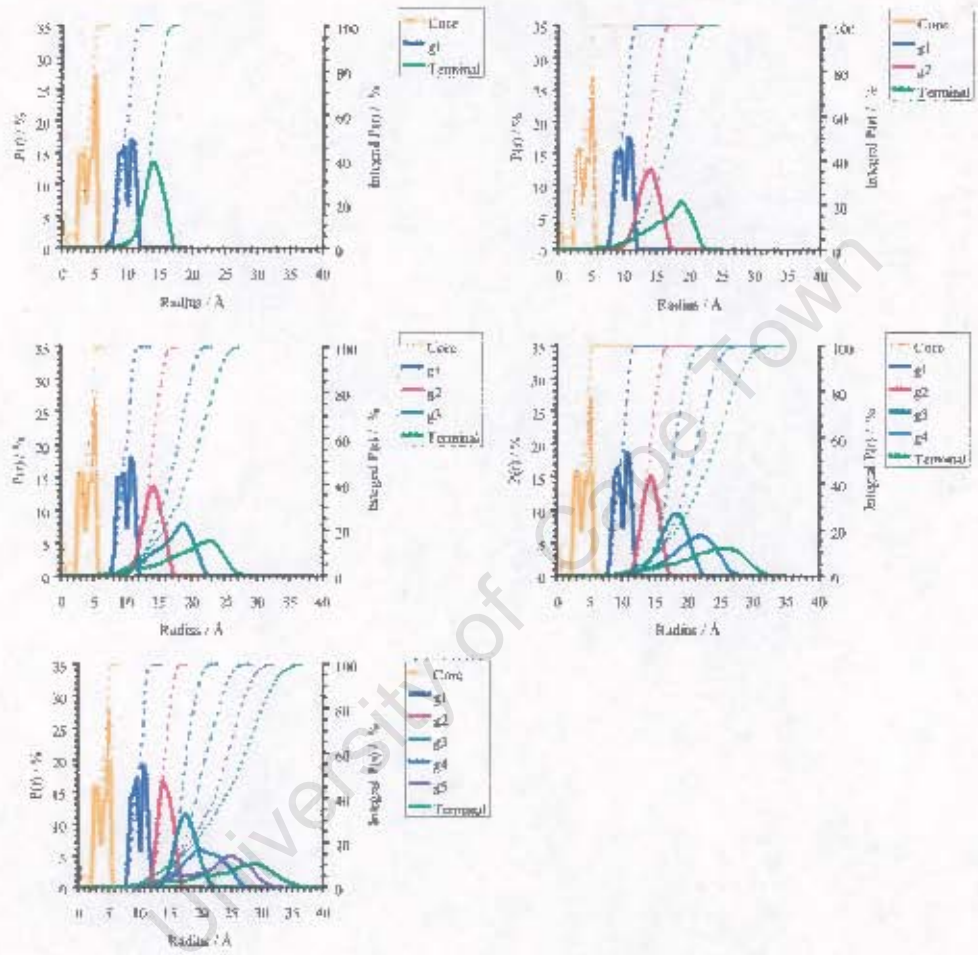

Figure B.6: $P_i(r)$ of each layer of dendrimers G1 to G5 in chloroform. This includes the integration of these distributions showing their accumulation within the dendrimer as one progresses to its periphery.

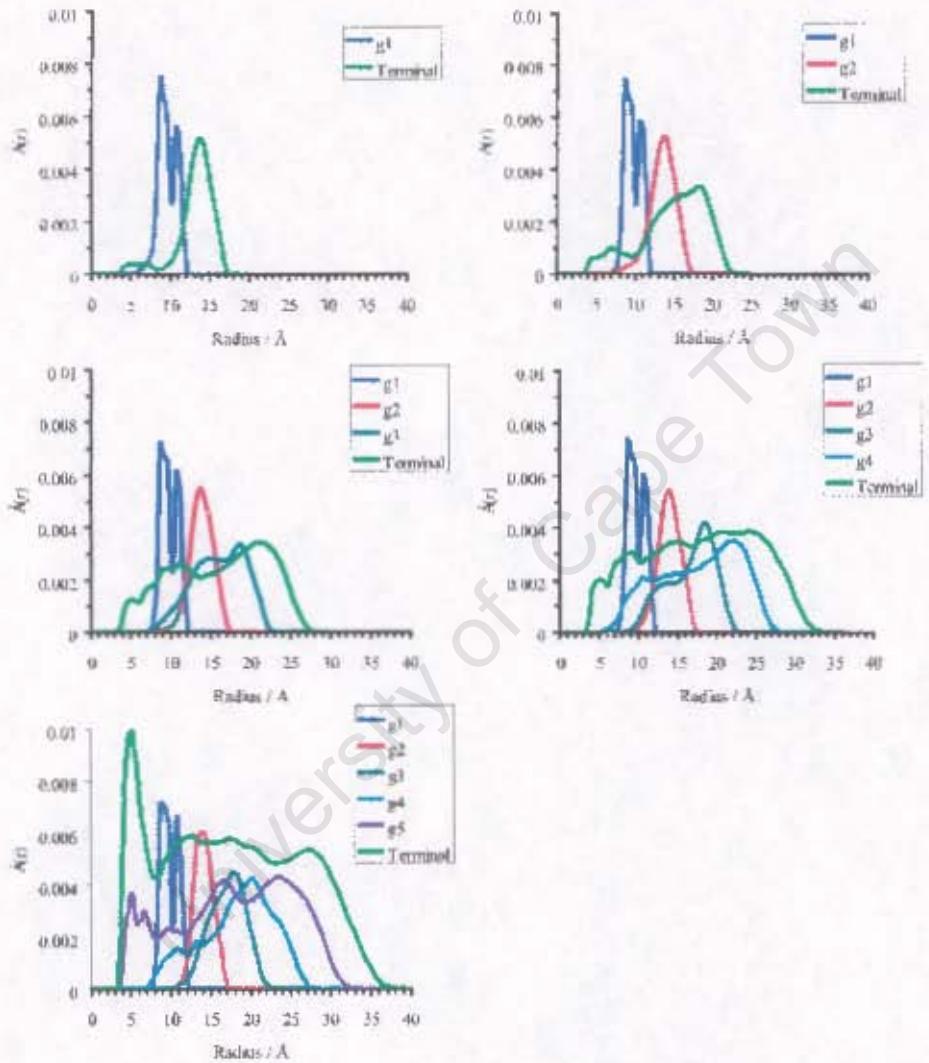

Figure B.7: $p_l(r)$ of the topological layers of dendrimers G1 to G5 in THF.

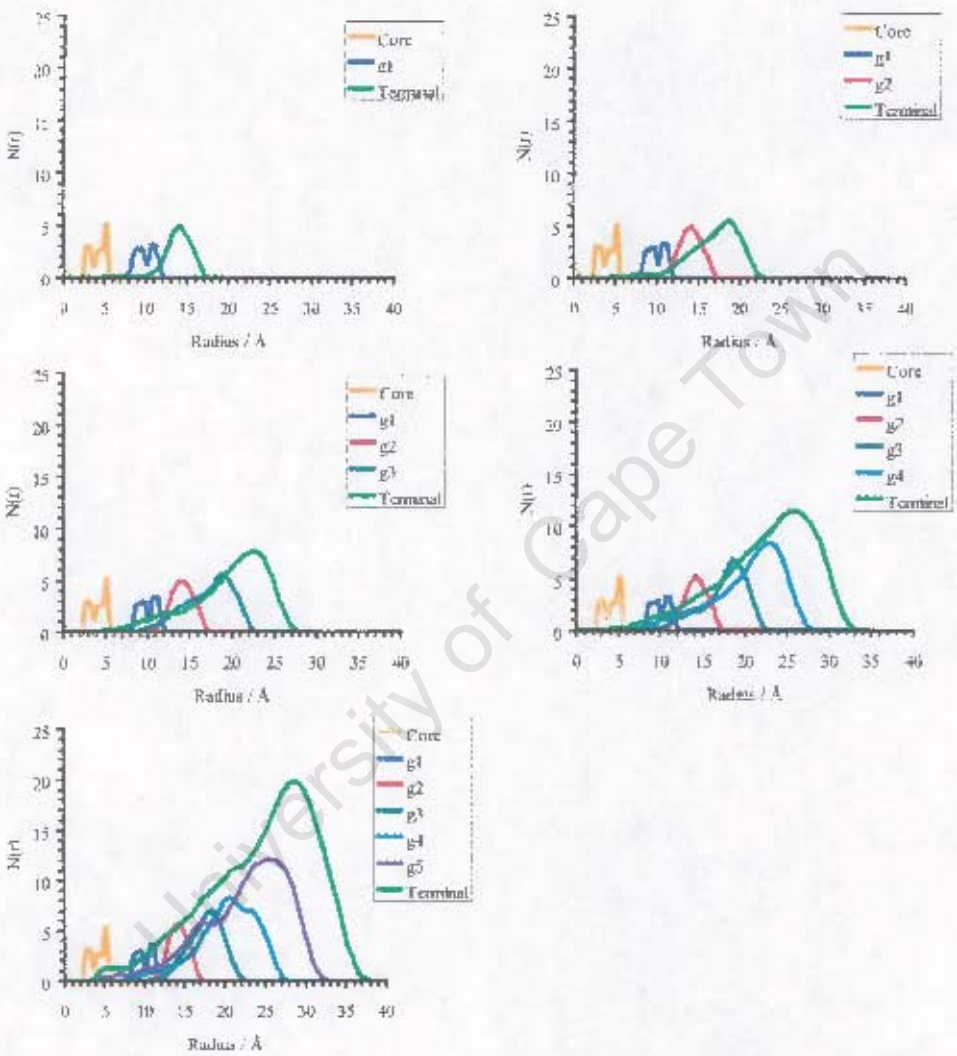

Figure B.8: $N_l(r)$ of the topological layers of dendrimers G1 to G5 in THF

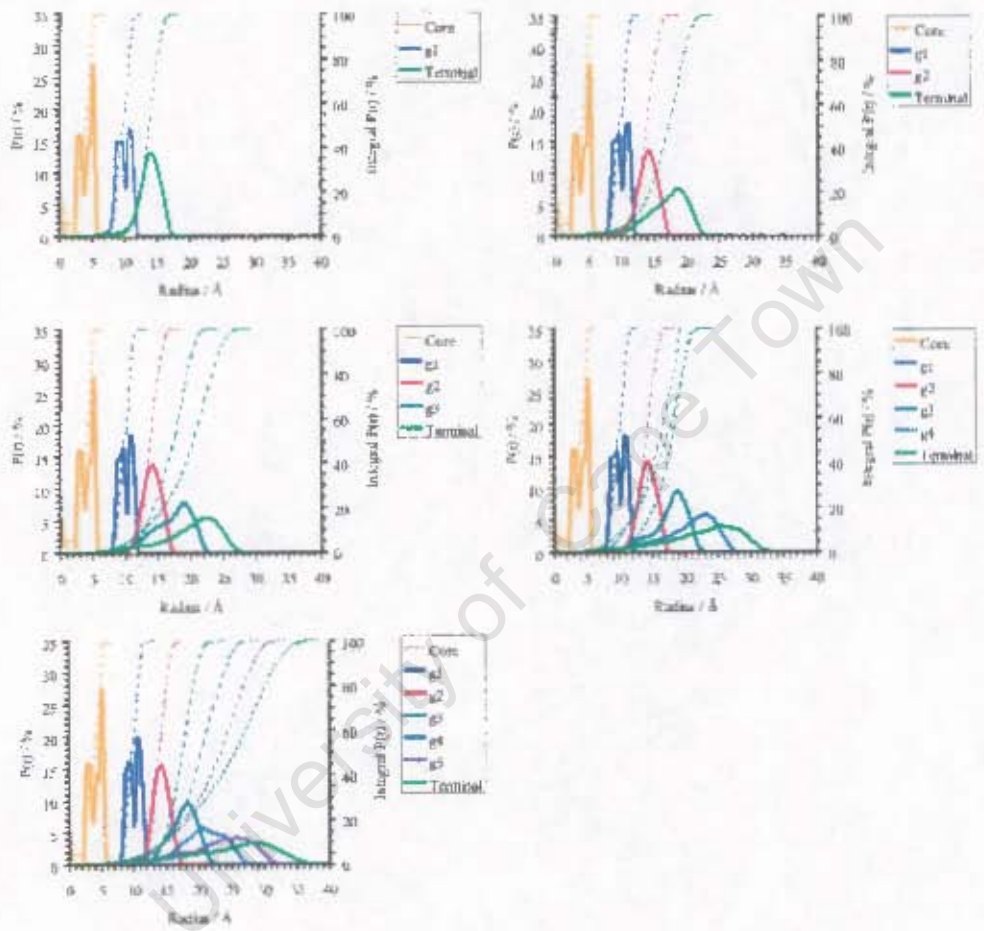

Figure B.9: $H(r)$ of each layer of dendrimers G1 to G5 in THF. This includes the integration of these distributions showing their accumulation within the dendrimer as one progresses to its periphery.

Appendix C

Overall spatial distribution profiles

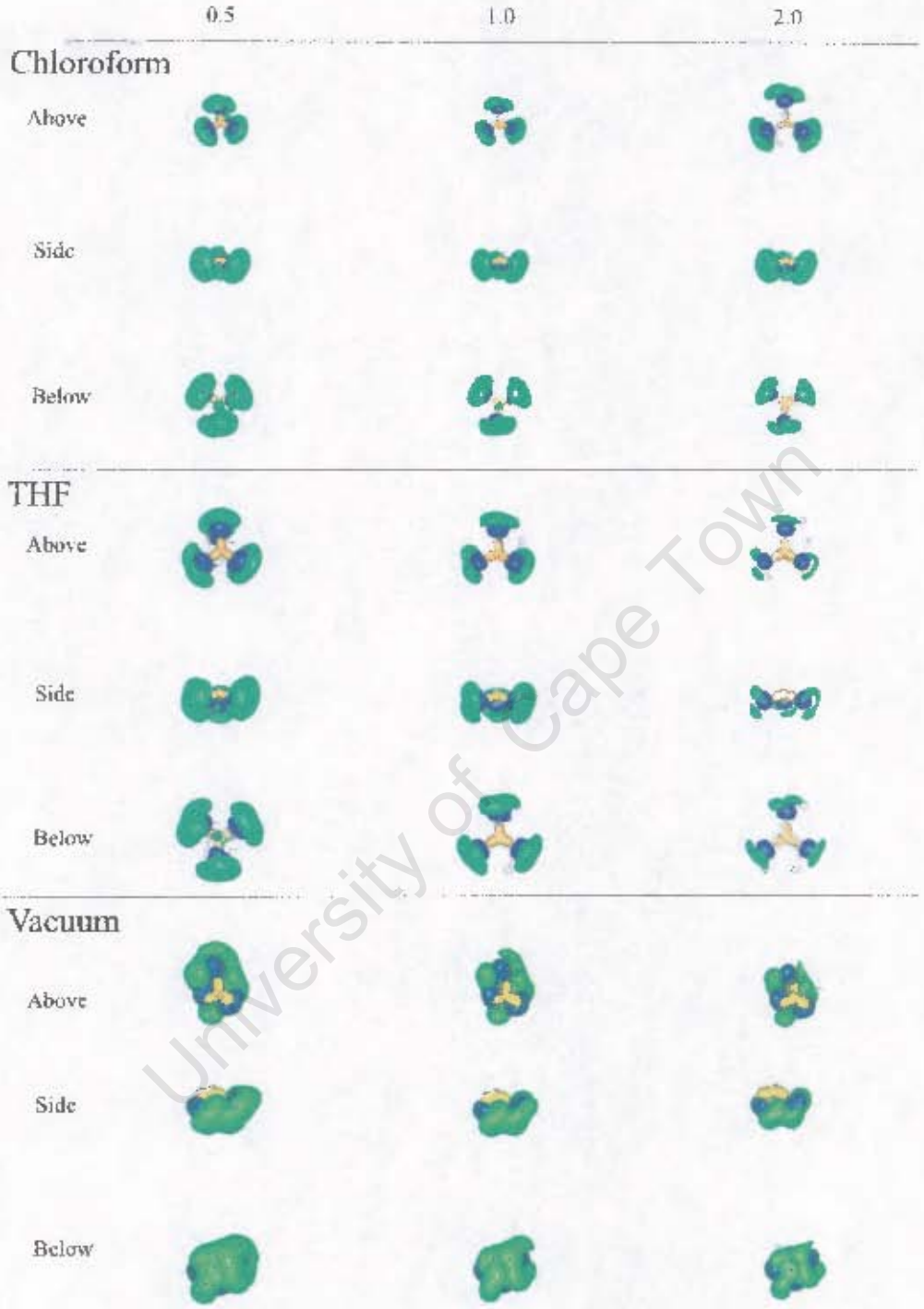

Figure C.1: Views of the G1 dendrimer from above, side and below of the complete set of SDFs for the dendrimer in vacuum, THF and chloroform at half bulk density (0.5), bulk density (1.0) and twice bulk density (2.0)

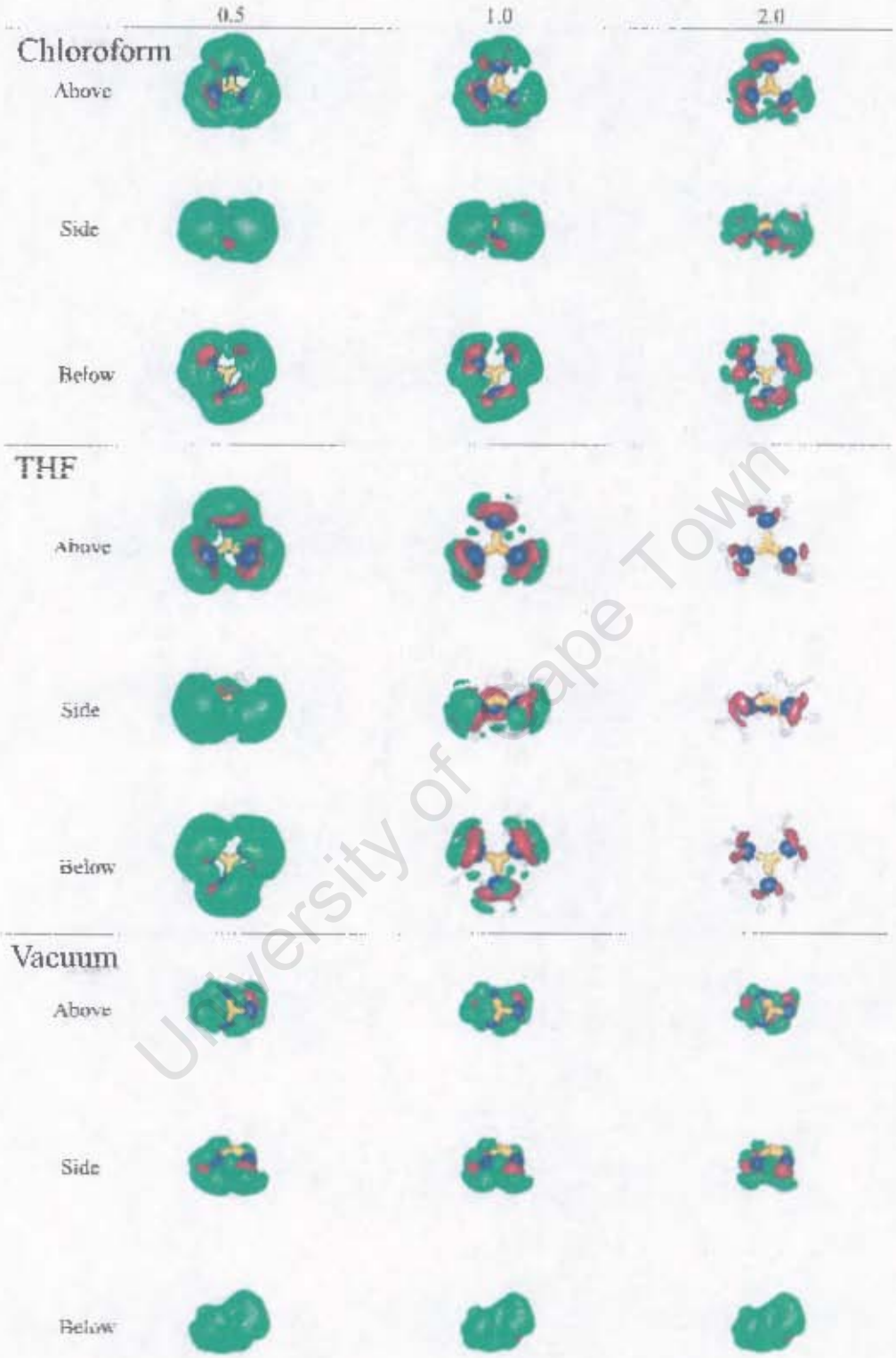

Figure C.2: Views of the G2 dendrimer from above, side and below of the complete set of SDFs for the dendrimer in vacuum, THF and chloroform at half bulk density (0.5), bulk density (1.0) and twice bulk density (2.0)

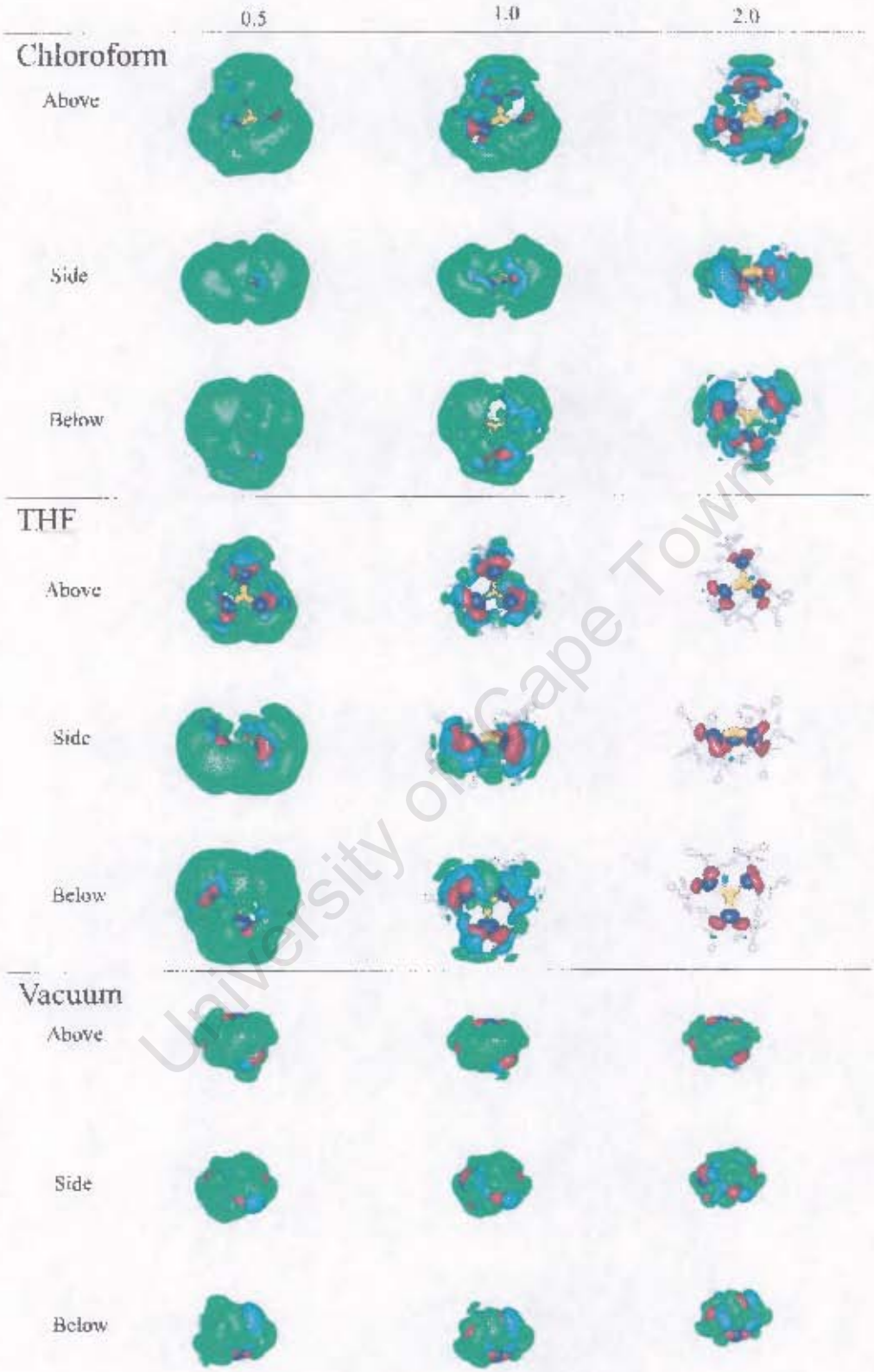

Figure C.3: Views of the G3 dendrimer from above, side and below of the complete set of SDFs for the dendrimer in vacuum, THF and chloroform at half bulk density (0.5), bulk density (1.0) and twice bulk density (2.0)

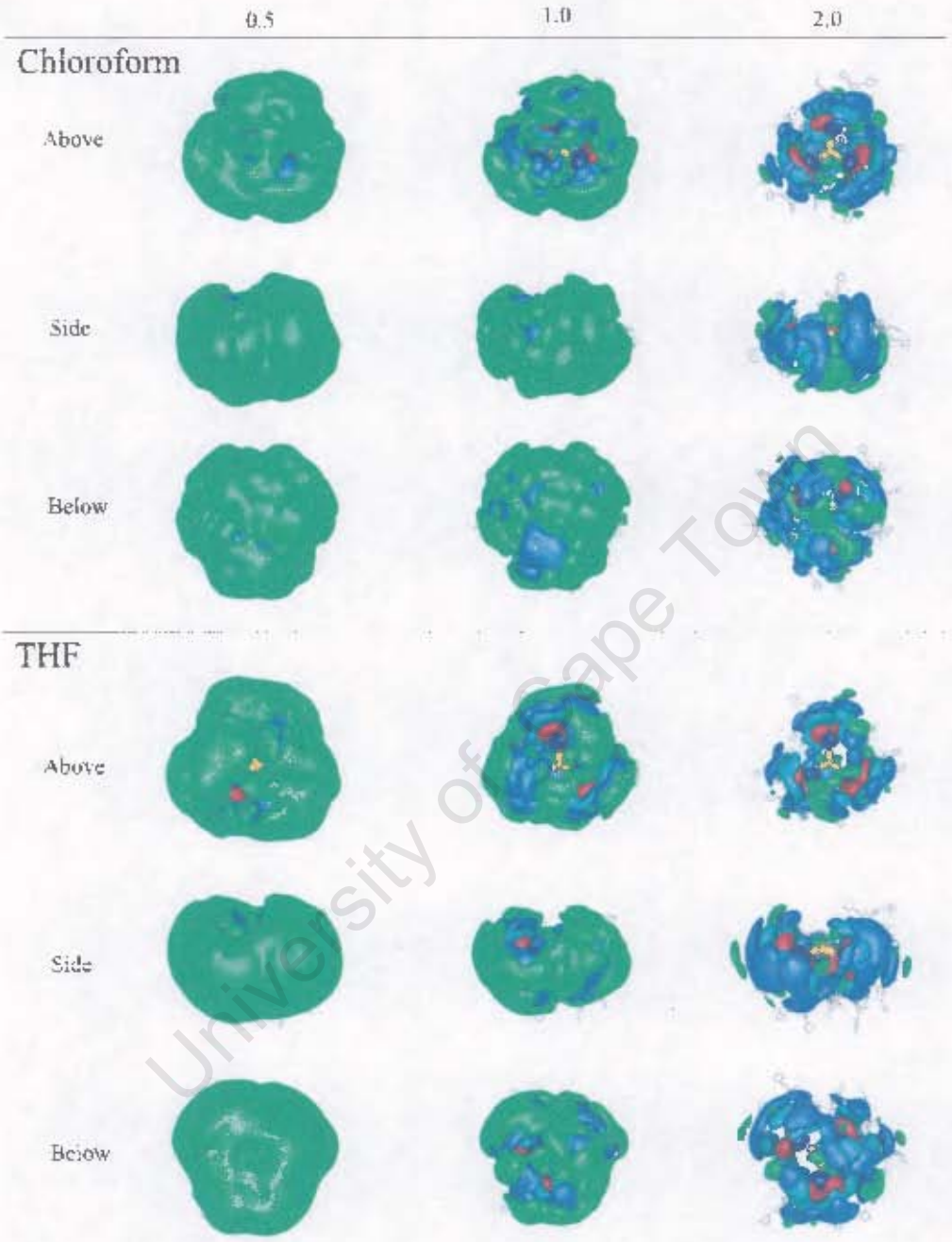

Figure C.4: Views of the G dendrimer from above, side and below of the complete set of SDFs for the dendrimer in THF and chloroform at half bulk density (0.5), bulk density (1.0) and twice bulk density (2.0)

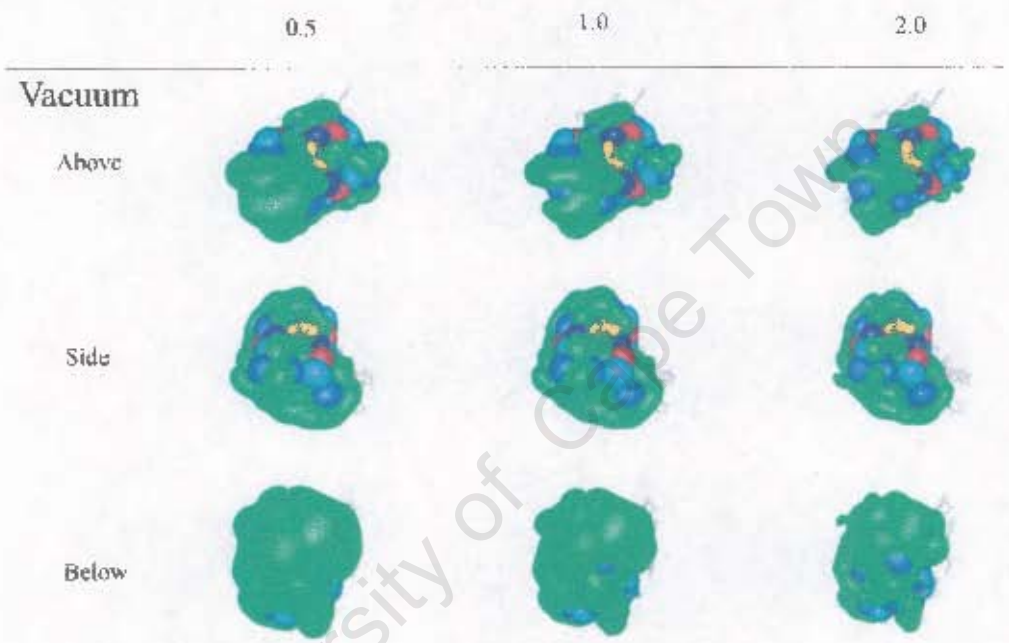

Figure C.5: Views of the G3 dendrimer from above, side and below of the complete set of SDFs for the dendrimer in vacuum at half bulk density (0.5), bulk density (1.0) and twice bulk density (2.0)

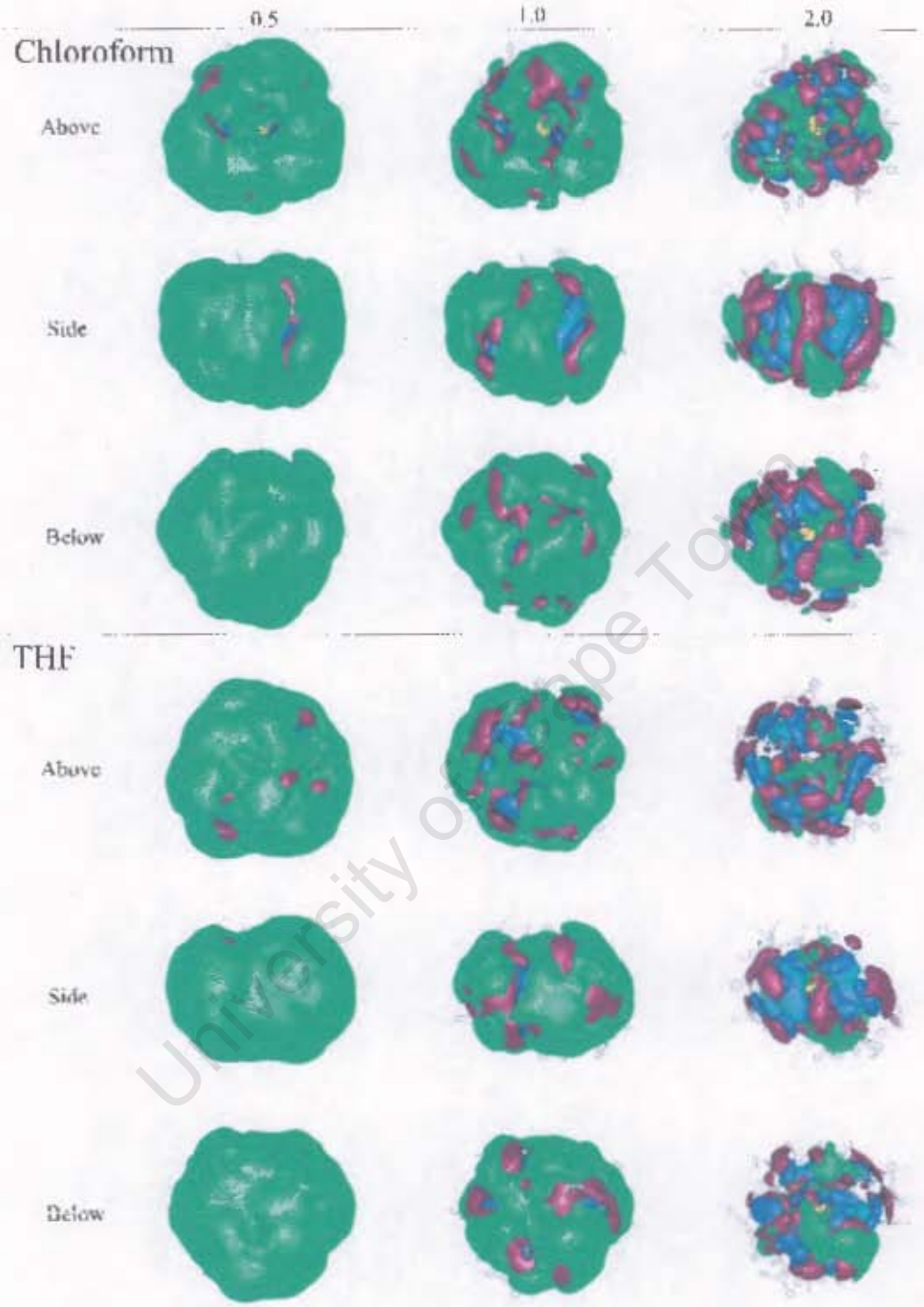

Figure C.6: Views of the G5 dendrimer from above, side and below of the complete set of SDFs for the dendrimer in THF and chloroform at half bulk density (0.5), bulk density (1.0) and twice bulk density (2.0)

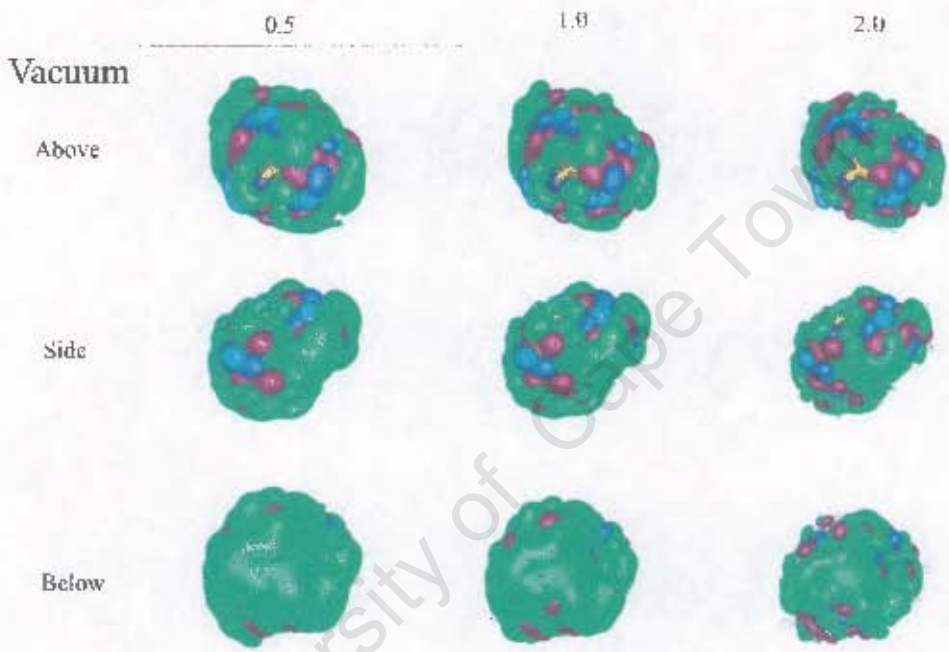

Figure C.7: Views of the G5 dendrimer from above, side and below of the complete set of SDFs for the dendrimer in vacuum at half bulk density (0.5), bulk density (1.0) and twice bulk density (2.0)

Appendix D

SDFs of topological layers of dendrimers - Vacuum

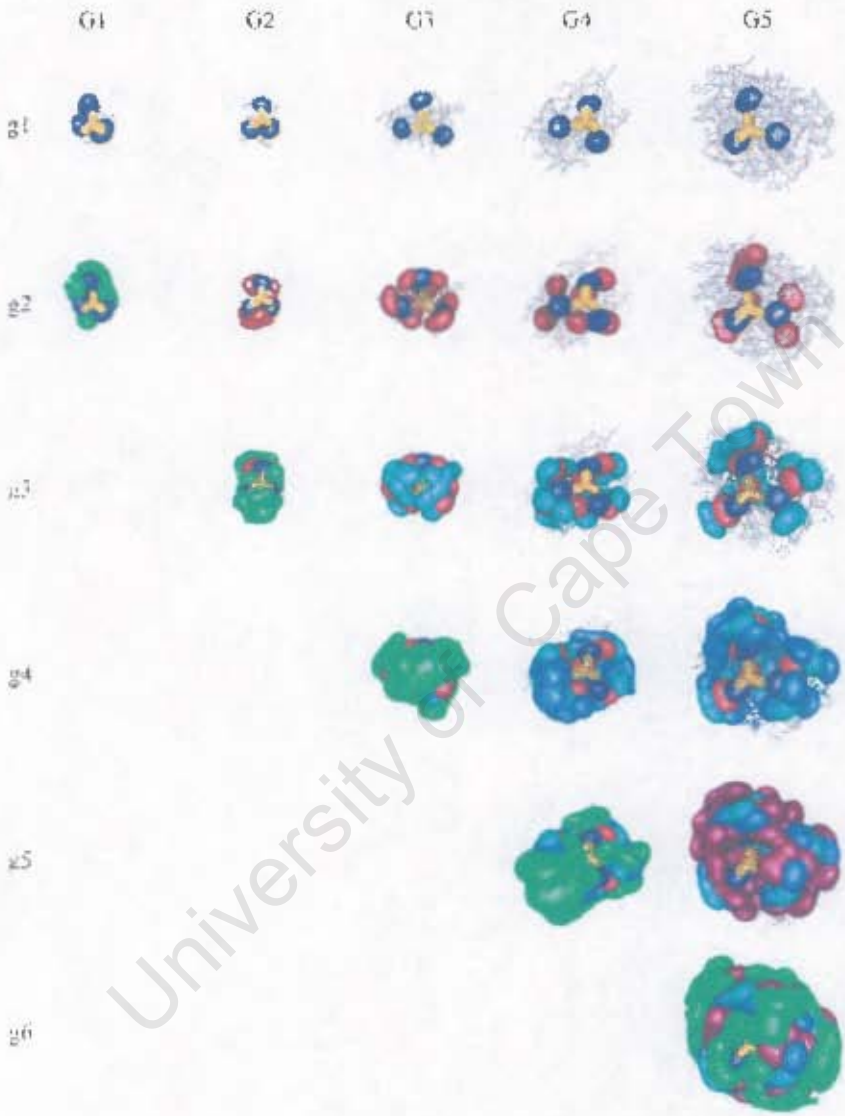

Figure D.1: The SDFs at half of bulk density of each topological layer (g1 - g6) of dendrimers G1 to G5 in vacuum.

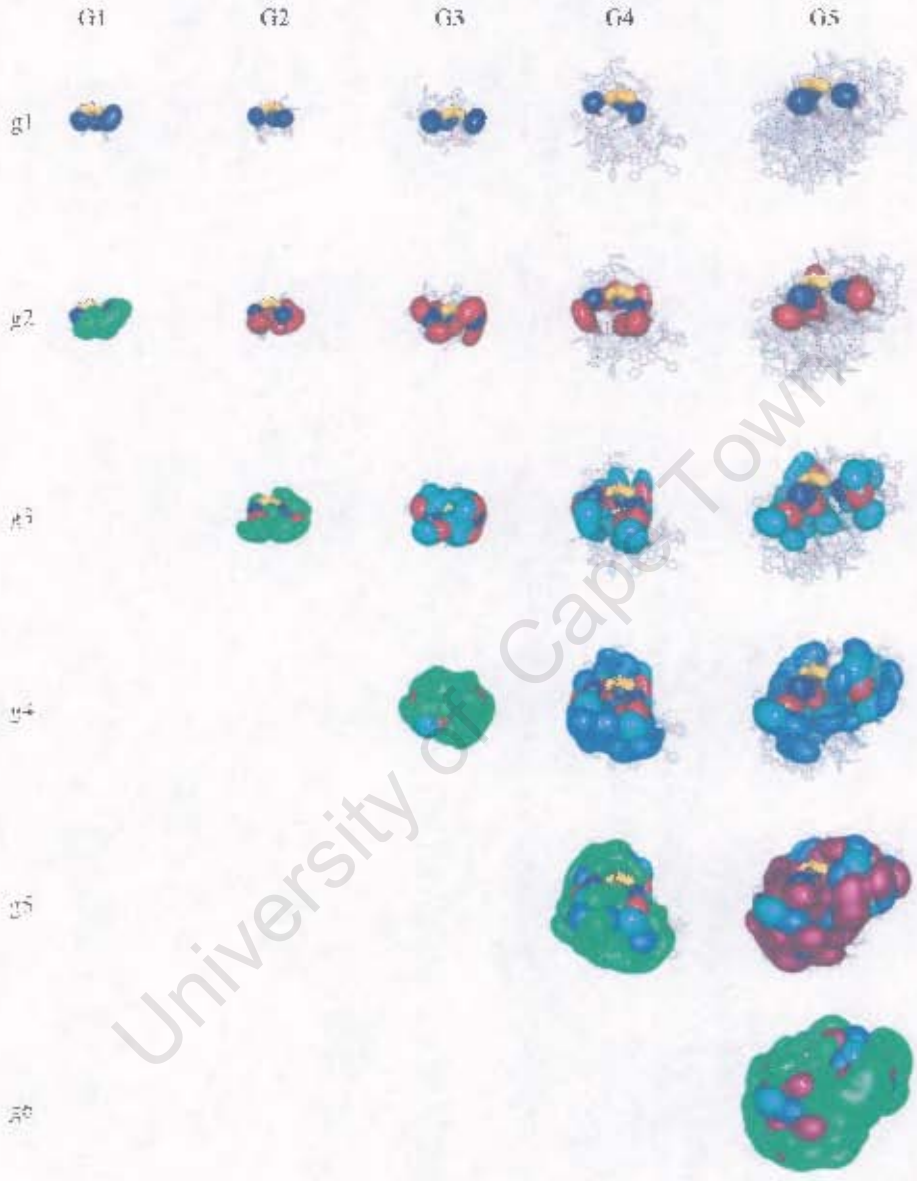

Figure D.2: A side view of the SDFs at half of bulk density of each topological layer (g1 - g6) of dendrimers G1 to G5 in vacuum.

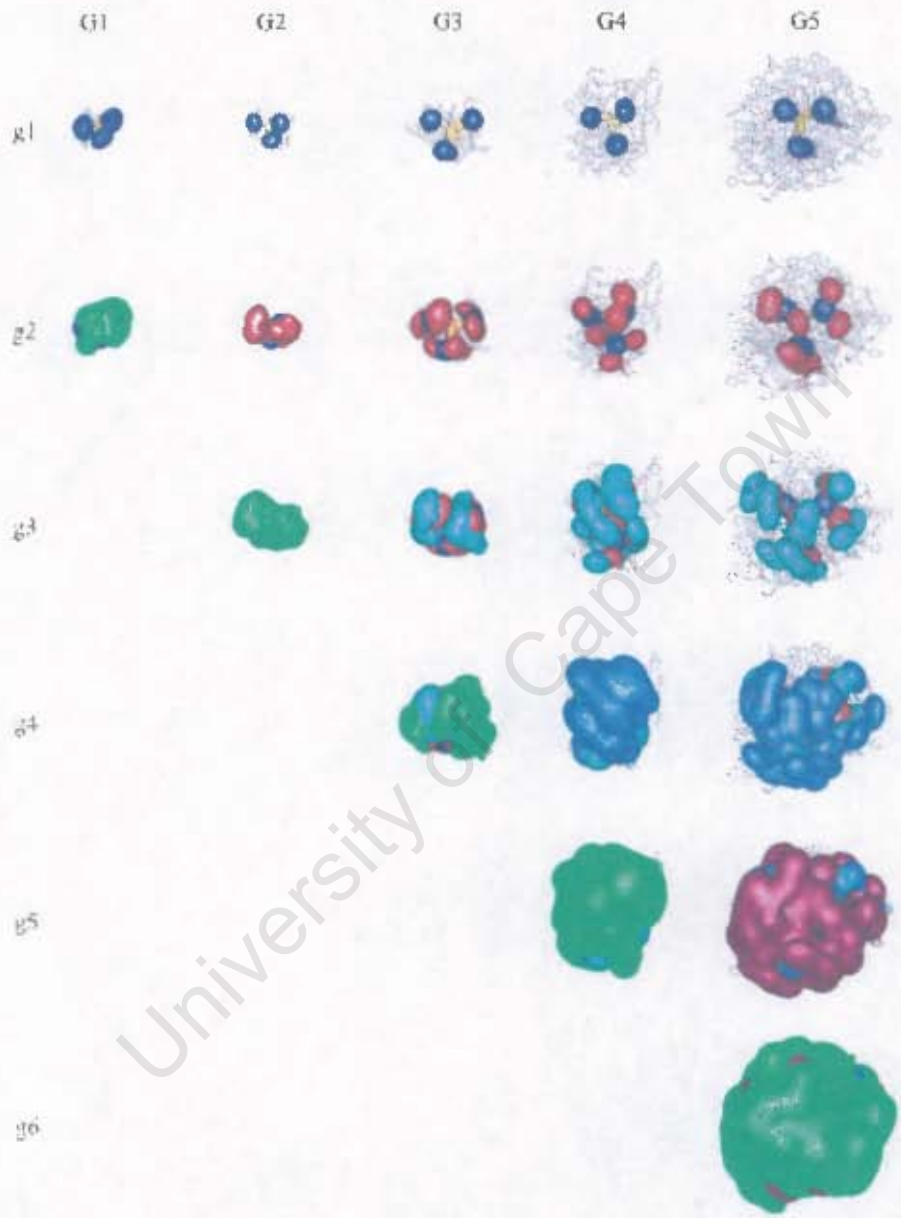

Figure D.3: A view from below the core of the SDFs at half of bulk density of each topological layer (g1 - g6) of dendrimers G1 to G5 in vacuum.

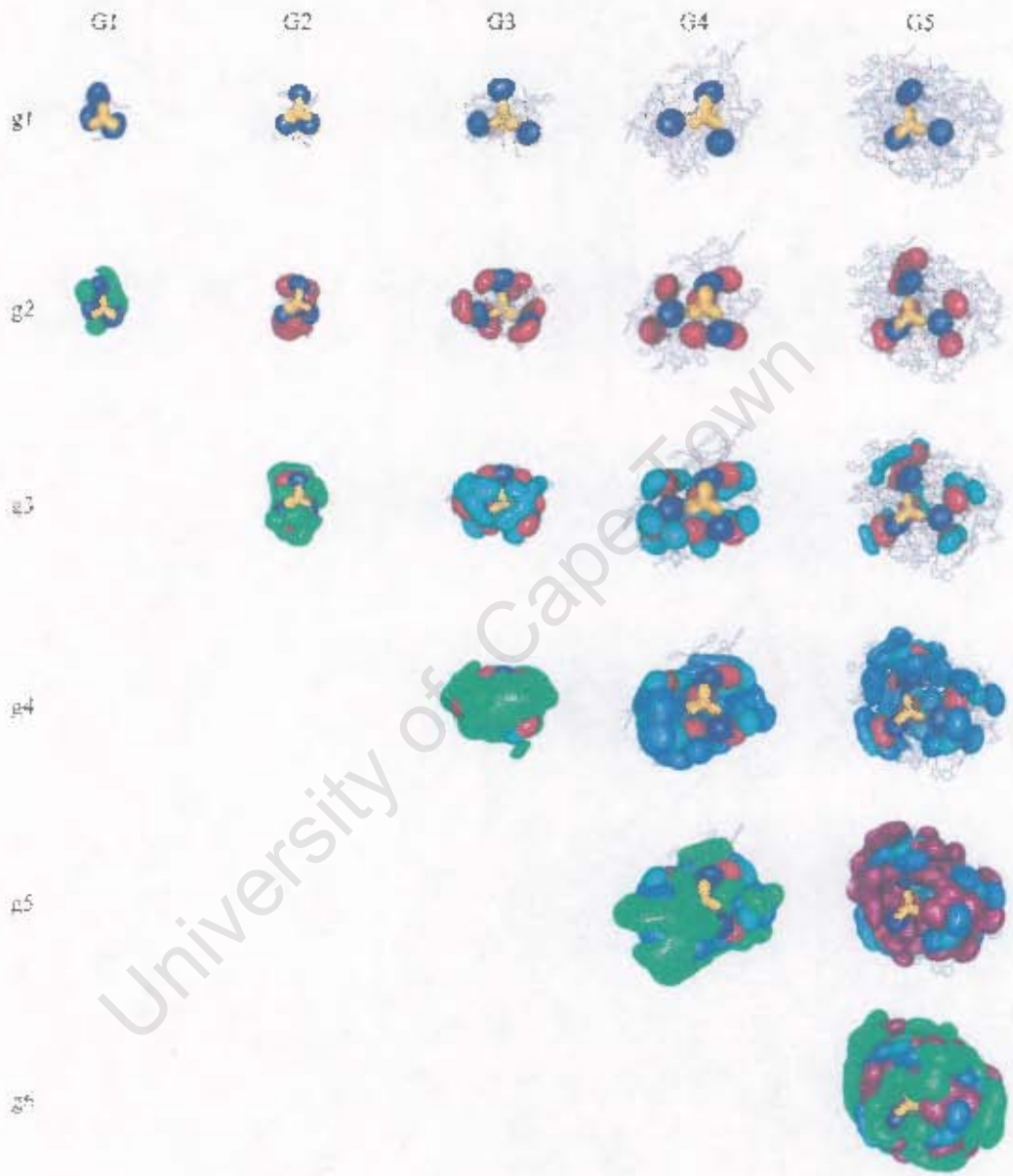

Figure D.4: The SDFs at bulk density of each topological layer (g1 - g6) of dendrimers G1 to G5 in vacuum.

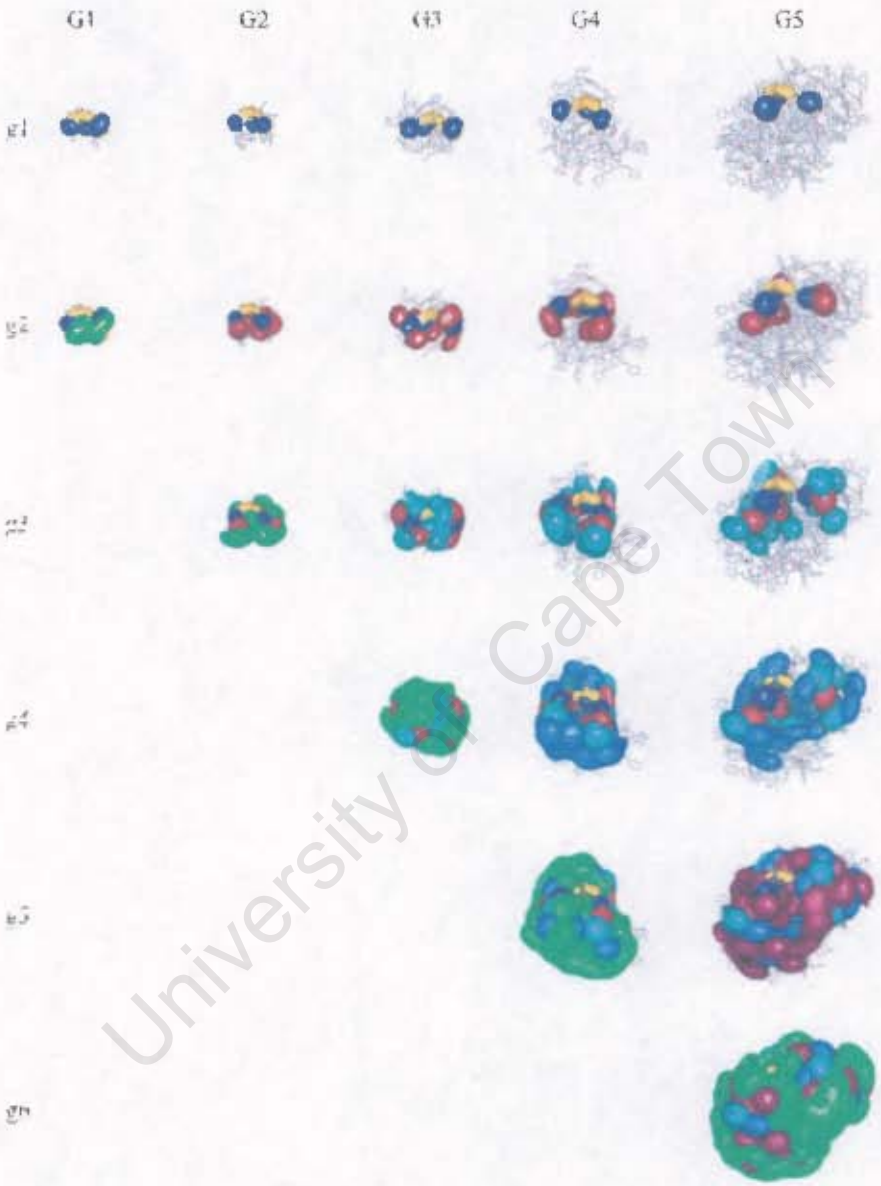

Figure D.5: A side view of the SDFs at bulk density of each topological layer (g1 - g6) of dendrimers G1 to G5 in vacuum.

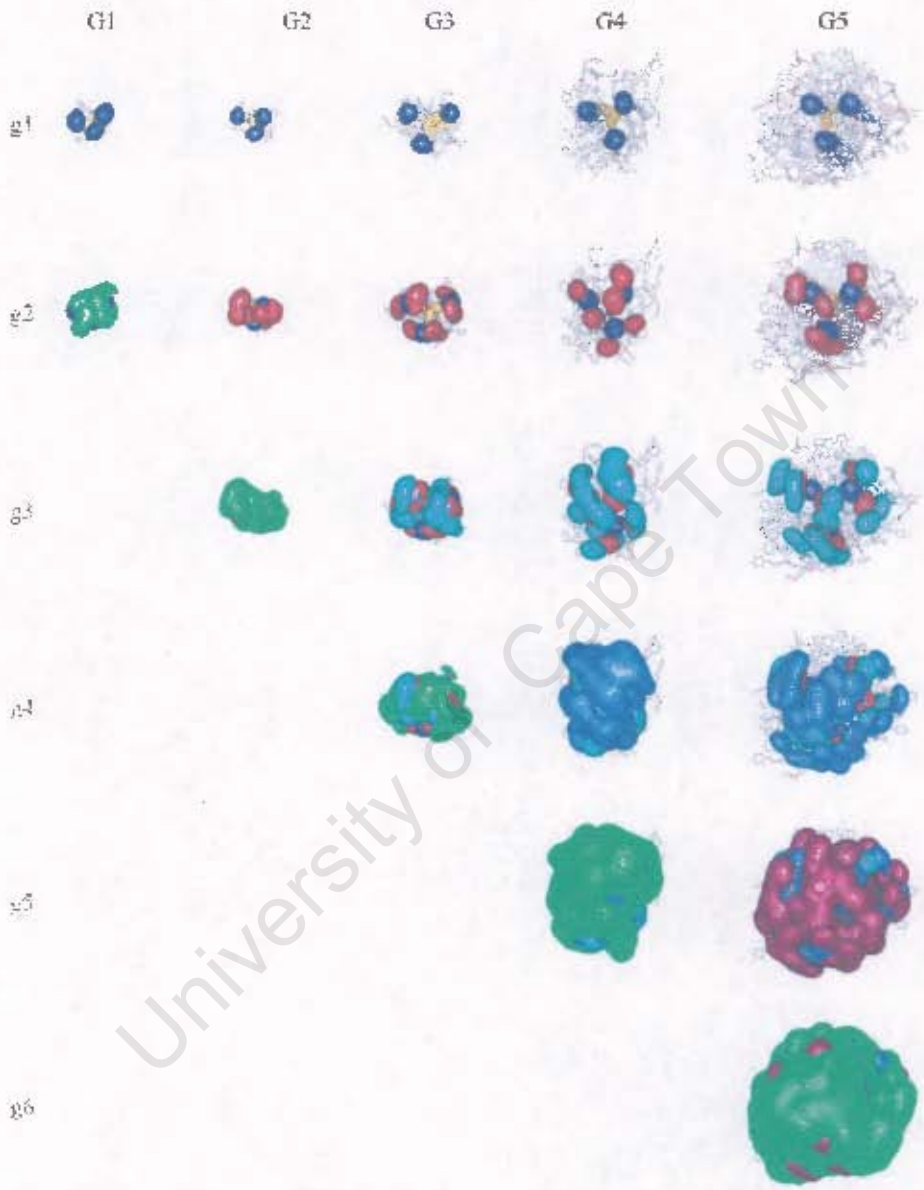

Figure D.6: A view from below the core of the SDF's at bulk density of each topological layer (g1 - g6) of dendrimers G1 to G5 in vacuum.

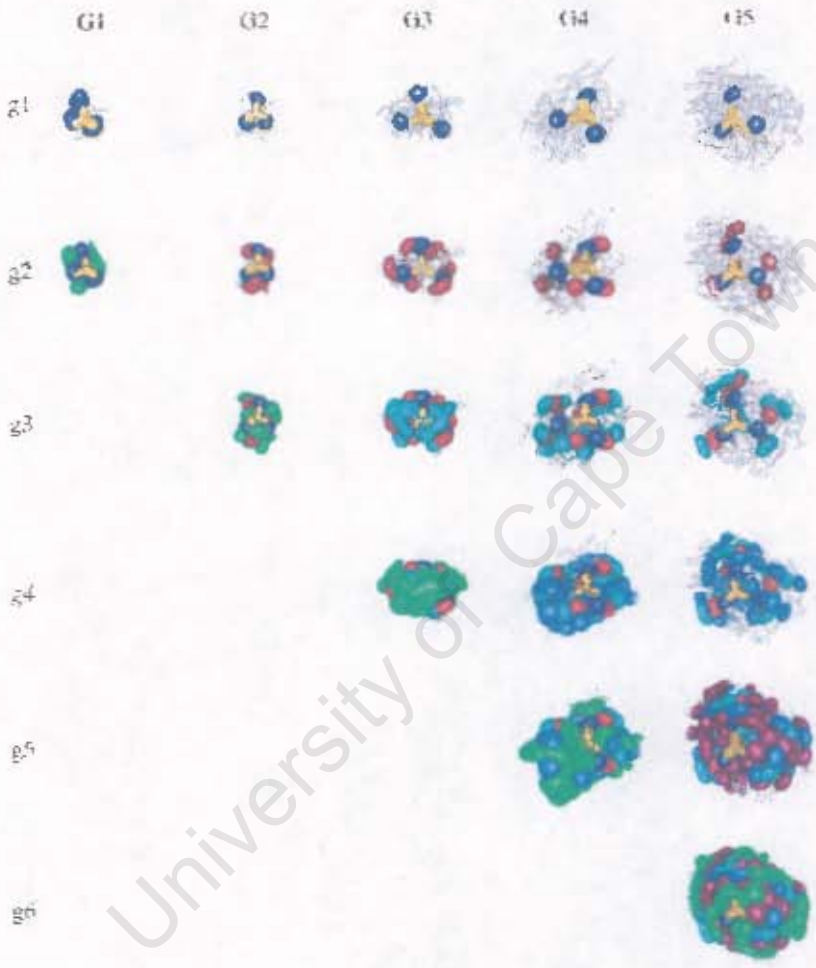

Figure D.7: The SDFs at twice bulk density of each topological layer (g1 - g6) of dendrimers G1 to G5 in vacuum.

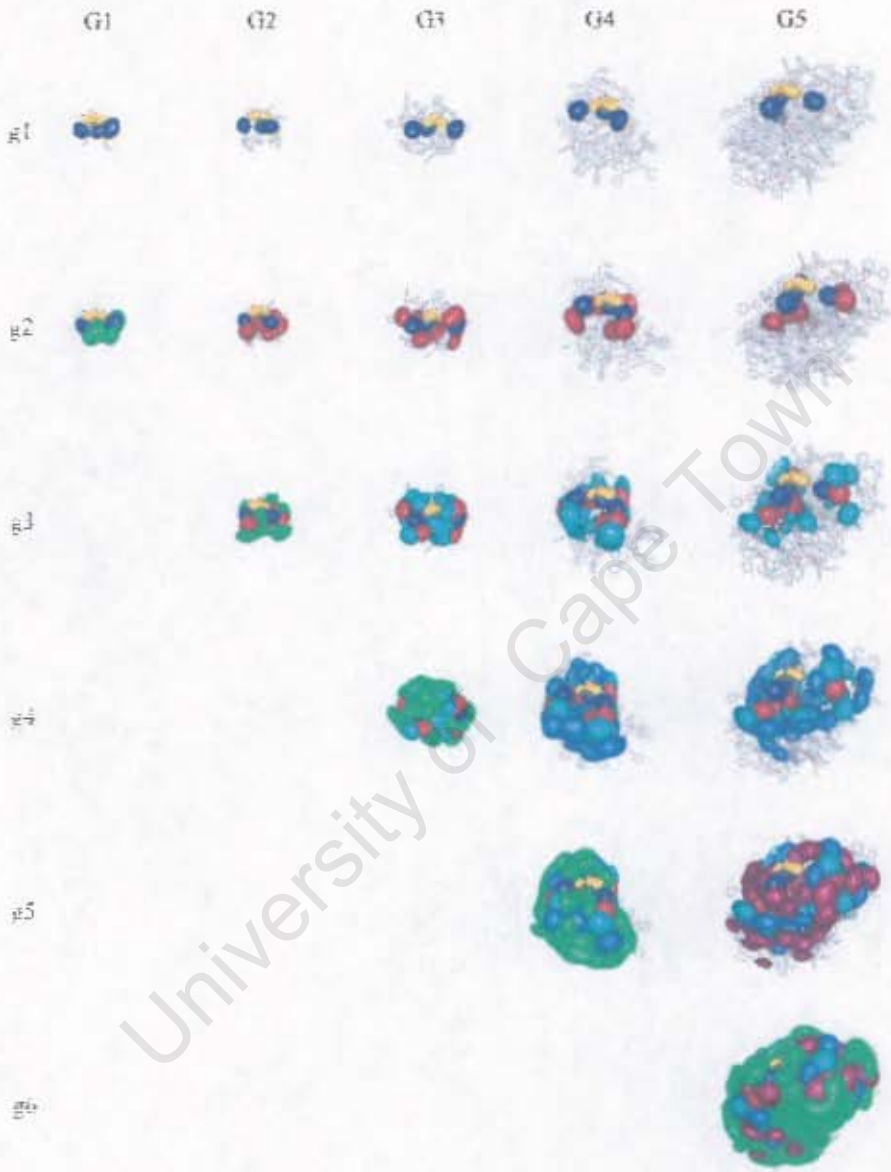

Figure D.8: A side view of the SDFs at twice bulk density of each topological layer (g1 - g6) of dendrimers G1 to G5 in vacuum.

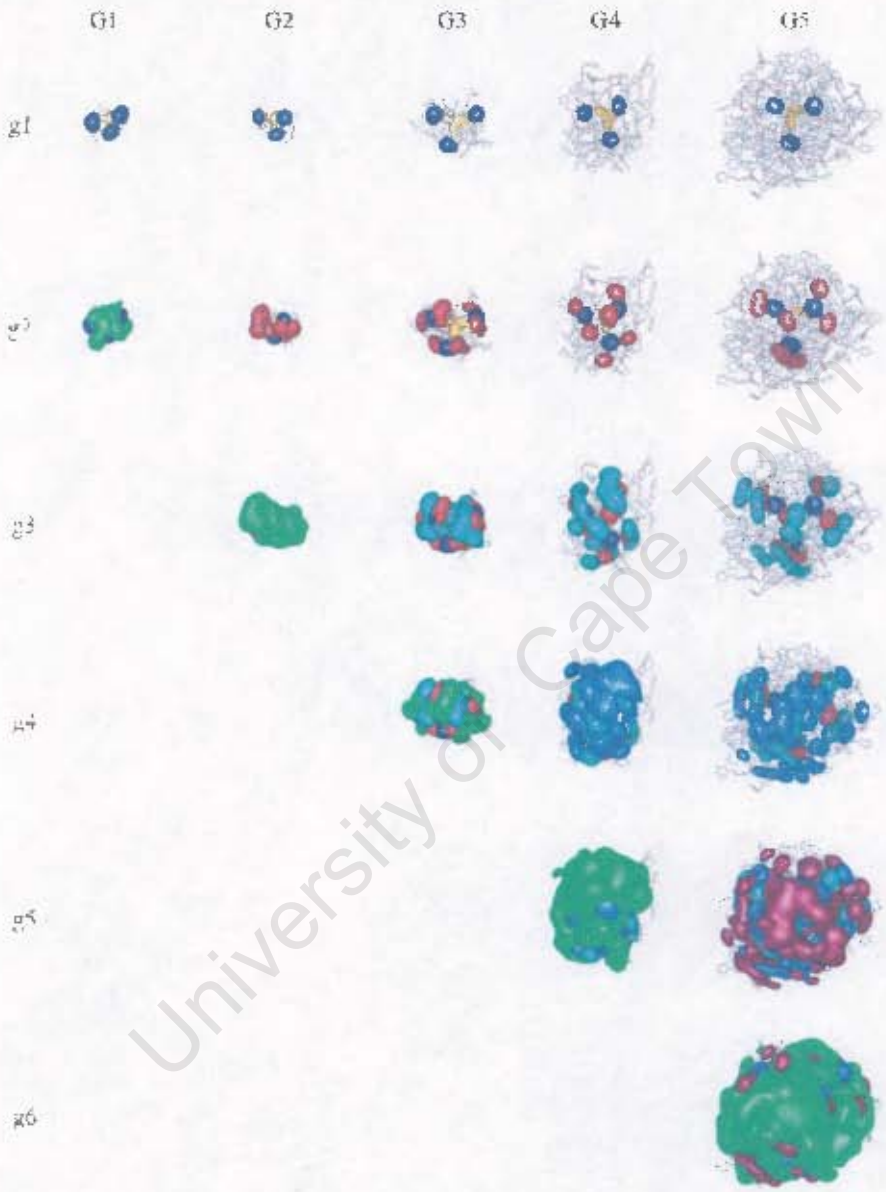

Figure D.9: A view from below the core of the SDFs at twice bulk density of each topological layer (g1 - g6) of dendrimers G1 to G5 in vacuum.

Appendix E

SDFs of topological layers of dendrimers - Chloroform

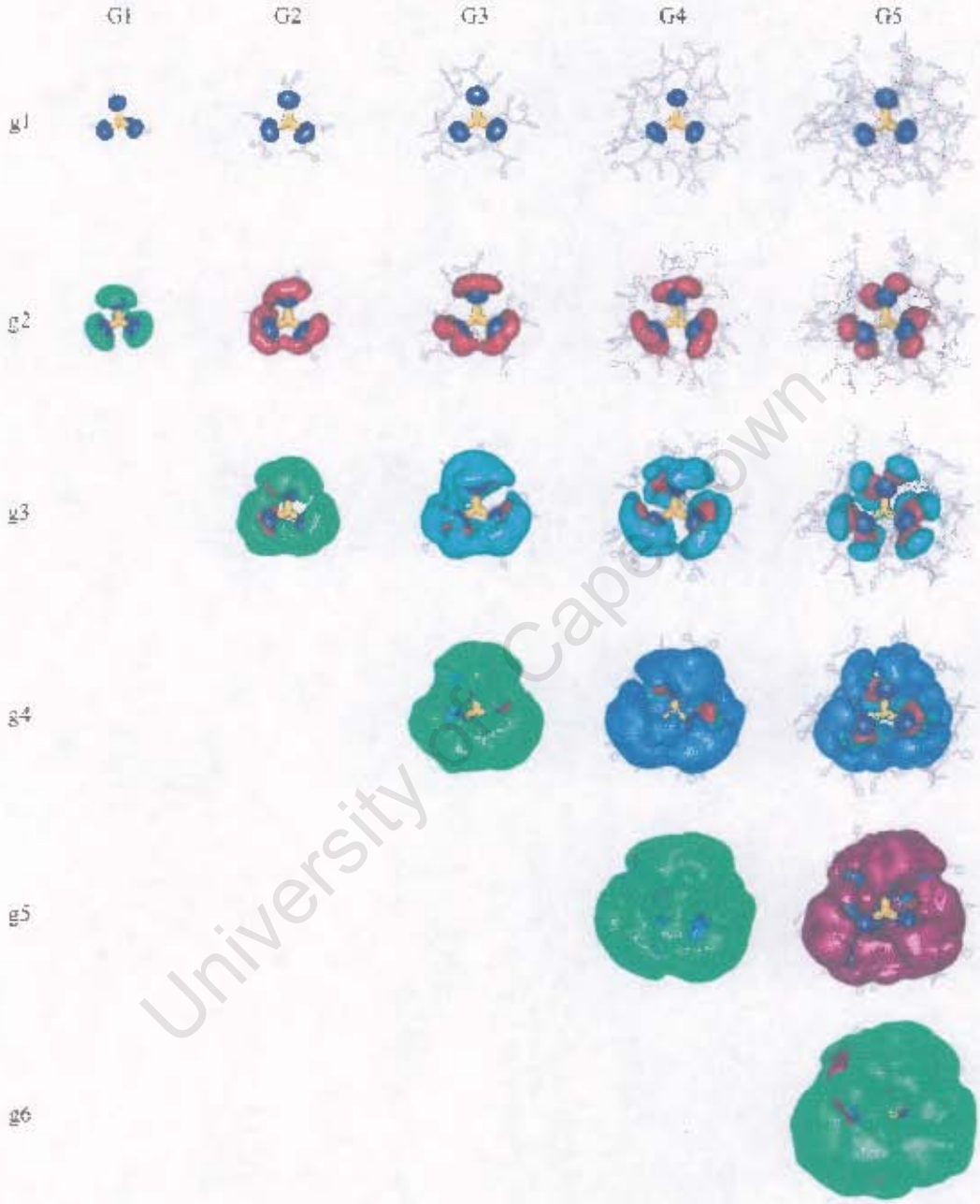

Figure E.1: The SDFs at half bulk density of each topological layer (g1 - g6) of dendrimers G1 to G5 in chloroform.

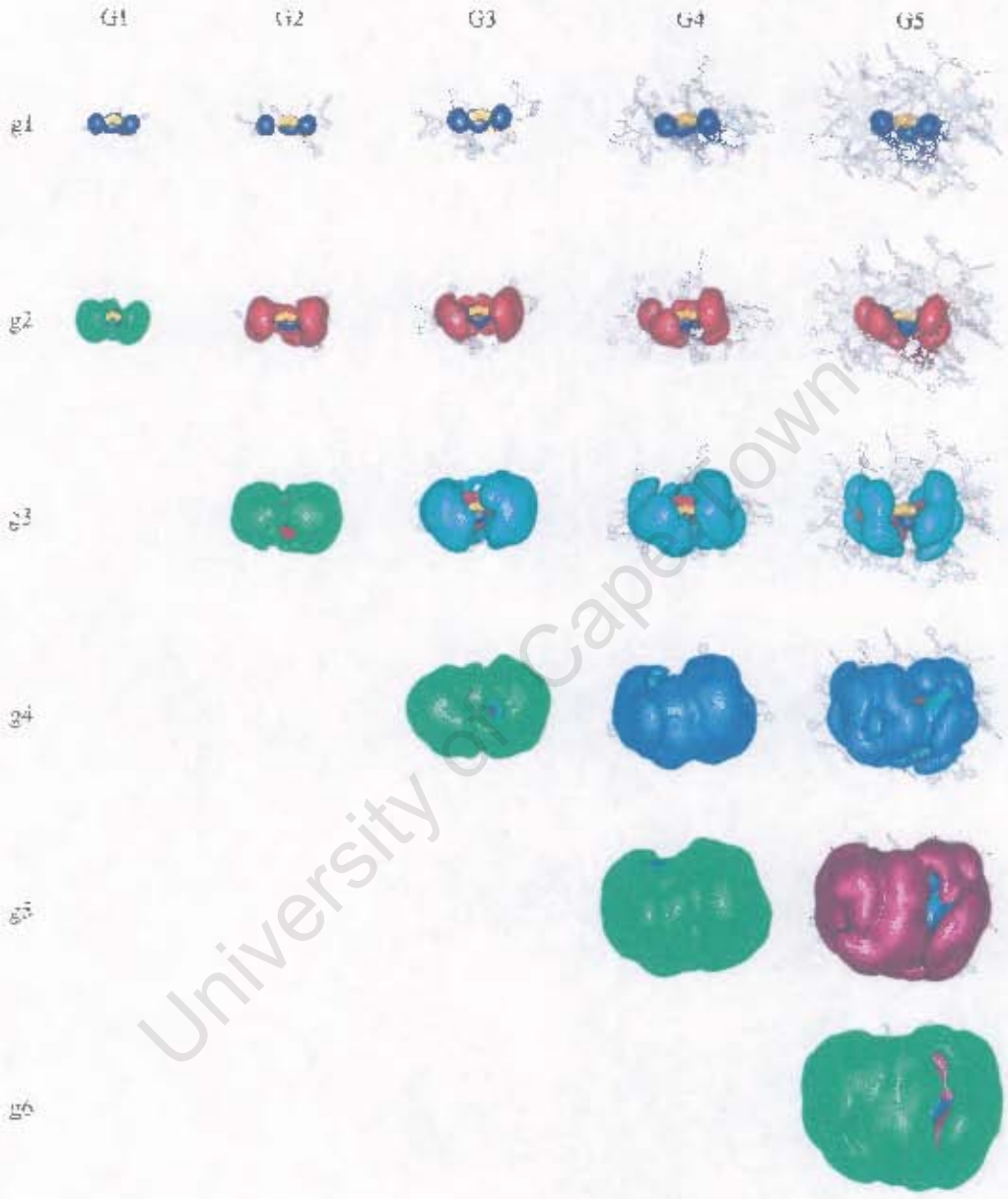

Figure E.2: A side view of the SDFs at half bulk density of each topological layer (g1 - g6) of dendrimers G1 to G5 in vacuum.

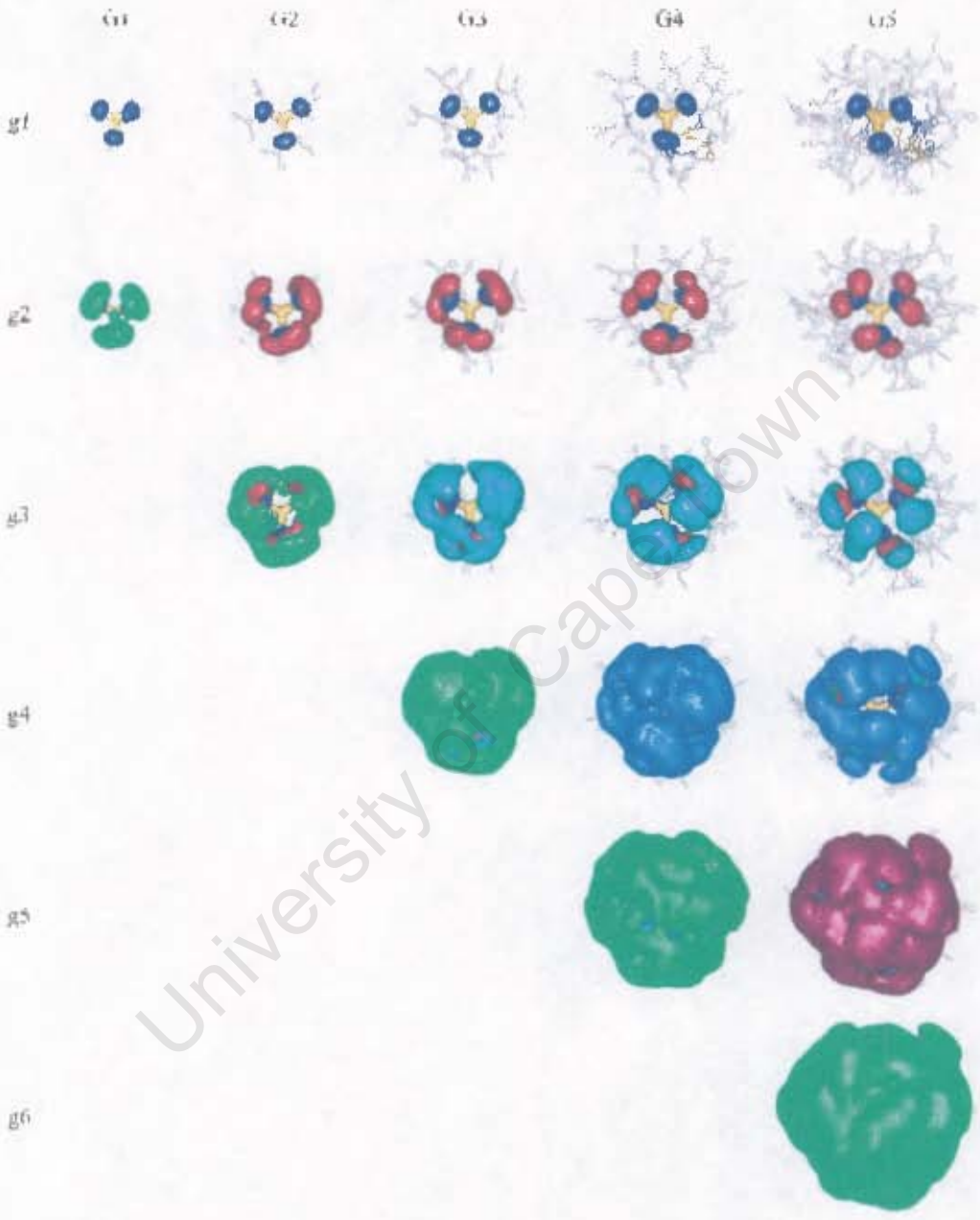

Figure E.3: A view from below the core of the SDFs at half bulk density of each topological layer (g1 - g6) of dendrimers G1 to G5 in chloroform.

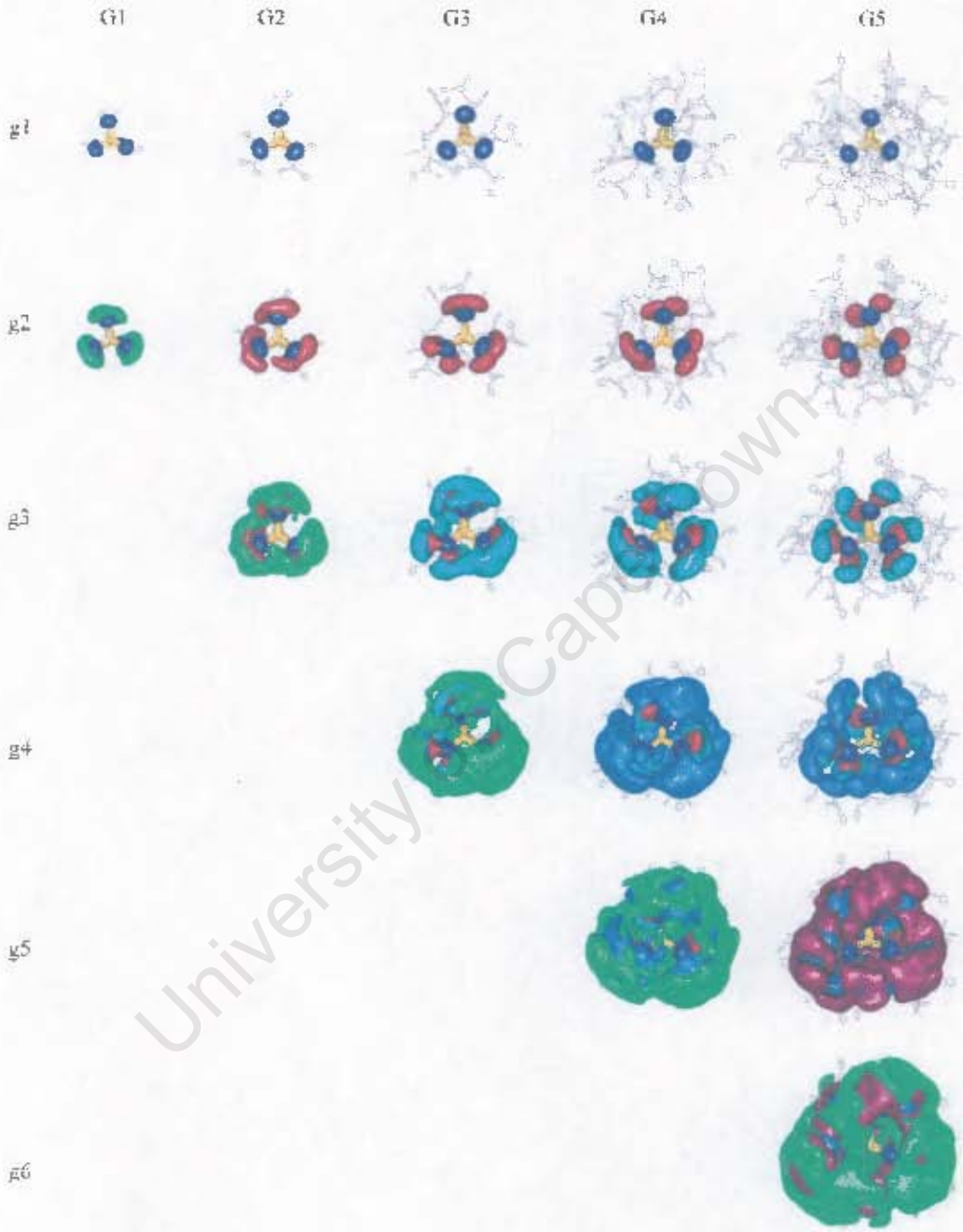

Figure E.4: The SDFs at bulk density of each topological layer (g1 - g6) of dendrimers G1 to G5 in chloroform.

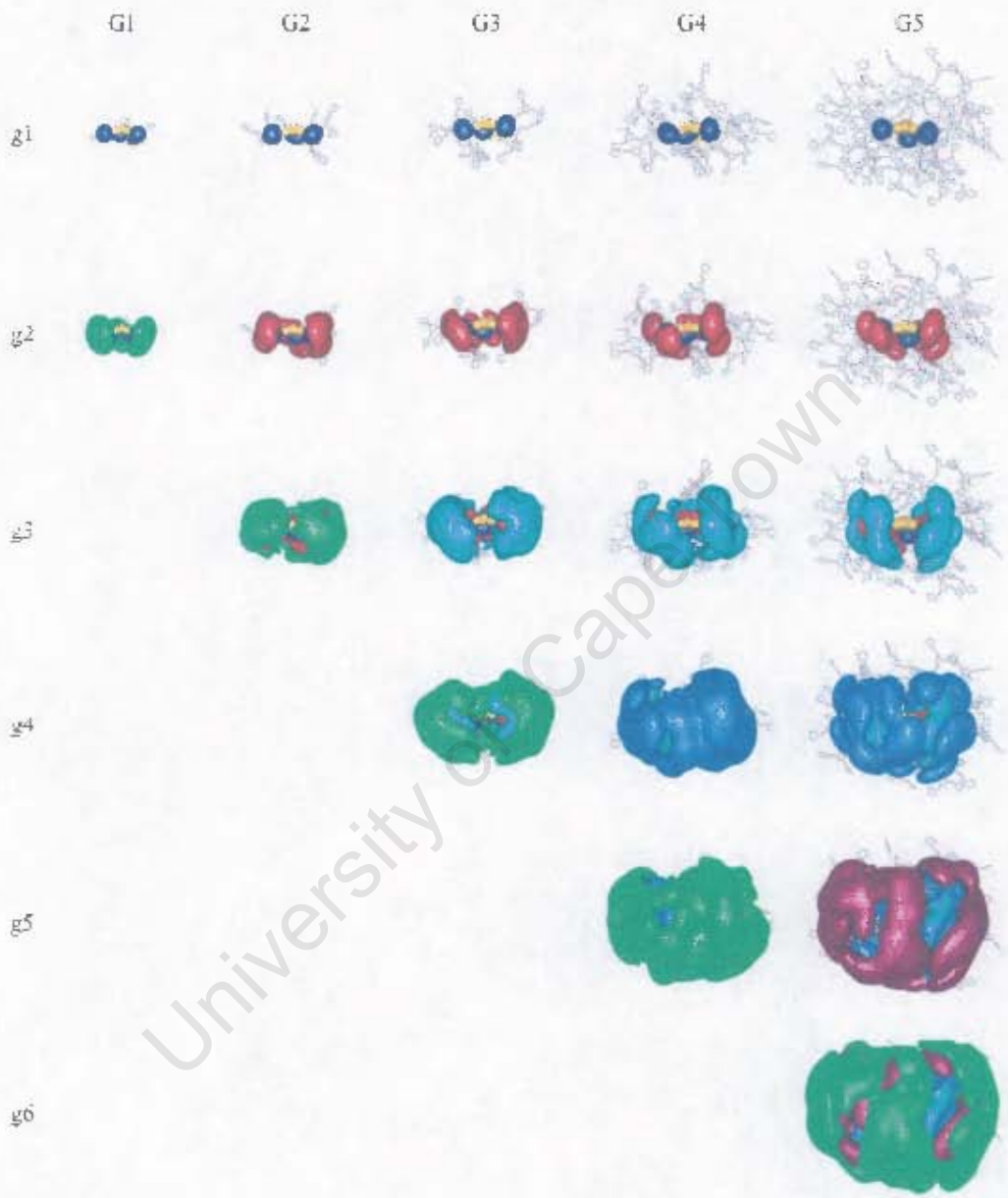

Figure E.5: A side view of the SDFs at bulk density of each topological layer (g1 - g6) of dendrimers G1 to G5 in vacuum.

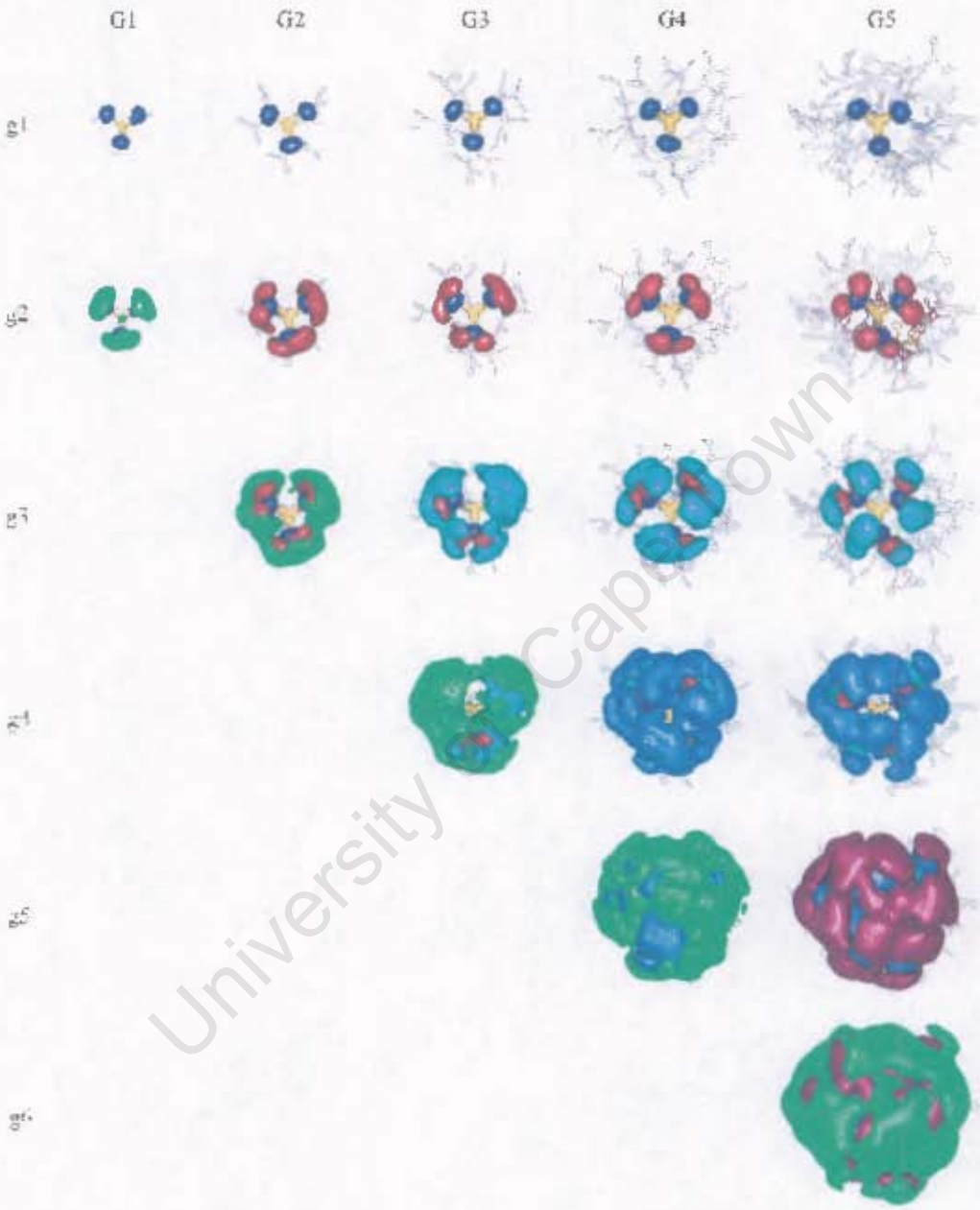

Figure E.6: A view from below the core of the SDFs at bulk density of each topological layer (g1 - g6) of dendrimers G1 to G5 in chloroform.

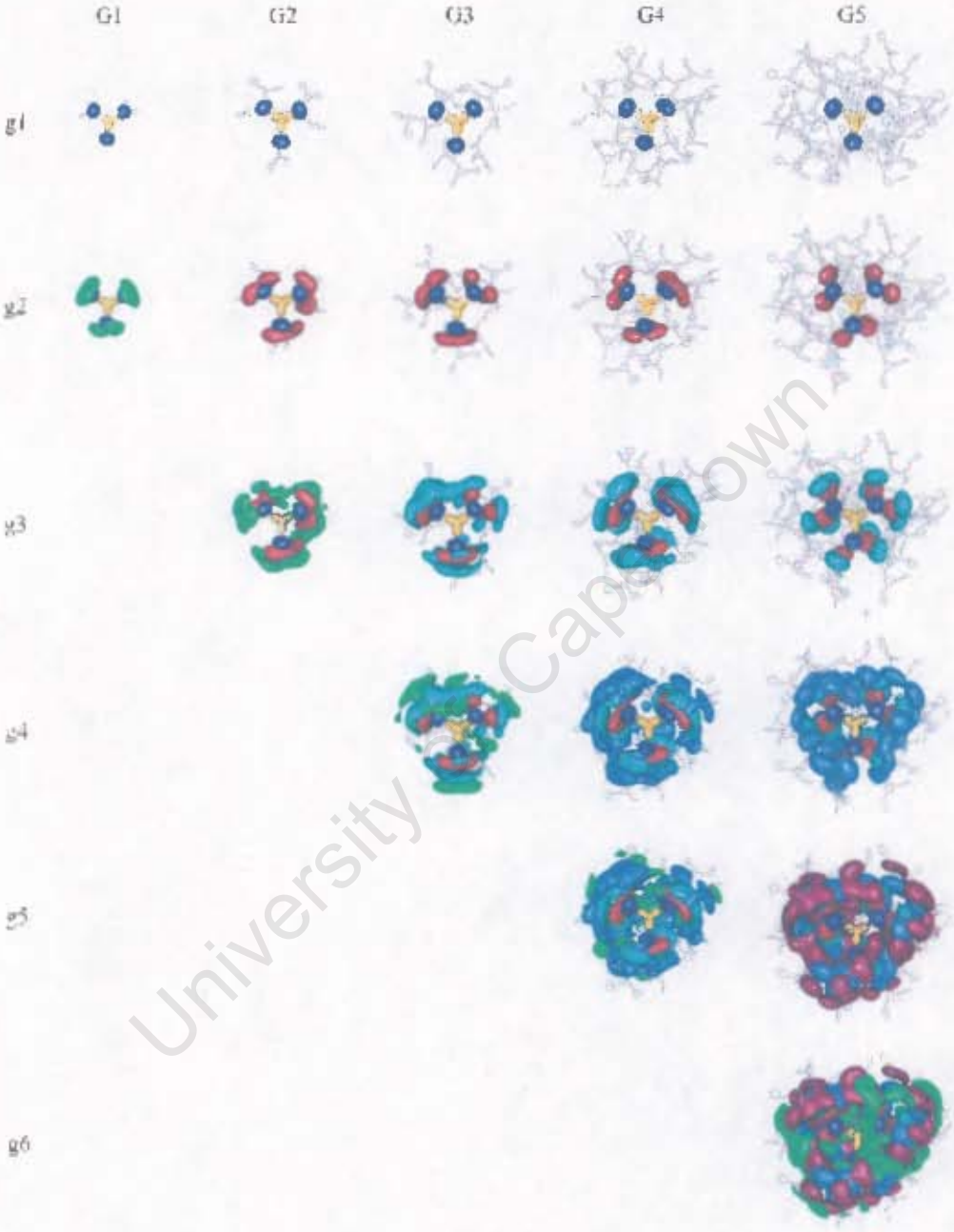

Figure E.7: The SDFs at twice bulk density of each topological layer (g1 - g6) of dendrimers G1 to G5 in chloroform.

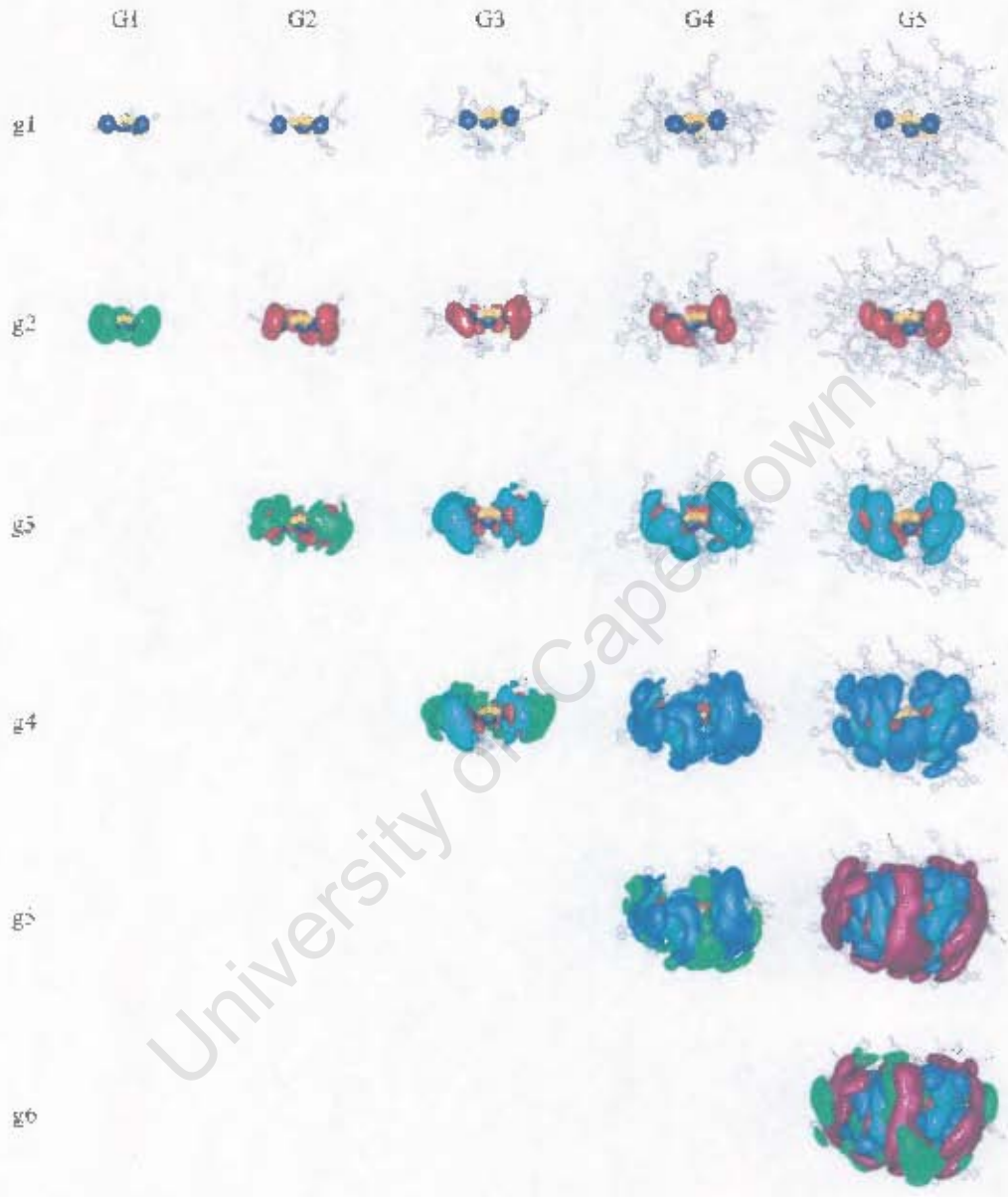

Figure E.8: A side view of the SDFs at twice bulk density of each topological layer (g1 - g6) of dendrimers G1 to G5 in vacuum.

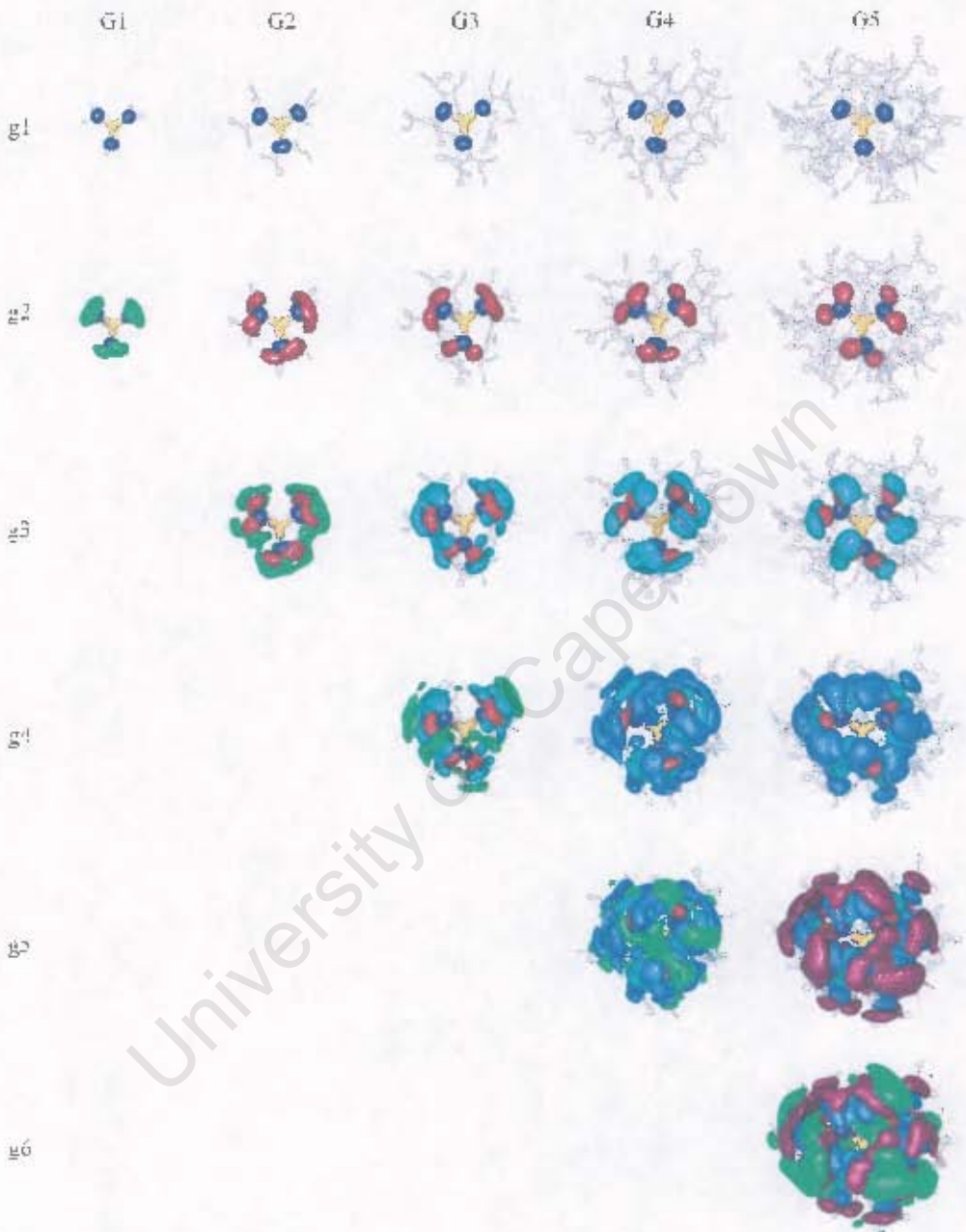

Figure E.9: A view from below the core of the SDFs at twice bulk density of each topological layer (g1 - g6) of dendrimers G1 to G5 in chloroform.

Appendix F

SDFs of topological layers of dendrimers - THF

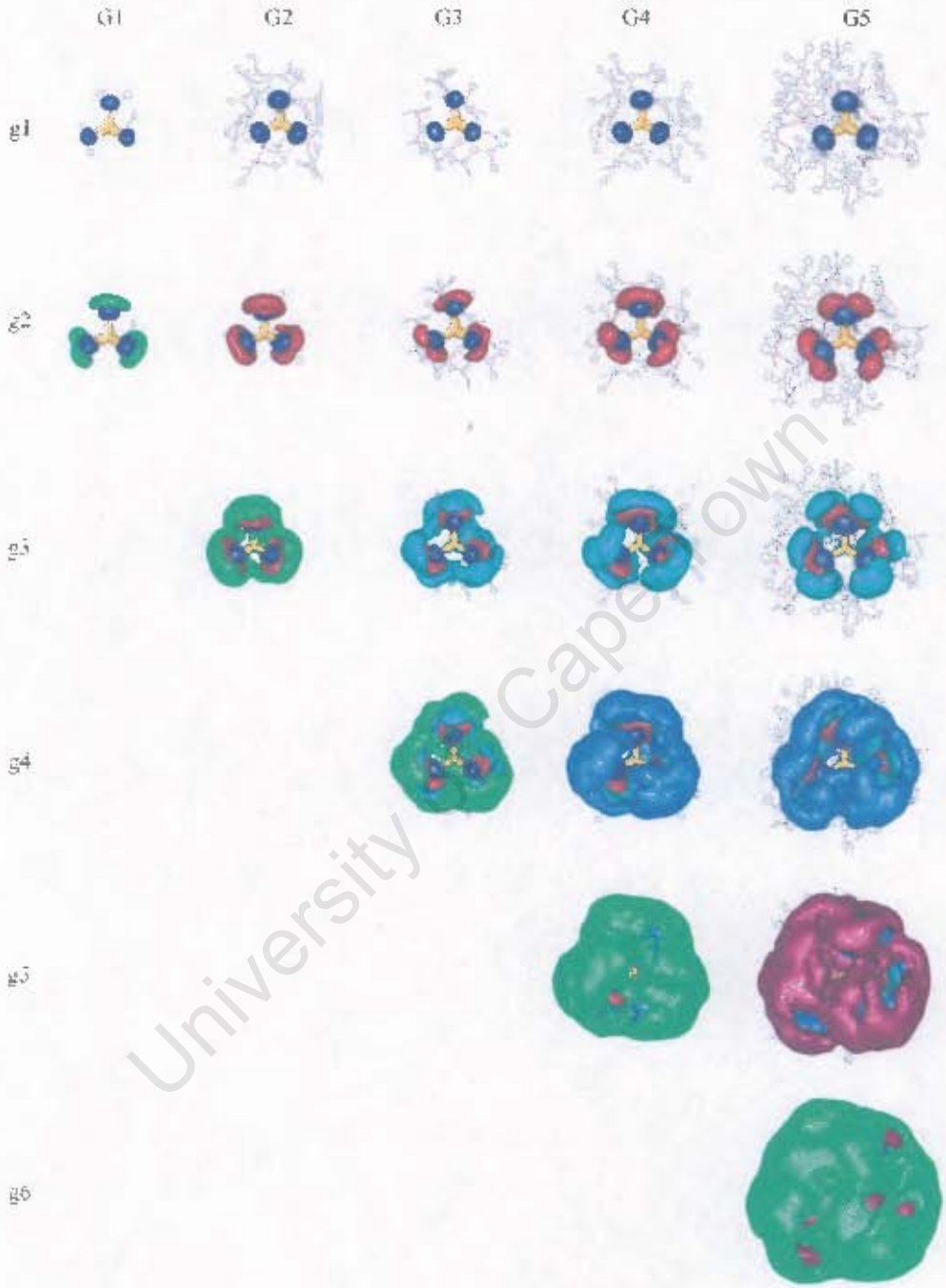

Figure F.1: The SDFs at half bulk density of each topological layer (g1 - g6) of dendrimers G1 to G5 in THF.

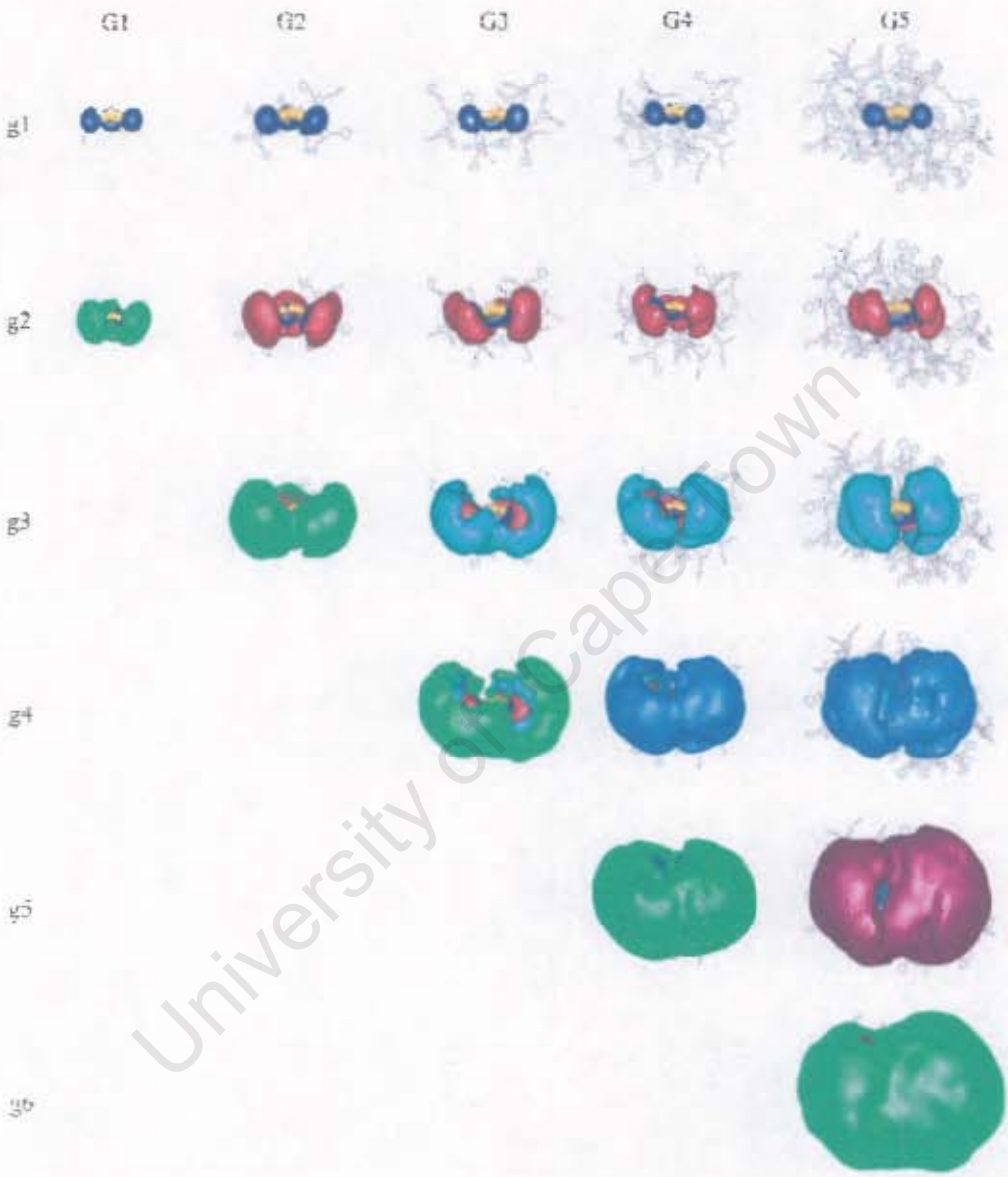

Figure F.2: A side view of the SDFs at half bulk density of each topological layer (g1 - g6) of dendrimers G1 to G5 in THF.

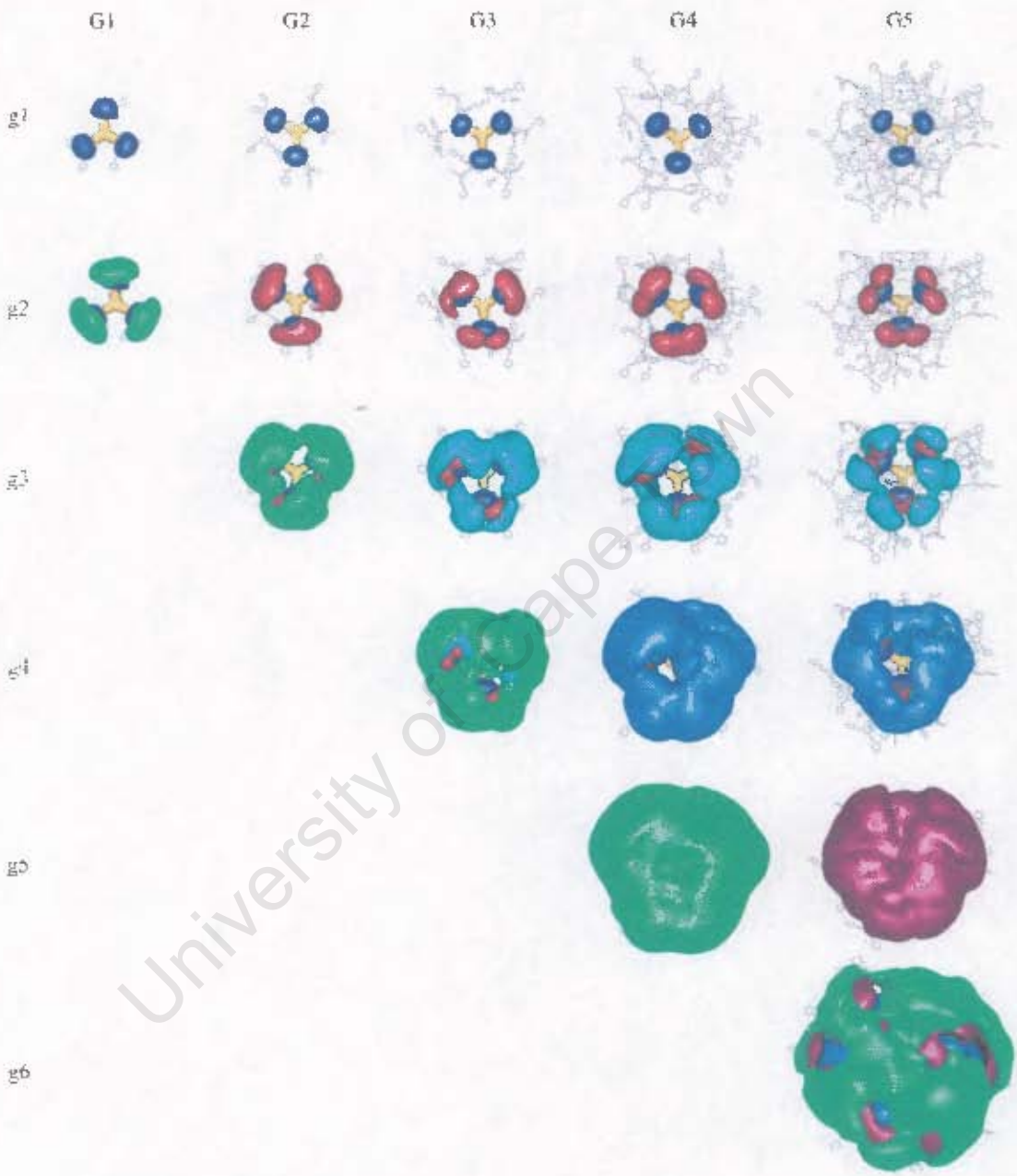

Figure F.3: A view from below the core of the SDFs at half bulk density of each topological layer (g1 - g6) of dendrimers G1 to G5 in THF.

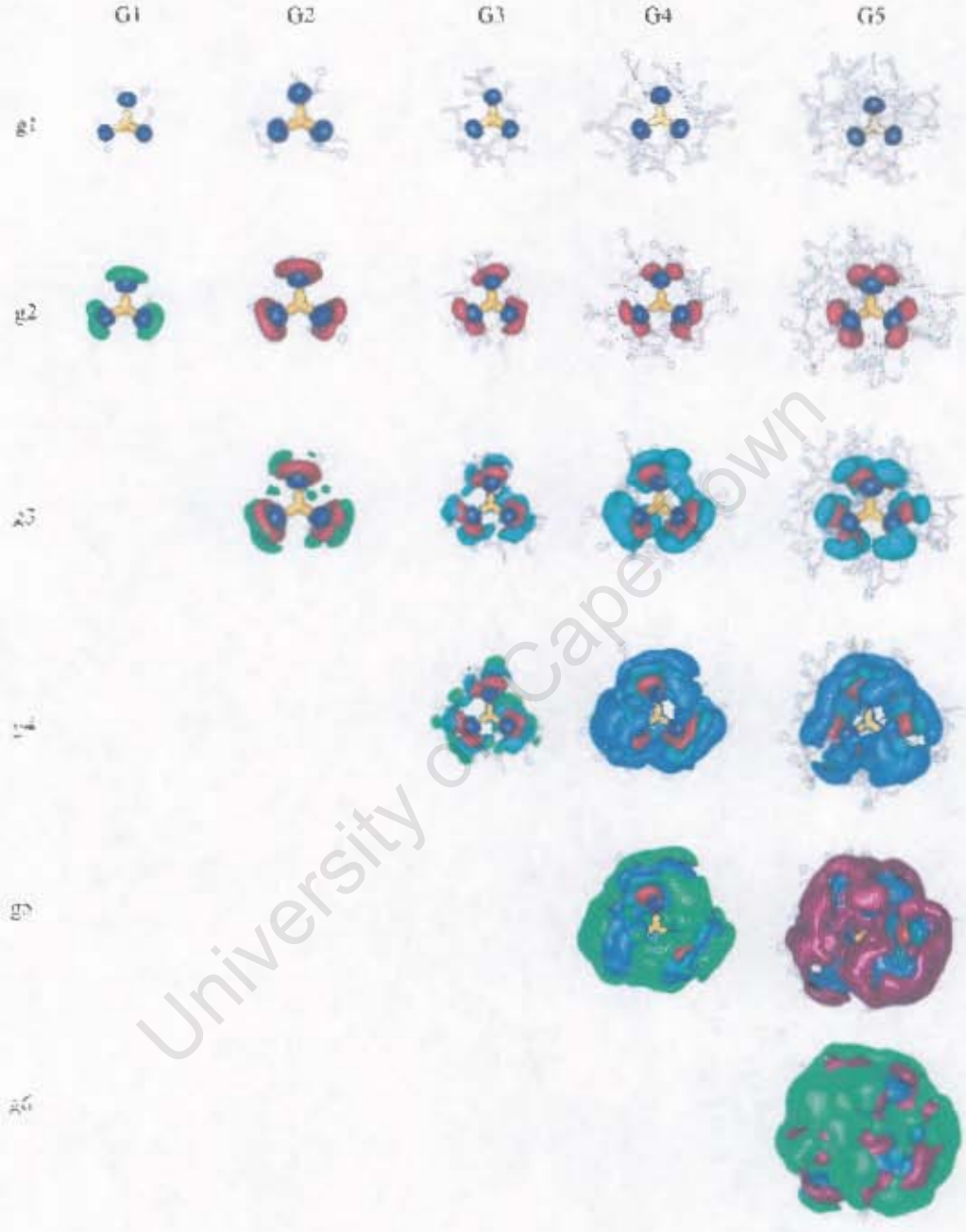

Figure F.4: The SDFs at bulk density of each topological layer (g1 - g6) of dendrimers G1 to G5 in THF.

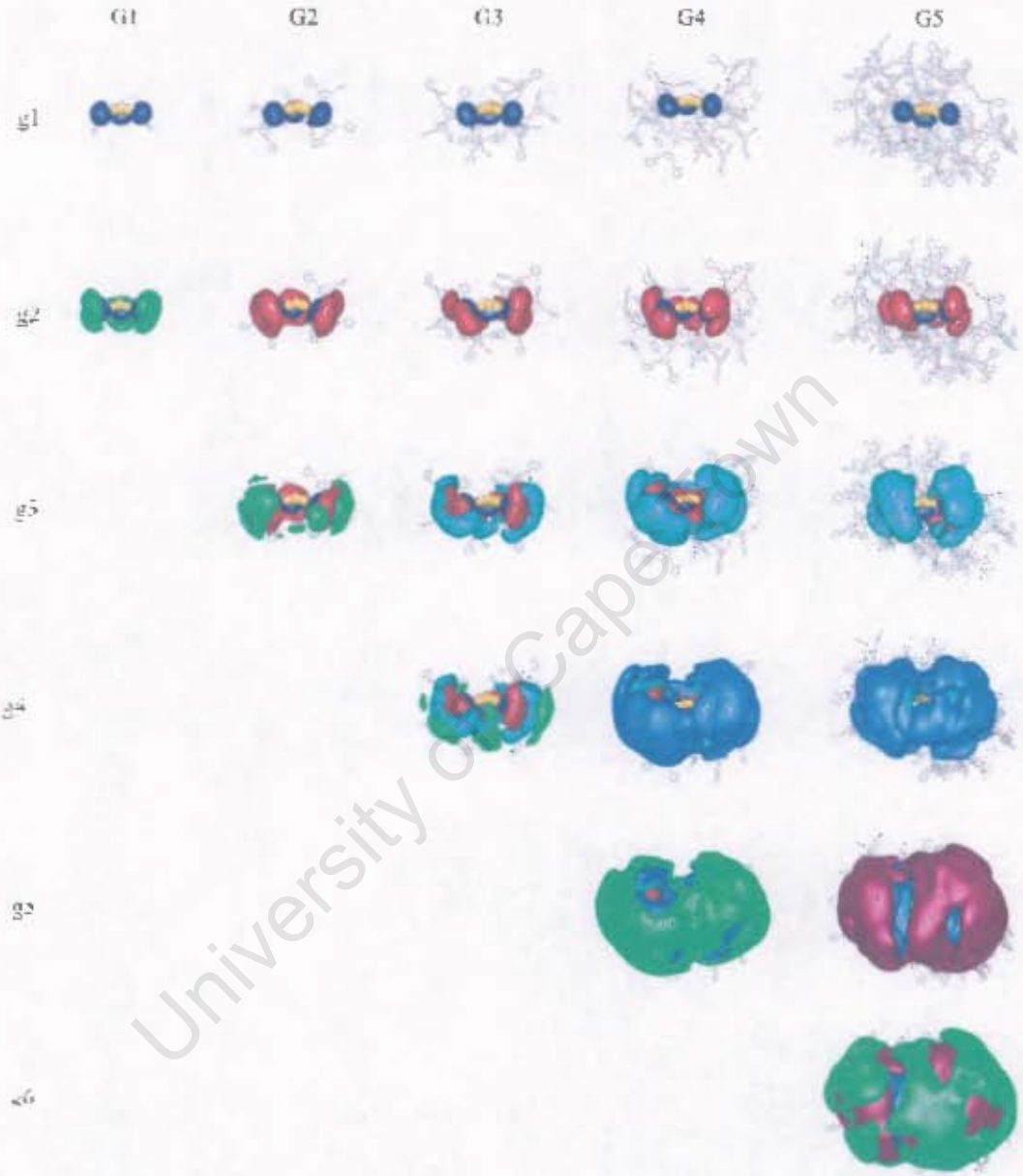

Figure F.5: A side view of the SDFs at bulk density of each topological layer (g1 - g6) of dendrimers G1 to G5 in THF.

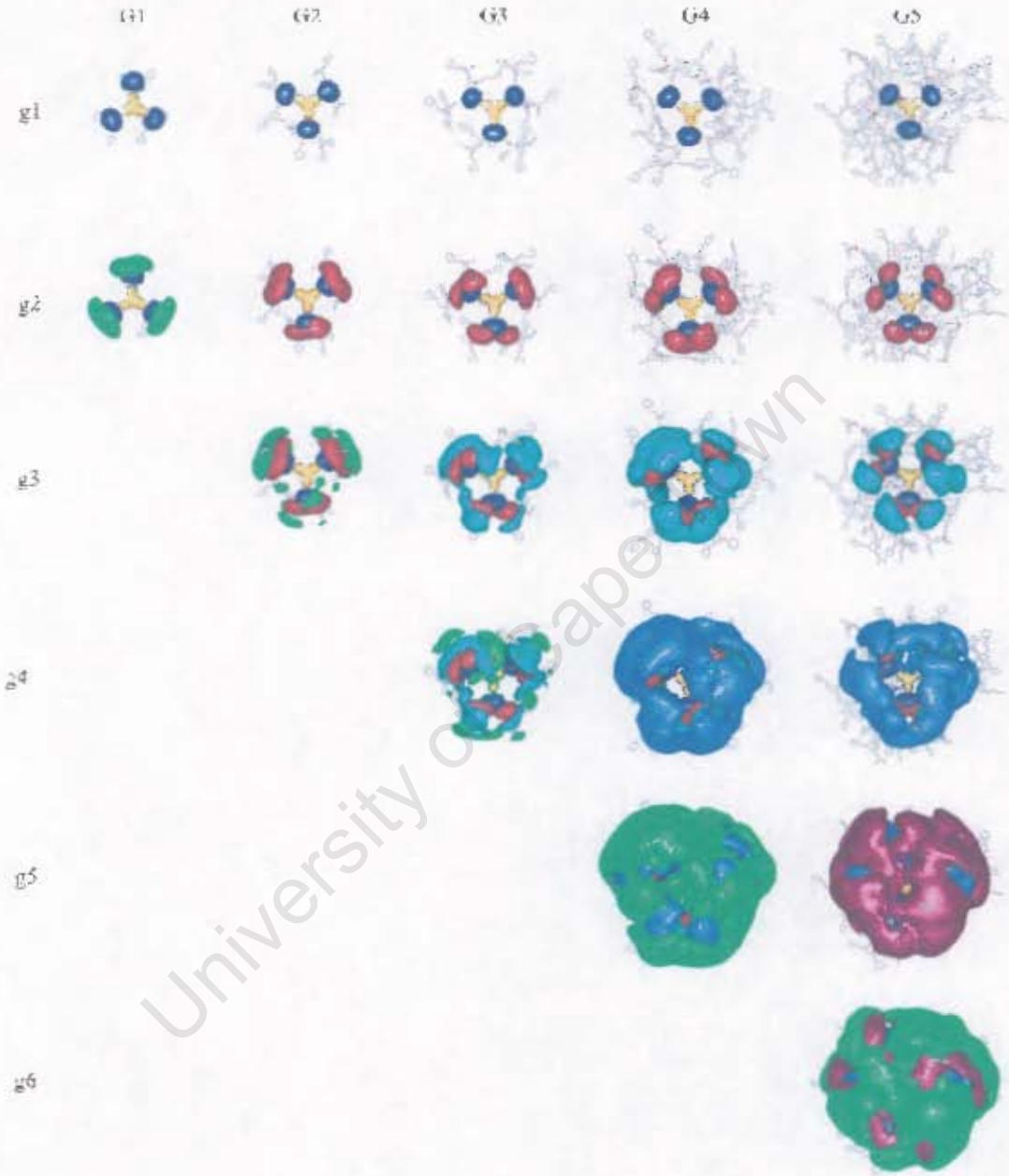

Figure F.6: A view from below the core of the SDFs at bulk density of each topological layer (g1 - g6) of dendrimers G1 to G5 in THF.

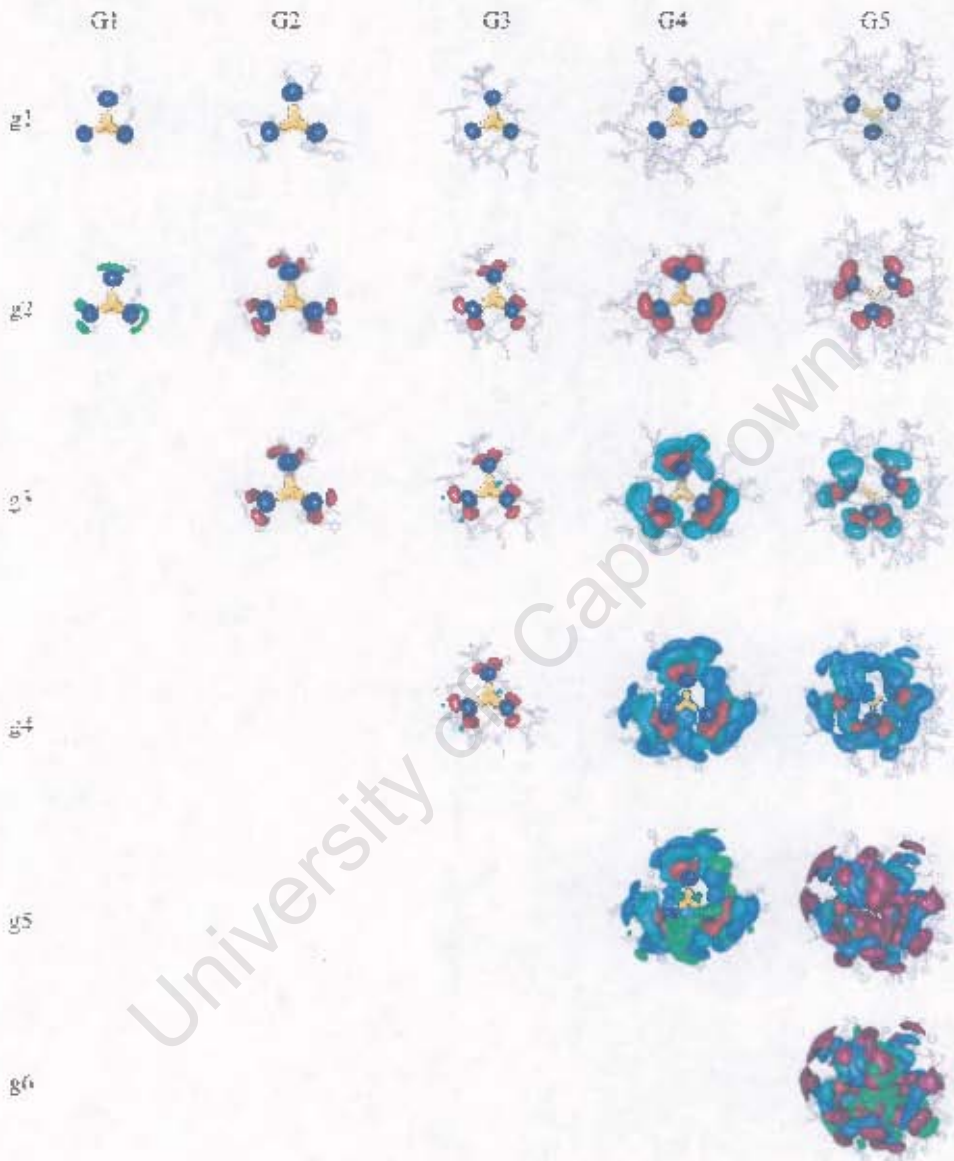

Figure F.7: The SDFs at twice bulk density of each topological layer (g1 - g6) of dendrimers G1 to G5 in THF.

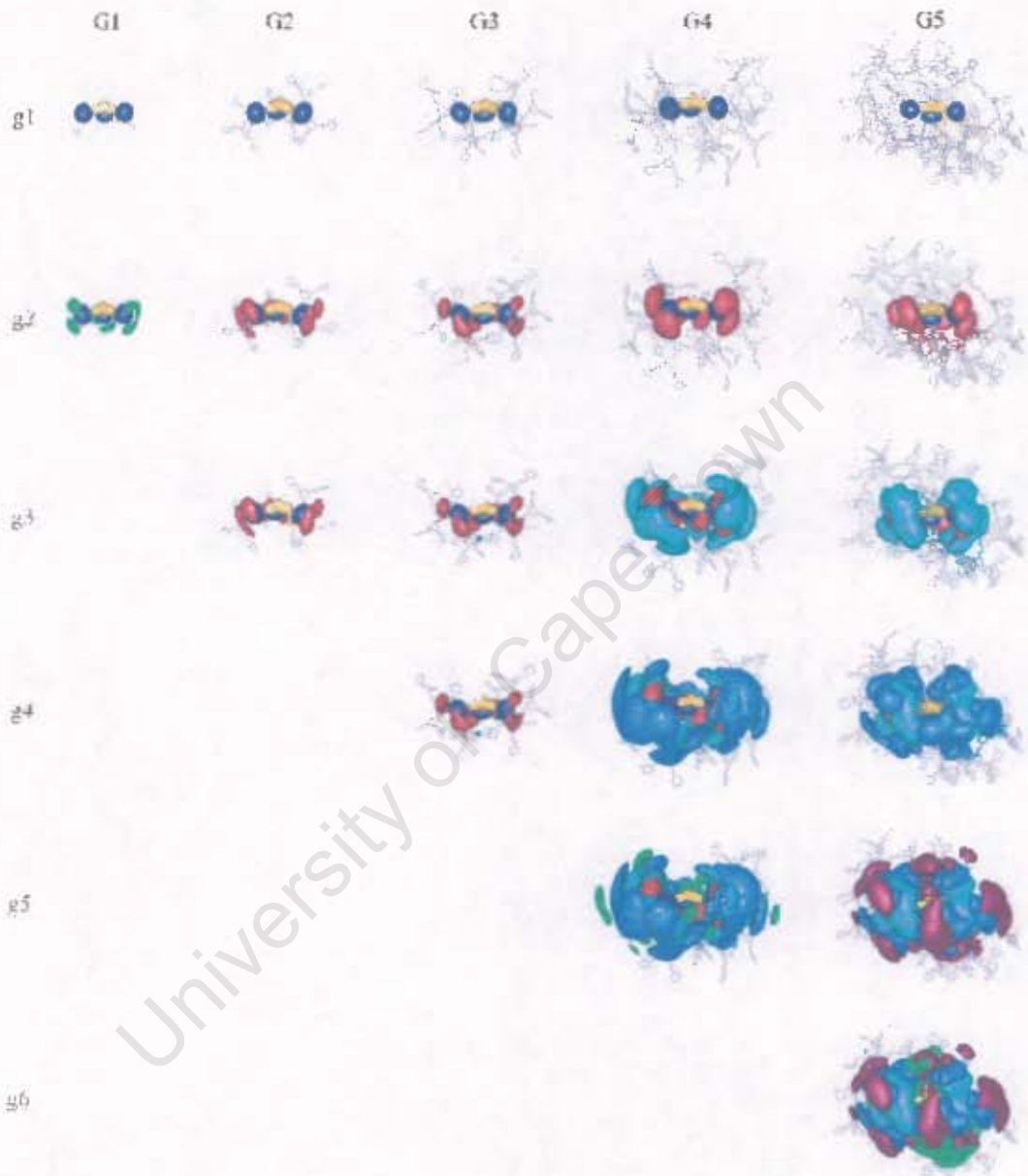

Figure F.8: A side view of the SDFs twice at bulk density of each topological layer (g1 - g6) of dendrimers G1 to G5 in THF.

Figure F.9: A view from below the core of the SDFs at twice bulk density of each topological layer (g1 - g6) of dendrimers G1 to G5 in THF.

Appendix G

Cutplanes through SDFs of dendrimers

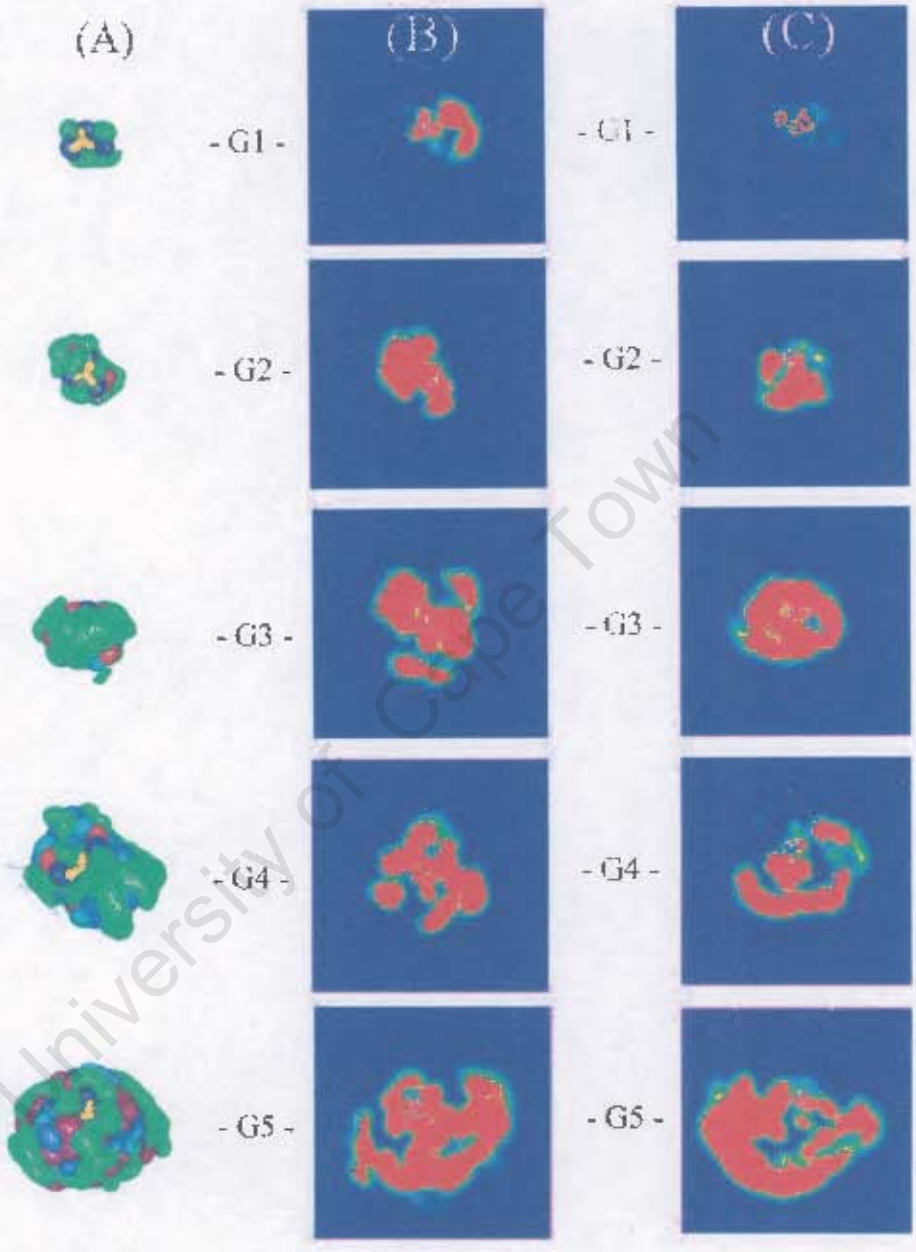

Figure G.1: Cutplanes through the SDFs of dendrimers G1 to G5 in vacuum. (A)Spatially averaged density functions (SDF) of the vacuum series at bulk density containing only the core and the terminal layers. (B) represents a cutplane through the SDF the plane of the three core phenyl rings' and (C) a cutplane orthoganol to the first cutplane. The key is represented in Figure 3.4.

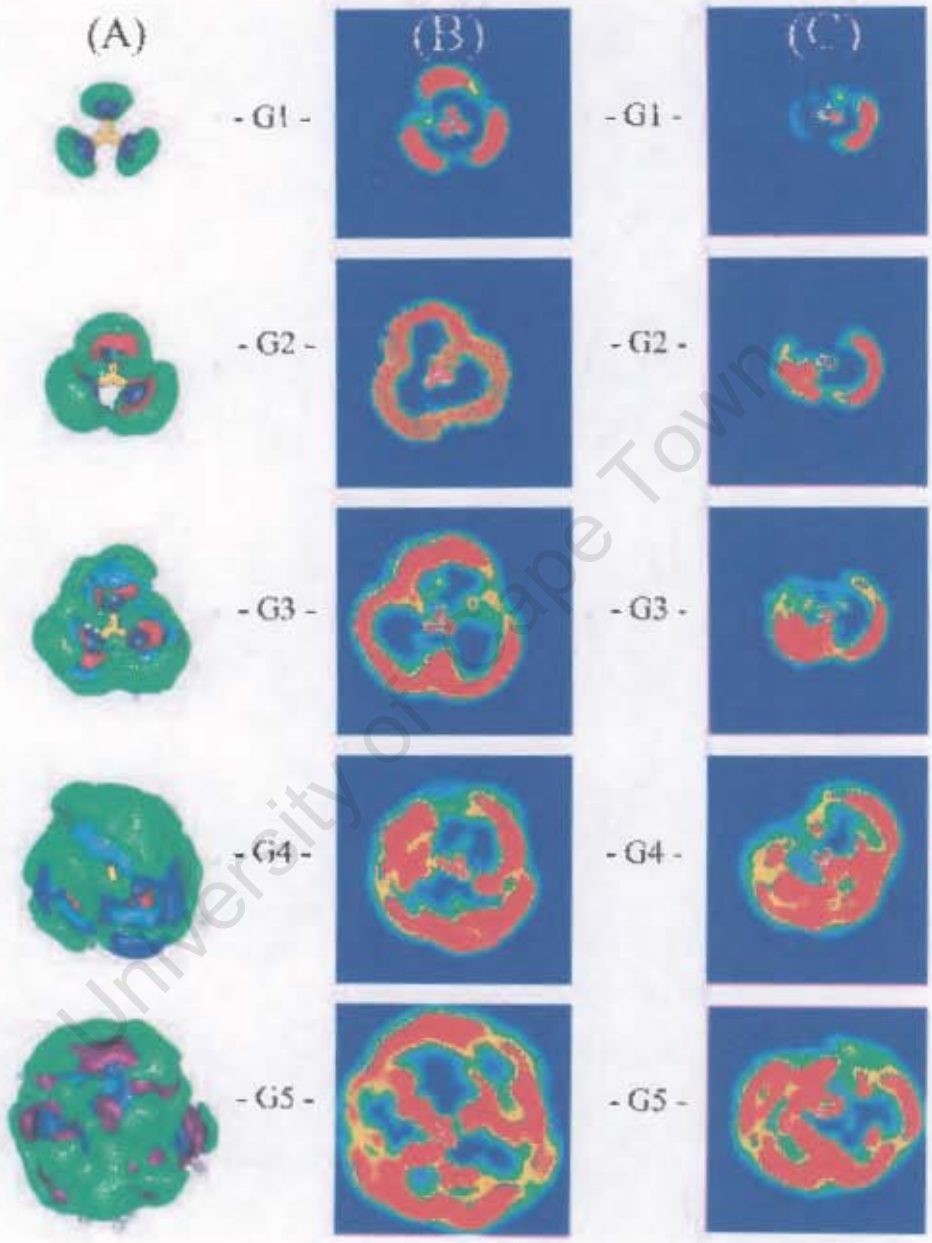

Figure G.2: The equivalent series of SDFs and cutplanes as Figure G.1 for the THF series.

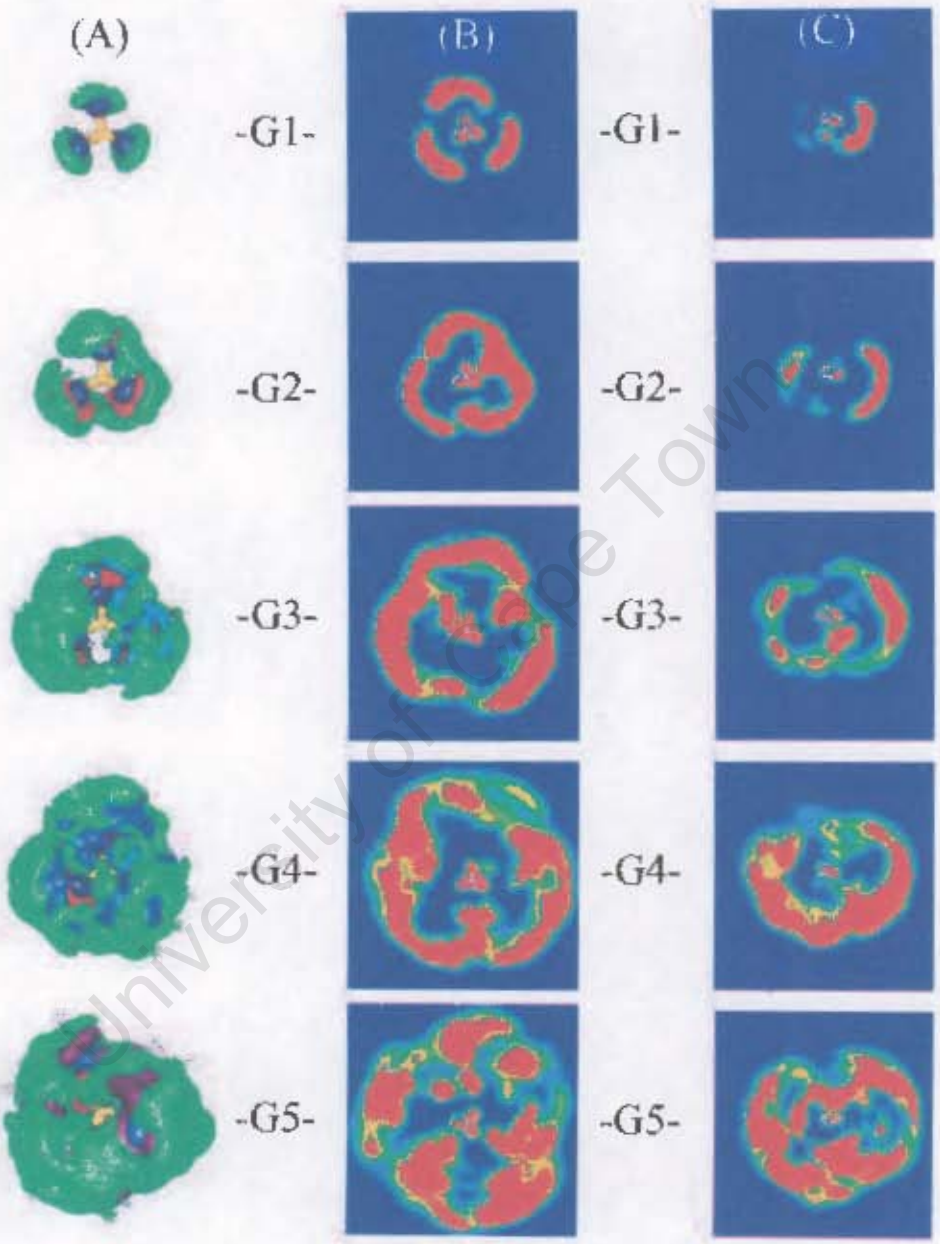

Figure G.3: The equivalent series of SDFs and cutplanes as Figure G.1 for the chloroform series.